The Molecular Mechanisms of rhIGF1 in the Treatment of Rett Syndrome and Related Disorders: Studies in Patients, Mouse and Cellular Models

---

Volume 1 of 2

A thesis submitted for the degree of

Doctor of Philosophy (PhD)

14/07/2022

Submitted by:

Stephen Shovlin

Under the supervision of:

Daniela Tropea

Declaration

I declare that this thesis has not been submitted as an exercise for a degree at this or any other university and it is entirely my own work.

I agree to deposit this thesis in the University's open access institutional repository or allow the Library to do so on my behalf, subject to Irish Copyright Legislation and Trinity College Library conditions of use and acknowledgment.

I consent to the examiner retaining a copy of the thesis beyond the examining period, should they so wish (EU GDPR May 2018).

Fort this thesis, data from an experiment previously conducted by Albert Sanfeliu Bosch, for his PhD thesis entitled "Exploring the molecular mechanisms of Rett Syndrome", was used for part of this analysis in Chapter II. Albert's contributions are acknowledged in the text of the thesis, where applicable.

30/11/2021

Stephen Shovlin **Submission Date**

Acknowledgments

I would like to thank my supervisor Dr. Daniela Tropea, for facilitating this project and working tirelessly with me throughout the last 4 years. Thank you to my colleagues in the lab, Albert Sanfeliu and Phuong Bach, who were great team-mates and Trojan workers when the going got tough. Thank you to my collaborators in MIT and Boston Children's Hospital, and all the families and patients for enabling this research to be conducted.

To all my colleagues in TTMI and Neuropsychiatric Genetics group, thank you for your support, comradery and friendship over the years. Particular mentions to the members of thesis writing club; Anna Bogdanska, Emma Leacy, Gráinne Jameson, and Niall Cook, who made writing a PhD thesis seem like a reasonable thing to do. Thank you to the Comparative Medicine Unit team; Viola, Rustam, Mark and Daniel, for helping to train me and care for the mice used in this project.

Thank you to my wonderful partner, Sophie Hennessy, who was there for every minor, and major calamity, you kept me going.

Thank you to my parents Ian Shovlin, and Ursula Keegan, who enabled me to pursue this career in academia, to my grandparents Mary and James Keegan, who have melted their weight in candle wax keep a light lit for me in Carraroe chapel. Thank you to Dallan and Ruth Shovlin for the company, cooking and gaming during lockdown when everything was up in the air.

A special thank you to two people who have had a great influence on my career and own personal development, Phil Shovlin and Dr Marion Rowland. You have always kept me grounded and self-aware and have helped me see the wood from the trees when needed.

Finally, to my friends who have helped me and provided an escape from things when I was overwhelmed, to Dallan, Marty, Aiden, Conor, Killian, Richard, John, Eoin, Jack, Oisín, Mark and Tweed, thank you.

You all got me through the grim grey days when equipment and reagents turned against me. I'm looking forward to bright shiny days in the future now.

Thank you.

Thesis Outputs:

The work described in this thesis has been partially published in the following peer-reviewed articles:

Shovlin, S. & Tropea, D. Transcriptome level analysis in Rett syndrome using human samples from different tissues. Orphanet J. Rare Dis. 13, 1–15 (2018).

Bach, S., Shovlin, S., Moriarty, M., Bardoni, B. & Tropea, D. Rett Syndrome and Fragile X Syndrome: Different Etiology With Common Molecular Dysfunctions. Front. Cell. Neurosci. 15, 1–16 (2021).

The work presented in Chapter I is currently being prepared as a manuscript for submission to a peer-reviewed journal.

Summary

Recombinant human Insulin-like Growth Factor 1 (rhIGF1) is an approved treatment for growth failure and IGF1 deficiency. IGF1 has multiple functions in the body including growth, cell survival, metabolism, ageing and neurodevelopment. The neuroprotective effects of rhIGF1 and its metabolite glycine-proline-glutamate (GPE), has led to a number of related clinical trials in neuropsychiatric disorders, including Rett Syndrome (RTT). RTT is a devastating X-linked neurodevelopmental disorder strongly associated with mutations in the *Methyl-CpG Binding Protein 2* (*MECP2*) gene. Patients with RTT generally have neuro-typical development up until 6 to 18 months of age, followed by the onset of symptoms and developmental regression. Patients display a wide variety of symptoms, including; severe cognitive impairment, motor dysfunction, cardiorespiratory abnormalities, impaired gait, and repetitive hand stereotypies. The X-linked nature of *MECP2* means that the presentation is more severe in males, usually leaving them non-viable, hence the vast majority of patients are female. Mutation of *Mecp2* in mouse models result in phenotypes that recapitulate many of the features of RTT.

This thesis aims to understand the molecular mechanisms of rhIGF1 treatment in the context of RTT. In Chapter I, we assessed the gene expression data of whole blood samples from patients with RTT in a phase I clinical trial. This analysis revealed different transcriptional profiles of gene expression depending on whether patients showed response to treatment, as measured by the improvement to apnoeic index. This analysis highlighted the importance of IGF signaling and regulation, immune modulation, and cell cycle progression in response to treatment.

In Chapter II, *Mecp2*$^{-/+}$ and *Mecp2*$^{-/y}$ mice were treated with rhIGF1. Locomotor activity and gene expression of the cerebellum and blood was measured to determine the effects of treatment. In *Mecp2*$^{-/+}$ mice, rhIGF1 affected Central Nervous System (CNS) specific functions, while in *Mecp2*$^{-/y}$ mice, rhIGF1 resulted in changes in cellular and metabolic processes. We analysed locomotor and gene expression of *Mecp2*$^{-/+}$ mice, while a colleague Albert Sanfeliu Bosch, provided sequencing data for the *Mecp2*$^{-/y}$ mice.

In the final chapter we performed *in vitro* experiments in neuronally differentiated SH-SY5Y cell line to identify the mechanism of action of rhIGF1 and its tripeptide GPE. Despite rhIGF1 and GPE being strongly interconnected, these drugs elicited different

effects on canonical downstream signalling pathways of IGF1, including PI3K-AKT and MAPK signaling.

In this way we will examine mechanisms of rhIGF1 in RTT patients, *Mecp2* mouse model and a cellular model, making use the advantages of each system in the context of RTT.

Thesis Aims

The aim of this thesis, is to determine the molecular mechanism of recombinant human Insulin-like Growth Factor I (rhIGF1) in Rett Syndrome, this analysis will aid future clinical trials in assessing IGF1 and related treatments.

Three different approaches will be used to complete this aim:

Chapter I: Patients with Rett Syndrome - Gene expression analysis will be conducted on RNA from whole blood of patients with Rett Syndrome treated with Mecasermin (rhIGF1), during a phase I clinical trial, in order to determine the effects of treatment, and to compare gene expression in patients with different clinical responses to treatment.

Chapter II: *Mecp2*$^{\mathbf{tm1.1Bird/J}}$ Mouse Model – These mice will be treated with rhIGF1 and have motor activity measured before and after treatment. Gene expression analysis will be conducted in blood and cerebellum of *Mecp2*$^{-/+}$ mice, while the blood can be compared to the results in Patients and the Cerebellum can be used to investigate the effects of treatment in the CNS.

Additionally, the gene expression measured in rhIGF1 treated female *Mecp2*$^{-/+}$ mice can be compared with a similar experiment, previously conducted by a colleague Albert Sanfeliu Bosch, in rhIGF1 treated male *Mecp2*$^{-/y}$ mice. This comparison is highly relevant as there are discrepancies between *Mecp2*$^{-/+}$ and *Mecp2*$^{-/y}$ mice phenotypes and the presentation of the disorder in humans.

Chapter III: SH-SY5Y Neuronally Differentiated Cell Line – This cell model will be used to determine the effects of rhIGF1 and its tripeptide derivative Glycine-Proline-Glutamate (GPE) stimulation *in vitro*.

The results of this analysis are not only important for Rett Syndrome, but could have applications to other neurodevelopment disorders, currently testing the efficacy of IGF1 based therapeutics at clinical trials.

Contents

List of Tables

List of Figures

List of Abbreviations

A

AKT	Serine-Threonine Kinase
ALB	Albumin
ALS	Acid Labile Subunit
AMPAR	α-Amino-3-Hydorxyl-5-Methyl-4-Isoxazolepropionic Acid Receptor
APOA2	Apolipoprotein A2
APS	Ammonium persulfate
ASD	Autism Spectrum Disorder
AURKB	Aurora Kinase B

B

BDNF	Brain Derived Neurotrophic Factor
BL	Blood
BSA	Bovine Serum Albumin

C

CAMK2A	Calcium Calmodulin-Dependent Kinase 2A
CAMK4	Calcium Calmodulin-Dependent Kinase VI
CBP	CREB Binding Protein
CCNB2	Cyclin B2
CDKL5	Cyclic Dependent Kinase-Like 5
CENPF	Centromere Protein F
CENPM	Centromere Protein M
cGP	cyclic Glycine-Proline
cKO	Conditional Knock-Out

CMU	Comparative Medicine Unit
CNS	Central Nervous System
CO1	Cytochrome C Oxygenase 1
CpG	Cytosine-Phosphate-Guanosine
CPM	Counts Per Million
CRB	Cerebellum
CREB	CAMP Response Element-Binding Protein
Cre-ER	Cre recombinase and modified Estrogen Receptor
CSF	Cerebrospinal Fluid
CT	Cycle Threshold
C-term	Carboxy-terminus
D	
ddCT	Delta Delta Cycle Threshold
DEG	Differentially Expressed Gene
DGE	Differential Gene Expression
DMSO	Dimethylsulfoxide
dNTPs	Deoxynucleoside Triphosphates
E	
EAE	Experimental Autoimmune Encephalomyelitis
EDTA	Ethylenediaminetetra acetic acid
EEG	Electroencephalogram
E/I	Excitation/Inhibition
EPSC	Excitatory Postsynaptic Current
EPI-743	α-Tocotrienol Quinone

ERK1/2	Extracellular Signal-Receptor Kinases 1/2
ERVMER34-1	Endogenous Retrovirus Group MER34 Member 1, Envelope
ESCO2	Establishment of Sister Chromatid Cohesion N-Acetyltransferase 2
F	
FABP1	Fatty Acid Binding Protein1
FDR	False Discovery Rate
FOXG1	Fox-Head Box Protein G1
FXS	Fragile X Syndrome
G	
GA	Glatiramer Acetate
GABA	Gamma Aminobutyric Acid
GAPDH	Glyceraldehyde 3-phosphate dehydrogenase
GFAP	Glial Fibrillary Acid Protein
GH	Growth Hormone
GHR	GH Receptor
GHRH	Growth Hormone Releasing Hormone
GO	Gene Ontology
GPE	Glycine-Proline-Glutamate
GRB2	Growth Factor Receptor-Bound Protein 2
GRIN2B	NMDA receptor 2B
H	
HDT	Hypothesis Driven Testing
HET	*Mecp2*$^{-/+}$ Mice
HFT	Hypothesis Free Testing

HLA-DRB5	Histocompatibility Complex Class II DRβ5
Hr	Hour
HRP	Horseradish Peroxide
I	
ID	Interdomain
IDT	Integrated DNA Technology
IGF1	Insulin-like Growth Factor 1
IGF2	Insulin-like Growth Factor 2
IGFBP	Insulin-like Growth Factor Binding Protein
IGFBP1	Insulin-like Growth Factor Binding Protein 1
IGFBP3	Insulin-like Growth Factor Binding Protein 3
IGFBP6	Insulin-like Growth Factor Binding Protein 6
IGF1R	Insulin-like Growth Factor 1 Receptor
IGF2R	Insulin-like Growth Factor 2 Receptor
IPSC	Induced Pluripotent Stem Cell
IR	Insulin Receptor
IRS	Insulin Receptor Substrate
IRS1	Insulin Receptor Substrate 1
IRS2	Insulin Receptor Substrate 2
K	
KO	Knock-Out
L	
LPS	Lippolysaccharide
LTP	Long Term Potentiation

M

MAD	Multiple Ascending Dose
MAPK	Mitogen Activated Protein Kinase
MASP	Mannose-Binding Lectin Associated Serine Proteases
MBD	Methyl Binding Domain
mCA	Methylated Cytosine-Adenine
mCAC	Methylated Cytosine-Adenine-Cytosine
mCG	Methylated-Cytosine-Gaunine
MDM2	Minute Double Minute 2
MECP2	Methyl CpG Binding protein 2
MIT	Massachusetts Institute of Technology
MRD	MECP2 Related Disorder
MRI	Magnetic Resonance Imaging
MTOR	Mechanistic Target Of Rapamycin

N

NaCl	Sodium Chloride
NaOH	Sodium Hydroxide
NCoR/SMRT	Nuclear Co-Repressor/Silencing Mediator for Thyroid-Hormone Receptor
NFkB	Nuclear Factor k-light-chain-enhancer-of-activated B cell
NMD	Non-Sense Mediated Decay
NMDA	N-Methyl-D Aspartate
NMDAR	N-Methyl-D Aspartate Receptor
NLS	Nuclear Localisation Signa

O

OLE	Open Label Extension
P	
pAKT	Phosphorylated-AKT
PBS	Phosphate Buffered Saline
PC	Principle Component
PCA	Principal Component Analysis
PCR	Polymerase Chain Reaction
pCREB	Phosphorylated-CREB
pERK1/2	Phosphorylated ERK1/2
PFA	Paraformaldehyde
pIGF1R	Phosphorylated-IGF1R
PI3K	Phosphatidylinositol 3 Kinase
PLL	Poly-L-Lysine
PK	Pharmacokenetics
PKA	Protein Kinase A
PKO	Peripheral Knock-Out
Pro-BDNF	Pro-Brain Derived Neurotrophic Factor
PPP	Picropodophyllin
PSD-95	Postsynaptic Density Protein-95
PTEN	Phosphatase and Tensin Homolog
PV	Parvalbumin
PVDF	Polyvinylidene Fluoride
Q	
QLFT	Quasi-Likelihood F test

qPCR	quantitative-Polymerase Chain Reaction
R	
rhIGF1	Recombinant Human Insulin Like Growth Factor 1
RNA	Ribonucleic Acid
RNAi	Ribonucleic Acid interference
RNA-Seq	RNA Sequencing
ROI	Regions of Interest
RRM2	Ribonucleotide Reductase Regulatory Subunit M2
RTT	Rett Syndrome
RVMSR	Responders versus MSRs
S	
SDS	Sodium Dodexyl Sulfate
SE	Standard Error
SERPINA1C	Alpha-1 Antitrypsin 1-3
SERPING1	Serpin Family G Member 1
SHC	Src-Homology and Collagen
SH-SY5Y	Neuroblastoma cell line
SIN3A	SIN3 Transcriptional Regulator Family A
siRNA	small interfering Ribonucleic Acid
SMCR5	Smith-Magenis Syndrome Chromosome Region, Candidate 5
T	
TBSI	Trinity Biomedical Science Institute
TBST	Tris Buffered Saline with Tween
TCD	Trinity College Dublin

TEMED	Tetramethylethlenediamine
TK1	Thymine Kinase 1
TMEM176A	Transmembrane Protein 176A
TMEM176B	Transmembrane Protein 176B
TOP2A	DNA Topoisomerase II α
TRD	Transcriptional Repression Domain
Tris-HCl	Tris-Hydrochloric acid
TrkB	Tyrosine Receptor Kinase B
TTR	Transthyretin
TUBB2A	Tubulin β 2A
T0	Pre-MAD
T1	Post-MAD
T2	Pre-OLE
T3	Post-OLE
U	
UBE2C	Ubiquitin Conjugating Enzyme E2 C
UTR	Untranslated Region
V	
V1	Primary Visual Cortex
VIP	Vasoactive Intestinal Peptide
W	
WT	Wildtype
WTF	Wildtype Female
WTM	Wildtype Male

X

XCI X-Chromosome Inactivation

#

3’DGE 3’ Digital Gene Expression

5hmC 5-hydroxymethylcytosine

COVID Impact Statement

During the final two years of the PhD program, the global and national SARS CoV2 pandemic detrimentally impacted my research project. This is a summary statement to list the ways in which my research was affected and to provide context for what was completed during my 4-year program.
The pandemic and lockdowns affected me in the following ways:

- The initial intension for the project was to compare the effects of mecasermin rhIGF1 and trofinetide (GPE) in the treatment of Rett Syndrome (RTT). Blood samples from a phase II clinical trial using Trofinetide as a treatment in RTT were meant to be sent from BCH to compliment the phase I mecasermin trial. However, the shipping of these samples were delayed and the study had to be omitted from my PhD project.
- A collaboration with the University of Rochester, to examine the effects of GPE on microglial cells in *Mecp2* mutant mice *in vivo*, was proposed during my third year. I had planned to travel and conduct in April. However, the national and international lockdowns implemented in March of that year meant that this collaboration had to abandoned.
- The national lockdowns meant that the lab groups *Mecp2* mouse colony had to be reduced to a minimal size. This was done to preserve the colony without risking animal welfare due to limited access to the facilities. Re-establishing the colony was difficult and time consuming. This meant that sample sizes in chapter II were limited, and results were delayed particularly for rhIGF1 treatments.
- Due to reallocation of resources in TTMI towards COVID research, the cell culture facilities that I was using for the experiments in chapter III of this thesis were not available. This required me to make alternative arrangements and set up cell culture in another lab, which had not used cell culture facilities for a few years. This delayed the results for chapter III of the thesis and prevented me from further investigating the cellular mechanisms of rhIGF1 and GPE. I had planned to explore the effect of GPE on NMDAR, using a specific inhibitor MK-801.
- Several consumables required for this research were in high demand due to ongoing research efforts into vaccines and therapeutics for SARS-CoV2, the

syringes and needles had significant delays up to 4 months which further delayed the treatment of *Mecp2* mice with rhIGF1 in chapter II.

The limited time and resources allocated due to the restrictions of the pandemic significantly impacted the scope of chapters II & III in this thesis. Beyond this, many months of my PhD were very stressful due to the uncertainty of the situation and work from home guidelines imposed by the Irish government.

1.0 Introduction

1.1 Insulin-like Growth Factor I (IGF1) and Glycine-Proline-Glutamate (GPE)

1.1.1 Basic Structure and Function of IGF1 and GPE

Insulin-like Growth Factor I (IGF1) is a growth hormone found throughout the body with a variety of anabolic functions related to growth, development, and metabolism. It has specific roles in the CNS such as growth, cell survival, synaptic plasticity and neurogenesis [1–3]. IGF1 is synthesised primarily in the liver, and it regulated by Growth Hormone (GH) secretion in the pituitary gland [4]. IGF1 levels are high during early development and decrease over time postnatally [5]. Although there are many different IGF1 isoforms, the proteins share a common mature peptide which is biologically active. The immature pro-IGF1 protein is cleaved by posttranslational processing, which removes the so-called E-peptide, leaving the /mature active IGF1 peptide [6].

IGF1 activity is mediated primarily through direct binding to the IGF1 Receptor (IGF1R), although IGF1 also binds the Insulin Receptor (IR) with lower affinity, and to a lesser extent Insulin-like Growth Factor 2 Receptor (IGF2R) [7]. IGF1R and IR have similar structures; two extracellular α-subunits bind via disulphide bonds and two transmembrane β-subunits allow for tyrosine kinase activity [8]. Ligand binding occurs in the α-subunits and leads to conformational changes in the β-subunits, which result in auto-phosphorylation and activation of downstream signaling [9].

IGF1 is a 70 amino acid long polypeptide, which is cleaved into a tripeptide glycine-proline-glutamate (GPE) and the remaining des-IGF1 [10–12].

IGF1's bioavailability for receptor activation is tightly regulated through the binding of Insulin-like Growth Factor Binding Proteins (IGFBPs). IGF1 has a higher affinity for IGFBPs than IGF1R and therefore they competitively prevent IGF1R activation [7] . There are 6 primary human IGFBPs, named IGFBP1 to IGFBP6. 75-80% of IGFs are bound by a ternary complex which contains IGF, IGFBP3 and Acid Labile Subunit (ALS), 20-25% of IGFs are bound by one other IGFBP and only 1% of IGFs are freely available in circulation [13]. Free IGF1 has a half-life of only 10 minutes. When bound to

an IGFBP IGF1's half-life is increased to ~ 25 min and when bound to the ternary complex half-life increases to ~ 16 hours [14].

1.1.2 Signaling pathways in IGF1 and GPE

IGF1R can form a homodimer (IGF1R-IGF1R) or the heterodimer (IGF1R-IR) with IR, due to their shared homology. IGF1-IR has different properties depending on the isoform of IR. The heterodimer IGF1R-IR binds IGF1 with high affinity, however, heterodimers containing IR-A isoform have more affinity for IGF2 and insulin compared to heterodimers containing IR-B [15]. When ligand binding of IGF1R occurs at the α-subunit, there is subsequent auto-phosphorylation of the β-subunit. These auto-phosphorylated tyrosine kinase sites are the same on IR as they are on IGF1R [16]. The interaction between docking proteins of IGF1R and receptor itself mediates the downstream signaling pathways. These docking proteins include; insulin Receptor Substrate-1 (IRS1), IRS2, and Src-Homology and collagen (SHC).

The two primary pathways activated by IGF1R are the Phosphatidylinositol 3-Kinase pathway (PI3K) and Ras-Mitogen activated protein kinase (MAPK), as depicted in figure 1.1. The PI3K activates the Serine-threonine kinase (AKT), which is essential for neuronal survival [17]. Sustained activation of the PI3K pathway by IGF1 has been found to induce cell proliferation [18]. MAPK signaling is shared by a number of different cascades, Extracellular Signal-Receptor Kinases 1/2 (ERK1/2) is associated with functions such as cell proliferation, differentiation, migration, senescence and apoptosis [19].

Different phosphorylation sites of IRS1 and IRS2 docking proteins induce different phosphorylation sites on downstream substrates. The IRS1 sites 608, 628, and 658, and IRS2 sites 649, 671, 734, and 814 were all found to be associated in p85 regulation of PI3K. IRS1 tyr-891 is a binding site for Growth Factor Receptor-Bound Protein 2 (GRB2), which activates the MAPK pathway. IRS can also be sensitised or desensitised by certain serine phosphorylation; S312, S616, S636 and S1101 desensitise IR signaling while S1223 can sensitise IR signaling [20].

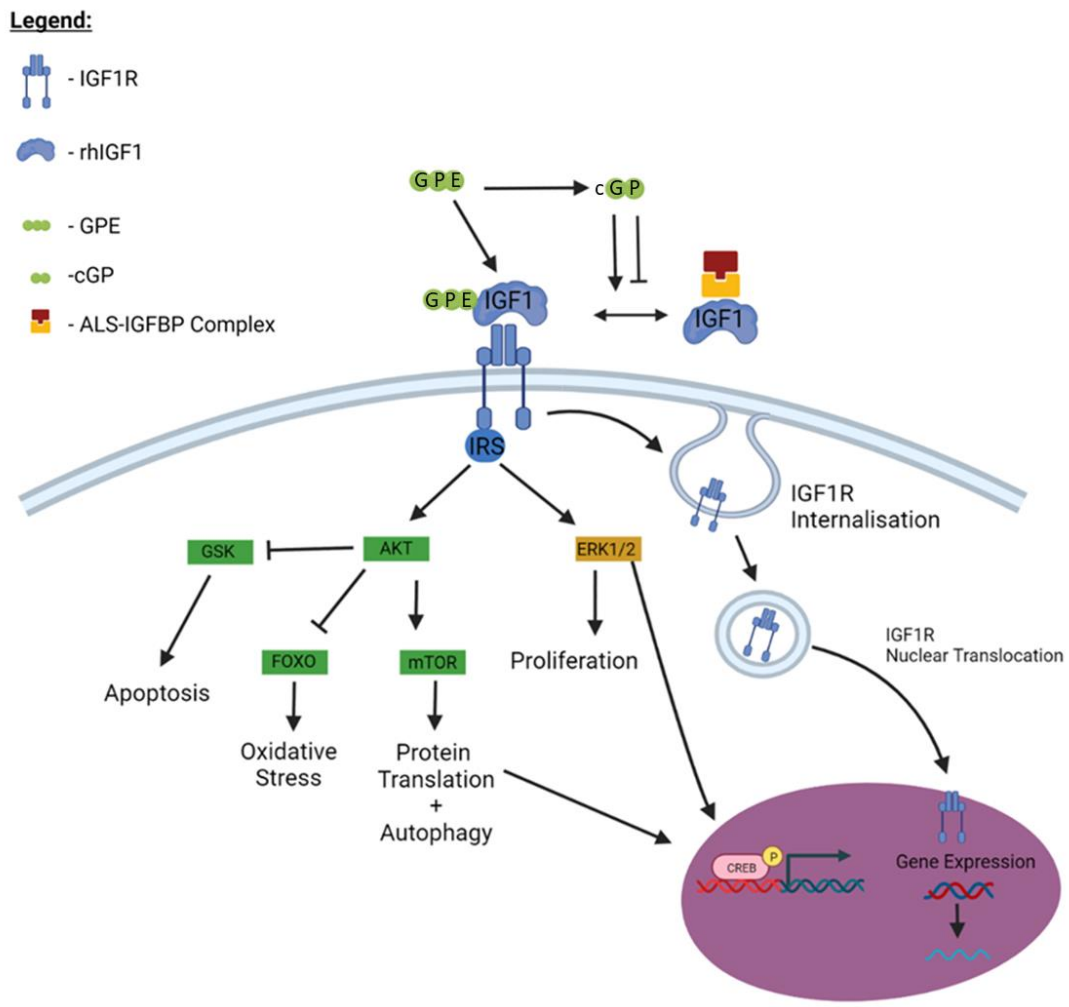

Figure 1.1 – IGF1 Signaling and Regulation

IGF1 preferentially binds the IGF1 receptor inducing auto-phosphorylation and subsequent phosphorylation of IRS docking proteins. IRS protein phosphorylation leads to activation to the two major pathways of canonical IGF1 signaling, that AKT and MAPK (ERK1/2) pathways. The AKT pathway is important for neuronal survival function of IGF1 [17]. The ERK1/2 pathway is involved in cell proliferation and differentiation [19].

The IGF1 derivative GPE also has neuroprotective properties. GPE does not directly bind the IGF1R [10] but can indirectly affect IGF1R signaling by increasing endogenous levels of IGF1 [30]. The metabolite of GPE, cyclic Glycine-Proline (cGP), has a regulatory effect on the bioavailability of IGF1 through the binding affinity of IGF1 and IGFBP3 in a homeostatic manner [11].

Activation of IGF1R can lead to internalisation of the receptor by endocytosis. This internalisation happens by two distinct pathways; at physiological concentrations of IGF1, Mouse double minute 2 (Mdm2)-ubiqutination mediates clathrin dependent endocytosis [179], at higher levels of IGF1 stimulation IGF1R internalisation is mediated by caveolin pathway [179].

Legend:

ALS-IGFBP complex = Acid Labile Subunit-IGF Binding Protein, cGP = cyclic Glycine-Proline

Picropodophyllin (PPP) is a specific inhibitor of IGF1R, that prevents the phosphorylation of IGF1R at the tyrosine 1136 completely [251]. This tyrosine residue is essential for the auto-phosphorylation loop and subsequently downstream signalling, without effecting insulin receptor activity [251]. PPP decreases activation of both ATK and ERK1/2 signalling inducing apoptosis in IGF1R positive tumour cells cultured in *in vitro* while its levels of cytotoxicity is relatively low [239].

1.1.3 IGF1 and GPE's Role in Neuroprotection and Neurodevelopment

IGF1 also has critical functions in neurodevelopment. While knock-out (KO) of IGF1 resulted in growth deficiency of 60% of wildtype (WT) birth weight, KO of IGF1R in mice was lethal [21]. IGF1 levels were found to be highest during perinatal and early postnatal development in the hippocampus and cerebral cortex and decreased thereafter [5]. Exogenous application of IGF1 has been demonstrated to prevent the effects of ocular dominance shift caused by monocular deprivation in mice. In this model, one eye is sutured closed during a critical period of development, this deprivation results in an increase in neuronal activity ratio response to signals from the open eye in primary visual cortex (V1) [22]. IGF1 was shown to be a crucial factor in accelerating maturation of gamma aminobutyric acid (GABA)-ergic neurotransmission and promoting the GABA polarity switch in the early life of rats. IGF1 treatment resulted in the accelerated development of visual acuity [23]. These studies underline the importance of IGF1 in neurodevelopment and its ability to regulate synaptic connectivity during development.

Both IGF1 and GPE treatments were neuroprotective in rodent models of brain injury [24,25]. Early work showed lesions in the rat hippocampus have elevated IGF1 levels [26]. In rats with hypoxic ischemic injury, IGF1 treatment two hours after injury reduced neuronal loss [24,27]. These studies suggest that IGF1 is involved in neuronal repair after injury.

Initial studies on GPE's mechanisms found that it did not bind IGF1R or IGFBP, and did not affect the binding efficiency of IGF1 to IGF1R. GPE elicited a number of neuro-modulatory effects including the release of acetylcholine and potentiating activity in glutamatergic neurons [10]. GPE was found to activate the N-Methyl D-Aspartate (NMDA) receptor, but only at non-physiologically high concentrations, therefore it is considered only a weak NMDA agonist [28]. GPE treatment reduced Aβ-induced cell death in the hippocampus of a Parkinson's disease mouse model [29]. One study that directly compared IGF1 and GPE in primary mouse neuronal culture proposed, that GPE increased endogenous levels of IGF. This study also found that IGF1 activated both AKT and ERK1/2 signaling, while GPE activated AKT in glial cells. Although GPE does not directly bind IGF1R [30], cyclic Glycine-Proline (cGP), a metabolite of GPE, has been found regulate the binding affinity of IGF1 and IGFBP3 in a homeostatic manner [11]. These studies illustrate that not only does GPE have a separate mechanism to IGF1 but also regulates IGF1 activity. However the exact mechanisms of GPE have yet to be determined.

1.2 Rett Syndrome

1.2.1 Clinical presentation of RTT

RTT is a neurodevelopmental disorder that typically occurs from 6 to 18 months of age and results in a variety of symptoms that can occur with variable severity. Typical RTT diagnosis requires a regression period followed by stabilisation and the presence of 4 core criteria [31]:

1. Loss of acquired speech, and communication.
2. Loss of purposeful hand movement.
3. Gait abnormality.
4. Hand stereotypies, such as wringing or flapping.

Atypical RTT diagnosis requires 2 of the 4 core criteria along with 5 of the 11 supportive criteria. These supportive criteria can also occur in typical RTT. These supportive criteria are [31]:

1. Breathing abnormality.
2. Bruxism.
3. Impaired sleep.
4. Abnormal muscle tone.
5. Peripheral vasomotor disturbance.
6. Scoliosis.
7. Growth retardation.
8. Small cold extremities.
9. Inappropriate laughing/screaming spells.
10. Diminished response to pain.
11. Eye pointing.

RTT was initially observed by Andreas Rett in 1966 in a group of 22 girls. This study provided details of many of the common RTT features and originally described the disorder as one of cerebral atrophy and hyperammonemia [32]. Later the disorder was characterised as having four distinct stages; stage I - early onset stagnation, stage II – developmental regression, stage III – pseudostationary, and stage IV – late motor deterioration [33].

The critical discovery for RTT research came when a number of mutations to *Methyl-CpG Binding Protein 2* (*MECP2*) gene were identified in RTT patients [34]. Since this discovery, a deeper understanding has emerged of the relationship between *MECP2* mutation and RTT. However, there are few patients who have RTT, but do not have mutations in *MECP2* and some people with *MECP2* mutations do not present with RTT [35,36]. However, there remains a very strong association between RTT and *MECP2* mutations, accounting for over 95% of classic RTT and 75% of atypical RTT [37]. This discovery led to the development of *Mecp2*-null mice (*Mecp2* $^{-/y}$). This mouse model created a phenotype that mimicked many of the features of RTT. These mice display severe neurological symptoms, gait abnormality, breathing abnormality and hind-limb clasping [38]. *Mecp2* $^{-/y}$ mice have been used by researchers to explore the relationship

between *Mecp2* and the developing brain, bringing a new level of molecular granularity to RTT.

1.2.2 Comorbidities in RTT

Beyond the core diagnostic criteria, RTT is associated with a range of comorbidities with different severity and prevalence. There is much discussion on nuance of the term comorbidity, but in essence it is the presence of more than one distinct condition in an individual [39]. The main comorbidities observed in RTT include; breathing abnormalities, gastrointestinal dysfunction, epilepsy, sleep disturbance and autonomic dysfunction. The severity of these symptoms leads to complex clinical scenarios and management.

Breathing disturbances in RTT can present in a number of different ways. These include hyperventilation, hypoventilation, apnoea, irregular breathing patterns (Valsalva, Cheyne-Stokes, Biot's breathing) and breath holding [40,41]. Breathing disturbances can be accompanied by cardiorespiratory dysregulation, which is consistent with an autonomic dysregulation [42]. Autonomic dysregulation in RTT was further supported by increased prevalence of sudden death (by 25%) in these patients and imbalanced sympathovagal tone [43].

An important feature of RTT in the context of this thesis is apnoea, as it is the primary readout of Chapter I. Apnoea is defined as the cessation of breathing and are usually associated with inspiration activity [41]. It has been noted that RTT patients demonstrate a specific feature of central apnoea where the lungs remain inflated which is more typical of breath-holding [41]. In female *Mecp2*$^{-/+}$ mice, which model symptoms of RTT, the Kölliker-Fuse nucleus of the dorsolateral pons was identified as a centre of control for respiratory dysfunction. GABAergic stimulation of the pons could decrease apnoeas and respiratory dysfunction in these mice [108]. Additionally, combination treatment targeting serotonin-1a receptor (5HT-1AR), and GABA reuptake blockade could rescue respiratory dysfunction in *Mecp2*$^{-/+}$ mice [272]. Efforts to translate the 5HT1AR agonist, Sarizotan, to therapeutic in RTT patients were not successful, the treatment did not show efficacy in primary or secondary aims and the clinical trial was terminated (NCT02790034).

Gastrointestinal dysfunction in RTT is common. Based on a survey of the RTT patient parents registered in the International Rett Syndrome Foundation; 92% had dysmotility, 81% had difficulty chewing/swallowing, 47% were over or under weight, 45% had growth deficits and 37% had low bone mineral content [44]. Investigations into the microbiota of RTT patients compared to healthy controls has yielded contradictory findings. Strati and colleagues reported significant differences in relative abundances of bacterial and fungal components, these differences were found to be independent of constipation status in RTT patients [44]. In contrast, Thapa and colleagues did not detect a significant difference between RTT patients and healthy controls, though gut microbiome did differ within the RTT cohort depending on clinical severity. Additionally, gut bacterial end-products, GABA and tyrosine were significantly decreased in RTT patients [45].

The occurrence of epilepsy in RTT is common. Estimations vary between 50-80% [47,48], and estimated cumulative prevalence goes as high as 90% [49]. A study with relatively large sample size demonstrated that severe atypical RTT was associated with increased prevalence of epilepsy [49]. Despite the high prevalence of epilepsy in RTT, it appears predominantly to have a relapsing remitting presentation, with only 16% of patients showing drug resistant epilepsy without remission[49].

Sleep disturbance and impaired sleeping patterns are another common comorbidity in RTT patients. A longitudinal study with 320 families registered with the Australian RTT database showed over 80% of individuals with RTT had sleep problems and that prevalence decreased with age [50]. A recent systematic review of animal studies identified characteristics of RTT sleep impairment. These animals had more frequent nocturnal awakening across a 24 hour cycle, poor maintenance of sufficient sleep, impaired sleep homeostasis and circadian rhythmicity, and breathing abnormalities during sleep [51]. In support of the breathing abnormalities during sleep, polysomnography in a small cohort of individuals with RTT revealed 69% had obstructive sleep apnoea [52]. However, different studies report different prevalence of obstructive sleep apnoea in RTT; Hagebeuk and colleagues report 50% in a cohort of 12 patients, and Amaddeo and colleagues report 82% in a cohort of 17 patients [53,54]. In *Mecp2*$^{-/y}$ mice the suprachiasmatic nucleus, which is responsible for the central circadian clock, showed significant decrease in vasoactive intestinal peptide (VIP)

neurons and abnormal neural activity [55]. This study presents a potential mechanism for the sleep disturbances observed in individuals with RTT.

1.2.3 Variant Forms of RTT

As well as the distinct clinical presentations of classic and atypical RTT, there are a number of specific RTT variants. These variants include; preserved speech variant, congenital variant, and early-onset seizure variant. Due to the difference in clinical presentation, it has been argued that some of these variants should constitute impendent disorders [56,57]. However, they currently fall under the umbrella of atypical RTT according to the diagnostic criteria [31].

Preserved speech or Zappella variant individuals tend to present with milder impairments compared to the same stages in classic RTT and the majority displaying known mutation to the *MECP2* gene. These individuals are more mobile, have persevered language, and can even retain manual skills such as drawing or writing [58].

The congenital variant individuals present with hypotonia, unresponsiveness, and irritability from birth. These patients have severe motor impairment, microcephaly, and lack the neuro-typical development [59] . Only a handful of cases of congenital variant have identified *MECP2* mutations [60], while a number of studies identified an association between congenital RTT and *Fork-head box protein G1* (*FOXG1)* gene mutation [59–61].

Finally, the early-onset seizure variant of RTT or the "Hanefeld variant" was initially identified in 1985 [62]. Early-onset seizure variant patients develop seizures before 5 months of age, infantile spasms, refractory myoclonic epilepsy, and lack of some of the main RTT criteria [56]. Genetic screening identified the *Cyclic Dependent Kinase-Like 5* (*CDKL5*) mutations are associated with this variant [63].

1.3 Molecular Pathways and Potential Treatments for Rett Syndrome

1.3.1 MeCP2 Protein and Molecular Functions

The *MECP2* gene encodes the protein MeCP2 which functions as a transcriptional regulator by binding specifically to methylated promoter sites of DNA [64]. It is expressed

at a steady state across different tissues and species [65], but has highest expression in the CNS, lungs, and spleen [66].

Structurally, the *MECP2* gene consists of 4 exons which give rise to two primary isoforms, called MeCP2 E1 and MeCP2 E2, due to alternate splicing of exon 2. MeCP2 E1 is 10 times more concentrated in the brain relative to MeCP2 E2 [67]. MeCP2 also has an untranslated region (UTR) with variable size that leads to three distinct transcripts 1.8kb, 10kb and 8.5kb [68]. The Methyl Binding Domain (MBD) was identified in MeCP2 at residues 78-161 and was found to bind fragments with A/T bases adjacent to methyl Cytosine-phosphate-Guanosine (CpG) [69]. MeCP2 is thought to facilitate repression through interaction with histone deacetylase, SIN3A complex and the Nuclear co-Repressor/Silencing Mediator for Thyroid-hormone Receptor (NCoR/SMRT) complex [70]. MeCP2 has been observed to bind at methylated Cytosine-Adenine (mCA) and methylated Cytosine-Adenine-Cytosine (mCAC), this binding was associated with transcriptional repression [71]. As MeCP2 is a nuclear protein it was thought that it would require a Nuclear Localisation Signal (NLS) to gain access to the nuclear compartment. The putative NLS was thought to be located in the Transcriptional Repression Domain (TRD) [64]. However, recently it was shown that MeCP2 can access the nucleus independently of the NLS [72]. The TRD contains a site essential for binding with the NCoR/SMRT complex, when this site (*Mecp2*^{R306C}) was mutated in mice they developed a RTT-like phenotype similar to *Mecp2*$^{-/+}$ mice and lost the ability to bind NCoR/SMRT [73].

MeCP2 has also been found to function as an activator of transcription, as well as a repressor. This observation was made based on gene expression analysis showing most genes are down-regulated in *Mecp2*$^{-/y}$ mice and up-regulated in transgenic *Mecp2* (*Mecp2*^{TG}) mice, which overexpress *Mecp2*, the opposite of what would be expected if MeCP2 was acting simply as a repressor [74]. A possible mechanism for MeCP2 activation could be through its ability to bind 5-hydroxymethylcytosine (5hmC) in post-mitotic neurons [75,76].

Another view considers MeCP2 a global regulator of transcription rather than a specific activator or repressor of genes. In *Mecp2* mutated mice, the neuronal chromatin structure was altered and there was an increase in repetitive transcriptional elements. Given these changes, and how highly concentrated MeCP2 is, it may be functioning to

dampen transcriptional noise genome-wide [77]. The main binding sites of MeCP2 other than methylated-Cytosine-Gaunine (mCG) in the brain were proportional to mCAC+mCG density [71]. MeCP2 has been demonstrated to be a dynamic component of heterochromatin condensate, further supporting its role as a global regulator [78]. Altogether, these data all suggest that MeCP2 has a global transcriptional role. A recent review of the topic of MeCP2's role as a transcriptional regulator was provided by Ip and colleagues, this group provided different models for how these functions might manifest in RTT patients [79]. The role of this transcriptional regulation in synaptic plasticity and maturation will be discussed in section 1.4.

Other Mutations of RTT

Some patients that have a classic form RTT do not have any mutation in *MECP2*, and other individuals have mutations to *MECP2* do not have RTT, although they do suffer from other developmental disorder [36,80]. There are other mutations that more frequently result in variant forms of RTT. Early onset seizure variant of RTT is associated with mutations to *CDKL5*, however, recent analysis proposes that CDKL5 related disorder should be a separate clinical entity to RTT [56,57]. *CDKL5* and *MECP2* are both nuclear proteins and are involved in maturation and synapse function [81,82].

Another transcriptional factor gene *FOXG1*, is involved in the development of the telencephalon, and has been attributed to the congenital RTT [60]. This form of the disorder is more severe than classic RTT, particularly affecting walking, fine motor skills, communication ability, and sleep [83]. *FOXG1* regulates neuronal stem cell proliferation and suppresses premature neuronal differentiation [84]. Interestingly, increased FOXG1 levels have been shown to prevent neuronal apoptosis induced by elevated MeCP2 Exon 2 (E2). IGF1 has also been found to protect against the neurotoxicity of MECP2 E2 [85].

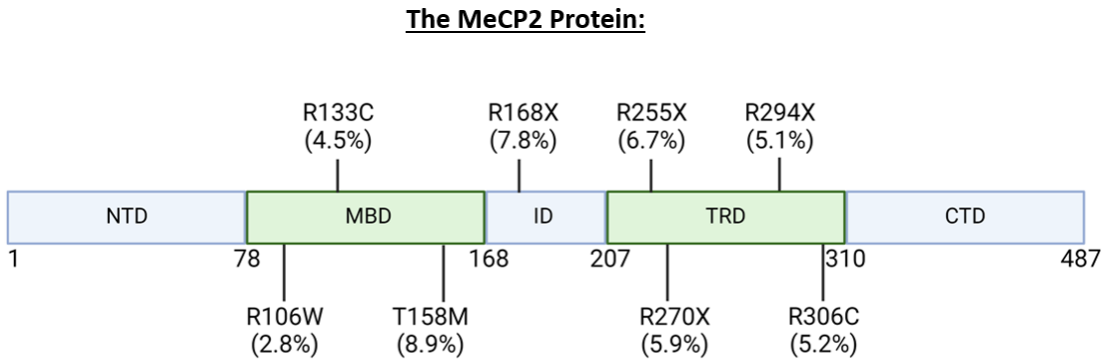

Figure 1.2 *MECP2* Mutations in RTT

Though RTT is characterised by *de novo* mutations to *MECP2*, eight of the most common mutations account for approximately 46.9% of all mutations in RTT patients [37]. This figure displays the MeCP2 protein and the locations of these common mutations [129]. These common mutations occur between the two functional domains of *MECP2:* the MBD and the TRD.

R106W, R133C and T158M are located on the MBD and binds CpG [69], and therefore interfere with the binding of methylated DNA. R168X and T158M are typically associated with severe presentation, but significant skewing of XCI can result in a milder phenotype of RTT [272].

The other common mutations (R255X, R270X, R294X, and R306C) are located on the TRD, therefore MeCP2 with these point mutations could result in protein that still binds methylated DNA but with aberrant transcriptional activity. Patients with R270X have reduced mortality and compared to the other common mutation and have severe clinical presentation [273]. Mouse model knock-ins mutation of common point mutations of *Mecp2* reveal that T158M results in a more severe phenotype compared to R306C and R133C, which display intermediate severity and milder severity respectively [274]. Mouse models of the R255X and R294X mutations have been generated, their phenotypes can be rescued by WT expression of *Mecp2* [275, 276]. An analysis of international RTT databases examining the genotype-phenotype relationship in the eight common mutations and C-terminal deletions, found R270X and R255X had the most severe presentation, while R133C and R294X had the least severe presentation [277]. C-terminal deletions appear to have an intermediate severity [278].

Legend:

NTD = N-Terminal Domain, MBD = Methyl-CpG-Binding Domain, ID = Inter-Domain, TRD = Transcriptional Repression Domain, CTD = C-Terminal Domain

1.4 Neurophysiology of Rett Syndrome

1.4.1 Gross Morphology of RTT

In terms of morphology, brain weight is decreased in patients with RTT, *Mecp2*$^{tm1.1Bird/J}$, and *Mecp2*$^{tm1.1Jae}$ mouse models [86,87] . Post-mortem analysis of RTT brains revealed neuronal size was reduced, while neuronal density was increased [88], and dendritic complexity was decreased in layers 3 and 5 of the motor and frontal cortices [89]. In a mouse model with conditional KO of *Mecp2* the following observations were made on morphology; dendritic spine density decreased, dendritic arbours shortened, neuronal density increased, and astrocytic complexity decreased [90]. These changes in gross and neuronal morphology suggest that proper development of neuronal dendrites is impacted in RTT and functionality is likely impacted by these changes.

1.4.2 MeCP2 and Synaptic Development

MeCP2's role in the developing nervous system is crucial and correlates with maturation of cells [91]. Initially, *MECP2* is expressed at low-levels and then increases after early postnatal development in response to synaptic activity [92]. Interestingly, when *Mecp2* is re-expressed in neurons there is a robust reversal of the RTT-like phenotype [93]. This finding supports the hypothesis that *Mecp2* is required for the maturation of neurons. It also shows that the majority of symptoms are caused by dysfunction in the CNS. A peripheral KO of *Mecp2* generated by Ross and colleagues confirms this, and identifies a subset of symptoms that persist in the periphery. These include hypoactivity, exercise fatigue, and bone abnormality [94].

Brain Derived Neurotrophic Factor (BDNF) is a well characterised neuromodulator and target of MeCP2 action. The regulation of BDNF and posttranscriptional processing have differential effects on neurons. While the precursor BDNF (Pro-BDNF) promotes apoptosis and inhibits dendritic spine formation, mature BDNF increases neuronal survival and Long Term Potentiation (LTP) [95]. Conditional KO of *Bdnf* in *Mecp2* mutant mice results in earlier presentation of symptoms, conversely *Bdnf* overexpression was found to improve RTT-like features [96]. BDNF-induced Tyrosine

Receptor Kinase B (TrkB) activation regulates glutamatergic synaptic density in an autonomous and autocrine manner [97]. A specific phosphorylation site on MeCP2 serine 421 (S421) regulates dendritic complexity, spine morphogenesis and activity dependent induction of *Bdnf* expression [98].

This critical period of plasticity is characterised by the development of neuronal networks in an activity-dependent manner. The postnatal critical period involves the development of the primary sensory cortex and higher cognitive functioning [99]. Mouse model studies can be used to understand how this critical period in development is impacted by *Mecp2* mutation.

Due their location on arm q.28 of the X chromosome, *MECP2* mutations can be subject to X Chromosome Inactivation (XCI) [34]. While most classic patients display a random pattern of XCI (91%), some patients display a skewing of XCI [172]. A study examining the two most common mutations in RTT, R168X and T158M, found a significant correlation between clinical severity score and the ratio of mutant *MECP2* allele expressed in peripheral blood leukocytes [272]. A recent study found only a weak positive correlation between skewed XCI and severity in RTT with maternal allele being preferentially expressed but not the paternal allele [279].

A mouse model that investigates the role of XCI in RTT phenotype is the double mutation of *Tsix* and *Mecp2* in female mice. These mice have reduced mosaicism and their phenotype is more severe in presentation akin to the male *Mecp2*$^{-/y}$ mice [152]. Importantly the rescue of 5-10% of wildtype *Mecp2* in these mice was enough to extend lifespan and rescue some RTT features, demonstrating the therapeutic value of such a strategy [152].

The relationship between XCI and severity of RTT presentation is not simple. Another study examining the methylation pattern of MeCP2 in RTT patients' blood could not find a correlation between XCI and clinical presentation [280]. Additionally, these authors found differences in the level of XCI in blood and cortex of the same patients [280], given that RTT is primarily a neurological condition it questions the utility of using blood to determine skewing of the X Chromosome. Many factors determine the clinical severity of RTT and favourable skewing of XCI could be an effective therapeutic strategy. For RTT research it is an influential variable and ideally should be accounted for.

1.4.3 Neuronal Circuits and RTT

MeCP2 is known to be essential for the proper development of GABAergic parvalbumin (PV)-interneurons in the visual cortex. In *Mecp2*$^{-/y}$ mice, there was a precocious development of interneurons resulting in deficiencies in binocular vision [100]. Furthermore, *Mecp2*$^{-/+}$ mice were found to respond to monocular deprivation at P60, while this plasticity is not present in WT mice at this age [101] . This suggests that *Mecp2*$^{-/+}$ neurons are in an immature state. Additionally, the retinogeniculate synapse of the visual system fails to strengthen during the experience-dependent critical period in *Mecp2*$^{-/y}$ mice [102]. These studies illustrate how *MECP2* mutations lead to dysfunction in activity-dependent manner.

As a consequence of altered synaptic functioning in *Mecp2* mutant mice, circuit-wide alterations in excitation and inhibition (E/I) balance have been observed. Several studies have found that *Mecp2* mutations lead to shifts in E/I balance reducing excitation and increasing inhibition [103–105]. Impaired inhibitory inputs lead to disinhibition and favouring excitation in a number of regions including CA1/CA3 of hippocampus, and areas of the brainstem of *Mecp2*$^{-/y}$ and *Mecp2*$^{-/+}$ mice [106–108]. Furthermore, the changes in GABAergic (inhibitory) and glutamatergic (excitatory) activity in *Mecp2*$^{-/y}$ mice are age dependent [109]. The role of E/I balance in RTT is dependent on the many cell types contributing to overall excitation and inhibition.

GABAergic interneurons are important regulators of E/I balance and appear to be critical in the RTT phenotype. Conditional Knock-Out (cKO) of *Mecp2* from GABAergic neurons results in 30-40% reduction in inhibitory neurotransmission and recapitulates many of the RTT-like features of the global KO [110]. In cKO *Mecp2*$^{-/y}$ mice affecting PV- expressing neurons, GABAergic drive was found to be dysfunctional with an overall increase in E/I balance in the primary visual cortex. Treating these mice with rhIGF1 improved both inhibitory and excitatory responses rescuing GABA drive [111].

Understanding how *Mecp2* affects E/I balance and the underlying neural circuitry is crucial to allow researchers to develop targeted therapeutic approaches.

1.4.4 Glial Function in RTT

Glia are the non-neuronal cells that support the functioning of the CNS by providing nutrients, maintaining ionic concentrations, facilitating synaptic connections, structurally supporting neurons, and responding to injury and threats. The main glial cell types are astrocytes, microglia, and oligodendrocytes. Despite this integral role in the CNS only in the last 10 years has the importance of glial cells in RTT begun to emerge.

Astrocytes are the most abundant glial cell type and support neuronal function by regulating the extracellular environment, controlling ionic concentration, and providing metabolites. Astrocytes are also important in responding to acute CNS injury where they become reactive astrocytes. Reactive astrocytes up-regulate Glial Fibrillary Acidic Protein (GFAP) which induces hypertrophy and cellular proliferation, this mechanism aims to reduce damage and restore homeostasis [112]. Early evidence of the role of glial cells in RTT came from a microarray analysis of cerebral cortex where glial transcripts including *GFAP*, *CRYAB*, and *S100A13* were significantly increased [113]. Re-expression of WT *Mecp2*, preferentially in astrocytes of a global KO of *Mecp2* significantly rescued RTT-like phenotype and prolonged life [114]. Postnatal loss of *Mecp2* decreased astrocytic morphology along with retraction of dendritic spines [90]. The RTT-like dysfunction caused by astrocytes does not appear to be due to impaired growth of astrocytes, as astrocytes from *Mecp2*$^{-/y}$ mice grow at a normal rate and RTT IPS cells differentiate to astrocytes at a normal rate [115]. Instead it appears that RTT astrocytes have abnormal vesicular transport and impaired clearance of cytotoxic glutamate [115,116]. Stimulation of astrocytes in WT *Mecp2* mice caused increased excitatory synaptic activity, this response is lost in *Mecp2*$^{-/y}$ mice. This loss of excitation response is dependent on *Mecp2* mutation status in astrocytes but not neurons [117].

Microglial are CNS resident macrophages and integral to the immune functioning in the brain. These cells release cytokine, refine synapses and provide immune surveillance of the environment [118]. Immune response to Lipopolysaccharide (LPS) in mixed glial *Mecp2*$^{-/y}$ cells is exaggerated and induces oxidative stress [119]. RTT-like microglia damage dendritic spines and synapses due to glutamate neurotoxicity in *Mecp2*$^{-/y}$. This neurotoxicity was not associated with astrocytes but due to microglial dysfunction [120]. However, the direct evidence of microglial involvement in RTT pathology has been controversial. An initial report found that WT microglia can rescue the RTT phenotype

in *Mecp2*$^{-/y}$ mice through bone marrow transplant [121], but a later study contradicted this finding [122]. Differentiating RTT Induced Pluripotent Stem (IPS) cells into microglia produced a significantly smaller cell compared to WT *Mecp2* [123]. RNA-Seq of *Mecp2*$^{-/+}$ microglia before and after onset of symptoms revealed a decrease in 9 heat-shock genes, implying these cells sense environmental cues differently [124].

These studies highlight the important role that both astrocytes and microglia appear to have in the RTT pathophysiology.

1.5 Animal and Cell Modelling of Rett Syndrome

Animal and cell models contribute a large amount to the understanding of RTT pathophysiology. RTT is primarily a neurodevelopmental disorder and has low prevalence in the general population, this makes studying primary human tissue very challenging. Utilising the strong association between RTT and *MECP2,* several mouse models have been generated to mimic the disorder *in vivo*. Different types of mutations such as whole exon deletion or common point mutations, help illustrate the molecular mechanisms of *Mecp2*. Here we will discuss some of those models and how they have informed the RTT literature.

1.5.1 Mecp2 Mouse Models

In 2001, Guy and colleagues generated the *Mecp2* KO mouse for the first time using Cre-*lox*P recombination KO of exons 3 and 4. This model is referred to as the *Mecp2*$^{tm1.1Bird/J}$ mouse [38]. *Mecp2*$^{tm1.1Bird/J}$ mice recapitulate many of the aspects of RTT pathology including the delayed onset of symptoms, after a period of apparently normal development. Other symptoms of this model include neurological crises affecting gait posture, breathing and movement [38]. Another striking feature of *Mecp2*$^{tm1.1Bird/J}$ mice is hind limb clasping which is thought to mimic the hand stereotypies observed in RTT individuals [38,96].

A separate study by Chen and colleagues developed a *Mecp2* KO mouse using Cre-*loxP* recombination, this time deleting only exon 3, it is referred to as *Mecp2*$^{tm1.1Jae}$ [125]. The *Mecp2*$^{tm1.1Jae}$ model again recapitulated many of the symptoms of RTT including delayed onset of symptoms, trembling, hypoactivity and respiratory problems. A CNS-specific

Mecp2 deletion was generated and mirrored the phenotype of the *Mecp2*$^{tm1.1Jae}$ model. This confirmed that the RTT phenotype was caused by central MeCP2 deficiency. When the *Mecp2* deletion was introduced into neurons postnatally, a similar RTT phenotype was produced at a later age. These findings highlight the important role of *Mecp2* in neuronal maturation [90]. Notably, both *Mecp2*$^{tm1.1Bird/J}$ and *Mecp2*$^{tm1.1Jae}$ mice displayed phenotypic differences between male and female mice; female onset of symptoms occurs much later and severity is milder relative to male counterparts [38,125].

To further understand the role of mature neurons in the RTT pathology, Guy and colleagues examined if re-expressing *Mecp2* could rescue the RTT phenotype. The *Mecp2*$^{lox-Stop}$ mouse model displayed a similar phenotype to other KO mice and could conditionally re-express *Mecp2* using a Cre recombinase and modified estrogen receptor (*cre-ER*), which was activated by tamoxifen [93]. Interestingly, the re-expression of *Mecp2* in eight of 17 mice led to absence of symptoms and normal life-span compared to WT, and the nine remaining mice died. These deaths were associated with toxically high levels of *Mecp2* expression. A similar phenotype has been observed when *Mecp2* levels were overexpressed in mice. These so-called transgenic mice (*Mecp2*^{Tg1}) displayed a two-fold increase in MeCP2 and developed symptoms around 10 weeks of age [126]. Symptoms of *Mecp2*^{Tg1} mice included; enhanced synaptic plasticity, motor and contextual learning, and the late-stage phenotype resulted in seizures, hypoactivity and death [126].

In most cases, RTT is associated with point mutations of *MECP2* (~65%) [37], therefore mouse models of specific point mutations can be very informative. The *Mecp*^{308} model was generated by a truncation of *Mecp2* at codon 308, this model produced a milder phenotype and has been commonly studied [66]. In *Mecp2*$^{308/y}$ mice, symptom onset occurs by 5 weeks of age, where tremor and motor dysfunction became apparent, in *Mecp2*$^{308/+}$ mice symptoms appeared by 1 year of age. Furthermore, point mutation mouse models have been generated using other common RTT mutations, such as R270X, R306C, R106W and T158M mutations [73,127–129]. These mouse models inform our understanding of RTT pathophysiology and specifically can reveal the pathogenicity of individual amino acid mutations in the MeCP2 protein.

1.5.2 Cell Culture Models of RTT

Cell culture models allow researchers to study mechanistic questions through *in vitro* experiments. Although lacking the biological context of complex tissues and cell compositions, cell culture experiments can describe the fundamental processes and molecular pathways in RTT pathology.

Small interfering RNA (siRNA) can be used to knockdown gene expression also known as RNA interference (RNAi). However, RNAi is imperfect, only 35% of siRNA achieved more than 90% silencing and almost 20% had efficacy of less than 50% [130]. The efficacy of knockdown experiments is dependent on the delivery system used to carry the siRNA to the desired site of action. These delivery systems include; viral vectors, polymer-based, peptide-based, lipid-based and conjugate systems [131]. RNAi cell models knocking down *Mecp2* have been useful for validating or elaborating on previous findings. For example, transcriptomic studies in post-mortem brain tissue identified *cytochrome c oxygenase 1* (*CO1*) as differentially expressed and RNAi experiments were used to confirm this was due to aberrant *MECP2* [132]. RNAi has also been used to determine detailed mechanisms of genes like *Mecp2* in primary neuronal cell culture of mice. One study used this method to find the reciprocal relationship between *Mecp2* and *Phosphatase and Tensin Homolog* (*Pten)* which was regulated through microRNA [133].

The development of neuronally differentiated IPS cells has greatly enhanced the understanding of RTT pathophysiology. Electrophysiology, morphology, and molecular mechanisms can be readily examined in this cell model. Examining these properties helps to describe the functioning of neurons in an early developmental state. X-chromosome inactivation (XCI) is the random inactivation of either mutant or WT *MECP2* allele, and this feature can be controlled in IPS cell experiments. IPS cells can generate either mosaic (mixed) or isogenic (homogenous) populations of mutant or WT *MECP2* [134]. This property of IPS cells is very informative, as isogenic controls can parse out mutational-specific and cell autonomous effects of RTT.

RTT derived IPS cells enable a personalised medicine approach to be taken. Different specific RTT mutations result in variable severity of disease [135]. Therefore, using RTT derived IPS cells from a particular patient can reveal different patterns of gene expression and phenotypes [136]. A recent study by Chen and colleagues, characterised

electrophysiological and morphological features of RTT derived IPS cells and embryonic stem cell knockdown of *Mecp2*. This study found that both models had immature phenotype affecting action potential firing and passive membrane potential, reduced soma size, and dendritic complexity [137]. Similar observations have been made in *Mecp2*$^{-/y}$ mice, though evoked action potentials appear not to be significantly different [101]. Importantly, this study also found that R106W *MECP2* mutant IPS cells were still partially functional compared to *MECP2* knockdown [137].

IPS cells can also be useful for identifying potential treatments. RTT derived IPS cells had reduced acetylation of α-tubulin, which could be reversed by inhibitors of HDAC6 [138]. Another study used RTT IPS cells to derive a mutant *MECP2* astrocytes in an isogenic population [139]. These cells caused dysfunction and aberrant morphology in WT neurons, suggesting a non-cell autonomous function in mutant *MECP2* astrocytes. Interestingly, both rhIGF1 and GPE partially rescue morphological deficits in neurons induced by these mutant *MECP2* astrocytes [140]. The non-cell autonomous role of *Mecp2* astrocytes has also been suggested in *Mecp2*$^{-/y}$ mice [139].

3D brain organoids take IPS cell culture a step further by mimicking the conditions of early nervous system development. This model has been informative not only for understanding temporal and spatial development of the nervous system but also the assembly of neuronal circuitry [141]. A recent study used a dorsal ventral brain organoid to identify premature development of the deep cortical layer and impaired interneuron migration [142]. Encouragingly, another recent study using RTT derived brain organoids found this model was capable of complex network dynamics and displayed abnormal epileptiform-like activity, similar to what is seen in the human disorder [143].

Further studies of individual RTT mutations in *MECP2* can be facilitated through use of RTT derived IPS cells and 3D brain organoids. These models can give insight to researchers into cellular and developmental processes of specific *MECP2* mutations, and with brain organoids it is now possible to characterise complex network activity.

1.5.3 Non-Human Primate Models of RTT

Non-human primate models of disease share more genetic, physiological, social and developmental similarities with humans than rodent models. This arguably makes them a more reliable resource for preclinical studies. Recently a Talen-edited *MECP2* mutant

Cynomolgus monkey that has recapitulate some of the RTT phenotype have been developed. This model displayed sleep disturbance, impaired pain response, and increased stereotypic behaviours similar to those observed in patients with RTT [144]. The Cynomolgus *MECP2*$^{-/+}$ monkey, was used to examine white matter microstructure revealing delayed white matter myelination in the first 9 months of postnatal development followed by abnormal anatomical network development. The changes in white matter myelination were also associated with abnormal behaviour including environmental exploration, conflict, and avoidance [145]. The strength of this model is the ability to study complex behaviours in a biological system more akin to humans than traditional rodent models. The similarity of non-human primates to humans makes this model useful in testing the efficacy of therapeutics, particularly gene therapies, for example in Parkinson's disease [146]. However, the *MECP2*$^{-/+}$ Cynomolgus model has not been thoroughly characterised yet, and requires further evaluation to understand how close the behavioural phenotype is to the RTT patient condition.

1.5.4 Limitations of RTT Animal and Cell Models

There are many advantages and disadvantages to studying the various models for RTT discussed in section 1.5. In humans, researchers cannot readily access the brain of RTT individuals without invasive means. Due to the physical disability of patients neuroimaging tools are not always viable; although there have been some studies that use Magnetic Resonance Imaging (MRI) and Electroencephalogram (EEG) in RTT patients due to their non-invasive nature [147,148].

In mice, a wide array of tools can be used to conduct *in vivo* or *ex vivo* experiments. Additionally, fluorescent probes can be genetically engineered to tag cellular targets, this process can be combined with different imaging or optogenetic techniques for the manipulation or isolation of specific cell populations. Mouse models control for age and genetic background which increases biological homogeneity and improves statistical power of experiments.

Unlike the condition in RTT patients, both female heterozygous (*Mecp2*$^{-/+}$) and male Mecp2-null (Mecp2$^{-/y}$) mice are viable and develop RTT-like symptoms. In patients with RTT, only a few male cases have been reported, as they rarely survive past infancy [37,149]. This distinction can be a confounding factor for translation of mouse model

studies to RTT patients. In *Mecp2*$^{-/y}$ mice symptoms begin around three weeks of age and become severe, while *Mecp2*$^{-/+}$ mice symptoms develop around three months and show a milder phenotype [38]. Progression and severity is dependent on the individual mouse model used [38,66,125]. Variability in *Mecp2*$^{-/+}$ female mice is due to mosaic expression of *Mecp2* at a cellular level caused by XCI [150].

The sex specific differences in mouse models which are not seen in RTT patients are important to note [150]. In *Mecp2*$^{-/y}$ male mice severity of symptoms and time of onset is more similar to that of RTT patients, which has led researchers to primarily focusing on these mice for development of therapeutics [101,150,151]. However, these mice do not have mosaic expression of *Mecp2*, which is seen in RTT patients. A double mutation of *Tsix* and *Mecp2* in female mice was shown to disrupt XCI and induce a RTT-like phenotype closer to that of the *Mecp2*$^{-/y}$ mouse [152]. In this thesis both the male and female *Mecp2* mutant mice will be studied and analysed.

RNAi and IPS based cell culture models link aberrant *MECP2* function to a cellular context that can be easily measured and manipulated. However, these techniques lack the structural and functional context of *in vivo* systems. IPS cell models can remove confounding factors such as XCI, variable genetic backgrounds, and heterogeneous tissue composition. Impressively, 3D brain organoid models can better replicate the human architecture of the brain and demonstrate the functional network activity.

The variability that characterises the presentation of RTT can be a double-edged sword. While reducing variability allows researchers to determine specific mechanisms, the context of the actual pathophysiology can be lost. A better approach is to use a number of models taking advantage of the strengths of each system to construct a robust biological mechanism.

1.6 Treating Rett Syndrome with IGF1 and GPE

1.6.1 Mecasermin (rhIGF1) and Trofinetide (A GPE Derivative) in Clinical Trials

Currently there is no treatment to address the underlying pathology of RTT. The limited genetic aetiology of RTT has meant there are good preclinical models, yet translation to approved treatments has not materialised. Considering the evidence that RTT patients

and *Mecp2* KO mice have disrupted neuronal maturation, rhIGF1 and GPE have been investigated pre-clinically as potential therapeutics for RTT.

Both rhIGF1 and GPE functionally improved a number of RTT symptoms, including improvements to lifespan, locomotor activity, heart rate, breathing abnormalities, and synaptic maturation. The rescued synaptic parameters were restored spine density, increased Excitatory Postsynaptic Current (EPSC) amplitude and increased Postsynaptic Density Protein-95 (PSD-95), which is a marker of synaptic maturation [101,151]. RhIGF1 also restores PV-expressing neurons caused by global and PV specific *Mecp2* deletion in mice [111].

A phase I clinical trial using rhIGF1 or Mecasermin in RTT patients found the treatment was well tolerated. Mecasermin increased IGF1 protein levels in both cerebrospinal fluid (CSF) and serum after 29 days of treatment. This trial had an additional open label extension (OLE) to provide preliminary evidence of efficacy. Apnoeic index improved significantly from the start to the end of the trial suggesting Mecasermin is efficacious at treating the RTT phenotype [153]. A phase II cross-over trial found Mecasermin again to be safe, however, measures of efficacy were mixed. Though there were some improvements to secondary measures for hand stereotypy and social communication other clinical parameters showed a worsening [154].

The GPE analogue, NNZ-2566 was designed to have improved half-life by adding a methyl group to the proline amino acid. Safety of NNZ-2566 was first assessed in healthy individuals in phase I clinical trials (NCT01420042 and NCT00961779) and its pharmacokinetics were determined using a meta-analysis [155]. Phase II trials using NNZ-2566 or Trofinetide to treat RTT were found to improve core variables of disease including communication and speech, behaviour, breathing, hand movement, motor dysfunction and seizures, as well as showing no clinically significant worsening of the condition [156]. Phase III clinical trials are ongoing testing Trofinetide in RTT (NCT04279314, NCT04776746, and NCT04181723). Additionally, Trofinetide has shown efficacy in treating Fragile X Syndrome (FXS), a neurodevelopmental disorder characterised by intellectual disability, Autism Spectrum Disorder (ASD), and emotional dysregulation [157].

The efficacy of Mecasermin in other neurodevelopmental disorders like ASD (NCT01970345) and Phelan-McDermid Syndrome (NCT01525901) is still being

assessed at phase II level. The difference in results at clinical trials demonstrate the mechanisms of rhIGF1 and GPE are important for translating these drugs to effective therapeutics.

1.6.2 Additional Clinical Trials in RTT

Breathing dysregulation in RTT has been investigated as a therapeutic target through modulation of serotonin system in mouse models. The serotonin system has been found to be dysregulated in RTT mouse models and in RTT patients leading to abnormalities in vagal tone [158,159]. Strategies to modulate serotonin receptors specifically 5-HT_{1a}R and 5-HT7R improve RTT symptoms including breathing abnormality and apnoea [160,161]. Unfortunately, a phase II/III trial of Sarizotan, a 5-HT1A agonist, was terminated recently for not showing improvement to primary or secondary measures of efficacy (NCT02790034).

Another therapeutic strategy used in a clinical trial for treatment of RTT is to address the mitochondrial dysfunction using the drug EPI-743 (α-tocotrienol quinone). The aims of the open-label phase II trial (NCT01822249) were not met, though some improvements in oxygenation and hand function were identified in a subset of patients [162]. The immunomodulatory Glatiramer Acetate (GA) was shown to increase Bdnf in mouse models of multiple sclerosis and *Mecp2* null mice. However, clinical trials of GA in RTT patients had to be stopped due to severe post-injection reactions in some patients [163].

The difficulty in translating potential treatments to approved therapeutics for RTT patients could greatly be aided by development of biomarkers. The heterogeneous presentation and rarity of RTT means that most studies in RTT patients are underpowered. A consistently performing biomarker predicting positive response to treatment would allow researchers to mitigate the lack of statistical power and better assess treatments.

1.7 Concluding Remarks

Developing therapeutics for the treatment of RTT is a unique challenge for researchers. On the one hand, the strong association between the disorder and *de novo* mutations to

MECP2 allows models to mimic different aspects of the disorder's clinical presentation. On the other hand, many of these studies require a level of nuance, due to fundamental differences between the model and the human condition or factors that cannot be accounted for by that model.

In this thesis, we used several tissues and models to examine the mechanisms of rhIGF for the treatment RTT at different levels. In chapter I, the use of RTT whole blood treated with mecasermin (rhIGF1) addresses the systemic effects of the treatment, but this does not represent the primary pathophysiology of the brain. The CNS pathophysiology and systemic effects are explored in chapter II, using the *Mecp2* mouse model. These first two chapters explore the effects of rhIGF1 on a tissue level. To understand rhIGF1 at a cell signaling level, neuronally differentiated SH-SY5Y cell cultures were used in chapter III. Another benefit of these cell cultures was the ability to compare rhIGF1 treatment with its tripeptide derivative GPE. GPE has been used to develop the therapeutic trofinetide which has recently showed efficacy in phase III clinical trials.

These studies provide important findings and information that can be used to design future development of clinical trials using rhIGF1 to treat RTT and related disorders.

2.0 Chapter I: Gene Expression of RTT Patients Treated with Mecasermin (rhIGF1) from Whole Blood

2.1 Introduction

In this chapter, gene expression data of whole blood from patients in a phase I trial of Mecasermin (rhIGF1) was used to understand molecular profiles of patients and the effect of treatment. This analysis will provide information to guide future design of clinical and pre-clinical studies of rhIGF1 treatment in RTT.

The purpose of the clinical trial was:

1. To establish the safety of the Mecasermin in RTT patients.

2. To find preliminary measures of efficacy of the Mecasermin in RTT patients.

For this reason, the trial had multi-phase approach. Figure 2.1 displays a schematic of the trial design and gene expression analysis conducted in this chapter. The clinical trial and subsequent RNA sequencing was conducted by colleagues at Boston Children's Hospital (BCH) and Massachusetts Institute of Technology (MIT) BioMicro Centre, I then conducted the downstream analyses at Trinity College Dublin (TCD). To summarise the clinical trial, a total of 12 patients were enrolled initially in the trial, including 9 patients with classic RTT and 3 patients with *MECP*-related disorders (MRD). Patients with MRD have pathological *MECP2* mutations but do not fulfil criteria for either the classic or atypical RTT as determined by Neul and colleagues [31].

For establishing the safety and pharmacokinetics of the treatment, all patients were included in an initial Multiple Ascending Dose (MAD) phase. This treatment phase used an escalating dose of 40 µg/kg in the first week, 80 µg/kg in the second week and maximum dose of 120 µg/kg for the final two weeks (a total of 4 weeks of treatment during MAD phase). Patients were then taken off treatment for a period of 12 to 30 weeks to allow for levels of systemic IGF1 to normalise. 10 patients returned for the Open Label Extension (OLE) treatment phase, which included in 9 patients with classic RTT and one patient with MRD. The 10 continuing patients received the same escalating doses as before but the maximum dose was continued for 17 weeks (as opposed to 2 weeks during the MAD) for a total time of 20 weeks of treatment during OLE phase.

The purpose of the MAD phase was to assess the pharmacodynamics and pharmacokinetics of Mecasermin, as well as assessing the safety and tolerability of the treatment. While the OLE was used to obtain preliminary measures of efficacy.

An important measure that was recorded before and after treatment was the autonomic/cardiorespiratory assessment. Autonomic and breathing dysfunction in RTT has been observed in patients and mouse models [40,101,151,164]. To assess the patient's autonomic function a wireless plethysmograph device (BioRadio, Great Lakes Neurotechnologies) was used, this device measured breathing dysfunction and breathholding. It revealed clinically significant apnoea (episodes > 10 seconds long) in 5 of the RTT patients in the trial. 4 of these 5 had moderate-severe apnoea (>5 episodes per hour) that decreased to mild (<5 episodes per hour) by the end of OLE. Details of pharmacokinetics and preliminary efficacy measures were described by Khwaja and colleagues [153].

Gene expression from whole blood samples was measured in trial patients at four timepoints: T0 = Before MAD, T1 = End of MAD, T2 = Before OLE, and T3 = End of OLE. These RNA samples were collected using PAXgene™ Blood collection tubes and sequenced by 3'Digital Gene Expression (3'DGE). A schematic for the trial structure and analysis is displayed in figure 2.1. Sample data on the RTT and MRD patients from the trial including the *MECP2* mutations are detailed in methods section in table 6.1.1.

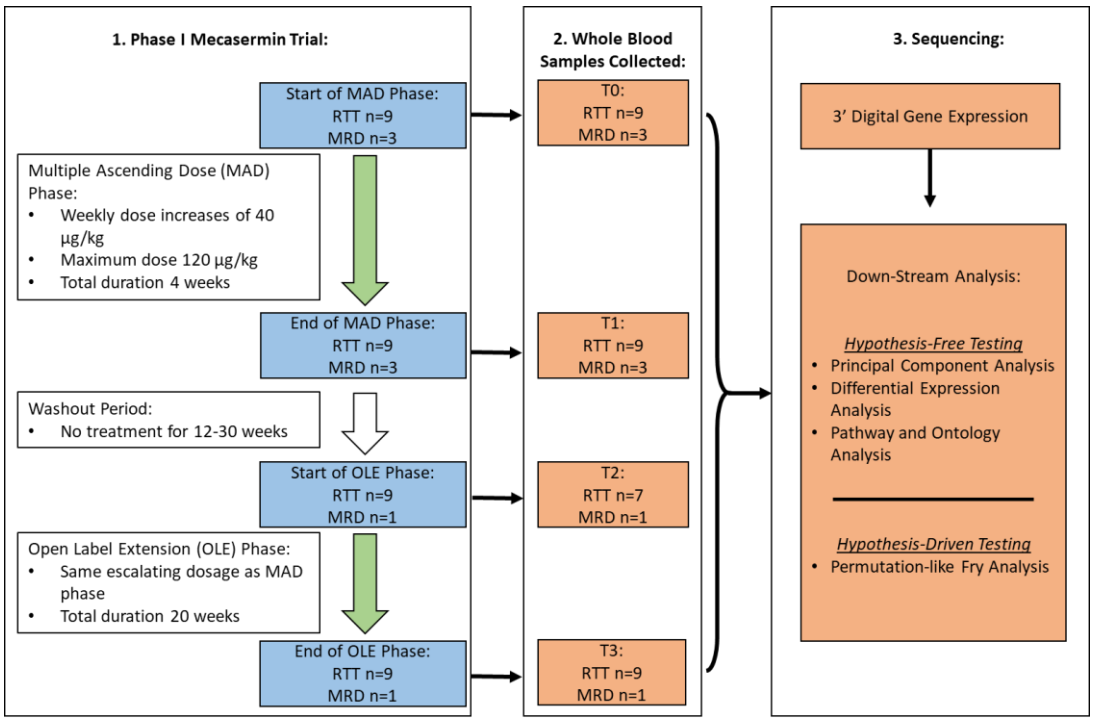

Figure 2.1 - Study Design and Dosing Schedule of Phase I Mecasermin Trial in RTT All patients (n = 12) were included in the multiple ascending dose (MAD) period while only those with RTT (n = 9) and one other patient with MRD progressed onto the open label extension (OLE) component. Patients were administered Mecasermin twice daily by subcutaneous injection. Timepoints when blood sampling was performed are denoted by T0 (start of MAD), T1 (end of MAD), T2 (start of OLE) and T3 (end of OLE). Whole blood samples were used for 3'DGE sequencing and gene expression analysis.

Legend:

MAD = Multiple Ascending Dosage, OLE = Open Label Extension

To understand the molecular mechanisms of response to Mecasermin treatment, differential gene expression (DGE) was quantified using the software edgeR, which was specifically designed for analysing sequencing data from small sample sizes [165]. Due the small sample numbers in this trial, a common problem in RTT studies because of low prevalence, two approaches of analysing the gene expression were adopted; Hypothesis Free Testing (HFT) and Hypothesis Driven Testing (HDT).

The HFT approach examines DGE using all the annotated genes expressed in all trial patients, 26,116 genes in total. This method detects gene expression without bias, however, because of the large number of genes tested there is a high false discovery rate (FDR). Therefore a severe multiple testing correction using Benjamini-Hochberg method is applied to HFT. In contrast, the HDT analyses asks specifically if a given number of gene sets are differentially expressed. This list of gene sets was derived based off findings from the literature. The HDT addresses specific hypotheses that are based on previous findings of other studies and does not suffer the same level of multiple testing correction, because of the smaller numbers of the genes tested. The gene sets analysed in HDT belong to 5 main categories.

1. IGF1 and BDNF pathways
2. Metabolic homeostatic mechanisms including; mitochondria, protein ubiquitination and chromatin mediated processes [166]
3. Inflammatory microglia responses [167]
4. Pathways linked to apnoeic phenotype i.e. Monoamine metabolism [169–171]
5. ASD IPS derived neuronal response to rhIGF1 [171]

Gene sets were obtained either directly from the list of significant results, as in the case for the Linker study [171], or were taken from the relevant ontology from the Gene Ontology (GO) data base. By using two distinct methods of statistical analysis to measure gene expression, we aim to increase the level of the specificity of testing i.e., the percentage of true negatives detected.

Chapter I aims to measure gene expression in whole blood of patients with RTT who participated in a phase I clinical trial of Mecasermin (rhIGF1) treatment. Differential gene expression analysis will be used to investigate the effects of treatment, and determine if patients with different clinical responses have distinct transcriptional effects.

2.2 Results

2.2.1 Gene expression profiles of RTT and MRD Patients

During the MAD phase of the trial both RTT and MRD Patients were used to determine the pharmacokinetic profile of Mecasermin. The OLE treatment phase was used to

elongate the period of treatment and allow clinicians to access the preliminary efficacy of Mecasermin. All 12 trial patients were treated during the MAD while only one MRD patient was included during the OLE along with the 9 other RTT patients. RTT patients 3 (RTT3) and 9 (RTT9) had blood samples for only T0, T1 and T3 (Note, 2 samples at T2 were not taken. These patients correspond to samples; RTT3 a Mecasermin Study Reference patient, and RTT9 a responding patient).

All molecular profiles of gene expression are included in Appendix I, supplementary figures 1, and 2. The average expression of RTT patients and MRD patients across each timepoint (T0, T1, T2 and T3) as well as the average profile of all RTT and MRD samples are included in Appendix I supplementary figure 3.

Although both MRD and RTT patients have pathogenic *MECP2* mutations, MRD patients do not have the clinical presentation of either classic or atypical RTT diagnosis. Therefore patients with MRD and RTT were directly compared at T0 and T1 using edgeR Quasi-like F Test (QLFT). These comparisons showed no significant differential expression. All Subsequent analysis in Chapter I uses data from classic RTT patients (n = 9).

2.2.2 Gene expression profiles of Responders and Mecasermin Study Reference before treatment

Based on improvements in apnoeic index of patients across the trial, T0 to T3, two subgroups were determined Responders (RTT5, RTT7, RTT8 and RTT9) and Mecasermin Study Reference (MSR) (RTT1, RTT2, RTT3, RTT4, and RTT6) [154]. Responders showed a significant decrease in apnoeic index from severe-moderate to mild during the trial (a decrease of frequency >50% or a reduction to $\leq$ 5 apnoeic episodes per hour), while MSR patients did not show improvement.

To understand the relationship between Responders (n = 4) and MSR patients (n = 5), Principal Component Analysis (PCA) was performed before treatment. A plot of the two largest principal components (PC1 and PC2) is shown in figure 2.2.A. Responders (red) and MSR (blue) were divided by PC1, with Responders to the right and MSRs to the left of PC1's origin. Of the 5 MSR samples 4 were clustered closer together in the upper left quadrant of the plot. MRD patients at T0 (data not shown) occupied an

intermediate between Responders and MSRs. PC1 was plotted against apnoeic index at T0 and the spearman correlation test was performed figure 2.1.B which showed significant degree of correlation with high R value.

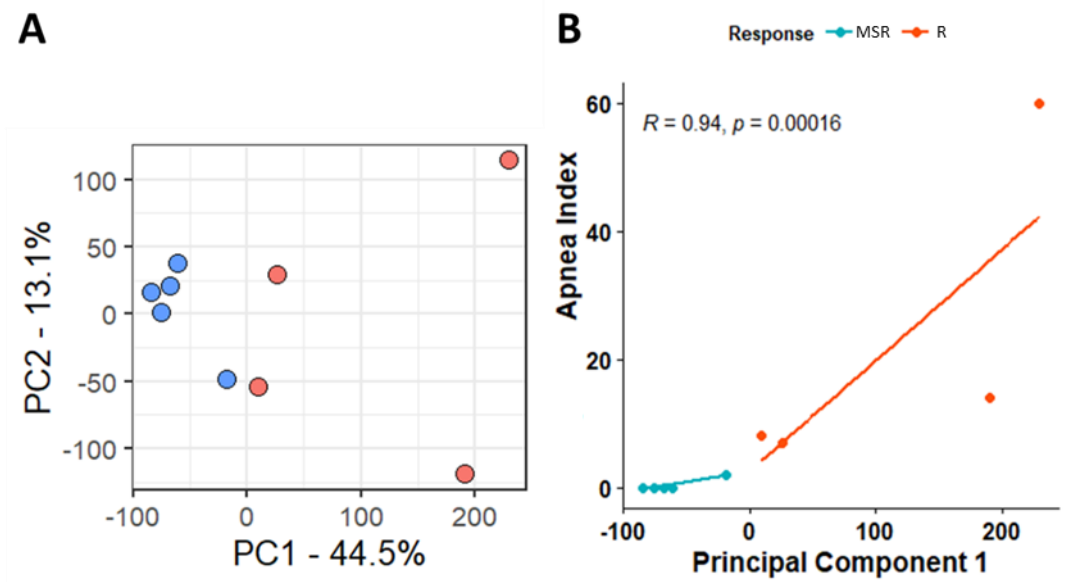

Figure 2.2 - RTT Patients show Responders and MSRs Distinction based on Gene Expression and Apnoea Index

A – Bi-plot of PC1 and PC2 accounting for 44.5% and 13.1% of total variance of gene expression. **B –** PC1 plotted against Apnoea Index for RTT patients at T0 as represented with scatter plot and linear regression lines for each group.

Legend:

R = Responders (Red) MSR = Mecasermin Study Reference (Blue), correlation measured using Spearman's test, sample size (n = 9)

2.2.3 Gene Expression Profiles Comparing Responders and MSRs at Different Timepoints in the Trial

DGE analysis was conducted directly comparing Responders and MSRs (RVMSR) at different timepoints of the study (T0, T1, T2, and T3). The results of this analysis are shown in figure 2.3

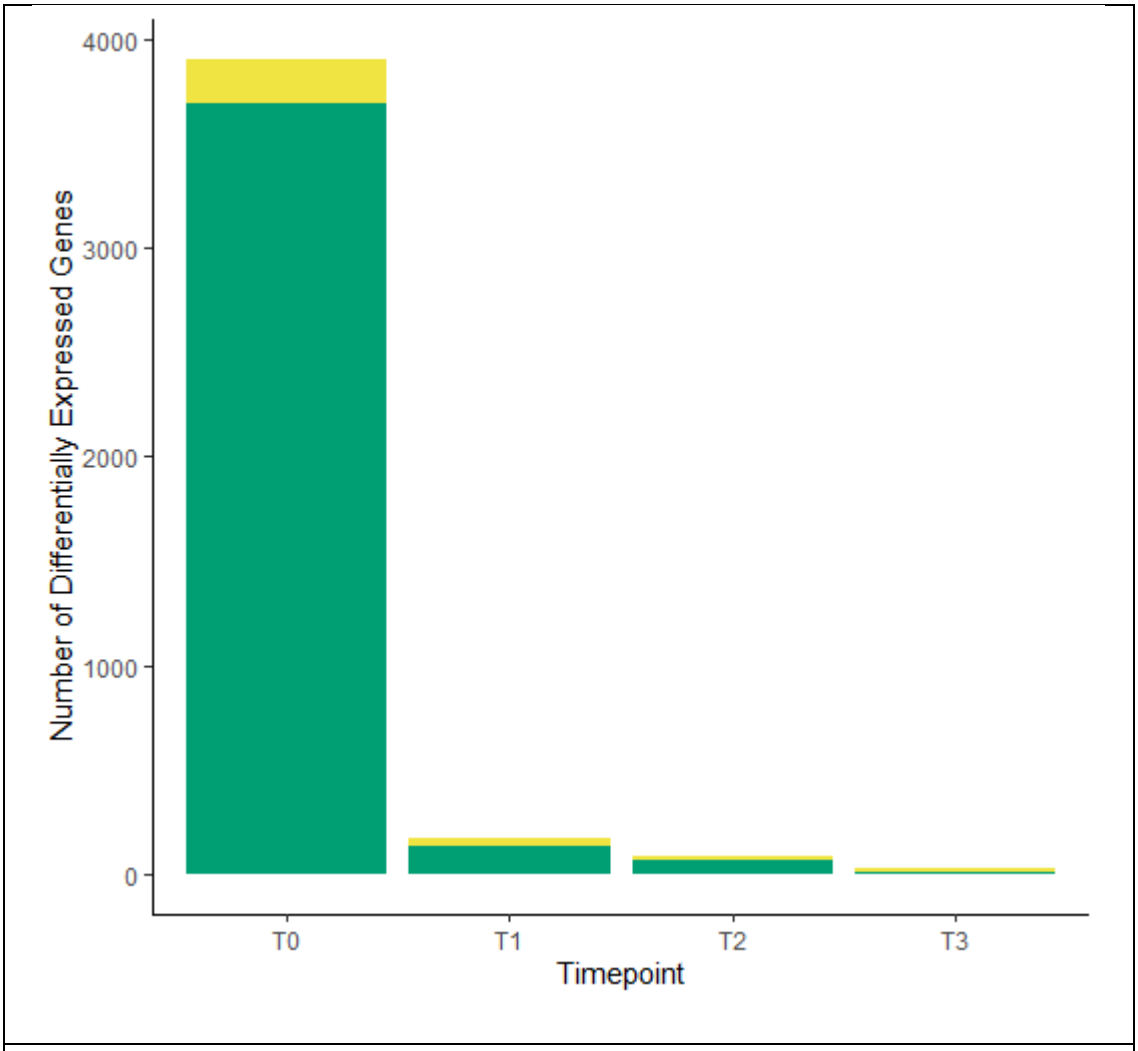

Figure 2.3 - Levels of Differential Gene Expression Decreased Over the Course of Mecasermin Trial in RTT Patient Blood

Number of genes differentially expressed comparing Responders and MSRs at different timepoints; T0, T1, T2 & T3.

Legend:

Up-regulated genes (Green), Down-regulated genes (Yellow), significant genes tested using edgeR with FDR corrected P-Value < 0.05, sample size (n= 4 vs. 5)

The greatest difference in gene expression was observed at T0 before treatment (3693 up-regulated, 221 down-regulated), followed by T1 (133 up-regulated, 34 down-regulated) and T2 (66 up-regulated, 16 down-regulated). At T3, the least number of differentially expressed genes (DEG) was detected and the pattern of transcription was reversed compared to the other comparisons (2 up-regulated, 28 down-regulated).

Overall, these results show that number of DEG in RVMSR decreased over the course of the trial.

To understand the large number of DEGs functional network analysis was conducted using Reactome and GO. Genes that were not recognised by this software were filtered out, so as not to affect the multiple testing correction. The full list of GO and Reactome results are included in Appendix I supplementary Tables 2 and 3. The significant ontologies and pathways detected using HFT were then validated using the edgeR's Fry() function which was used for HDT. This was to strengthen the results of the pathway analysis by using a permutation-like based test as well as the enrichment analysis. The top significant validated results for these analyses are shown in Table 2.1.

Top Significant Reactome Pathways in RVMSR			
Reactome Pathway and Identifier	**Comparison**		**FDR**
Developmental Biology (R-HSA-1266738)	T0		7.38E-07
Extracellular matrix organization (R-HSA-1474244)	T0		2.50E-04
Keratinization (R-HSA-6805567)	T0		0.01
Degradation of extracellular matrix (R-HSA-1474228)	T0		0.01
Extracellular matrix organization (R-HSA-1474244)	T2		0.028
Alpha-defensins (R-HSA-1462054)	T2		0.028
RUNX1-regulated genes involved in differentiation of keratinocytes (R-HSA-8939242)	T2		0.028
Degradation of extracellular matrix (R-HSA-1474228)	T2		0.029
Top Significant GO Ontologies in RVMSR			
GO: Biological Process	**Comparison**	**Fold Enrichment**	**FDR**
Positive regulation of vasoconstriction (GO:0045907)	T0	3.51	2.97E-02
Regulation of vascular permeability (GO:0043114)	T0	3.07	2.69E-02

Heterophilic cell-cell adhesion via plasma membrane cell adhesion molecules (GO:0007157)	T0	2.91	2.89E-02
Killing of cells of other organisms (GO:0031640)	T0	2.4	2.46E-02
Regulation of tube diameter (GO:0035296)	T0	2.32	4.29E-03

Table 2.1 - Pathways and Mechanisms Significantly Different Comparing Responders versus MSRs

Reactome analyses show top results based on FDR, as fold enrichment was not calculated. GO analyses show top results (up to 5) based on fold enrichment of significant ontologies.

Legend:

FDR = False Discovery Rate, significant genes determined using edgeR with FDR corrected P-Value < 0.05, then inputted to GO and Reactome analysis and results were validated using edgeR Fry analysis, sample size (n= 4 vs. 5)

2.2.4 Preliminary assessment of mechanisms underlying response to Mecasermin in RTT

In order to evaluate the changes induced by the Mecasermin administration, the gene expression pattern across different intervals of the trial was compared (T0-T1, T0-T2, T0-T3, T1-T2, T1-T3, and T2-T3). For these timepoint intervals, 3 different groups/subgroups were used; all RTT patients (n = 9), Responders (n = 4), and MSRs (n = 5).

In the full RTT cohort (n = 9) there was no DGE between T0 to T1 (MAD phase), T0 to T2, T0 to T3 (whole trial) or T1 to T3. During the period off-treatment (T1 to T2) two genes were down-regulated, *TMEM176A* and *TMEM176B*. Expression levels of *TMEM176B* then significantly increased during the OLE treatment phase (T2 to T3) along with another three genes *Ribonucleotide Reductase Regulatory Subunit M2* (*RRM2)*, *Centromere Protein F (CENPF)*, and Endogenous Retrovirus Group MER34 Member 1, Envelope (*ERVMER34-1)*. These results are displayed in Table 2.2.

Interval	Gene	Log_2 Fold Change	P-Value	FDR
T0 to T1	-	-	-	-
T0 to T2	-	-	-	-
T0 to T3	-	-	-	-
T1 to T2	*TMEM176B*	-2.53	1.54×10^{-11}	3.41×10^{-07}
	TMEM176A	-2.72	2.61×10^{-11}	3.41×10^{-07}
T1 to T3	-	-	-	-
T2 to T3	*ERVMER34-1*	2.35	3.22×10^{-09}	7.81×10^{-05}
	TMEM176B	2.07	5.98×10^{-09}	7.81×10^{-05}
	RRM2	2.06	3.42×10^{-06}	0.03
	CENPF	2.81	5.07×10^{-06}	0.03

Table 2.2 - DGE in All RTT Patients show a Small Number of Expression Changes

The table shows differentially expressed genes detected by QLFT comparing different time intervals using all RTT patients.

Legend:

FDR = False Discovery Rate, significant genes determined using edgeR with FDR corrected P-Value < 0.05, sample size (n= 4 vs. 5)

In the Responders subgroup (n = 4) only two DEG were detected during the trial, these were a gene encoding the Major Histocompatibility Complex Class II DRβ5 (*HLA-DRB5*), and non-coding Smith-Magenis Syndrome Chromosome Region Candidate 5 gene (*SMCR5*). *HLA-DRB5* decreased from T0 to T1 (MAD phase) and from T0 to T2, this gene then increased in expression from T2 to T3 (OLE phase). *SMCR5* also decreased only from T0 to T2.

In MSRs subgroup (n = 5) there was a much greater level of DGE compared to Responders and all RTT patients. At all intervals of the trial MSRs showed differential expression; 13 genes from T0 to T1, 24 genes from T0 to T2, 28 genes from T0 to T3,

49 genes from T1 to T2, 27 genes from T1 to T3 and 37 genes from T2 to T3. These results are summarized in Table 2.3 for all intervals using each of the 3 different groups. The full list of results were included in Appendix I.

Interval	**Number of Genes (All RTT, n=9)**	**Number of Genes (Responders, n=4)**	**Number of Genes (MSRs, n=5)**
T0 to T1	-	1 (0 ↑, 1 ↓))	13 (1 ↑, 12 ↓)
T0 to T2	-	2 (0 ↑, 2 ↓)	24 (0 ↑, 24 ↓)
T0 to T3	-	-	28 (16 ↑, 12 ↓)
T1 to T2	2 (0 ↑, 2 ↓)	-	49 (5 ↑, 44 ↓)
T1 to T3	-	-	27 (21 ↑, 6 ↓)
T2 to T3	4 (4 ↑, 0 ↓)	1 (1 ↑, 0 ↓)	37 (36 ↑, 1 ↓)

Table 2.3 - Summary of DEG in Each Group shows Highest Levels of DGE in MSRs

Legend:

↑ = Up-regulated genes, ↓ = Down-regulated genes, significant genes determined using edgeR with FDR corrected P-Value < 0.05, sample size (All Rett n= 9, Responders n = 4, MSRs n = 5).

All the DEG found in the full RTT comparisons (n = 9) were also identified in MSRs subgroup. This suggests that the lack of significant gene expression in all RTT patients

was due to the limited DGE in Responders. The top most differentially expressed genes from MSRs are listed in table 2.4.

Comparison	Gene	Log_2 FC	FDR
T0 to T1	*ERVMER34-1*	-3.13	2.33 E-09
	C4B_2	-2.80	2.33 E-09
	C4A	-2.90	1.47 E-06
	ELK2AP	1.80	1.30 E-03
	RPL26	-1.65	5.13 E-03
	TUBB2A	-1.67	9.31 E-03
	IFI44L	-1.48	2.72 E-03
	CD177	-1.47	2.72 E-03
	CISD2	-1.51	3.08 E-02
	UQCRB	-1.67	3.08 E-02
T0 to T2	*ERVMER34-1*	-4.33	3.05 E-12
	CHPT1	-2.29	1.53 E-04
	TRIM58	-2.00	1.53 E-04
	OSBP2	-2.24	1.53 E-04
	SIAH2	-2.00	1.53 E-04
	C4B_2	-1.90	2.07 E-03
	BPGM	-1.77	4.43 E-03
	CA1	-1.66	9.29 E-03
	YOD1	-1.81	9.37 E-03
	SLC4A1	-1.64	9.44 E-03
T0 to T3	*CD177*	-4.09	3.04 E-16
	DEFA3	3.84	2.95 E-12
	DEFA4	3.31	5.14 E-12
	DEFA1B	3.64	4.67 E-08
	DEFA1	3.64	4.67 E-08
	IFI44L	-2.19	2.38 E-05
	FAM90A10P	-1.93	9.25 E-04
	RSAD2	-2.00	1.19 E-03
	SMIM1	-1.96	1.77 E-03

	CHI3L1	1.85	1.92 E-03
T1 to T2	*TMEM176B*	-3.54	3.39 E-19
	TMEM176A	-3.62	5.28 E-15
	SLC4A1	-2.03	2.71 E-10
	KRT1	-2.14	2.79 E-10
	AHSP	-1.70	8.63 E-07
	TRIM58	-1.51	1.19 E-04
	FAM210B	-1.40	4.07 E-04
	RSAD2	-2.26	4.07 E-04
	SMIM1	-1.68	4.07 E-04
	BLVRB	-1.37	5.01 E-04
T1 to T3	*DEFA4*	3.60	3.90 E-18
	DEFA3	3.68	4.87 -16
	DEFA1B	3.58	4.22 E-11
	DEFA1	3.58	4.22 E-11
	ERVMER34-1	2.89	7.82 E-08
	CD177	-2.60	3.42 E-06
	C4B_2	2.29	9.77 E-06
	CAMP	1.78	5.44 E-05
	TMEM176A	-2.08	1.60 E-04
	SMOX	1.78	5.98 E-04
T2 to T3	*DEFA3*	4.80	9.43 E-27
	DEFA1B	4.72	2.79 E-22
	DEFA1	4.72	2.79 E-22
	DEFA4	4.09	3.92 E-19
	CAMP	2.88	1.13 E-11
	ERVMER34-1	4.12	4.82 E-11
	ELANE	3.18	1.58 E-06
	AHSP	2.06	3.52 E-06
	SLC4A1	2.03	4.40 E-06
	LTF	2.89	5.04 E-05

Table 2.4 – Summary of the DEG in MSRs

The table shows differentially expressed genes detected by QLFT comparing different time intervals using MSRs. The top significant 10 DEG of each comparison are listed.

Legend:

FDR = False Discovery Rate, Log_2FC = Log_2 Fold Change, significant genes determined using edgeR with FDR corrected P-Value < 0.05, sample size (n = 5)

From the DEGs in the groups (All RTT patients, Responders, and MSRs) Reactome and GO analysis was performed and similarly to the RVMSR comparison, validated using fry() permutation-like analysis. The only results that were significant after validation were in MSRs (n =5). GO identified Mitotic Cell Cycle Process (GO:1903047) at T2 to T3 (OLE phase) and Reactome identified Non-Sense Mediated Decay (NMD) and NMD enhanced by Exon Junction Complex (R-HSA-927802 and R-HAS-975957) at T1 toT2 (Off-treatment phase). The full list of GO and Reactome results and the validation results of fry() analysis were included in Appendix I supplementary tables 2, 3 and 5.

2.2.5 Hypothesis Driven Testing

For testing the role of mechanisms previously associated with RTT or response to rhIGF1, edgeR fry permutation-like analysis was conducted for a list of specific gene sets. These gene sets were obtained from relevant Gene Ontology database, or in the case of response to rhIGF1 treatment in ASD IPS neurons, the list of significant genes from each comparison; Chronic ASD, Acute ASD, Chronic Control and Acute Control, from publication was taken [171]. The linker study analysed responses to rhIGF1 treatment in ASD IPS derived neuronal culture after 48hr (Acute) and 7 days (Chronic) of treatment. These responses were measured in ASD and matched controls.

All subgroups and comparisons were analysed in HDT, the significant results are displayed in table 2.5. All results are listed in Appendix I supplementary table 4. The majority of results were identified in RVMSR comparison at T0.

Gene set	ID	Comparison	P Value	FDR
IGF receptor signaling pathway	GO.0048009	T0 (RVMSR)	0.0166	0.0202
MAPK cascade	GO.0000165	T0 (RVMSR)	0.0010	0.0060
Phosphatidylinositol 3-kinase signaling	GO.0014065	T0 (RVMSR)	0.0036	0.0062
Brain-derived neurotrophic factor receptor signaling pathway	GO.0031547	T0 (RVMSR)	0.0212	0.0234
Serotonin receptor signaling pathway	GO.0007210	T0 (RVMSR)	0.0016	0.0060
Dopamine receptor signaling pathway	GO.0007212	T0 (RVMSR)	0.0002	0.0033
Response to catecholamine	GO.0071869	T0 (RVMSR)	0.0018	0.0060
Respiratory electron transport chain	GO.0022904	T0 (RVMSR)	0.0063	0.0090
Protein ubiquitination	GO.0016567	T0 (RVMSR)	0.0024	0.0060
Reactive oxygen species metabolic process	GO.0072593	T0 (RVMSR)	0.0024	0.0060
Chromatin organization	GO.0006325	T0 (RVMSR)	0.0083	0.0108
Microglial cell immune response	GO.0002282	T0 (RVMSR)	0.5544	0.5544
Inflammatory response	GO.0006954	T0 (RVMSR)	0.0025	0.0060
Response to Chronic rhIGF-1 in ASD IPS neuronal culture	Linker.ASD_Chronic	T0 (RVMSR)	0.0028	0.0060
Response to Acute rhIGF-1 in Control IPS neuronal culture	Linker.Control_Acute	T0 (RVMSR)	0.0040	0.0062
Response to Chronic rhIGF-1 in Control IPS neuronal culture	Linker.Control_Chronic	T0 (RVMSR)	0.0039	0.0062
Response to Acute rhIGF-1 in ASD IPS neuronal culture	Linker.ASD_Acute	T0 (RVMSR)	0.0220	0.0234
Insulin-like growth factor receptor signaling pathway	GO.0048009	T1 (RVMSR)	0.0005	0.0088
Phosphatidylinositol 3-kinase signaling	GO.0014065	T2 (RVMSR)	0.0004	0.0031
response to catecholamine	GO.0071869	T2 (RVMSR)	0.0000	0.0005

brain-derived neurotrophic factor receptor signaling pathway	GO.0031547	T2 (RVMSR)	0.0065	0.0220
dopamine receptor signaling pathway	GO.0007212	T2 (RVMSR)	0.0043	0.0202
serotonin receptor signaling pathway	GO.0007210	T2 (RVMSR)	0.0088	0.0249
reactive oxygen species metabolic process	GO.0072593	T2(RVMSR)	0.0048	0.0202
Insulin-like growth factor receptor signaling pathway	GO.0048009	T1-T2 (Responders)	0.00106	0.01795
Marchetto.ASD_Chronic	Marchetto.ASD_Chronic	T1-T2 (MSRs)	6.93E-09	1.18E-07

Table 2.5 – Significantly Expressed Gene Sets from Hypothesis-Driven Testing in Responders versus MSRs Comparisons

All groups, entire RTT cohort (n = 9), Responders (n = 4) and MSRs (n = 5), were used to compare different timepoints (T0-T1, T0-T2, T0-T3, T1-T2, T1-T3, T2-T3). Responders and MSRs were also directly compared at T0, T1, T2 and T3. Gene sets were considered differentially expressed with a FDR< 0.05.

Legend:

FDR = False Discovery Rate, ID = Identifier

All gene sets, bar Microglial cell immune response, were differentially expressed at T0 in RVMSR comparison. At T1 the only gene set that was differentially expressed IGF1R signaling pathway which corresponds to the end of MAD phase. At T2 a number of signaling pathways were differentially expressed including PI3K, BDNF Receptor, Dopamine Receptor and Serotonin Receptor signaling. At T3 no gene sets were differentially expressed.

In Responders (n = 4) there was only one significant result, IGF1R signaling pathway that was differentially expressed at T1 to T2 (Off-Treatment Phase). Similarly, MSRs subgroup (n = 5) identified one significant result, Response to Chronic rhIGF1 in ASD

IPS neuronal culture from the Linker study which was differentially expressed at T1 to T2.

2.3 Discussion

This chapter aims to understand the molecular effects of Mecasermin treatment through gene expression of whole blood of RTT trial patients from phase I clinical trial [154]. These results have implications for design of future trials accessing Mecasermin in RTT and may inform the analysis of the ongoing trials in RTT and other related disorders.

Currently there is no treatment for RTT that rescues the phenotype. Despite the promising preclinical evidence and preliminary measures of efficacy from the phase I clinical trial, Mecasermin administration did not produce significant improvement to selected primary outcomes in phase II trial. However, two of the secondary outcomes; hand stereotypy and social communication were significantly improved [151,153,154]. These results further support the ongoing clinical trials for the use of Mecasermin in ASD and Phelan McDermid Syndrome (NCT01970345, NCT01525901). Therefore, analysis conducted in Chapter I is important for determining the future direction of Mecasermin/rhIGF1 treatment in RTT and related disorders.

2.3.1 Heterogeneity of RTT patients in Mecasermin trial

RTT is known to have a varied clinical presentation and many comorbidities, as discussed in sections 1.1.1 and 1.1.2. PCA before treatment (T0) shows the relationship between samples before Mecasermin administration. PC1, the component accounting for the greatest amount of variance, was then plotted against apnoeic index at T0. The PCA and correlation analysis suggested that apnoeic index strongly contributed to the overall variation in gene expression before treatment. The change in Apnoeic Index from beginning of MAD to the end OLE was the key significant improvement attributed to Mecasermin. Patients were considered Responders if they had significant moderate-severe apnoea before treatment which reduced to mild, and patients without moderate-sever apnoea were considered a reference group MSR to compare with. The presence or absence Apnoeic index before treatment could be used as a means of stratification of patients to target patients that could benefit from the effects of

Mecasermin treatment. This study characterises the gene expression profiles of both Responders and MSR blood samples across the trial and comparing Responders samples to MSR samples at each timepoint.

An important factor in the severity of RTT is the mosaic expression of WT and mutant *MECP2* due to XCI [173,174]. In the Responders versus MSRs (RVMSR, n = 4 vs 5) comparisons there was a large number of DEG that were identified, particularly at T0. One DEG related to XCI is *TSIX*. *TSIX*'s expression is significantly increased in Responders relative to MSRs at T0, T1 and T2. *TSIX* and *XIST* are long non-coding genes that function to control the levels of XCI, *XIST* induces inactivation while *TSIX* represses *XIST* expression. A double mutation of *Tsix* and *Mecp2* in female mice resulted in a severe RTT-like phenotype akin to the *Mecp2*$^{-/y}$ mice. The mutation in *Tsix* had the effect of reducing levels of mosaicism and preferentially expressing mutant *Mecp2* [153].

One hypothesis to explain the difference in response to treatment is that *TSIX* mediated the ratio of mutant to WT *MECP2* expression. This could have made MSRs resistant to treatment due to greater levels of pathogenic mutant *MECP2* and Responders malleable to treatment due to greater mosaic expression of *MECP2*. However, finding of increased *TSIX* in responders, contradicts what was observed that Responders were more severely affected with moderate-severe apnoea before treatment. Further experiments are required to investigate the relationship between XCI in RTT and response to rhIGF1 treatment.

A key observation on the RVMSR comparisons, was that the overall decrease in DEG during the trial (Figure 2.2). The difference was highest before treatment and decreased at subsequent timepoints. The hypothesis driven testing was generally consistent with this observation with more gene sets differentially expressed at T0 and no significant changes by T3. These data suggest a homeostatic effect of Mecasermin/rhIGF1 treatment on gene expression in Responders and MSR. Additional findings in Chapter II of this thesis based on *Mecp2* mouse model treated with rhIGF1 support this observation. These results suggest a homeostatic role of rhIGF1, which is supported in the literature. IGF1 signaling is strongly regulated through IGFBP binding, and the relative abundance of IGF1R in the membrane, which is controlled by internalisation processes and desensitisation of IRS [7,8]. Furthermore, the IGF1 metabolite cGP has

been found to regulate IGF1 function in the context of lymphoma tumour and ischaemic brain injury. The normalisation of IGF1 function occurred in homeostatic manner through effecting binding affinity with IGFBP3 [11].

Further studies examining the ratio of endogenous cGP:IGF1 in other disease contexts, have been used to predict the clinical recovery from ischemic stroke and predict the cognitive status in Parkinson's Disease patients [174,175]. All these various control mechanisms need to be investigated to fully understand the homeostatic role of rhIGF1 in RTT pathophysiology.

Based on the results of the hypothesis driven and hypothesis free testing there are mechanisms that can explain the different efficacy of Mecasermin treatment depending on stratification of RTT patients.

2.3.2 IGF1 Signaling and Regulation

The IGF system has many functional roles in the body and is highly regulated. Several results from both HDT and HFT suggest that IGF signaling regulation could be an important factor in determining RTT patient's response to treatment.

HDT found that the majority of significant results were found in the RVMSR comparisons. Nearly all gene sets were significantly expressed at baseline T0. This included 'Insulin-like growth factor receptor signaling pathway' (GO:0048009) and the primary downstream IGF1 signaling pathways, PI3K and MAPK signaling (GO:0014065 and GO:0000165 respectively). Both the PI3K and MAPK signaling have neuroprotective functions by increasing survival and protecting against oxidative damage [8,17]. These signalling pathways have also been demonstrated to be controlled by MeCP2 regulated miRNA during early neurogenesis [1776]. Therefore, these pathways could be central to functional improvements in RTT pathophysiology.

At T1 only IGF receptor signaling pathway (GO: 0048009) remained differentially expressed. At T2 PI3K signaling along with other pathways like BDNF receptor signaling (GO: 0031547) and serotonin receptor signaling (GO: 0007210) were differentially expressed. By the end of the trial at T3 no gene sets were differentially expressed between Responder and MSRs. This suggested that the difference between

patients with different stratification was affected by IGF1 signaling and its downstream pathways, but by the end of treatment there were no differences.

The difference in response may be a feature of rhIGF1/Mecasermin treatment in RTT rather than failing of the clinical trial. Work by Linker and colleagues found heterogeneous transcriptional responses to rhIGF1 in ASD IPS derived neuronal cultures, which correlated with *IGF1R* gene expression. The authors suggested there may have been a stronger negative feedback IGF1R pathway in ASD compared to control samples [171]. While ASD and RTT have a subset of overlapping symptoms and features such as impaired communication and repetitive behaviours, these are distinct disorders and are defined clinically. However, due to the relevance of the Linker study gene sets from the analysis were included in the hypothesis driven testing.

Interestingly the only significant gene sets observed comparing timepoints were during off treatment period (T1 to T2) in Responders (n=4) and MSRs (n=5). In MSRs it was the chronic response to rhIGF1 in ASD and in Responders it was IGF receptor signaling (GO: 0048009). These results suggest that only after finishing initial Mecasermin treatment during MAD phase were the transcriptional changes elicited. This highlights the fact that first exposure to Mecasermin/rhIGF1 strongly effected OLE treatment phase.

In hypothesis free testing the RVMSR comparisons at T0 and T1, *IGF1* was increased in Responders compared to MSRs. *Growth Hormone 2* (*GH2*) and *Growth Hormone Releasing Hormone* (*GHRH*) were also increased at T0 in Responders compared to MSRs. Considering that growth hormone stimulates the secretion of IGF1 in the liver and this process is controlled by GHRH levels [178], an interpretation of these results is that Responders have enhanced endogenous *IGF1* levels driven by the increased expression of *GH* and *GHRH*. After exogenous Mecasermin (rhIGF1) is applied negative feedback mechanism are triggered to regulate *IGF1* and *GH* related gene expression. As a consequence, *IGF1* levels remain higher in Responders at T1 but become indistinguishable from MSRs at T2 and T3.

Both IGF1 and GH signaling are strongly regulated and interlinked as part of the so-called GH-IGF1 axis. IGF1 treatment has been shown to induce a negative feedback of *Gh* expression in rat somatotroph cell line which in turn reduces IGF1 synthesis in the liver. This mechanism is dependent on cAMP response element-binding protein

(CREB)- Binding Protein (CBP) [178]. IGF1 negative feedback is known to occur via endocytic internalisation which regulates the bioavailability of IGF1R. Membrane bound IGF1R is endocytosed in response to IGF1 stimulation by two distinct mechanisms, clathrin-mediated endocytosis occurs at physiological levels of IGF1 stimulation and then at higher non-physiological IGF1 concentrations via the caveolin route [179]. Alternatively, desensitisation of IGF1 via degradation of its substrate IRS-1 via PI3K and m-TORC signalling could mediate decreased IGF signalling [8]. Many of these endogenous regulatory mechanisms of IGF1 could have contributed to the IGF1 signaling in RTT patients during this trial.

Another possible interpretation of the effects of Mecasermin is related to BDNF signalling. BDNF is an important target of MeCP2 and functions through the same signaling pathways as IGF1 signaling (PI3K and MAPK). *BDNF-Anti Sense* (*BDNF-AS*) long noncoding RNA is known to repress the expression of BDNF levels and inhibition of this gene leads to increased neuronal out-growth and differentiation [181].

At T0 *BDNF-AS* expression was increased in Responders relative to MSRs in hypothesis free testing. In hypothesis driven testing BDNF Receptor signaling pathway was differentially expressed in T0 to T2 in Responders compared to MSRs, therefore BDNF signaling could also mediate the beneficial effects of treatment. Bdnf expression is known to be decreased in *Mecp2*$^{-/y}$ mice and *Bdnf* overexpression in *Mecp2*$^{-/y}$ rescued RTT-like the phenotype [97].

2.3.3 Immune System Modulation in RTT Patients Treated with Mecasermin

This analysis found a number of DEG and pathways that implicate immune functioning as an effect of Mecasermin treatment, particularly in the timepoint comparisons of MSRs. While neuronal dysfunction in RTT has been thoroughly studied, initially the role of immune functioning in RTT was not investigated, since *MECP2* was not thought to be expressed in glial cells [183]. In recent years, there has been a growing consensus that immune function plays a key role in the RTT pathology [116,121,184], and crucially restoration of *MECP2* expression in immune cells resulted in functional improvements to the RTT phenotype, including astrocytes, microglia, macrophages and

oligodendrocytes [91,115,122]. However, there is contradictory evidence that normalising *Mecp2* expression in microglia can rescue RTT symptoms [122,123,184].

Several genes related to immune function emerged from analysis of RTT patients. A decrease in *TMEM176A* and *TMEM176B* expression was observed comparing before and after the off-treatment phase (T1 to T2) in all RTT patients (n=9). *TMEM176B* expression was found to subsequently increase during the OLE phase (T2 to T3). Minimal DGE was observed comparing timepoints including all RTT patients (n=9), only 3 other genes were significantly altered. The proteins these genes encode are thought to be involved in maintaining immature dendritic cell status [185]. However, a recent preprint study using double knockout of *Tmem176a* and *Tmem176b* demonstrated normal levels of precursor dendritic cells, and instead found a role for *Tmem176a/b* in major histocompatibility class II interaction with CD4+ T-cell for dendritic cell priming [186].

In Responders (n = 4) comparing different timepoints across the trial, *HLA-DRB5* was found to be decreased initially during MAD phase and subsequently increased during the OLE. *HLA-DRB5* was also decreased in MSRs at T2 to T3 (OLE) and therefore is unlikely to be mediating the improvements observed in Responders. There was only one additional DEG identified in Responders comparisons (n = 4) across the trial, indicating minimal effect of Mecasermin on expression in the whole blood. This major histocompatibility class II gene transcribes a protein that is involved in antigen presentation for recognition by CD4 T-Cells [187]. *HLA-DRB5* methylation in the brain is associated with diagnosis of Alzheimer's disease and loss of *HLA-DRB5* has been associated with progression of Multiple Sclerosis [188,189].

In the MSRs sub-group (n = 5) comparing different timepoints across the trial. Three genes associated with the regulation of complement cascade were found to be differentially expressed in the MAD phase of MSRs *Complement C4A* (*C4A*), *Complement C4B Copy 2* (*C4B_2*), and *Serpin Family G Member 1* (*SERPING1*). *C4A* and *C4B_2* were decreased while *SERPING1* was increased. Aberrant complement cascade gene expression and protein concentrations have been noted in a number of neurodevelopmental conditions including Schizophrenia, ASD and RTT [190]. An integrated analysis of different transcriptomic studies of RTT human tissues found that *SERPING1* was increased in brain tissue and fibroblasts but decreased in cell culture

experiments [191]. The protein encoded by this gene is the C1 complex inhibitor which plays a key role in complement regulation, by inactivating C1r, C1s and mannose-binding lectin associated serine proteases (MASP)-1/2 thereby inhibiting the classical and lectin complement pathways [191]. Another component of the C1 complex, C1q genes have been identified as a convergence point between RTT patients and *Mecp2* mutant mouse model gene expression [167]. The *C1q* KO mouse develops altered synaptic connectivity and epilepsy [192]. These studies suggest that immune functioning and specifically complement pathway related DEG can have consequences for neuropathology of RTT.

In MSRs (n = 5), several genes associated with α-defensins and neutrophil degranulation were increased during OLE and considering the whole trial (T0T3). These DEG included *DEFA1*, *DEFA1B*, *DEFA3*, *DEFA4*, *CAMP*, *LTF*, *ELANE* and *CENPF*, and was supported by GO and Reactome analysis which found neutrophil degranulation (GO:0043312 and R-HSA-6798695), α-defensins (R-HSA-1462054) and antimicrobial humoral response mediated by antimicrobial peptides (GO:0061844) significantly over-represented. However, these ontologies and pathways were not validated by fry() analysis. IGF1 is known to potentiate pro-inflammatory cytokines in PBMCs via MAPK signalling [193]. Recently *Mecp2*$^{308/y}$ mice displayed imbalance immune response to autoimmune challenge, where pro-inflammatory response was up-regulated and immune regulation was down-regulated [194].

It is difficult to determine whether increased immune response in MSRs is due to patient stratification or is a result of Mecasermin treatment or a combination of both. In Chapter II, evidence from *Mecp2*-null and –heterozygous mice demonstrate innate immune functions are abnormal in blood which suggests that immune changes were linked to RTT pathology. However, *Igfbp3* expression was increased in activated *Mecp2*$^{-/y}$ microglia and myeloid cells suggesting that RTT pathology, immune function, and IGF1 signaling are all linked [184,195]. Hypothesis driven testing at T0 found inflammatory response (GO:0006954) but not microglial cell immune response (GO:0002282) as being differentially expressed comparing Responders and MSRs.

An explanation for this results is that MSRs were more immune compromised than Responders and therefore did not experience the beneficial effects of Mecasermin

treatment. These results provide an intriguing direction for future experiments in understanding how Mecasermin/rhIGF1 in RTT.

2.3.4 Cell Cycle Progression

Though little DEG was observed across timepoints when testing all RTT samples (n=9), two genes were up-regulated during OLE (T2 to T3) were CENPF and *RRM2*. These genes are associated with mitotic cell cycle. Reactome analysis identified the pathways G2/M (R-HSA-69206) and G1/S (R-HSA-69206) transition to be over-represented in this comparison. IGF1 treatment has been found to promote the progression from G2 to M phase in cerebral cortex thyroid cell line of rat via Cyclin D1 [196,197]. Interestingly work in *MECP2* deficient IPS cells found enhanced cell reprogramming that was dependent on IGF1/AKT/mTOR signalling activating G1/S phase transition [198].

Analysis of MSRs during MAD and OLE phases also found a number DEGs associated with cell cycle progression, G1/S and G2/M transition. These genes include *Tubulin β 2A* (*TUBB2A*), *Cyclin B2* (*CCNB2*), *CENPF, Centromere Protein M (CENPM), RRM2, DNA Topoisomerase II α* (*TOP2A*), *Ubiquitin Conjugating Enzyme E2 C* (*UBE2C*), *Thymine Kinase 1* (*TK1*), *Establishment of Sister Chromatid Cohesion N-Acetyltransferase 2 (ESCO2)* and *Aurora Kinase B* (*AURKB*). Reactome analysis of these DEG found G2/M transition (R-HSA-69275), mitotic G2-G2/M phases (R-HSA-453274), mitotic metaphase and anaphase (R-HSA-2555396), and resolution of sister chromatid cohesion (R-HSA-2500257) over-represented in both treatment phases. Given IGF1s role in growth and its mitogenic effects it is not surprising to find that Mecasermin influencing cell cycle dynamics in patients with RTT. Though these cell cycle progression genes were found in OLE of all RTT patients, there was a greater number of DEG and associated pathways linked to cell cycle in both treatment phases in MSRs. This suggests that the regulation of cell cycle progression though an effect of treatment was probably not mediating the beneficial effects of treatment.

2.3.5 Overview and Limitations

This Chapter provides new insights on the molecular effects of Mecasermin/rhIGF1 administration in patients with RTT. However due to the nature of the clinical trial

design, there are a number of limitations that need to be considered. Gene expression analysis was completed in RNA derived from whole blood, therefor may not be informative of changes in other tissues, though there is a subset of RTT-like phenotype in peripheral tissues that reflect the changes that occur in the CNS [91,95]. The studies in animal models discussed in Chapter II are used to clarify the correlation between changes observed in the blood and other tissues i.e. the brain.

The low sample size in this study is another limiting factor in this analysis. This is a common issue in studying primary tissues of RTT patients because of low occurrence is in the population, especially for brain samples which must be obtained post-mortem [199]. Therefore, analysis of blood samples represents a more attractive resource to use. Blood samples can be taken longitudinally and is less invasive than taking CSF sample by lumbar puncture. Longitudinal samples control for genetic background as they come from the same individual which reduces noise, and therefore increasing statistical power.

A further complication of this analysis is the complexity of the trial design. The trial had two treatment phases with an off period of between 12-30 weeks. The benefit of this design was the ability to assess the pharmacokinetics, dynamics and safety then separately in OLE assess efficacy of treatment. The treatment phases are not equivalent in length though they had the same escalating dosage in the opening 3 weeks. As discussed in section 2.3.2 IGF1 signaling is highly regulated, therefore shorter exogenous application of Mecasermin during MAD could desensitise IGF1 signaling so that response to Mecasermin during OLE.

2.4 Conclusion

This analysis provides a first look at the transcriptional profiling RTT patients treated with Mecasermin/rhIGF1. These results indicate that there was a varied response to treatment with a subgroup of patients showing significant decrease to apnoeic index. A potential mechanism for mediating this heterogeneous response to treatment is IGF receptor signalling. Neuronally differentiated IPS cells from ASD patients also support the idea of Responder MSR distinction and suggest it could be mediated by expression of IGF1R [171].

Gene expression analysis found immune system functioning was altered by Mecasermin treatment. This effect was minimal in Responders, with only *HLA-DRB5* expression decreasing during MAD and increasing during OLE. In MSRs, an extensive innate immune response linked to activation of complement cascade during MAD and in neutrophil degranulation and antimicrobial peptide α-defensins during OLE.

This study on the mechanisms of Mecasermin/rhIGF1 treatment in the context of whole blood in RTT patients suggests that regulation of IGF1 signalling and innate immunity may play a role in response to treatment and should be investigated further. In chapter II *Mecp2* –null and –heterozygous mice will be used to further assess rhIGF1's effects on both CNS and whole blood and potentially expand on the findings in chapter I.

3.0 Chapter II: Behavioural and Molecular Correlates of Administration of rhIGF1 in *Mecp2* Mouse Model

3.1 Introduction

Mouse models play a key role in understanding the RTT pathology. These mice provide researchers with a readily available source of neuronal tissues and their behaviour can be monitored and analysed. Additionally, the conditions in mouse models can be controlled, which avoids the variability present in patients with RTT and increases the statistical power of experiments. In addition, the mouse models present molecular endophenotypes and behavioural traits also identified in RTT patients, and these parameters can be measured for quantifying the severity of the presentation for evaluating the benefits of candidate treatments.

Mecp2-null (*Mecp2*$^{-/y}$) and –heterozygous (*Mecp2*$^{-/+}$) mice were generated using the *Mecp2*$^{tm1.1Bird}$ model [38] females cross-bred with WT C57/BL6 male mice. The original *Mecp2*$^{tm1.1Bird}$ females were purchased from Jackson's Laboratory, and the males were provided by the Department of Comparative Medicine Unit in Trinity Biomedical Science Institute (TBSI). The *Mecp2*$^{-/+}$ female offspring were used to breed with WT C57/BL6 male mice to maintain the colony. These mice have functional loss of MeCP2 due to KO of exons 3 and 4, a mutation present in some patients with RTT (including one of the patients in Chapter I, see Supplementary table 1).

There are a number of advantages and disadvantages of studying *Mecp2* mouse models over RTT patients. These advantages include:

1. Controlled genetic background with consistent *Mecp2* mutation, i.e. deletion of exons 3 and 4.
2. Controlled environment, diet and ability to have age matched controls.
3. Ability to conduct behavioural analysis that would not be possible in humans.
4. Access to CNS tissues.
5. Ability to test preclinical therapeutics.

The disadvantages include:

1. Differences in underlying biology of mice compared to humans.

2. Unlike the vast majority of RTT patients, *Mecp2*$^{-/y}$ mice can survive postnatally and are similar to RTT patients in severity of symptoms and age of onset, while *Mecp2*$^{-/+}$ mice are less similar.
3. *Mecp2*$^{-/y}$ mice do not have mosaic expression of *Mecp2*, which is a feature of female RTT patients.
4. *Mecp2*$^{-/+}$ mice do not have onset of symptoms until maturity ~ 3 months and display a milder phenotype.

It has also been shown that the maternal behaviour of *Mecp2*$^{-/+}$ mothers was significantly impaired compared to WT surrogate mothers, specifically pup gathering [200]. This impairment could affect the development of both male and female *Mecp2* mutant mice from an early age.

To better understand how rhIGF1 treatment can affect the RTT phenotype, *Mecp2*$^{tm1.1Bird}$ female and male mice were treated with rhIGF1 or vehicle control. Locomotor performance was measured before and after treatment along with recording body weight to provide measures of physiological condition and measure of treatment efficacy. After completion of treatment and measurement of physiological performance, all mice were culled using CO_2 and tissues were harvested and stored.

RNA was extracted from cerebellum and peripheral whole blood tissues and used for quantification of gene expression, by 3'DGE and quantitative Polymerase Chain Reaction (qPCR). For 3'DGE experiments *Mecp2*$^{-/+}$ cerebellum and blood was sequenced in MIT BioMicro Centre. Two additional reference samples from a previous experiment by Albert Sanfeliu Bosch, a member of this research group, using rhIGF1 treatment in *Mecp2*$^{-/y}$ mice were included. This allowed for comparison between the two sets of experiments. In this way, the effects of rhIGF1 treatment in male and female *Mecp2* mice were analysed by 3'DGE. The original preclinical evidence for rhIGF1 as a treatment for RTT focused on using male mice, although some experiments were conducted in female mice [151].

One of the primary findings from the phase I Mecasermin trial (Chapter 1), was that some of the patients showed an improvement in apnoeic index, while some patients show no improvements (MSRs), and the analysis of transcripts between these two groups showed significant differences even before the start of the treatment. This study was limited to DEG in whole blood.

Chapter II aims to measure differential expression in cerebellum and blood of *Mecp2*-null and –heterozygous mice treated with rhIGF1 to determine the effects of treatment in RTT pathology. Additionally, gene expression and motor activity in the treated *Mecp2*-null and –heterozygous mice will be compared to investigate the different phenotypes of these animals.

3.2 Results

3.2.1 Locomotor Analysis of Mecp2 Mice

The *Mecp2*$^{-/y}$ and *Mecp2*$^{-/+}$ mice have reduced nocturnal activity using infrared beam detectors [125]. In *Mecp2*$^{-/y}$ mice, this deficiency was recovered by treatment with rhIGF1 or GPE [101,151]. Here, the severity of RTT phenotype was characterised through nocturnal locomotor activity in *Mecp2*$^{-/y}$ and *Mecp2*$^{-/+}$ mice compared to WT control.

Locomotor activity, which described in detail in section 6.2.4, was measured by number of beambreaks (interruptions) per hour using infrared beam detectors (47420, Ugo Basille). A schematic of the cage and infrared beams is displayed in methods section 6.2.4 in figure 6.1. Mice were placed in the cage at least 3 hours (3hr) before starting nocturnal measurement. Mice were kept on a 12hr light cycle, nocturnal activity was measured during 12hr lights off period. Beambreaks were captured by the horizontal receiver and transmitter set at ground level of the cage, and by the vertical receiver and transmitter set higher in line with grid bars containing food diet and water. Three variables were considered for locomotor activity: horizontal, vertical and total (horizontal + vertical) activity.

3.2.1 Nocturnal Activity in Mecp2$^{-/+}$ *and Mecp2*$^{-/y}$ *Mice*

The sum of locomotor activity during the night, as measured by infrared beambreaks per hour, in *Mecp2*$^{-/+}$ and *Mecp2*$^{+/+}$ mice is shown in figure 3.1. Mice were measured at various ages after age of symptom onset (p120 ~ 4 months), to capture the variability of the phenotype. *Mecp2*$^{-/+}$ mice had significantly decreased horizontal, vertical and total nocturnal activity (Figure 3.1). Horizontal activity captured beambreaks along ground level of the cage, vertical activity captured beambreaks at the level of metal grid

holding food and water at the top of the cage and total activity was the sum of horizontal and vertical activity.

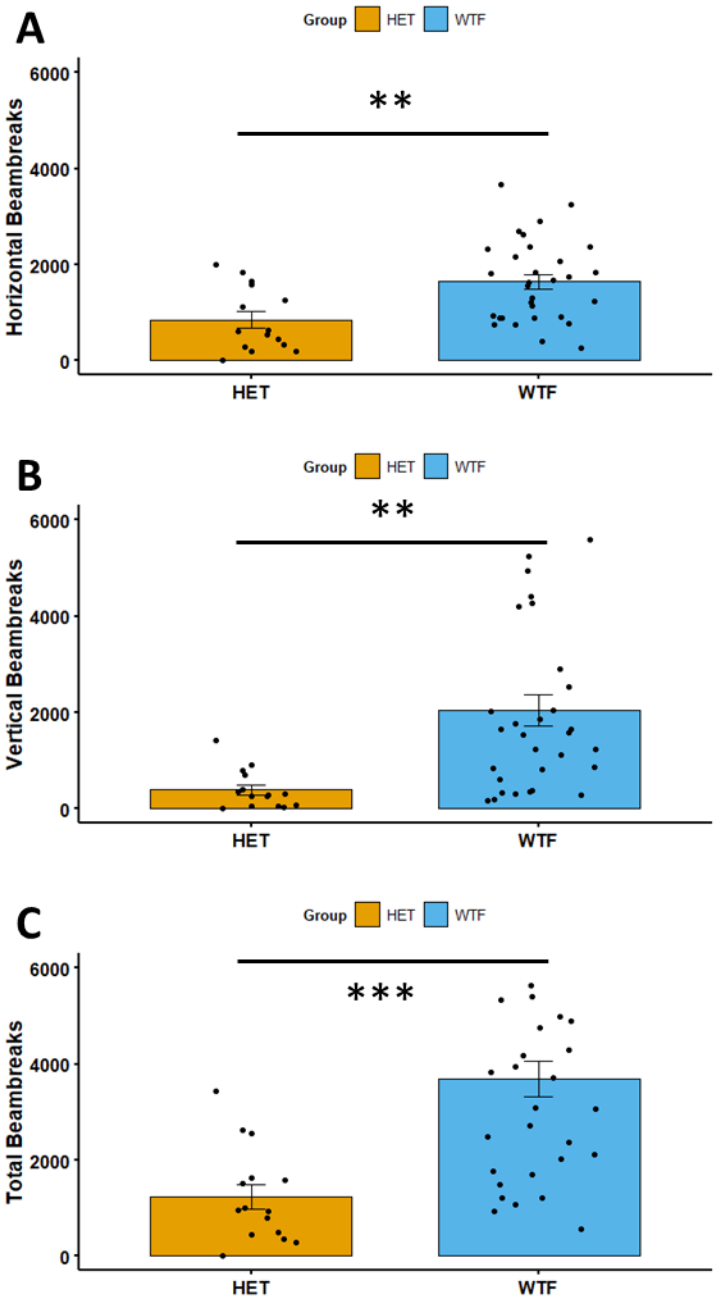

Figure 3.1 - *Mecp2*$^{-/+}$ Mice have Lower Locomotor Activity than WT Control

Average of the total beambreaks of HET and WTF mice as represented by bar-graph of mean ± Standard Error (SE) of the mean.

Legend:

HET = *Mecp2*$^{-/+}$, WTF = *Mecp2*$^{+/+}$, ** = Adjust P-Value < 0.005, *** = Adjusted P-Value < 0.0005, tested using Kruskal-Wallis post hoc Wilcox test unpaired, sample size (n = 25; 9 HET and 16 WTF)

In figure 3.2, the sum of nocturnal activity is reported for *Mecp2*$^{-/y}$ and *Mecp2*$^{+/y}$ mice. Mice were used at various ages after age of symptom onset (p28 ~ 4 weeks), to capture the variability of the phenotype. *Mecp2*$^{-/y}$ mice had significantly decreased horizontal, vertical and total nocturnal activity. Mice ranged in age from p28-p69 as *Mecp2*$^{-/y}$ mice tended not to survive beyond 10 weeks of age.

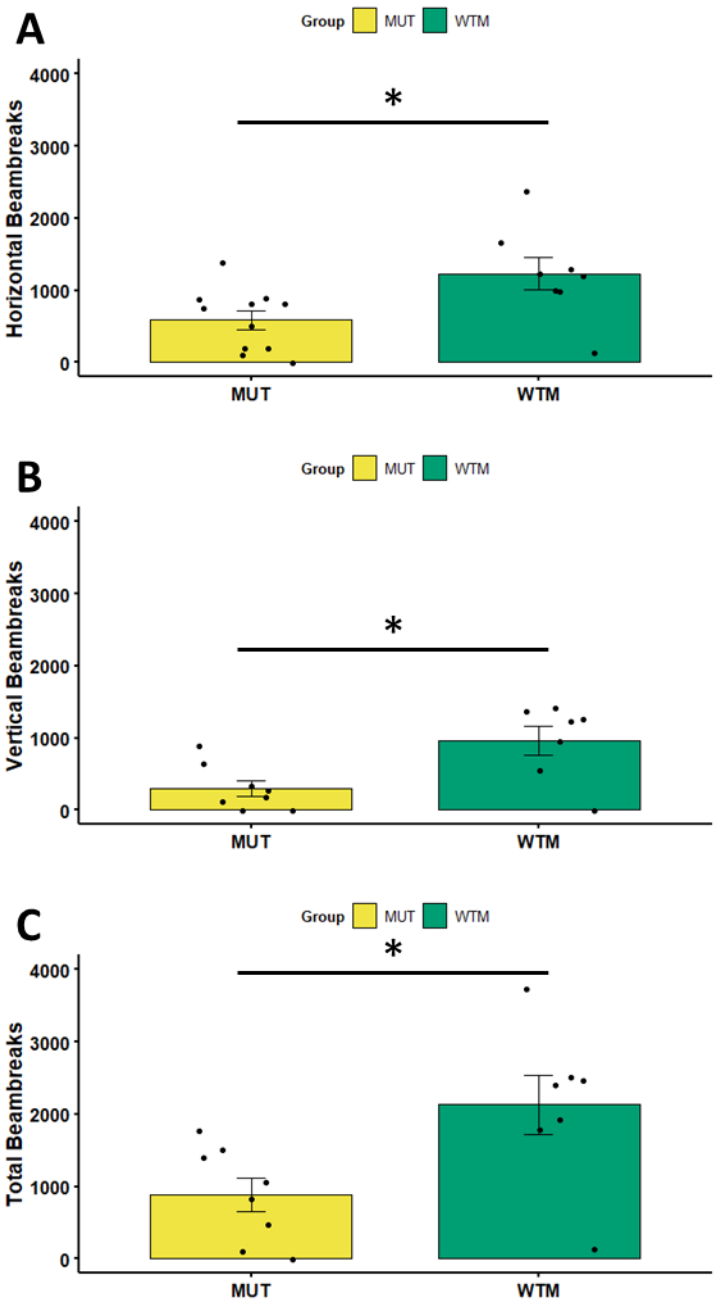

Figure 3.2 - *Mecp2*$^{-/y}$ mice have lower locomotor activity than WT control

Average of the total beambreaks of MUT and WTM mice as represented by bar-graph of mean ± SE of the mean.

Legend:

MUT = *Mecp2*$^{-/y}$, WTM = *Mecp2*$^{+/y}$, * = Adjust P-Value < 0.05, tested using Kruskal-Wallis post hoc Wilcox test unpaired, sample size (n = 17; 9 MUT, and 8 WTM)

3.2.2 Nocturnal Activity over Time in Mecp2$^{-/y}$ and Mecp2$^{-/+}$

To understand if the locomotor deficiency observed in section 3.2.1 varied over time, the cumulative nocturnal activity was plotted against 12hr of the night. *Mecp2*$^{-/+}$ and *Mecp2*$^{+/+}$ mice were plotted in figure 3.3. This analysis revealed that *Mecp2*$^{-/+}$ mice activity remained lower during the night compared to *Mecp2*$^{+/+}$ mice. This result suggests that *Mecp2*$^{-/+}$ mice were fatigued compared to WT control.

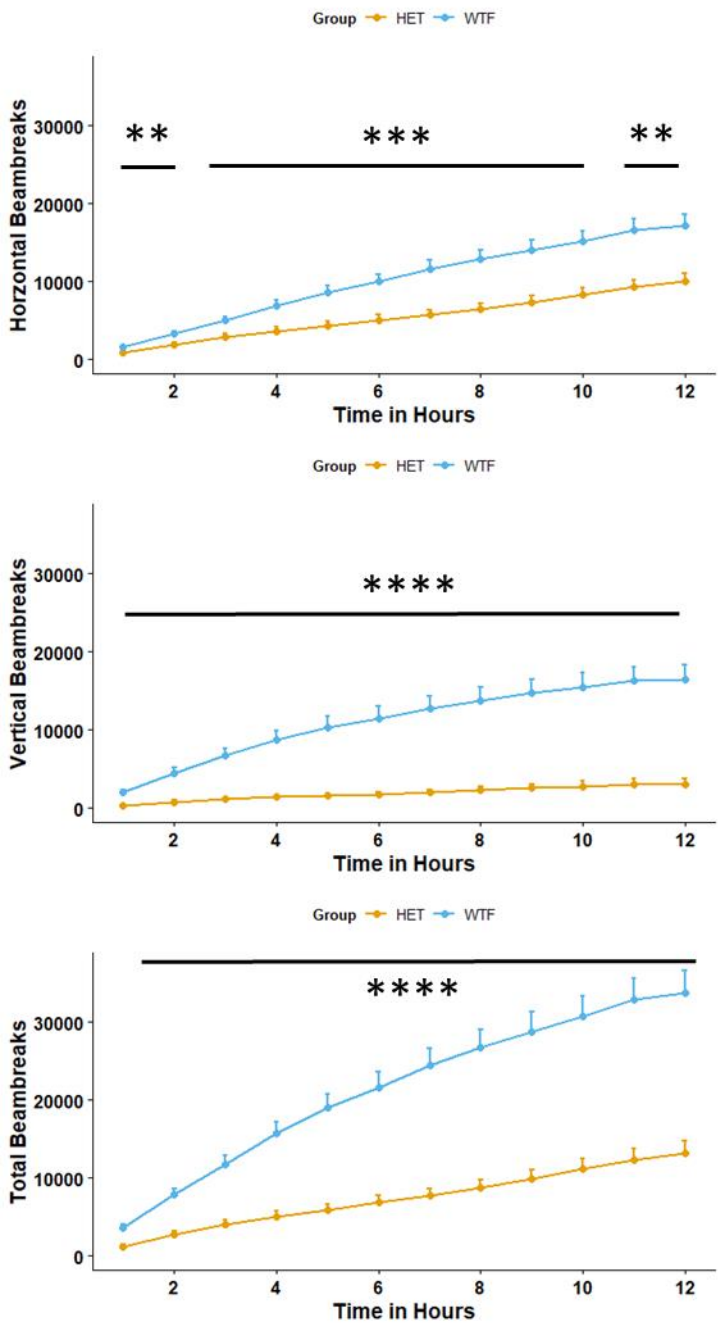

Figure 3.3 - Nocturnal Activity of *Mecp2*$^{-/+}$ Mice Demonstrate Fatigue

Average beambreaks per hour plotted against time during the night as presented as line-graph of mean ± SE of the mean.

Legend:

HET = *Mecp2*$^{-/+}$, WTF = *Mecp2*$^{+/+}$, ** = Adjusted p-value of less than 0.005, *** = Adjusted p-value of less than 0.0005, **** = Adjusted p-value of less than 0.00005, tested using Friedman test and post hox Wilcox test unpaired, sample size (n = 25; 9 HET and 16 WTF)

Nocturnal activity over time was plotted for *Mecp2*$^{-/y}$ and *Mecp2*$^{+/y}$ mice in figure 3.4. Although nocturnal activity in *Mecp2*$^{-/y}$ was always lower than *Mecp2*$^{+/y}$, this difference was only significant in the initial 7 hours of horizontal activity and the first hour of total activity. Vertical activity was not significantly different in *Mecp2*$^{-/y}$ compared to *Mecp2*$^{+/+}$ mice.

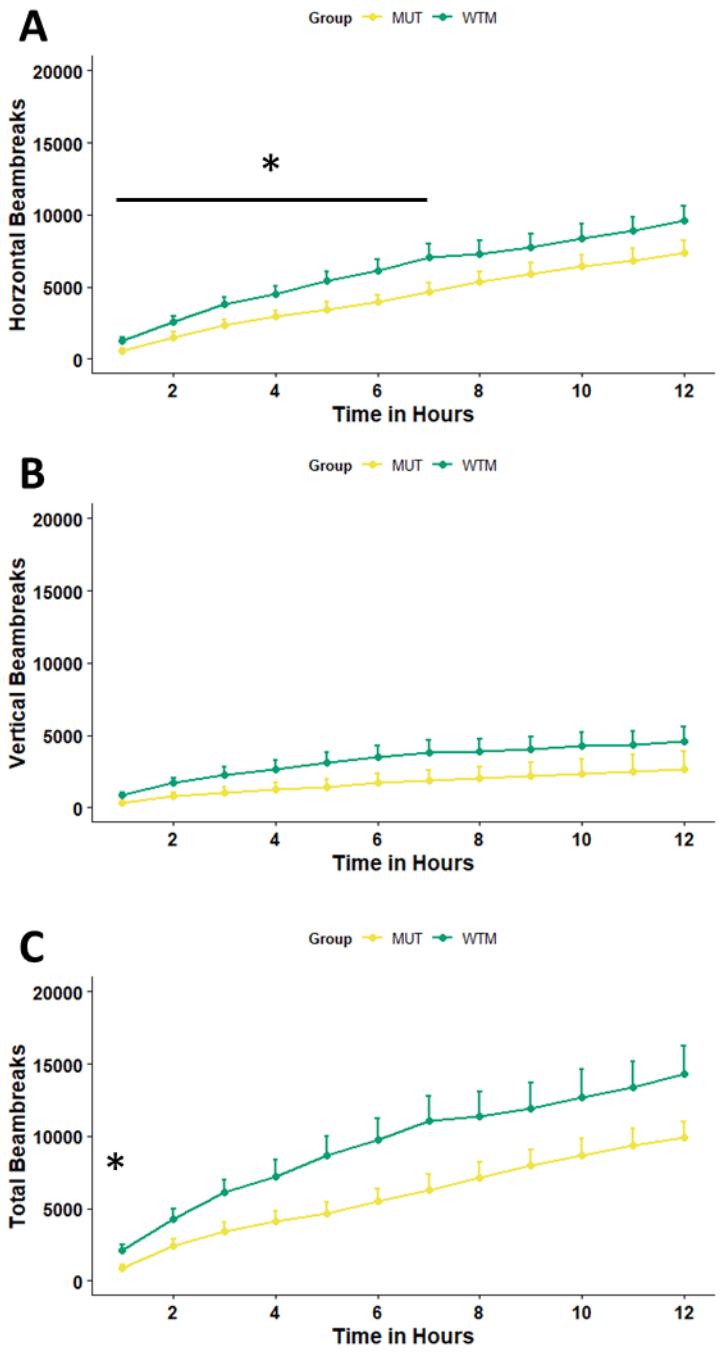

Figure 3.4 - Nocturnal Activity over Time in *Mecp2*$^{-/y}$ Compared to *Mecp2*$^{+/+}$ Mice was Lower Horizontal and Total Activity but Not Vertical Activity

Average beambreaks per hour plotted against time during the night as presented as line-graph of mean ± SE of the mean.

Legend:

MUT = *Mecp2*$^{-/y}$, WTM = *Mecp2*$^{+/y}$, * = Adjusted p-value of less than 0.05, tested using Friedman test and post hox Wilcox test unpaired, sample size (n = 17; 9 MUT and 8 WTM)

3.2.3 Correlation of Nocturnal Activity with Age

It has been observed that *Mecp2*$^{-/y}$ mice show an age-dependent decrease in locomotor activity at 8 weeks (P56), compared to 4 weeks (P28) the approximate age of symptom onset [151]. To understand the relationship between nocturnal activity and age, these activity variables were plotted against each other, and a non-parametric spearman test was used to determine correlation.

Although there was no significant correlation between age and locomotor activity, the analysis shows that female mice *Mecp2*$^{+/+}$ display a slight decline in activity with increasing age, while *Mecp2*$^{-/+}$ mice activity remained steady but lower across all ages.

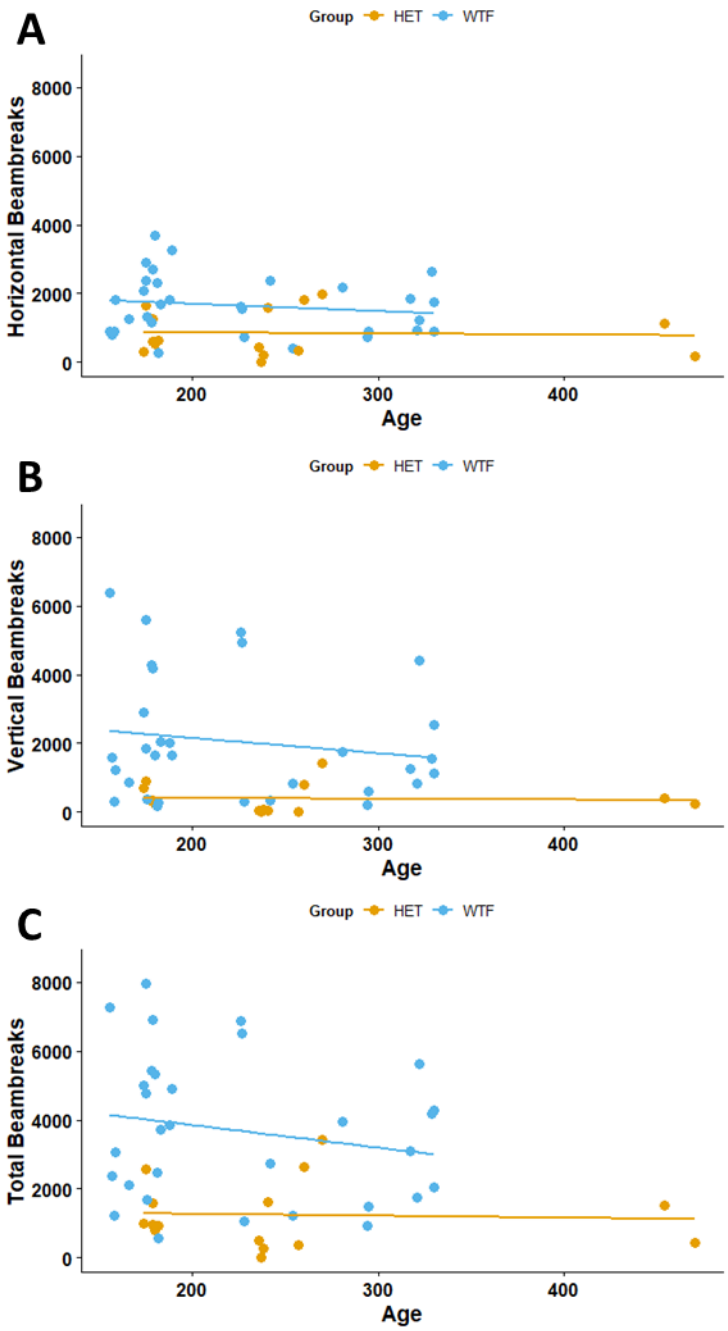

Figure 3.5 - Correlation of Locomotor Activity and Age in *Mecp2*$^{-/+}$ and *Mecp2*$^{+/+}$ Mice

Average beambreaks per hour plotted against the age of the mice in days postnatal, as represented by scatter plot with linear regression for each group.

A - Correlation of horizontal activity and age in HET (rho= 0.0375, p-value = 0.8944) and WTF (rho = -0.056, p-value = 0.7868), **B -** correlation of vertical activity and age in HET (rho = -0.1519, p-value = 0.5889) and WTF (rho = -0.1492, p-value

= 0.423), **C** correlation of total activity and age HET (rho = -0.034, p-value = 0.9044) and WTF (rho = -0.1696, p-value = 0.3617).

Legend:

HET = *Mecp2*$^{-/+}$, WTF = *Mecp2*$^{+/+}$, correlation tested using Spearman test, sample size (n = 25; 9 HET and 16 WTF)

In male *Mecp2*$^{+/y}$ mice, there was an increase in nocturnal activity with age and in *Mecp2*$^{-/y}$ mice there was a decrease in nocturnal activity with age. Although there was no significant correlation between age and nocturnal activity, there is a clear trend showing a decline in activity overtime in *Mecp2*$^{-/y}$ and increase in activity in *Mecp2*$^{+/y}$ mice.

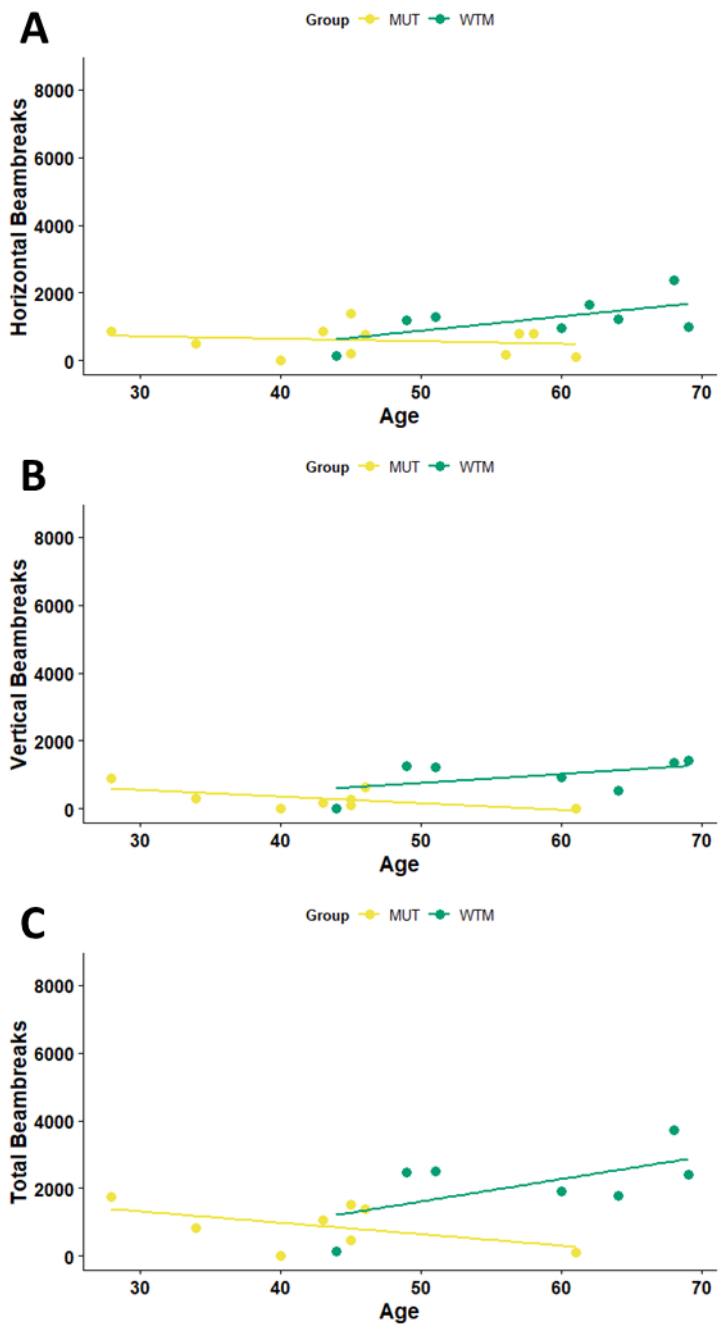

Figure 3.6 - Correlation of Locomotor Activity and Age in *Mecp2*-/y and *Mecp2*$^{+/y}$ Mice

Average beambreaks per hour plotted against the age of the mice in days postnatal, as represented by scatter plot with linear regression for each group.

A Correlation in horizontal component in MUT (rho= -0.1959, p-value = 0.5637) and WTM (rho = 0.4286, p-value = 0.2992), **B** correlation in vertical component in MUT (rho = -0.3975, p-value = 0.3294) and WTM (rho = 0.6429, p-value =0.1389), **C** MUT (rho = -0.2395, p-value = 0.5678) and WTM (rho = 0.3214, p-value = 0.4976).

Legend:
MUT = *Mecp2*$^{-/y}$, WTM = *Mecp2*$^{+/y}$, correlation tested using Spearman test, sample size (n = 17; 9 MUT and 8 WTM)

3.2.4 rhIGF1 Treatment and Locomotor Performance in Mecp2 Mice

Mecp2$^{-/+}$, *Mecp2*$^{+/+}$, *Mecp2*$^{-/y}$, and *Mecp2*$^{+/y}$ mice were treated with either rhIGF1 or vehicle. Their locomotor activity was measured over night before and after treatment. To find out whether treatment effected locomotor activity, the baseline activity was subtracted from the activity after treatment. This difference was plotted in figures 3.7 and 3.8 in female and male mice respectively.

Vehicle treated *Mecp2*$^{-/+}$ mice showed a significant decline compared to rhIGF1 treated *Mecp2*$^{-/+}$ in vertical activity. The same trend was observed in total activity, although it did not reach significance. This result indicates that rhIGF1 may be protecting against the locomotor deficits of the RTT-like phenotype. There was no significant difference between treatment in *Mecp2*$^{+/+}$ mice, suggesting that rhIGF1 improved locomotor activity only where deficits were present.

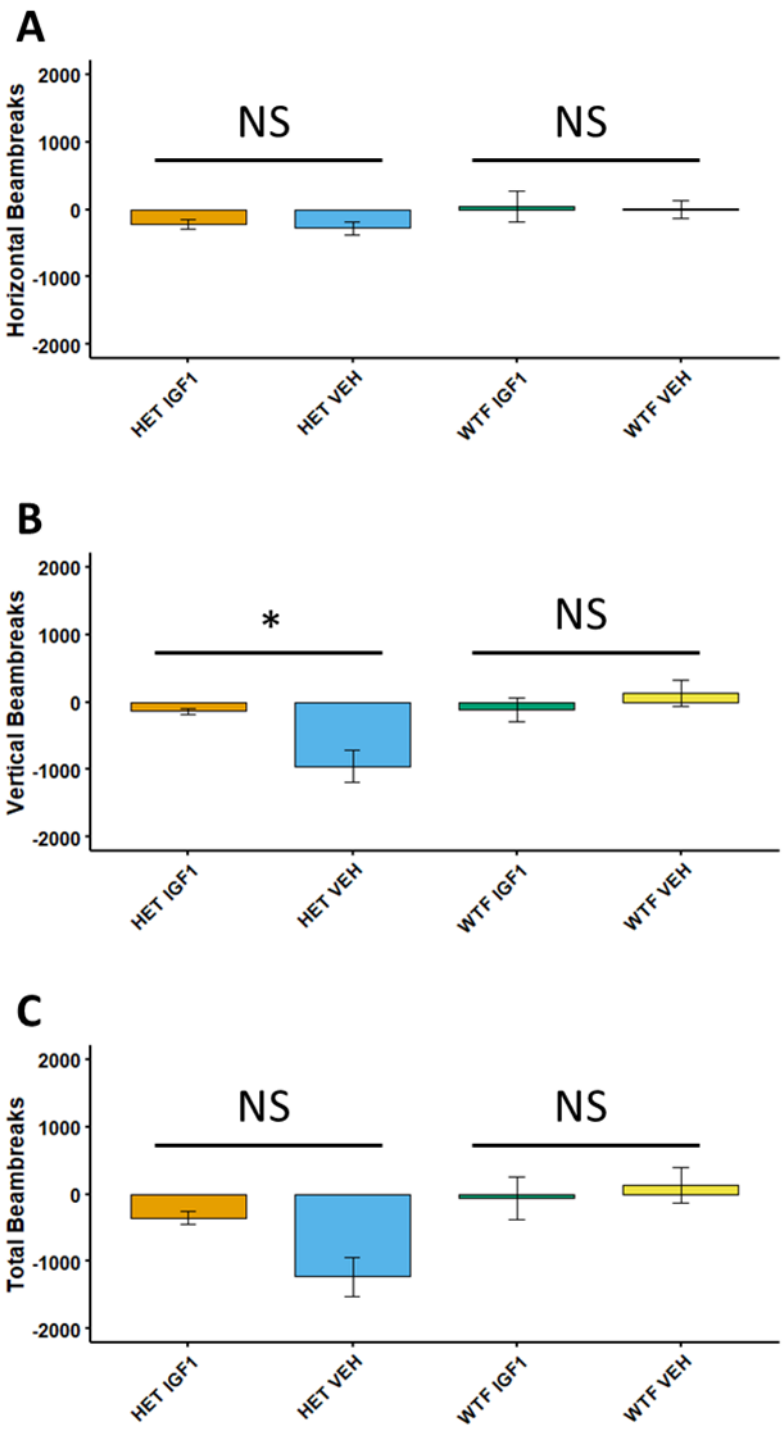

Figure 3.7 – Vertical Activity Decline in *Mecp2*-/+ Mice was Prevented by rhIGF1 Treatment

Difference between beambreaks per hour as represented by bar-graph with mean ± SE of the mean. Kruskal-Wallis test results **A.** p-value = 0.594, **B.** p-value = 0.009 and **C.** p-value = 0.161. Change in vertical beambreaks is significant comparing

rhIGF1 treated and vehicle treated *Mecp2*$^{-/+}$ mice (p-value = 0.045), the same trend is observed in total beambreaks, but it becomes insignificant (p-value = 0.46).
Legend:
HET_IGF1 = Difference before and after rhIGF1 in *Mecp2*$^{-/+}$, HET_VEH = Difference before and after vehicle in *Mecp2*$^{-/+}$, WTF_VEH = Difference before and after rhIGF1 in *Mecp2*$^{+/+}$, WTF_IGF1 = Difference before and after vehicle in *Mecp2*$^{+/+}$, * Adjusted p-value < 0.05, NS = Non-Significant, tested using Kruskal-Wallis and post hoc Wilcox test unpaired, sample size (HET_IGF1 n =5, HET_VEH n = 4, WTF_IGF1 n = 7, WTF_VEH n = 7)

In male mice, there was a stronger effect of rhIGF1 treatment on locomotor activity. In vehicle treated *Mecp2*$^{-/y}$ mice, there were significant declines in horizontal and total activity and a slight increase in vertical activity compared to rhIGF1 treated *Mecp2*$^{-/y}$ mice.

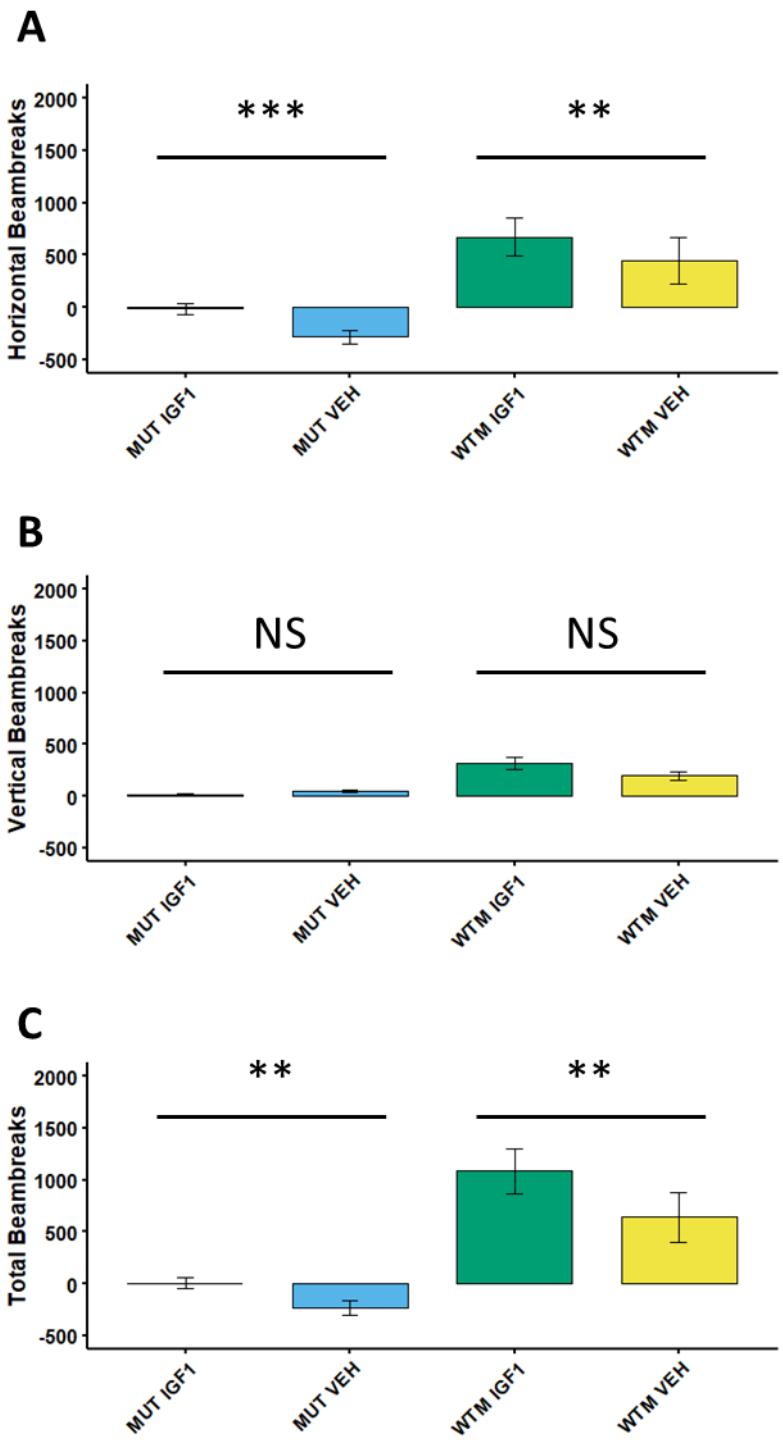

Figure 3.8 - Total and Horizontal Activity Decline in *Mecp2-/y* Mice was Prevented by rhIGF1 Treatment

Difference between beambreaks per hour as represented by bar-graph with mean ± SE of the mean. Kruskal-Wallis test results **A.** p-value = 2.71×10^{-07}, **B.** p-value = 1.05×10^{-07} and **C.** p-value = 3.30×10^{-08}.

Legend:

MUT_IGF1_T0T2 = Difference before and after rhIGF1 in *Mecp2*$^{-/y}$, MUT_VEH_T0T2 = Difference before and after vehicle in *Mecp2*$^{-/y}$, WTM_VEH_T0T2 = Difference before and after rhIGF1 in *Mecp2*$^{+/y}$, WTM_IGF1_T0T2 = Difference before and after vehicle in *Mecp2*$^{+/y}$, ** = Adjusted p-value < 0.05, NS = Non-Significant, tested using Kruskal-Wallis and post hoc Wilcox test unpaired, sample size (MUT_IGF1 n = 3, MUT_VEH n = 3, WTM_IGF1 n = 6, WTM_VEH n = 5)

The locomotor activity was plotted over time in hours to understand how the difference in activity was distributed throughout the night. This was done for both female and male treated mice before and after treatment. Total activity over the 12hr of the night was plotted and activity before and after treatment was compared.

In female mice in figure 3.9, there were no significant differences in locomotor activity before and after treatment in either *Mecp2*$^{-/+}$ or *Mecp2*$^{+/+}$ mice.

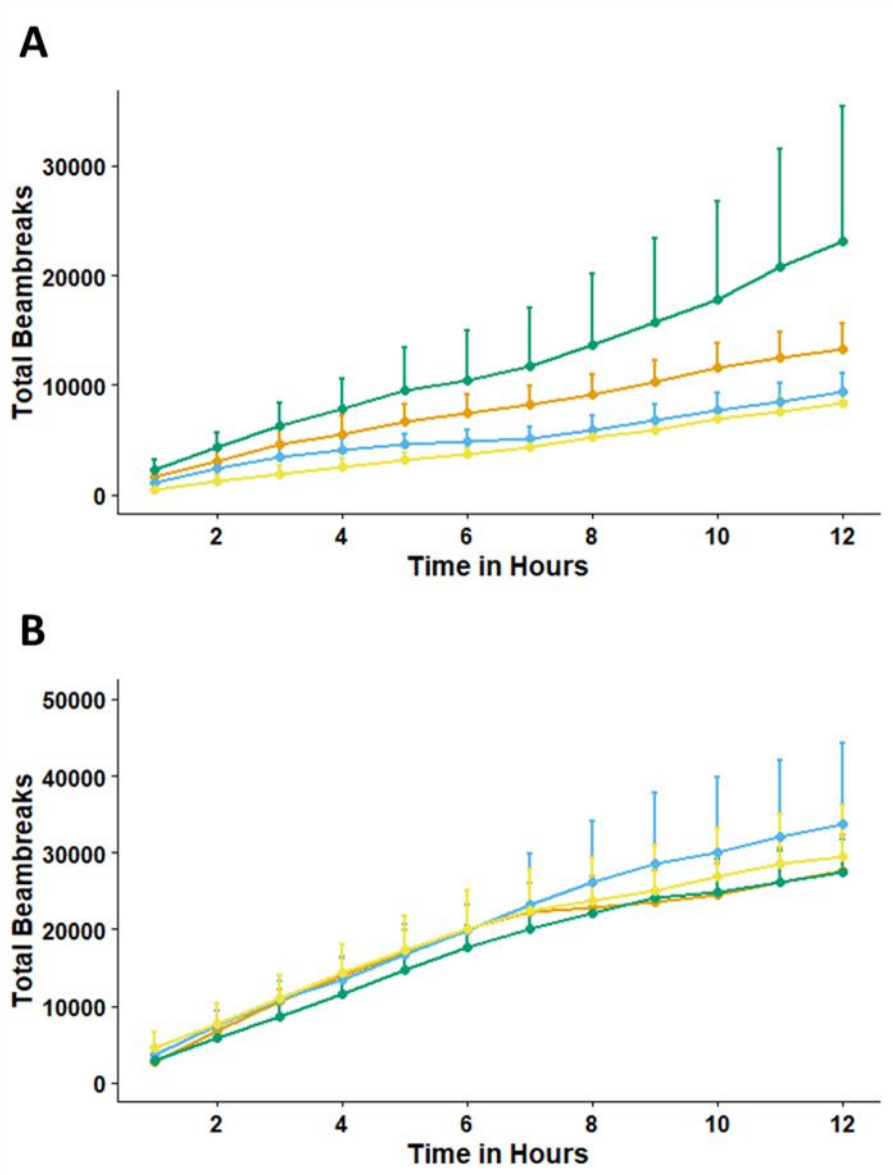

Figure 3.9 – Total Locomotor Activity over Time Before and After rhIGF1/Vehicle in Female Mice

Total beambreaks over time in hours were compared before and after treatment in *Mecp2*$^{-/+}$ (**A**) and *Mecp2*$^{+/+}$ (**B**) mice. There were no significant differences between these comparisons.

To test the variance by rank in this block designed experiment the Friedman test was used and post-hoc Wilcoxon paired test compared each hour comparing before and after treatment *Mecp2*$^{-/+}$ and *Mecp2*$^{+/+}$ mice, p-values were adjusted for multiple testing using Benjamini Hochberg method.

Legend:

IGF1 = rhIGF1 treated mice, VEH = Vehicle treated mice, Orange = Before rhIGF1, Blue = After rhIGF1, Green = Before VEH, Yellow = After VEH
Sample size: *Mecp2*$^{-/+}$ rhIGF1 treated (n = 5), *Mecp2*$^{-/+}$ VEH treated (n = 4), *Mecp2*$^{+/+}$ rhIGF1 treated (n = 7), *Mecp2*$^{+/+}$ VEH treated (n = 7)

In figure 3.10, there was significant increase in activity of *Mecp2*$^{+/y}$ mice treated with rhIGF1 before and after treatment throughout the night. There were also significant increases at hours 1 and 7 comparing vehicle treated *Mecp2*$^{+/y}$ mice before and after treatment. There were no significant differences comparing before and after treatment in *Mecp2*$^{-/y}$ mice.

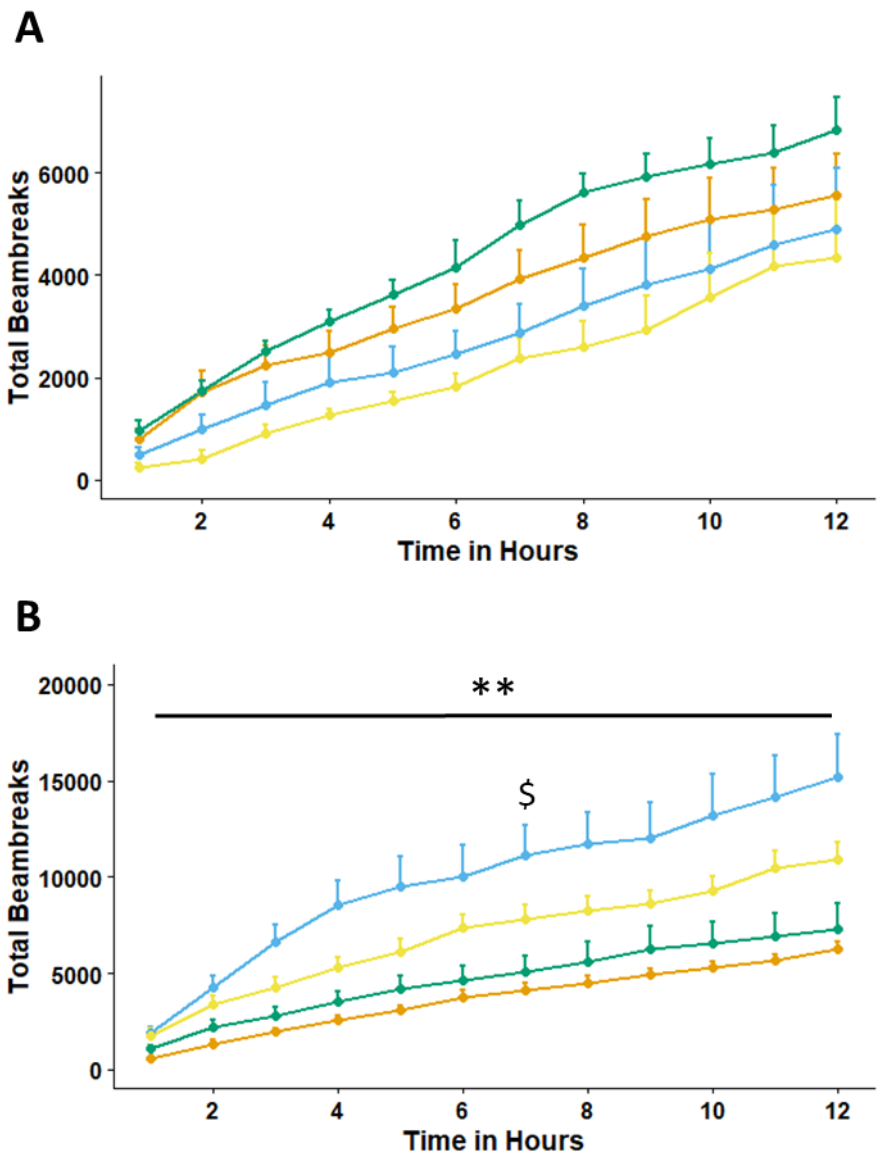

Figure 3.10 – Total Locomotor Activity Over Time Before and After rhIGF1/Vehicle in Male Mice

Total beambreaks over time in hours were compared before and after treatment in *Mecp2*$^{-/y}$ (**A**) and *Mecp2*$^{+/y}$ (**B**) mice. Only rhIGF1 treated *Mecp2*$^{+/y}$ mice showed a difference in locomotor movement overtime, where it increased significantly at all times. Given rhIGF1's role as an anabolic steroid and the period in development these mice are at this finding should be expected.

To test the variance by rank in this block designed experiment the Friedman test was used and post-hoc Wilcoxon paired test compared each hour comparing before and after treatment in *Mecp2*$^{-/y}$ and *Mecp2*$^{+/y}$ mice, p-values were adjusted for multiple testing using Benjamini Hochberg method.

Legend:

IGF1 = rhIGF1 treated mice, VEH = Vehicle treated mice, Orange = Before rhIGF1, Blue = After rhIGF1, Green = Before VEH, Yellow = After VEH

** = Adjusted p-value <0.005, comparing before and after rhIGF1 treatment in *Mecp2*$^{+/y}$ mice

$ = Adjusted p-value 0.05, comparing before and after VEH treatment in *Mecp2*$^{+/y}$ mice

Sample size: *Mecp2*$^{-/y}$ rhIGF1 treated (n = 3), *Mecp2*$^{-/y}$ VEH treated (n = 3), *Mecp2*$^{+/y}$ rhIGF1 treated (n = 6), *Mecp2*$^{+/y}$ VEH treated (n = 5)

The changes in *Mecp2*$^{+/y}$ mice can be explained by the normal growth and development that occurs during mouse adolescence. This growth was accelerated by rhIGF1 treatment in male *Mecp2*$^{+/y}$, mice but had no effect in already fully developed female *Mecp2*$^{+/+}$ mice, aged 4 to 5 months.

For *Mecp2*$^{-/+}$ and *Mecp2*$^{-/y}$ mice there was generally a larger decrease in vehicle treated mice before and after treatment compared to rhIGF1 treated mice, but there was no significant difference. Higher sample numbers are required to determine if this trend will continue and become significant.

Mecasermin/rhIGF1 is known to stimulate growth and has been used to treat growth failure associated with IGF1 deficiency [201]. Therefore, weight changes before and after treatment were compared in male and female mice in figure 3.11. There was no significant change in either *Mecp2*$^{-/+}$ or *Mecp2*$^{+/+}$ mice, while was a significant increases in both rhIGF1 and vehicle treated *Mecp2*$^{-/y}$ and *Mecp2*$^{+/y}$ mice.

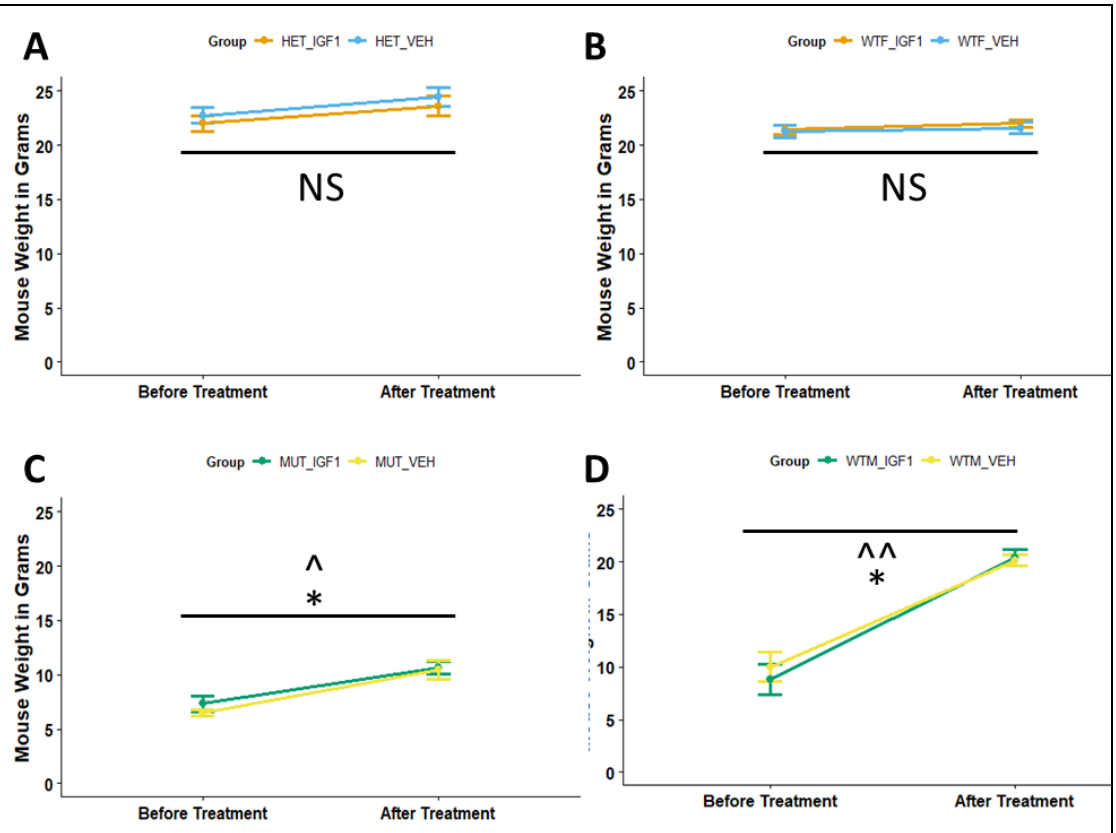

Figure 3.11 - Change in Weight of *Mecp2* Mice Before and After rhIGF1 and Vehicle Treatment

To test the variance in weight change before and after treatment in female and male mice, the Kruskal-Wallis test was used (p-value = 0.0881 for female mice **A -** and **B -** and p-value = 1.34 E-05 for male mice **C -** and **D-**), as Shapiro-Wilks test revealed these mice did not follow normal distribution (p-value = 0.0024 for females, p-value = 0.0007 male mice). For post-hoc testing the Wilcoxon paired test was used.

Legend:

* Adjusted p-value < 0.05, comparing before and after rhIGF1, ^ Adjusted p-value < 0.05, comparing before and after vehicle, ^^ Adjusted p-value <0.005, comparing before and after vehicle, Shapiro-Wilks test was used determine whether body weight followed normal distribution. Parametric testing using Kruskal-Wallis test followed by post-hoc Wilcoxon paired test.

A. HET_IGF1 = *Mecp2*$^{-/+}$ rhIGF1 treated mice (n=5), HET_VEH = *Mecp2*$^{-/+}$ vehicle treated mice (n=4), **B.** WTF_IGF1 = *Mecp2*$^{+/+}$ rhIGF1 treated mice (n=7), WTF_VEH = *Mecp2*$^{+/+}$ vehicle treated mice (n=7),

C. MUT_IGF1 = *Mecp2*$^{-/y}$ rhIGF1 treated mice (n=6), MUT_VEH = *Mecp2*$^{-/y}$ vehicle treated mice (n=4), **D.** WTF_IGF1 = *Mecp2*$^{+/y}$ rhIGF1 treated mice (n=5), WTF_VEH = *Mecp2*$^{+/y}$ vehicle treated mice (n=7)

3.2.5 High Throughput 3'DGE Sequencing in Female Mecp2 Mutant Mice Treated with rhIGF1

To understand the molecular changes associated with rhIGF1 or vehicle treatment in *Mecp2*$^{-/+}$ and *Mecp2*$^{+/+}$ mice, whole blood and cerebellum tissue was sequenced using High Throughput 3'DGE. By adding reference samples from a previous sequencing run conducted in this research group, it was possible to directly compare these results with a previous study examining the effects of rhIGF1 in *Mecp2*$^{-/y}$ mice.

After treatment and locomotor activity measurement, mice were culled by CO_2 euthanasia. Cerebellum and blood tissues were collected, and RNA was extracted. RNA concentration and integrity was measured using RNA Nano 6000 chips on a Bioanalyser system (Agilent Technologies). Due to each a limit of 24 samples per run for 3'DGE and the need for 2 reference samples, only 22 samples could be included. To accommodate for both cerebellum and blood samples to be measured, rhIGF1 treated *Mecp2*$^{+/+}$ blood samples were not included. Samples used for 3'DGE are listed in figure 3.1.

Sample Name	Genotype	Tissue	Treatment	RIN	Concentration (ng/µL)
HET_IGF1_CRB_1	*Mecp2*$^{-/+}$	CRB	IGF1	8	767
HET_IGF1_CRB_2	*Mecp2*$^{-/+}$	CRB	IGF1	8	368
HET_IGF1_CRB_4	*Mecp2*$^{-/+}$	CRB	IGF1	8	599
HET_IGF1_CRB_4	*Mecp2*$^{-/+}$	CRB	IGF1	9	637
HET_VEH_CRB_1	*Mecp2*$^{-/+}$	CRB	VEH	8	496
HET_VEH_CRB_2	*Mecp2*$^{-/+}$	CRB	VEH	8	451
HET_VEH_CRB_3	*Mecp2*$^{-/+}$	CRB	VEH	8	950
WTF_IGF1_CRB_1	*Mecp2*$^{+/+}$	CRB	IGF1	8	1015
WTF_IGF1_CRB_2	*Mecp2*$^{+/+}$	CRB	IGF1	9	1411
WTF_IGF1_CRB_3	*Mecp2*$^{+/+}$	CRB	IGF1	9	685
WTF_VEH_CRB_1	*Mecp2*$^{+/+}$	CRB	VEH	8	865

WTF_VEH_CRB_2	*Mecp2*$^{+/+}$	CRB	VEH	8	1213
WTF_VEH_CRB_3	*Mecp2*$^{+/+}$	CRB	VEH	8	724
HET_IGF1_BL_1	*Mecp2*$^{-/+}$	BL	IGF1	7	136
HET_IGF1_BL_2	*Mecp2*$^{-/+}$	BL	IGF1	8	48
HET_IGF1_BL_3	*Mecp2*$^{-/+}$	BL	IGF1	7	244
HET_VEH_BL_1	*Mecp2*$^{-/+}$	BL	VEH	7	54
HET_VEH_BL_2	*Mecp2*$^{-/+}$	BL	VEH	7	45
HET_VEH_BL_3	*Mecp2*$^{-/+}$	BL	VEH	7	139
WTF_VEH_BL_1	*Mecp2*$^{+/+}$	BL	VEH	9	19
WTF_VEH_BL_2	*Mecp2*$^{+/+}$	BL	VEH	8	49
WTF_VEH_BL_3	*Mecp2*$^{+/+}$	BL	VEH	7	15
REF_CRB	*Mecp2*$^{+/y}$	CRB	VEH	9	925
REF_BL	*Mecp2*$^{+/y}$	BL	VEH	8	391

Table 3.1 –Treated Female *Mecp2*$^{-/+}$ and *Mecp2*$^{+/+}$ Mice and Reference Samples included for High-Throughput 3' DGE Sequencing

Legend:

CRB = Cerebellum, BL = Blood, IGF1 = rhIGF1 treated mice, VEH = Vehicle treated mice, RIN = RNA Integrity Number

In figure 3.12, the distribution of Average $\log_2$ counts for each group has been plotted using. Distributions in each group were found to have similar overall profiles.

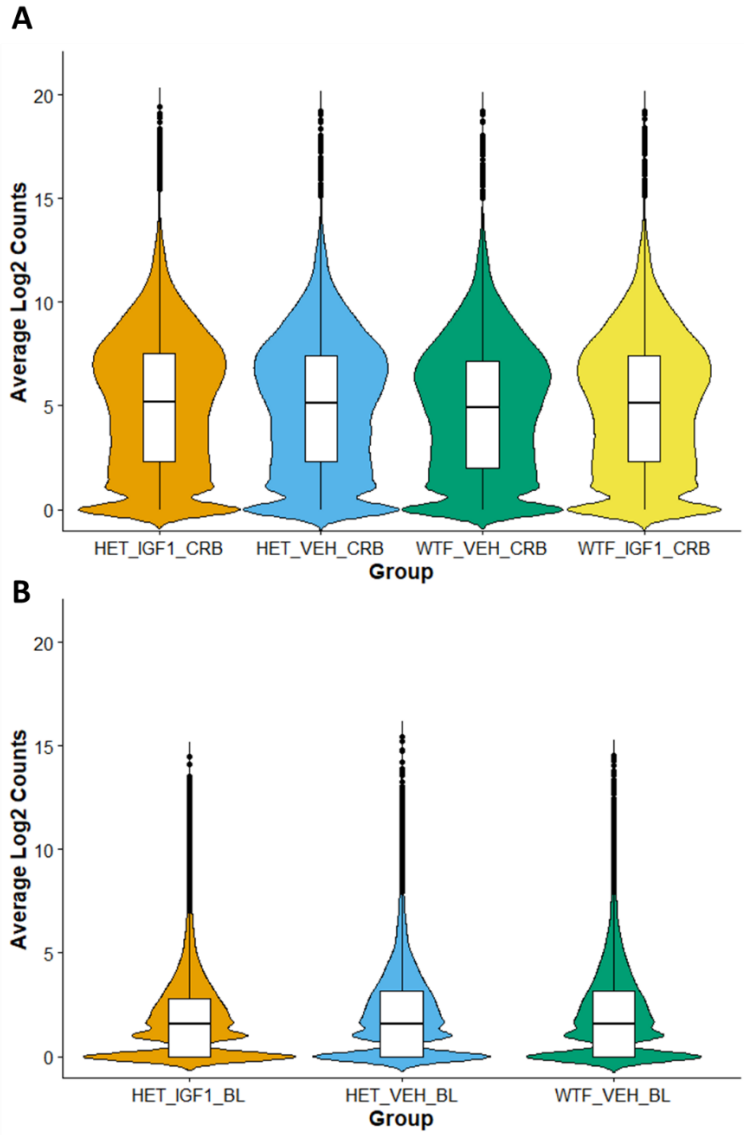

Figure 3.12 – Distribution of Average Log_2 Counts in Cerebellum and Blood of *Mecp2*$^{-/+}$ and *Mecp2*$^{+/+}$ Mice

A. Cerebellum tissue distributions, **B** Whole blood tissue distributions. These distribution were represented by violin plot with boxplot displaying mean interquartile range and whiskers displaying maximum and minimum values

Legend :

A. HET_IGF1_CRB = rhIGF1 treated *Mecp2*$^{-/+}$ cerebellum, HET_VEH = vehicle treated *Mecp2*$^{-/+}$ cerebellum, WTF_IGF1_CRB = rhIGF1 treated *Mecp2*$^{+/+}$ cerebellum, WTF_VEH_CRB = vehicle treated *Mecp2*$^{+/+}$ cerebellum. Sample size was n = 4, 3, 3, and 3 respectively.

B. HET_IGF1_BL = rhIGF1 treated *Mecp2*$^{-/+}$ blood, HET_VEH_BL = vehicle treated *Mecp2*$^{-/+}$ blood, WTF_VEH_BL = vehicle treated *Mecp2*$^{+/+}$ blood. Sample size was n = 3, 3, and 3 respectively.

Whole blood and cerebellum average counts per million (CPM) were plotted against each other in figure 3.13. All three comparisons found positive correlation between cerebellum and blood in rhIGF1 treated *Mecp2*$^{-/+}$ (R = 0.67), VEH treated *Mecp2*$^{-/+}$ (R = 0.68), and VEH treated *Mecp2*$^{+/+}$ (R = 0.66).

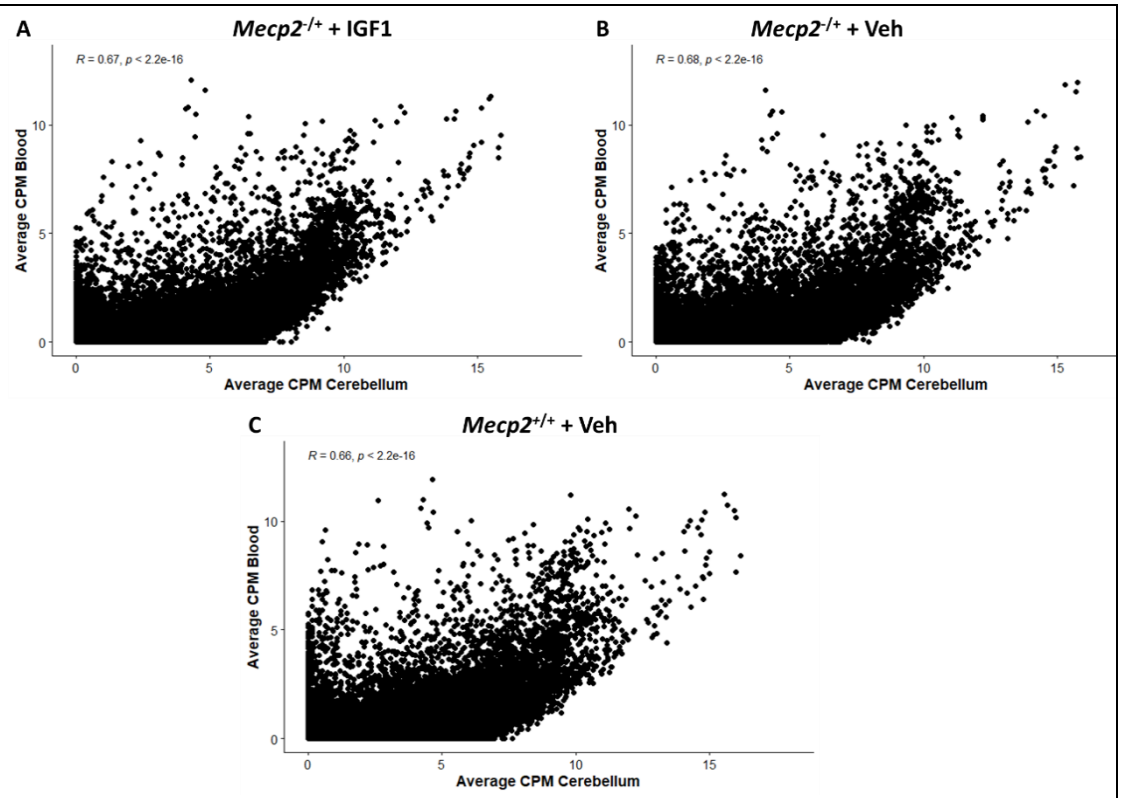

Figure 3.13 –Correlation of Cerebellum and Whole Blood Gene Expression in CPM

Correlation between gene expression in cerebellum and blood as represented by scatter plot of average CPM per gene in cerebellum against average CPM per gene in blood in *Mecp2*$^{-/+}$ treated with rhIGF1, *Mecp2*$^{-/+}$ treated with vehicle, and *Mecp2*$^{+/+}$ treated with vehicle. Each of these plots demonstrate significant correlation with R between 0.66 and 0.68.

Legend:

A *Mecp2*$^{-/+}$ treated with rhIGF1, **B** *Mecp2*$^{-/+}$ treated with VEH, **C** *Mecp2*$^{+/+}$ treated with VEH. Correlation was measured using Spearman's test with a sample size was n = 3, 3, and 3 respectively.

To determine differential gene expression (DGE), changes between the different experimental groups, the statistical R package, "empirical analysis of DGE in R" or EdgeR was used [165]. DGE was determined by QLFT and significant values were those with FDR corrected p-values < 0.05. Due to the restricted number of samples per run allowed by the sequencing facility the rhIGF1 treated *Mecp2*$^{+/+}$ blood samples were not included. Five meaningful comparisons for DGE were calculated, each of these asked a specific biological question. These comparisons were:

1. IGF1 treated *Mecp2*$^{-/+}$ vs. VEH treated *Mecp2*$^{-/+}$
2. VEH treated *Mecp2*$^{-/+}$ vs. VEH treated *Mecp2*$^{+/+}$
3. IGF1 treated *Mecp2*$^{-/+}$ vs. VEH treated *Mecp2*$^{+/+}$
4. IGF1 treated *Mecp2*$^{-/+}$ vs. IGF1 treated *Mecp2*$^{+/+}$
5. IGF1 treated *Mecp2*$^{+/+}$ vs. VEH treated *Mecp2*$^{+/+}$

The results of these comparisons in female mice are plotted in figure 3.14.

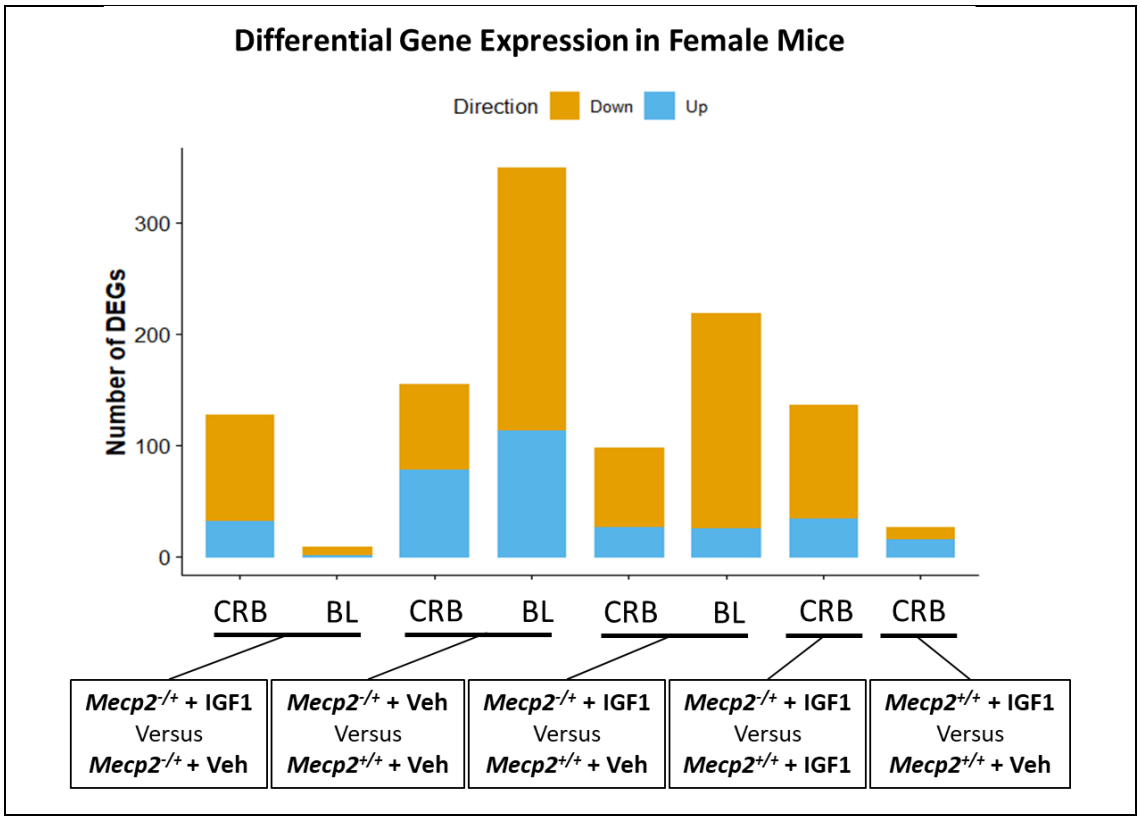

Figure 3.14 – DGE in Cerebellum and Blood of rhIGF1 and Vehicle treated *Mecp2*$^{-/+}$ and *Mecp2*$^{+/+}$ Mice

DEG were considered significant with FDR corrected p-Value <0.05. IGF1 treated *Mecp2*$^{-/+}$ versus VEH treated *Mecp2*$^{-/+}$ in cerebellum had a total of 127 genes differentially expressed (31 up-regulated, 96 down-regulated) and in blood a total of 8 genes differentially expressed (1 up-regulated and 7 down-regulated). VEH treated *Mecp2*$^{-/+}$ versus VEH treated *Mecp2*$^{+/+}$ in cerebellum had a total of 155 genes differentially expressed (78 up-regulated, 77 down-regulated) and in blood a total of 349 genes differentially expressed (113 up-regulated and 236 down-regulated). IGF1 treated *Mecp2*$^{-/+}$ versus VEH treated *Mecp2*$^{+/+}$ in cerebellum had a total of 97 genes differentially expressed (26 up-regulated, 71 down-regulated) and in blood had a total of 218 genes differentially expressed (25 up-regulated and 193 down-regulated). IGF1 treated *Mecp2*$^{-/+}$ versus IGF1 treated *Mecp2*$^{+/+}$ in cerebellum a total of 136 genes differentially expressed (34 up-regulated, 102 down-regulated). IGF1 treated *Mecp2*$^{+/+}$ versus VEH treated *Mecp2*$^{+/+}$ DGE in cerebellum had a total of 26 genes differentially expressed (15 up-regulated, 11 down-regulated)

Legend:

DEG = Differentially Expressed Genes, IGF1 = rhIGF1 treated mice, VEH = Vehicle treated mice, CRB = Cerebellum, BL = Blood, Down = Down-Regulated, Up = Up-Regulated, IGF1+*Mecp2*$^{-/+}$ versus VEH+*Mecp2*$^{-/+}$ in cerebellum (n = 4 vs. 3), IGF1+*Mecp2*$^{-/+}$ versus VEH+*Mecp2*$^{-/+}$ in blood (n = 3 vs. 3), VEH+*Mecp2*$^{-/+}$ versus VEH+*Mecp2*$^{-/+}$ in cerebellum (n = 3 vs. 3), VEH+*Mecp2*$^{-/+}$ versus VEH+*Mecp2*$^{-/+}$ in blood (n = 3 vs. 3), IGF1+*Mecp2*$^{-/+}$ versus VEH+*Mecp2*$^{+/+}$ in cerebellum (n = 4 vs. 3), IGF1+*Mecp2*$^{-/+}$ versus VEH+*Mecp2*$^{+/+}$ in blood (n = 3 vs. 3), IGF1+*Mecp2*$^{-/+}$ versus IGF1+*Mecp2*$^{+/+}$ in cerebellum (n = 4 vs. 3), IGF1+*Mecp2*$^{+/+}$ versus VEH+*Mecp2*$^{+/+}$ in cerebellum (n = 3 vs. 3). DEG was determined using QLFT in edgeR.

Previous work conducted in this group by Albert Sanfeliu Bosch used the same 3'DGE sequencing technique to measure gene expression in cerebellum and blood samples of male *Mecp2* mice. Two RNA reference samples from this previous experiment were included in this sequencing run along with the *Mecp2*$^{-/+}$ treated mice samples. To determine whether the two studies could be compared, a Spearman correlation test was

conducted on the reference samples in both sequencing runs. Both blood and cerebellum reference samples highly correlated across experiments, R = 0.87 (p-value < 2.2 x10^{-16}) and R = 0.86 (p-value < 2.2 x10^{-16}) respectively. DEG analysis was conducted using the same comparisons as described in female mice. The results of these analyses are shown in figure 3.15.

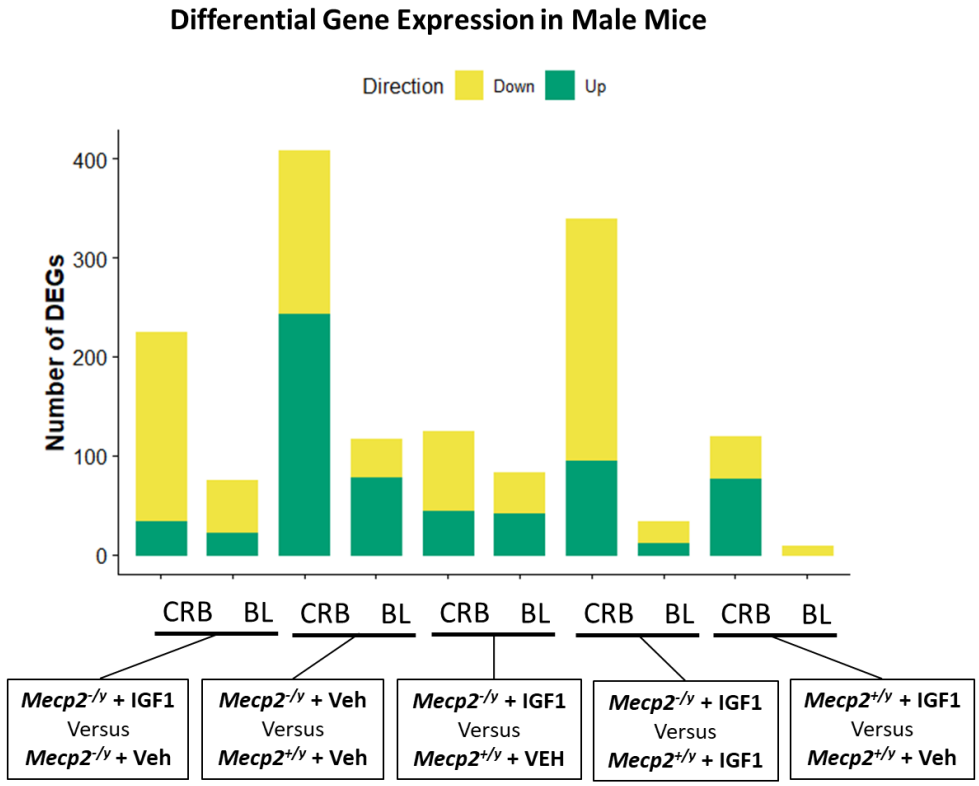

Figure 3.15 - DGE in Cerebellum and Blood of rhIGF1 and Vehicle treated *Mecp2*$^{-/y}$ and *Mecp2*$^{+/y}$ Mice

DEG were considered significant with FDR corrected p-Value <0.05.

IGF1 treated *Mecp2*$^{-/y}$ versus VEH treated *Mecp2*$^{-/y}$ in cerebellum had a total of 225 genes differentially expressed (34 up-regulated, 191 down-regulated) and in blood a total of 75 genes differentially expressed (22 up-regulated and 53 down-regulated).

VEH treated *Mecp2*$^{-/y}$ versus VEH treated *Mecp2*$^{+/y}$ in cerebellum had a total of 408 genes differentially expressed (243 up-regulated, 165 down-regulated) and in blood a total of 117 genes differentially expressed (78 up-regulated and 39 down-regulated).

IGF1 treated *Mecp2*$^{-/y}$ versus VEH treated *Mecp2*$^{+/y}$ in cerebellum had a total of 125 genes differentially expressed (44 up-regulated, 81 down-regulated) and in blood a total of 83 genes differentially expressed (41 up-regulated and 42 down-regulated).

IGF1 treated *Mecp2*$^{-/y}$ versus IGF1 treated *Mecp2*$^{+/y}$ in cerebellum had a total of 339 genes differentially expressed (94 up-regulated, 245 down-regulated) and in blood a total of 34 genes differentially expressed (11 up-regulated, 23 down-regulated). IGF1 treated *Mecp2*$^{+/y}$ versus VEH treated *Mecp2+/y* in cerebellum had a total of 119 genes differentially expressed (77 up-regulated, 42 down-regulated) and in blood 9 genes differentially expressed (9 down-regulated).

Legend:

DEG = Differentially Expressed Genes, IGF1 = rhIGF1 Treated Mice, VEH = Vehicle treated mice, Down = Down-Regulated, Up = Up-Regulated, IGF1+*Mecp2*$^{-/y}$ versus VEH+*Mecp2*$^{-/y}$ in cerebellum (n = 8 vs. 9), IGF1+*Mecp2*$^{-/y}$ versus VEH+*Mecp2*$^{-/y}$ in blood (n = 8 vs. 9), VEH+*Mecp2*$^{-/y}$ versus VEH+*Mecp2*$^{-/y}$ in cerebellum (n = 9 vs. 9), VEH+*Mecp2*$^{-/y}$ versus VEH+*Mecp2*$^{-/y}$ in blood (n = 9 vs. 9), IGF1+*Mecp2*$^{-/y}$ versus VEH+*Mecp2*$^{+/y}$ in cerebellum (n = 8 vs. 9), IGF1+*Mecp2*$^{-/y}$ versus VEH+*Mecp2*$^{+/y}$ in blood (n = 8 vs. 9), IGF1+*Mecp2*$^{-/y}$ versus IGF1+*Mecp2*$^{+/y}$ in cerebellum (n = 8 vs. 9), IGF1+*Mecp2*$^{-/y}$ versus IGF1+*Mecp2*$^{+/y}$ in blood (n = 8 vs. 9), IGF1+*Mecp2*$^{+/y}$ versus VEH+*Mecp2*$^{+/y}$ in cerebellum (n = 9 vs. 9), IGF1+*Mecp2*$^{+/y}$ versus VEH+*Mecp2*$^{+/y}$ in blood (n = 8 vs 9). DEG was determined using QLFT in edgeR.

3.2.6 Mecp2 Mutant versus WT

The comparisons between vehicle treated *Mecp2*-null and –heterozygous mice with vehicle treated WT mice, examined the effects of *Mecp2* mutation. The top significant 10 genes for both the cerebellum and blood are displayed in table 3.2.

In female mice, 155 genes in the cerebellum and 349 genes in blood were differentially expressed. In the cerebellum 78 genes were up-regulated and 77 genes were down-regulated and in blood 113 genes were up-regulated and 236 genes were down-regulated in *Mecp2*$^{-/+}$ relative to *Mecp2*$^{+/+}$ (See figure 3.14). These results did not suggest that *Mecp2* was specifically acting as a repressor or activator of gene transcription in the cerebellum. However, in blood, 66% of DEG were down-regulated and 33% of DEG were up-regulated suggesting that *Mecp2* may function more as a transcriptional activator in blood tissue.

In male mice, 408 genes in the cerebellum and 117 genes in blood were differentially expressed. In the cerebellum 243 genes were up-regulated and 165 genes were down-regulated in *Mecp2*$^{-/y}$ relative to *Mecp2*$^{+/y}$ (See figure 3.15). The proportion of activation to repression of DGE was 59% to 41% in the cerebellum and 67% to 33% in the blood. The proportion of DGE transcription was the same in the blood of female and male mice.

Of these DEG, 11 genes in the cerebellum were overlapping in the same direction in male and female mice. These genes were *AW551984*, *Calcb*, *Klk6*, *Meis2*, *Mog*, *Pdlim2*, *Resp18*, *Rims3*, *Slc5a7*, *Sncg*, and *Zcchc12*. In the blood there were 51 genes that overlapped between male and female mice. Of these 51 genes, only 3 genes were expressed in the same direction. These were *S100a8*, *S100a9* and *Retnlg* which were all up-regulated in *Mecp2* mutant mice.

	Female			**Male**		
Tissue	**Gene**	**LogFC**	**FDR**	**Gene**	**LogFC**	**FDR**
CRB	*Rpl31-ps8*	-11.16	3.55E-86	*Mir6236*	2.24	5.13E-29
	Crym	4.89	1.65E-39	*Usp1*	2.25	2.55E-23
	Lamp5	-2.25	2.39E-26	*Kcnj13*	-1.14	2.42E-14
	Neurod6	2.19	6.49E-24	*Fabp7*	-0.87	4.09E-14
	Calcb	-5.55	1.84E-22	*Scg2*	-0.75	6.35E-12
	Sncg	-2.21	2.13E-22	*Mecp2*	-2.13	2.10E-11
	Ptk2b	2.92	5.95E-22	*Klk6*	-1.07	4.61E-11
	Calca	-2.69	6.29E-21	*Snrpb*	0.84	7.44E-11
	Gh	-2.21	1.08E-20	*Etnppl*	0.84	1.39E-10
	Spink8	3.71	1.01E-19	*Acbd3*	1.51	1.06E-09
BL	*Mup3*	-6.54	2.62E-16	*Alb*	4.77	7.30E-31
	Serpina1d	-7.61	2.62E-16	*Apoa2*	4.63	4.12E-25
	Serpina1b	-6.45	5.51E-15	*Ttr*	4.78	2.58E-21
	Serpina1a	-6.48	1.42E-14	*Apoc1*	4.04	2.77E-13
	Mup19	-6.63	3.39E-14	*Irf7*	-2.73	3.17E-13
	Mup14	-5.90	9.81E-14	*Saa3*	2.30	7.46E-13
	Hpx	-6.84	4.36E-13	*Gzma*	-2.87	2.16E-11
	Mup11	-6.27	1.08E-12	*Cxcl13*	2.65	2.35E-11

	Mup9	-9.02	1.47E-12	*Wfdc17*	2.04	4.70E-11
	Serpina1c	-5.51	2.02E-12	*Ccl5*	-2.10	1.94E-10

Table 3.2 - Top Significant DEGs in the Cerebellum and Blood of Vehicle Treated *Mecp2*$^{-/+}$ versus *Mecp2*$^{+/+}$ Mice

Top DEG were determined by FDR corrected p-value significance, the top 10 genes were included.

Legend:

CRB = Cerebellum, BL = Blood, LogFC = Log_2 fold change in Vehicle treated *Mecp2*$^{-/+}$ relative to *Mecp2*$^{+/+}$, FDR = False Discovery Rate

To understand gene expression in the context of biological mechanisms, GO and Reactome analysis was used to determine over-represented ontologies and pathways in the DEG. GO analysis revealed a total of 206 ontologies significantly over-represented in the cerebellum and a total of 506 ontologies significantly over-represented in the blood in female mice. There were 17 and 322 ontologies over-represented in the cerebellum and blood in male mice respectively. The top 10 significant ontologies have been reported in table 3.3 and all ontologies have been reported in Appendix II.

Tissue	**Female**		**Male**	
CRB	**Gene Set**	**FDR**	**Gene Set**	**FDR**
	Behavior	2.65E-10	Sensory perception of smell	7.02E-05
	Regulation of trans-synaptic signaling	2.71E-08	Sensory perception of chemical stimulus	9.80E-05
	Modulation of chemical synaptic transmission	3.92E-08	Metabolic process	5.65E-03
	Positive regulation of synaptic transmission	4.50E-07	Cellular metabolic process	6.74E-03
	Regulation of transport	2.34E-06	Cellular process	1.35E-02
	Response to inorganic substance	2.77E-06	Response to organonitrogen compound	1.38E-02

	Anterograde trans-synaptic signaling	3.56E-06	Organonitrogen compound metabolic process	1.51E-02
	Chemical synaptic transmission	4.07E-06	Positive regulation of cellular process	1.87E-02
	Regulation of biological quality	4.52E-06	Response to nitrogen compound	2.25E-02
	Regulation of secretion by cell	4.68E-06	Regulation of cellular component	2.80E-02
BL	Small molecule metabolic process	2.73E-43	Regulation of hydrolase activity	7.42E-14
	Organic acid metabolic process	4.31E-43	Negative regulation of hydrolase activity	5.36E-12
	Oxoacid metabolic process	1.50E-41	Response to chemical	8.21E-11
	Carboxylic acid metabolic process	2.21E-41	Regulation of catalytic activity	4.17E-10
	Lipid metabolic process	5.11E-28	Negative regulation of catalytic activity	1.71E-09
	Monocarboxylic acid metabolic process	1.91E-24	Biological process involved in interspecies interaction between organisms	6.08E-09
	Cellular lipid metabolic process	4.71E-24	Response to biotic stimulus	7.72E-09
	Blood coagulation	1.31E-23	Small molecule metabolic process	1.39E-08
	Coagulation	1.48E-23	Response to external biotic stimulus	1.43E-08
	Hemostasis	1.85E-23	Negative regulation of peptidase activity	1.52E-08

Table 3.3 - Top Significant Ontologies Over-represented in the Cerebellum and Blood of Vehicle Treated *Mecp2*$^{-/+}$ versus *Mecp2*$^{+/+}$ Mice

Legend:

CRB = Cerebellum, BL = Blood, FDR = False Discovery Rate

Reactome pathway analysis found 37 pathways significantly over-represented in the cerebellum and 85 pathways significantly over-represented in the blood in females. In male mice, 12 and 72 pathways were over-represented in the cerebellum and blood respectively. The top 10 significant pathways have been reported in table 3.4 and all ontologies have been reported in Appendix II.

Notably, Transcriptional Regulation by MeCP2 was the top significant pathway in the cerebellum and Regulation of IGF transport and uptake by IGFBPs was in the top most significant pathway in the blood in both male and female. 44 of these pathways were found in both male and female mouse blood including, Platelet degranulation, Neutrophil degranulation, and MAP2K and MAPK Activation.

	Female		**Male**	
Tissue	**Gene Set**	**FDR**	**Gene Set**	**FDR**
CRB	Transcriptional Regulation by MECP2	7.35E-07	Transcriptional Regulation by MECP2	6.21E-07
	GPCR downstream signalling	7.07E-06	Cellular responses to stimuli	8.24E-06
	Signaling by GPCR	7.07E-06	Cellular responses to stress	2.00E-05
	GPCR ligand binding	5.82E-05	MECP2 regulates transcription of neuronal ligands	2.61E-04
	Long-term potentiation	1.98E-04	FOXO-mediated transcription	0.019158112
	Peptide ligand-binding receptors	5.75E-04	Aggrephagy	0.030455082
	Signal Transduction	5.75E-04	Translation	0.033761675
	Unblocking of NMDA receptors, glutamate binding and activation	0.00159278	Loss of MECP2 binding ability to 5mC-DNA	0.033761675
	Negative regulation of NMDA receptor-mediated neuronal transmission	0.00159278	Metabolism of proteins	0.033761675

	Class B/2 (Secretin family receptors)	0.00217 0402	Macroautophagy	0.035545 315
BL	Formation of Fibrin Clot (Clotting Cascade)	1.65E-14	Interferon alpha/beta signaling	1.88E-10
	Response to elevated platelet cytosolic Ca2+	1.65E-14	Post-translational protein phosphorylation	5.58E-09
	Platelet activation, signaling and aggregation	1.65E-14	Plasma lipoprotein assembly	8.88E-09
	Platelet degranulation	1.65E-14	Regulation of Insulin-like Growth Factor (IGF) transport and uptake by Insulin-like Growth Factor Binding Proteins (IGFBPs)	1.25E-08
	Hemostasis	1.65E-14	Plasma lipoprotein assembly, remodeling, and clearance	1.25E-08
	Regulation of Insulin-like Growth Factor (IGF) transport and uptake by Insulin-like Growth Factor Binding Proteins (IGFBPs)	2.72E-10	Immune System	1.03E-07
	Common Pathway of Fibrin Clot Formation	6.03E-10	Chylomicron remodeling	1.65E-07
	Post-translational protein phosphorylation	1.09E-08	Interferon Signaling	1.65E-07
	Intrinsic Pathway of Fibrin Clot Formation	1.57E-08	Plasma lipoprotein remodeling	3.74E-07
	Complement cascade	2.61E-07	Cytokine Signaling in Immune system	1.60E-06

Table 3.4 - Top Significant Pathways Over-represented in the Cerebellum and Blood of Vehicle Treated *Mecp2*$^{-/+}$ versus *Mecp2*$^{+/+}$ Mice

Legend:

CRB = Cerebellum, BL = Blood, LogFC = Log_2 fold change in Vehicle treated *Mecp2*-null and -heterozygous relative to Vehicle treated WT, FDR = False Discovery Rate

3.2.7 rhIGF1 treated versus Vehicle treated Mecp2 Mutant Mice

This comparison assessed what the effects of rhIGF1 were in *Mecp2*-null and –heterozygous mice. The top significant 10 genes for both the cerebellum and blood are displayed in table 3.5.

In female mice, 127 genes in the cerebellum and 8 genes in blood were differentially expressed. In the cerebellum, 31 genes were up-regulated and 96 genes were down-regulated and in blood 1 gene was up-regulated and 7 genes were down-regulated in rhIGF1 treated mice relative to vehicle treated mice. In male mice, 225 and 75 genes were differentially expressed in the cerebellum and blood respectively. 34 and 22 genes were up-regulated, and 191 and 53 genes were down-regulated in the cerebellum and blood respectively.

	Female			**Male**		
Tissue	**Gene**	**LogFC**	**FDR**	**Gene**	**LogFC**	**FDR**
CRB	*Crym*	-6.91	5.54E-71	*Mir6236*	2.24	5.13E-29
	Rpl31-ps8	9.93	1.11E-44	*Usp1*	2.25	2.55E-23
	Spink8	-5.30	1.64E-37	*Kcnj13*	-1.14	2.42E-14
	Gm4767	-9.31	6.77E-33	*Fabp7*	-0.87	4.09E-14
	Neurod6	-2.10	5.51E-31	*Scg2*	-0.75	6.35E-12
	Ptk2b	-2.82	8.02E-27	*Mecp2*	-2.13	2.10E-11
	Pcdha5	8.85	2.41E-22	*Klk6*	-1.07	4.61E-11
	Camk2a	-2.17	3.03E-22	*Snrpb*	0.84	7.44E-11
	Foxg1	-5.69	2.31E-19	*Etnppl*	0.84	1.39E-10
	Scn3b	-1.88	1.91E-18	*Acbd3*	1.51	1.06E-09
BL	*Alb*	-3.29	2.03E-04	*Alb*	-8.29	8.92E-30
	Fabp1	-4.58	5.01E-04	*Apoa2*	-7.76	1.86E-23
	Rps16-ps2	-6.89	9.03E-04	*Mir6236*	2.92	5.30E-16
	Apoa2	-3.32	1.32E-03	*Ttr*	-4.67	2.13E-13
	Ccl5	-2.18	1.32E-03	*Saa3*	-2.69	1.63E-12
	Rps13-ps1	3.04	3.56E-03	*Apoc1*	-4.36	5.28E-09

	Gm10240	-2.01	1.37E-02	*Apoa1*	-6.12	6.37E-09
	Ipo11	-2.11	4.56E-02	*Ahsg*	-5.91	1.12E-07
	NA	NA	NA	*Wfdc17*	-1.79	5.56E-06
	NA	NA	NA	*Fabp1*	-5.58	6.44E-06

Table 3.5 – Top Significant DEGs in the Cerebellum and Blood of rhIGF1 Treated versus Vehicle Treated in *Mecp2* –Null and –Heterozygous Mice

Legend:

CRB = Cerebellum, BL = Blood, LogFC = Log_2 fold change in rhIGF1 treated *Mecp2*-null and -heterozygous relative to Vehicle treated, FDR = False Discovery Rate

In female mice, GO analysis found a total of 92 ontologies in the cerebellum and there were no significant ontologies in blood. In male mice, 21 and 186 ontologies were over-represented in the cerebellum and blood respectively. The top 10 significant ontologies have been reported in table 3.6 and all ontologies have been reported in Appendix II.

	Female		**Male**	
Tissue	**Gene Set**	**FDR**	**Gene Set**	**FDR**
CRB	Behavior	3.04E-08	Metabolic process	3.97E-06
	Regulation of ion transport	9.02E-05	Cellular metabolic process	7.77E-06
	Nervous system development	9.24E-05	Organonitrogen compound metabolic process	1.18E-04
	generation of neurons	1.42E-04	Nitrogen compound metabolic process	3.56E-04
	Regulation of localization	2.94E-04	Primary metabolic process	1.23E-03
	Neurogenesis	5.04E-04	Organic substance metabolic process	1.46E-03
	Anterograde trans-synaptic signaling	5.82E-04	Cellular catabolic process	1.37E-02
	Regulation of synaptic plasticity	6.08E-04	Catabolic process	1.51E-02

	Chemical synaptic transmission	6.47E-04	Sensory perception of chemical stimulus	2.06E-02
	Cognition	7.07E-04	ATP metabolic process	2.08E-02
BL	-	-	Regulation of hydrolase activity	1.68E-06
	-	-	Lipid transport	1.79E-06
	-	-	Negative regulation of hydrolase activity	2.47E-06
	-	-	Response to inorganic substance	2.95E-06
	-	-	Regulation of plasma lipoprotein particle levels	3.06E-06
	-	-	Lipid localization	8.71E-06
	-	-	Cholesterol transport	9.95E-06
	-	-	Sterol transport	1.28E-05
	-	-	Response to chemical	1.29E-05
	-	-	Plasma lipoprotein particle organization	1.68E-06

Table 3.6 - Top Significant Ontologies Over-represented in rhIGF1 Treated versus Vehicle Treated in *Mecp2* –Null and –Heterozygous Mice

Legend:

CRB = Cerebellum, BL = Blood, FDR = False Discovery Rate

Reactome pathway analysis found 14 pathways were over-represented in the cerebellum and 15 pathways in the blood in female mice. In male mice, 93 and 32 pathways were over-represented in the cerebellum and blood of male mice respectively. The top significant 10 pathways have been reported in table 3.7 and all pathways have been reported in Appendix II.

No pathways in the cerebellum and 9 pathways in the blood were overlapping between female and male mice. These overlapping pathways in blood, included regulation of IGF transport and uptake by IGFBPs, post-translational protein phosphorylation and high-density lipoprotein remodelling.

	Female		Male	
Tissue	**Gene Set**	**FDR**	**Gene Set**	**FDR**
CRB	Signaling by GPCR	4.08E-05	NGF-stimulated transcription	1.23E-02
	GPCR downstream signalling	4.08E-05	Nuclear Events (kinase and transcription factor activation)	2.77E-02
	GPCR ligand binding	1.25E-04	Cellular responses to stimuli	2.77E-02
	Peptide ligand-binding receptors	1.49E-03	RHOH GTPase cycle	2.77E-02
	Transcriptional Regulation by MECP2	1.49E-03	Nuclear Receptor transcription pathway	2.77E-02
	Calcitonin-like ligand receptors	2.01E-03	Hh mutants are degraded by ERAD	2.77E-02
	Class B/2 (Secretin family receptors)	1.05E-02	Hh mutants abrogate ligand secretion	2.77E-02
	RUNX3 regulates RUNX1-mediated transcription	1.05E-02	Downstream signaling events of B Cell Receptor (BCR)	2.77E-02
	Class A/1 (Rhodopsin-like receptors)	1.80E-02	Cellular responses to stress	2.77E-02
	Long-term potentiation	2.31E-02	Defective CFTR causes cystic fibrosis	2.77E-02
BL	Formation of Fibrin Clot (Clotting Cascade)	1.65E-14	Plasma lipoprotein assembly	1.98E-06
	Response to elevated platelet cytosolic Ca2+	1.65E-14	Plasma lipoprotein assembly, remodeling, and clearance	5.32E-05
	Platelet activation, signaling and aggregation	1.65E-14	Chylomicron assembly	6.58E-05
	Platelet degranulation	1.65E-14	Chylomicron remodeling	9.25E-05
	Hemostasis	1.65E-14	Retinoid metabolism and transport	9.25E-05

	Regulation of Insulin-like Growth Factor (IGF) transport and uptake by Insulin-like Growth Factor Binding Proteins (IGFBPs)	2.72E-10	Metabolism of fat-soluble vitamins	1.44E-04
	Common Pathway of Fibrin Clot Formation	6.03E-10	Platelet degranulation	1.44E-04
	Post-translational protein phosphorylation	1.09E-08	Response to elevated platelet cytosolic Ca2+	1.76E-04
	Intrinsic Pathway of Fibrin Clot Formation	1.57E-08	Plasma lipoprotein remodeling	2.00E-04
	Complement cascade	2.61E-07	Post-translational protein phosphorylation	3.00E-04

Table 3.7 - Top Significant Pathways Over-represented in rhIGF1 Treated Vehicle Treated in *Mecp2* –Null and –Heterozygous Mice

Legend:

CRB = Cerebellum, BL = Blood, FDR = False Discovery Rate

3.2.8 rhIGF1 treated Mecp2-null and Mecp2-heterozygous mice versus Vehicle Treated WT Mice

rhIGF1 treated *Mecp2* –null and – heterozygous mice were compared to vehicle treated *Mecp2* WT mice, to assess whether rhIGF1 treatment returned mutant mice to WT levels of expression.

There were 97 genes in the cerebellum and 218 genes in blood were considered differentially expressed in female mice. In the cerebellum 26 genes were up-regulated and 71 genes were down-regulated, and in blood 25 genes were up-regulated and 193 genes were down-regulated in rhIGF1 treated $Mecp2^{-/+}$ relative to vehicle treated $Mecp2^{+/+}$. In male mice, 125 and 83 genes were differentially expressed in the cerebellum and blood of male mice. 44 and 41 genes were up-regulated, and 81 and 42 genes were down-regulated in the cerebellum and blood respectively. The top significant results of these analyses are listed in table 3.8 and the full list is reported in Appendix II.

	Female			Male		
Tissue	**Gene**	**LogFC**	**FDR**	**Gene**	**LogFC**	**FDR**
Cerebellum	*Gm14648*	-2.52	1.47E-35	*Fabp7*	-0.91	4.28E-15
	Gm4767	-8.99	6.98E-29	*Etnppl*	1.01	4.88E-15
	Gm32687	8.60	3.36E-18	*Sgk1*	0.95	4.88E-15
	Sncg	-1.50	4.75E-14	*Kcnj13*	-0.97	5.83E-12
	Lamp5	-1.21	3.02E-10	*Gh*	1.90	4.26E-10
	Rpl31-ps8	-1.41	8.05E-10	*Mt2*	0.73	1.12E-09
	Ighm	-1.59	1.29E-09	*Alb*	-1.70	5.73E-08
	Calca	-1.50	1.29E-09	*Klk6*	-0.95	8.48E-08
	Gh	-1.28	1.77E-09	*Sst*	-1.35	8.52E-08
	Gm10095	-1.05	1.63E-08	*Mecp2*	-1.73	4.83E-07
Blood	*Fabp1*	-8.97	1.81E-18	*Mir6236*	3.19	1.13E-22
	Mup3	-8.04	5.06E-18	*Arf5*	2.00	9.26E-10
	Alb	-7.87	5.06E-18	*Gzma*	-2.67	1.64E-07
	Apoa2	-7.90	9.16E-18	*Ifi27l2a*	-2.12	4.14E-06
	Apoc3	-8.35	1.42E-16	*Nkg7*	-2.25	5.53E-06
	Serpina1c	-8.31	1.72E-16	*Ccl5*	-1.74	5.53E-06
	Mup14	-7.29	3.57E-16	*Sftpc*	-5.57	6.76E-05
	Serpina1b	-7.81	1.09E-15	*E2f2*	1.39	2.52E-04
	Ahsg	-10.24	1.49E-15	*Pkn2*	1.63	2.52E-04
	Serpina3k	-10.22	1.77E-15	*Slc25a37*	1.21	8.37E-04

Table 3.8 – Top Significant DEGs in the Cerebellum and Blood of rhIGF1 Treated in *Mecp2* –Null and –Heterozygous Mice versus Vehicle Treated in WT Control

Legend:

CRB = Cerebellum, BL = Blood, LogFC = Log_2 fold change in rhIGF1 treated *Mecp2*-null and -heterozygous relative to Vehicle treated WT, FDR = False Discovery Rate

GO analysis revealed a total of 25 ontologies significantly over-represented in the cerebellum, and a total of 418 ontologies significantly over-represented in the blood of female mice. In male mice, 4 ontologies were over-represented in the cerebellum, and 7

ontology were significant in blood. The top significant 10 ontologies have been reported in table 3.9 and all ontologies have been reported in Appendix II.

Tissue	Female		Male	
	Gene Set	**FDR**	**Gene Set**	**FDR**
CRB	Neuropeptide signaling pathway	2.22E-05	Response to oxygen-containing compound	9.96E-03
	Regulation of glucocorticoid secretion	1.81E-03	response to external stimulus	1.10E-02
	Regulation of transport	5.45E-03	Cellular response to chemical stimulus	1.68E-02
	Positive regulation of glucocorticoid secretion	5.69E-03	Response to stimulus	3.39E-02
	Regulation of corticosteroid hormone secretion	5.75E-03	-	-
	Regulation of secretion	6.33E-03	-	-
	Regulation of amine transport	6.34E-03	-	-
	Regulation of corticosterone secretion	6.40E-03	-	-
	Regulation of steroid hormone secretion	6.51E-03	-	-
	Regulation of localization	7.34E-03	-	-
BL	Small molecule metabolic process	5.17E-41	Response to external biotic stimulus	3.21E-03
	Organic acid metabolic process	1.28E-38	Response to biotic stimulus	3.62E-03
	Carboxylic acid metabolic process	5.45E-37	Immune system process	3.72E-03
	Oxoacid metabolic process	1.29E-36	Biological process involved in interspecies interaction between organisms	3.90E-03
	Lipid metabolic process	3.00E-28	Response to other organism	4.20E-03
	Cellular lipid metabolic process	5.96E-24	Response to toxic substance	8.17E-03

	Monocarboxylic acid metabolic process	1.54E-22	Response to external stimulus	4.03E-02
	Steroid metabolic process	3.58E-20	-	-
	Fatty acid metabolic process	1.45E-19	-	-
	Small molecule catabolic process	1.83E-19	-	-

Table 3.9 - Top Significant Ontologies Over-represented rhIGF1 Treated in *Mecp2* –Null and –Heterozygous Mice versus Vehicle Treated in WT Control

Legend:

CRB = Cerebellum, BL = Blood, FDR = False Discovery Rate

In female mice Reactome pathway analysis identified 21 pathways significantly over-represented in the cerebellum and 76 pathways significantly over-represented in the blood. In male mice, 19 and 4 pathways were over-represented in the cerebellum and blood respectively. Two pathways overlapped in the cerebellum; MECP2 regulates transcription of neuronal ligand, and Transcriptional regulation by MECP2. The top 10 significant pathways have been reported in table 3.10 and all pathways have been reported in Appendix II.

	Female		**Male**	
Tissue	**Gene Set**	**FDR**	**Gene Set**	**FDR**
CRB	MECP2 regulates transcription of neuronal ligands	5.25E-05	MECP2 regulates transcription of neuronal ligands	2.85E-07
	Calcitonin-like ligand receptors	1.06E-03	Transcriptional Regulation by MECP2	5.57E-07
	GPCR ligand binding	1.06E-03	Loss of MECP2 binding ability to 5mC-DNA	1.11E-03
	rRNA processing in the mitochondrion	1.07E-03	Loss of MECP2 binding ability to 5hmC-DNA	1.04E-02
	GPCR downstream signalling	1.07E-03	Regulation of MECP2 expression and activity	1.04E-02

	tRNA processing in the mitochondrion	1.07E-03	Loss of function of MECP2 in Rett syndrome	1.04E-02
	ADORA2B mediated anti-inflammatory cytokines production	1.07E-03	Disorders of Developmental Biology	1.04E-02
	Class B/2 (Secretin family receptors)	1.15E-03	Disorders of Nervous System Development	1.04E-02
	G alpha (s) signalling events	1.30E-03	Pervasive developmental disorders	1.04E-02
	Signaling by GPCR	1.70E-03	Metallothioneins bind metals	1.04E-02
BL	Response to elevated platelet cytosolic Ca2+	1.03E-13	Interleukin-10 signaling	1.03E-02
	Platelet degranulation	2.56E-13	Interferon alpha/beta signaling	2.10E-02
	Platelet activation, signaling and aggregation	3.71E-12	Cytokine Signaling in Immune system	3.37E-02
	Regulation of Insulin-like Growth Factor (IGF) transport and uptake by Insulin-like Growth Factor Binding Proteins (IGFBPs)	3.74E-12	Cam-PDE 1 activation	3.37E-02
	Post-translational protein phosphorylation	6.07E-10	-	-
	Formation of Fibrin Clot (Clotting Cascade)	6.07E-10	-	-
	Metabolism	5.96E-09	-	-
	Common Pathway of Fibrin Clot Formation	6.02E-08	-	-
	Hemostasis	1.08E-07	-	-
	Plasma lipoprotein assembly, remodeling, and clearance	1.62E-07	-	-

Table 3.10 Top Significant Pathways of Over-represented in rhIGF1 Treated in *Mecp2* –Null and –Heterozygous Mice versus Vehicle Treated in WT Control

Legend:
CRB = Cerebellum, BL = Blood, FDR = False Discovery Rate

3.2.9 Comparisons of rhIGF1 Treatment in Female and Male Mice

The DEG identified in this comparison investigated whether rhIGF1 treatment had differential effects on gene expression depending on *Mecp2* mutation status, however because of timing of onset of symptoms in male and female mice were different, these mice were treated at completely different ages. This should be kept in mind throughout the whenever comparing the male and female mice.

In female mice, there were 136 genes in the cerebellum differentially expressed, 34 genes were up-regulated and 102 genes were down-regulated. This comparison was not possible in blood because rhIGF1 treated *Mecp2*$^{+/+}$ samples were not included in the sequencing experiment. In male mice, 339 and 34 genes were differentially expressed in the cerebellum and blood respectively. 94 and 11 genes were up-regulated, and 245 and 23 genes were down-regulated in the cerebellum and blood respectively. The results of these analyses are listed in table 3.11

	Female			**Male**		
Tissue	**Gene**	**LogFC**	**FDR**	**Gene**	**LogFC**	**FDR**
Cerebellum	*Gm4767*	-9.23	1.10E-31	*Mir6236*	-2.56	1.52E-35
	Prl	-1.67	2.28E-26	*Tmem59l*	-1.04	4.14E-19
	Gm32687	8.71	2.28E-20	*Usp1*	-2.16	1.24E-18
	Gh	-1.69	1.67E-19	*Rbm3*	1.04	6.98E-16
	Mamdc4	-4.55	4.69E-18	*Sgk1*	1.01	9.85E-16
	Lamp5	-1.45	3.27E-17	*Etnppl*	1.05	2.34E-15
	Ighm	-1.82	3.24E-14	*Hspa5*	-0.86	1.36E-12
	Tcea1-ps1	7.89	5.00E-11	*Fkbp2*	-0.74	2.17E-09
	Bc1	-0.99	1.17E-10	*Cirbp*	0.90	6.34E-09
	Resp18	-1.02	1.42E-09	*Fabp7*	-0.75	7.09E-09
Blood	-	-	-	*Mir6236*	3.09	3.22E-19
	-	-	-	*Gzma*	-2.80	1.44E-08
	-	-	-	*Prg4*	2.49	2.06E-06
	-	-	-	*Ccl5*	-1.81	6.27E-06
	-	-	-	*Tgtp2*	-2.49	1.42E-05

	-	-	-	*Cox5a*	-1.80	4.91E-05
	-	-	-	*Nkg7*	-2.12	4.91E-05
	-	-	-	*Ifi27l2a*	-1.91	9.66E-05
	-	-	-	*Arf5*	1.50	1.73E-04
	-	-	-	*E2f2*	1.46	3.51E-04

Table 3.11 – Top Significant DEGs in the Cerebellum and Blood of rhIGF1 Treated *Mecp2*-Null and -Heterozygous versus WT Mice

Legend:

CRB = Cerebellum, BL = Blood, LogFC = Log_2 fold change in rhIGF1 treated *Mecp2*-heterozygous relative to Vehicle treated WT, FDR = False Discovery Rate

Go analysis revealed a total of 54 ontologies significantly over-represented in the cerebellum of female mice. In male mice, 48 and 33 ontologies were over-represented in the cerebellum and blood respectively. The top 10 significant results of which have been reported in table 3.12 and all pathways have been reported in Appendix II.

Tissue	**Female**		**Male**	
	Gene Set	**FDR**	**Gene Set**	**FDR**
CRB	Neuropeptide signaling pathway	1.60E-06	Sensory perception of smell	2.61E-04
	Behavior	8.81E-06	Response to chemical	2.91E-04
	Regulation of transport	6.34E-05	Cellular component organization	3.52E-04
	Regulation of localization	1.97E-04	Protein-containing complex subunit organization	3.85E-04
	Regulation of system process	2.05E-04	Cellular component organization or biogenesis	3.87E-04
	Regulation of ion transport	2.56E-04	Regulation of cell death	5.78E-04
	Anterograde trans-synaptic signaling	7.74E-04	Regulation of programmed cell death	7.32E-04
	Synaptic signaling	8.43E-04	Regulation of apoptotic process	7.60E-04

	Chemical synaptic transmission	8.60E-04	Sensory perception of chemical stimulus	8.43E-04
	Regulation of multicellular organismal process	8.98E-04	Negative regulation of cellular process	1.02E-03
BL	-	-	Cellular response to cytokine stimulus	1.11E-04
	-	-	Response to cytokine	2.02E-04
	-	-	Cytokine-mediated signaling pathway	5.06E-04
	-	-	Biological process involved in interspecies interaction between organisms	8.45E-04
	-	-	Chemokine-mediated signaling pathway	1.91E-03
	-	-	Response to biotic stimulus	2.12E-03
	-	-	Response to external biotic stimulus	2.16E-03
	-	-	Response to other organism	2.48E-03
	-	-	Response to chemokine	2.59E-03
	-	-	Defense response	2.82E-03

Table 3.12 Top Significant Ontologies Over-represented in rhIGF1 Treated *Mecp2*-Null and -Heterozygous versus WT Mice

Legend:

CRB = Cerebellum, BL = Blood, FDR = False Discovery Rate

In female mice, Reactome pathway analysis identified 26 pathways significantly over-represented in the cerebellum. In male mice, 25 and 19 pathways were significantly over-represented in the cerebellum and blood respectively. The top significant 10 pathways have been reported in table 3.13 and all pathways have been reported in Appendix II.

	Female		Male	
Tissue	**Gene Set**	**FDR**	**Gene Set**	**FDR**
CRB	Transcriptional Regulation by MECP2	7.21E-05	Transcriptional Regulation by MECP2	7.92E-06
	Signaling by GPCR	1.12E-04	Cellular responses to stimuli	1.66E-05
	GPCR downstream signalling	1.12E-04	Cellular responses to stress	1.08E-04
	MECP2 regulates transcription of neuronal ligands	1.31E-04	ATF6 (ATF6-alpha) activates chaperone genes	1.08E-04
	Activation of HOX genes during differentiation	4.53E-04	ATF6 (ATF6-alpha) activates chaperones	1.78E-04
	Activation of anterior HOX genes in hindbrain development during early embryogenesis	4.53E-04	Loss of function of MECP2 in Rett syndrome	1.45E-03
	Class B/2 (Secretin family receptors)	1.76E-03	Disorders of Nervous System Development	1.45E-03
	Calcitonin-like ligand receptors	2.10E-03	Pervasive developmental disorders	1.45E-03
	GPCR ligand binding	2.48E-03	Disorders of Developmental Biology	1.45E-03
	Loss of MECP2 binding ability to 5hmC-DNA	2.48E-03	MECP2 regulates neuronal receptors and channels	3.14E-03
BL	-	-	Cytokine Signaling in Immune system	5.11E-08
	-	-	Chemokine receptors bind chemokines	3.40E-07
	-	-	Immune System	2.97E-05
	-	-	Interleukin-10 signaling	6.99E-05
	-	-	Interferon Signaling	7.84E-05
	-	-	Interferon alpha/beta signaling	1.10E-04

	-	-	Peptide ligand-binding receptors	1.58E-04
	-	-	Class A/1 (Rhodopsin-like receptors)	7.44E-04
	-	-	Signaling by Interleukins	1.48E-03
	-	-	GPCR ligand binding	5.91E-03

Table 3.13 Top Significant Pathways of Over-represented in rhIGF1 Treated *Mecp2*-Null and -Heterozygous versus WT Mice

Legend:

CRB = Cerebellum, BL = Blood, FDR = False Discovery Rate

3.2.10 Mecp2 WT Mice rhIGF1 treated versus Vehicle treated

The DEG identified in this comparison examined whether rhIGF1 treatment had an effect in WT mice. There were only 26 genes differentially expressed in the cerebellum, 15 were up-regulated and 11 were down-regulated. In male mice, 119 genes and 9 genes were differentially expressed in the cerebellum and blood. 77 genes were up-regulated, and 42 genes were down-regulated in the cerebellum, in blood all genes were down-regulated. The results of these analyses are listed in figure 3.14. The top significant DEG are listed in table 3.14 and the full list is reported in Appendix II.

	Female			**Male**		
Tissue	**Gene**	**LogFC**	**FDR**	**Gene**	**LogFC**	**FDR**
Cerebellum	*Gm14648*	2.87	9.23E-34	*Mir6236*	2.30	4.71E-30
	Tcea1-ps1	8.61	1.89E-17	*Usp1*	2.13	5.15E-20
	Pcdha1	-8.27	4.37E-13	*Hspa5*	0.85	9.07E-15
	Mamdc4	-4.23	8.79E-13	*Lamp5*	-3.07	1.09E-10
	Cers1	7.44	7.49E-07	*Acbd3*	1.54	5.26E-10
	Pcdha8	-7.21	4.19E-05	*Tmem59l*	0.50	2.61E-08
	Gm10095	0.94	1.47E-04	*Manf*	1.00	1.02E-06
	Prl	-0.88	2.24E-04	*Car8*	0.44	1.85E-06
	NA	1.84	2.41E-04	*Wapl*	0.90	6.37E-06
	Fxyd2	2.19	2.68E-04	*Apoa2*	-2.69	2.25E-10
Blood	-	-	-	*Prg4*	-1.99	2.18E-08
	-	-	-	*Fn1*	-2.77	9.62E-04

	-	-	-	*Ednrb*	-1.74	9.62E-04
	-	-	-	*Saa3*	-3.18	1.43E-02
	-	-	-	*Car3*	-1.43	2.27E-02
	-	-	-	*Alox15*	-1.69	3.04E-02
	-	-	-	*Itgam*	-4.31	3.44E-02
	-	-	-	*Mup2*	-3.20	3.55E-02
	-	-	-	*Cfd*	-2.69	2.25E-10
	-	-	-	-	-	-

Table 3.14 – Top Significant DEGs in the Cerebellum and Blood of rhIGF1 Treated versus Vehicle Treated *Mecp2* WT Mice

Legend:

CRB = Cerebellum, BL = Blood, LogFC = Log_2 fold change in rhIGF1 treated *Mecp2*$^{+/+}$ relative to Vehicle treated, FDR = False Discovery Rate

There were no significant ontologies identified in GO analysis in female mice and 2 ontology in the cerebellum of male mice. Reactome pathway analysis found 14 pathways over-represented in female cerebellum. In male mice, there were 14 and 50 pathways in the cerebellum and blood respectively. The top significant pathways have been reported in table 3.15 and the total pathways have been reported in appendix II.

	Female		**Male**	
Tissue	**Gene Set**	**FDR**	**Gene Set**	**FDR**
CRB	Potential therapeutics for SARS	1.11E-03	Unfolded Protein Response (UPR)	3.01E-10
	NOTCH3 Intracellular Domain Regulates Transcription	4.67E-03	ATF6 (ATF6-alpha) activates chaperone genes	4.23E-07
	SARS-CoV Infections	4.67E-03	ATF6 (ATF6-alpha) activates chaperones	5.92E-07
	Signaling by NOTCH3	6.19E-03	IRE1alpha activates chaperones	1.00E-04
	Ion homeostasis	6.19E-03	Cellular responses to stress	4.12E-04
	Ion transport by P-type ATPases	6.51E-03	Cellular responses to stimuli	4.58E-04

	Cardiac conduction	2.00E-02	Chk1/Chk2(Cds1) mediated inactivation of Cyclin B:Cdk1 complex	1.25E-02
	Ion channel transport	3.47E-02	PERK regulates gene expression	1.53E-02
	Muscle contraction	3.48E-02	Platelet activation, signaling and aggregation	1.54E-02
	Prolactin receptor signaling	3.48E-02	Activation of BAD and translocation to mitochondria	1.75E-02
BL	-	-	Interleukin-4 and Interleukin-13 signaling	7.01E-08
	-	-	Signaling by Interleukins	2.56E-05
	-	-	Cytokine Signaling in Immune system	3.72E-04
	-	-	Immune System	4.19E-03
	-	-	Integrin cell surface interactions	2.03E-02
	-	-	Platelet degranulation	3.23E-02
	-	-	Response to elevated platelet cytosolic Ca2+	3.23E-02
	-	-	Alternative complement activation	3.23E-02
	-	-	Fibronectin matrix formation	3.23E-02
	-	-	Biosynthesis of DPAn-6 SPMs	3.23E-02

Table 3.15 - Top Significant Pathways Over-represented in rhIGF1 Treated versus Vehicle Treated *Mecp2* WT Mice

Legend:

CRB = Cerebellum, BL = Blood, FDR = False Discovery Rate

3.2.11 Genes Targeted by rhIGF1 Treatment in Female and Male Mice

The primary function of MeCP2 is as a global transcriptional regulator [78,137,202]. Therefore, to understand whether rhIGF1 treatment could rescue transcripts that are

affected by *Mecp2* mutation, the overlapping genes in comparisons examining the effect of treatment in *Mecp2*$^{-/+}$ mice and the effect of the *Mecp2* mutation in female mice were examined. DEG expressed due to the *Mecp2* mutation whose expression was reversed by rhIGF1 treatment were considered to be likely due to rhIGF1 action.

In female mice, 75 genes in the brain and 3 genes in the blood were rescued, the top 10 significant overlapping genes and recalculated FDR are reported in table 3.16. A hypergeometric test was conducted to ensure this overlap was not by chance, described in section 6.2.6.

A hypergeometric test was performed on the number of overlapping genes to ensure that these overlaps were unlikely to be found by chance, the resulting p-values were 5.37 x10^{-145} for cerebellum and 8.78 x10^{-05} for blood.

	rhIGF1 vs Vehicle Treated *Mecp2*$^{-/+}$ Mice (Cerebellum)		**Vehicle Treated *Mecp2*$^{-/+}$ vs. *Mecp2*$^{+/+}$ Mice (Cerebellum)**	
Overlapping Gene	Log_2FC	New FDR	Log_2FC	New FDR
Crym	-6.91	4.26E-69	4.89	6.33E-38
Rpl31-ps8	9.93	4.28E-43	-11.16	2.74E-84
Spink8	-5.30	4.22E-36	3.71	8.67E-19
Neurod6	-2.10	1.06E-29	2.19	1.25E-22
Ptk2b	-2.82	1.23E-25	2.92	7.63E-21
Pcdha5	8.85	3.10E-21	-7.91	1.05E-10
Camk2a	-2.17	3.33E-21	2.00	4.71E-14
Foxg1	-5.69	2.22E-18	6.69	5.86E-16
Scn3b	-1.88	1.63E-17	1.13	6.68E-05
Enc1	-2.09	1.64E-15	1.63	9.85E-08
	rhIGF1 vs Vehicle Treated *Mecp2*$^{-/+}$ Mice (Blood)		**Vehicle Treated *Mecp2*$^{-/+}$ vs. *Mecp2*$^{+/+}$ Mice (Blood)**	
Overlapping Genes	Log_2FC	New FDR	Log_2FC	New FDR
Rps13-ps1	3.04	1.07E-02	-3.23	6.78E-03
Ipo11	-2.11	6.83E-02	2.69	7.40E-03
Rps16-ps2	-6.89	9.03E-04	7.09	5.28E-05

Table 3.16 - Target Genes of rhIGF1 Action in Female *Mecp2*$^{-/+}$ Mice Cerebellum and Blood

p-value of hypergeometric test in cerebellum was p = 5.37 x10^{-145}, and in blood p = 8.78 x10^{-05}

Legend:

FDR = False Discovery Rate, LogFC = Log_2 fold change

In male mice, 113 genes in the brain and 37 genes in the blood were rescued, the top 10 overlapping genes and recalculated FDR are reported in table 3.17.

	rhIGF1 vs Vehicle Treated *Mecp2*$^{-/y}$ Mice (Cerebellum)		**Vehicle Treated *Mecp2*$^{-/+}$ vs. *Mecp2*$^{+/y}$ Mice (Cerebellum)**	
Overlapping Gene	Log_2FC	New FDR	Log_2FC	New FDR
Mir6236	-2.51	3.75E-31	2.24	5.79E-27
Usp1	-2.30	2.14E-20	2.25	1.44E-21
Tmem59l	-1.14	1.35E-15	0.59	4.00E-07
Fam213b	-0.98	1.08E-10	0.65	6.53E-07
Gpx4	-0.85	3.60E-08	0.47	3.04E-04
Caly	-1.08	4.24E-07	0.45	2.93E-02
Tppp3	-0.93	7.61E-07	0.70	2.00E-05
Necap2	-1.32	1.01E-06	0.88	3.27E-04
Ywhaq	-0.77	1.37E-06	0.49	7.00E-05
Isca1	-0.78	1.53E-06	0.33	2.36E-02
	rhIGF1 vs Vehicle Treated *Mecp2*$^{-/y}$ Mice (Blood)		**Vehicle Treated *Mecp2*$^{-/+}$ vs. *Mecp2*$^{+/y}$ Mice (Blood)**	
Overlapping Gene	Log_2FC	New FDR	Overlapping Gene	Log_2FC
Alb	-8.29	3.30E-28	4.77	7.30E-31
Apoa2	-7.76	3.44E-22	4.63	4.12E-25
Ttr	-4.67	2.63E-12	4.78	2.58E-21
Saa3	-2.69	1.51E-11	2.30	7.46E-13
Apoc1	-4.36	3.90E-08	4.04	2.77E-13

Apoa1	-6.12	3.93E-08	4.06	3.76E-10
Ahsg	-5.91	5.93E-07	3.75	4.84E-08
Wfdc17	-1.79	2.57E-05	2.04	4.70E-11
Fabp1	-5.58	2.65E-05	3.61	3.28E-06
Cyp3a11	-5.40	1.58E-04	4.43	5.36E-07

Table 3.17 – Target Genes of rhIGF1 Action in Male *Mecp2*$^{-/y}$ Mice Cerebellum and Blood

p-value of hypergeometric test in cerebellum was p = 3.21 x10^{-135}, and in blood p = 4.97 x10^{-67}

Legend:

FDR = False Discovery Rate

These rhIGF1 target genes were analysed using GO and Reactome pathway analysis. The Reactome analysis in female mice revealed 7 over-represented pathways in the cerebellum but none in blood. In male mice, there were 7 pathways over-represented in the cerebellum and 45 pathways in the blood. GO analysis in female mice revealed 46 ontologies in the cerebellum and no ontologies in the blood over-represented. In male mice, there were 3 ontologies in cerebellum and 179 ontologies in the blood over-represented. Table 3.18 displays the top pathways from Reactome and table 3.19 displays the top significant ontologies from GO analysis. The full lists of results are reported in Appendix II.

	Female		**Male**	
Tissue	**Gene Set**	**FDR**	**Gene Set**	**FDR**
CRB	Calcitonin-like ligand receptors	1.98E-03	Cellular responses to stress	3.04E-02
	Signaling by GPCR	3.28E-03	Cellular responses to stimuli	3.04E-02
	GPCR downstream signalling	4.67E-03	RHOH GTPase cycle	3.06E-02
	Long-term potentiation	1.05E-02	Activation of gene expression by SREBF (SREBP)	3.06E-02

	Class B/2 (Secretin family receptors)	1.59E-02	Cellular response to starvation	3.84E-02
	Transcriptional Regulation by MECP2	1.59E-02	TP53 Regulates Metabolic Genes	3.84E-02
	GPCR ligand binding	3.40E-02	Regulation of cholesterol biosynthesis by SREBP (SREBF)	4.38E-02
BL	-	-	Plasma lipoprotein assembly	5.94E-08
	-	-	Plasma lipoprotein assembly, remodeling, and clearance	1.02E-06
	-	-	Chylomicron assembly	3.53E-06
	-	-	Retinoid metabolism and transport	3.53E-06
	-	-	Chylomicron remodeling	5.15E-06
	-	-	Metabolism of fat-soluble vitamins	5.15E-06
	-	-	Plasma lipoprotein remodeling	1.25E-05
	-	-	Post-translational protein phosphorylation	1.25E-05
	-	-	Regulation of Insulin-like Growth Factor (IGF) transport and uptake by Insulin-like Growth Factor Binding Proteins (IGFBPs)	2.77E-05
	-	-	VLDL assembly	4.13E-05

Table 3.18 - Top Significant Pathways Over-represented in Target Genes of rhIGF1 Action

Legend:

CRB = Cerebellum, BL = Blood, FDR = False Discovery Rate

	Female		Male	
Tissue	**Gene Set**	**FDR**	**Gene Set**	**FDR**
CRB	Nervous system development	1.52E-06	Cellular metabolic process	2.37E-03
	System development	9.90E-05	Metabolic process	7.51E-03
	Multicellular organism development	2.03E-04	Organonitrogen compound metabolic process	2.52E-02
	Behavior	5.44E-04	-	-
	Response to calcium ion	5.96E-04	-	-
	Developmental process	1.15E-03	-	-
	Regulation of synaptic plasticity	1.39E-03	-	-
	Multicellular organismal process	1.53E-03	-	-
	Anatomical structure development	1.58E-03	-	-
	Cellular response to metal ion	1.67E-03	-	-
BL	-	-	Protein-lipid complex remodeling	1.62E-06
	-	-	Cholesterol efflux	1.67E-06
	-	-	Protein-lipid complex assembly	1.73E-06
	-	-	Plasma lipoprotein particle assembly	1.74E-06
	-	-	Lipid localization	1.76E-06
	-	-	Plasma lipoprotein particle remodeling	1.81E-06
	-	-	Triglyceride metabolic process	1.88E-06
	-	-	Protein-containing complex remodeling	2.00E-06

	-	-	Plasma lipoprotein particle clearance	2.32E-06
	-	-	Regulation of hydrolase activity	3.41E-06

Table 3.19 - Top Significant Ontologies Over-represented in Target Genes of rhIGF1 Action

Legend:

CRB = Cerebellum, BL = Blood, FDR = False Discovery Rate

3.2.12 Gene Expression and Locomotor Performance in Untreated Mecp2$^{-/y}$ Mice

Based on previous findings from this analysis from Chapter I and the literature, 7 genes were chosen to:

1. Compare expression between KO and WT *Mecp2* mice.
2. Test if there was a correlation between expression and locomotor movement in the blood and cerebellum.

These genes were *Igf1*, *Igf1r*, *S100a8*, *S100a9*, *Ube2v1*, *Tmem176a* and *Tmem176b*. *Igf1* and *Igf1r* were chosen due to their relevance to rhIGF1 (Mecasermin) treatment and based on the finding in Chapter I section 2.2.5. In this analysis, IGF Receptor signaling pathway was found to be significantly differentially expressed, using hypothesis driven testing, comparing Responders and MSRs at T0, T1 and in the Responders comparing T1 to T2. *IGF1* expression was also observed to be elevated in Responders compared to MSRs at T0 and T1 using hypothesis free testing.

S100a9 was previously identified by Urdinguio and colleagues as a neuronal target of *Mecp2* through sequencing and chromatin immunoprecipitation [203]. In this group, *S100a9* has also been identified as being elevated in the blood of *Mecp2*$^{-/y}$ mice [204]. S100A8 and S100A9 are Ca2+ binding proteins that form a heterodimer (S100A8/A9) and a more short-lasting homodimer. During inflammation S100A8/A9 is released from neutrophils and monocytes to modulate the immune response affecting leukocyte recruitment and cytokine secretion [205].

Ube2v1 encodes for a protein that is a variant of the E2 ubiquitin conjugating enzyme family, though it has no enzymatic activity itself, when bound to UBE2N it forms ubiquitin chains needed in Nuclear Factor k-light-chain-enhancer-of-activated B cell (NFkB)-related inflammation [206]. *Ube2v1* has also been found to be down-regulated in the cerebellum of symptomatic *Mecp2*$^{-/y}$ mice [204]. *TMEM176A* and *TMEM176B* were also identified in Chapter I of this thesis as being decreased in the blood of MSRs in the wash-out period between treatment phases.

When comparing untreated *Mecp2*$^{-/y}$ with *Mecp2*$^{+/y}$ and correcting for multiple testing, there was no significant difference between these genes. *Tmem176a* did not amplify reliably in either the blood or cerebellum and therefore was not considered for multiple correction. In general blood RNA gene expression was difficult to detect in samples (Data not shown).

Figure 3.16 shows the gene expression and correlation to the total locomotor activity of *Igf1* and *Igf1r* in untreated *Mecp2*$^{-/y}$ and *Mecp2*$^{+/y}$ mice cerebellum. There was no significant change or correlation in these comparisons.

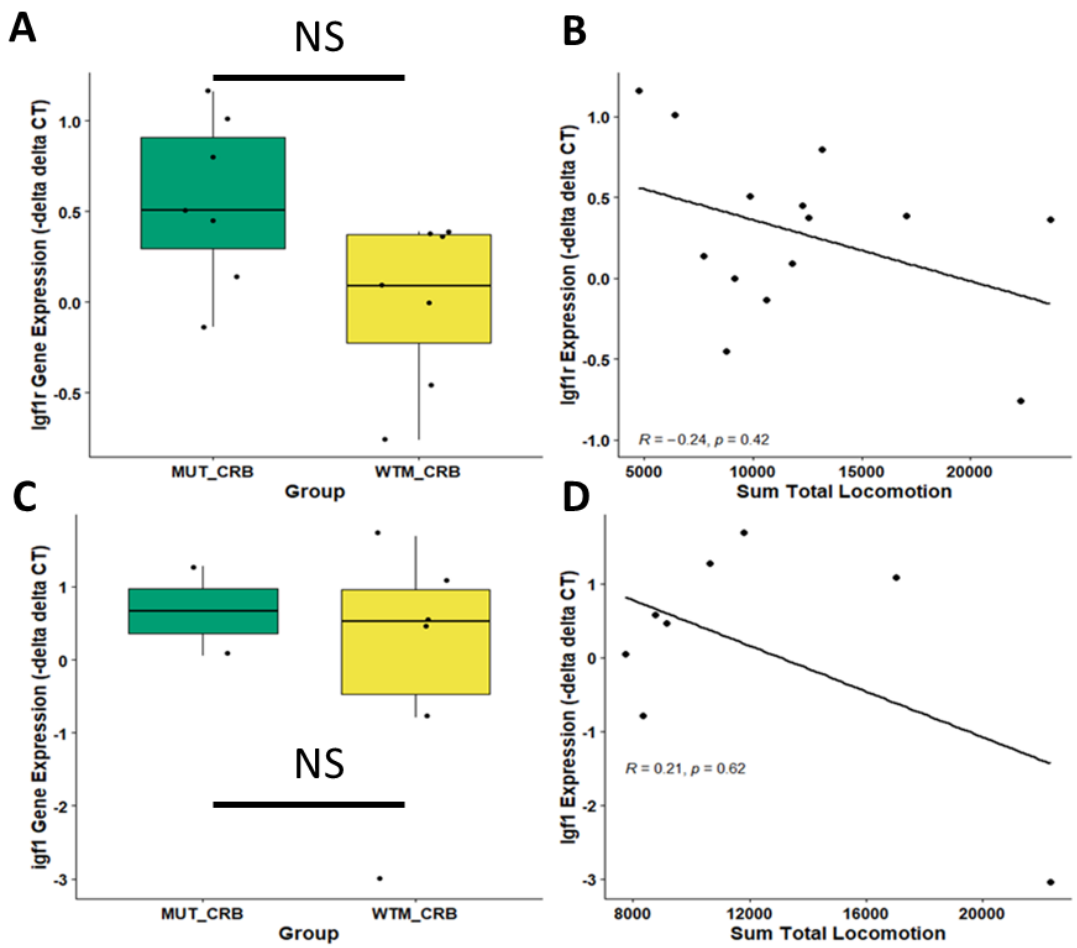

Figure 3.16 – Expression of *Igf1r* and *Igf1* in untreated *Mecp2*$^{-/y}$ and *Mecp2*$^{+/y}$ mice plotted against locomotion

Difference in *Igf1r* and *Igf1* expression in the cerebellum of *Mecp2*$^{-/y}$ and *Mecp2*$^{+/y}$ mice showing mean, and interquartile range as represented by boxplot with whiskers showing the maximum and minimum values (**A** and **C** respectively). Expression values of *Igf1r* and *Igf1* were plotted against the sum of total locomotor activity, as measured by beambreaks/hour during the night, in scatter plot with linear regression line displayed (**B** and **D** respectively).

For test comparing the means Wilcoxon test unpaired was used and corrected for testing of multiple genes using the Benjamini-Hochberg method. For correlation between gene expression and locomotor activity spearman's test reporting R and P-values.

Legend:

WTM_CRB = Cerebellum of *Mecp2*$^{+/y}$, MUT = Cerebellum of *Mecp2*$^{-/y}$, NS = Non-Significant, -ddCT = - delta delta CT, sample size (WTM_CRB n = 7, MUT_CRB n = 7)

Figure 3.17 shows the gene expression and correlation to the total locomotor activity of *S100a8* and *S100a9* in untreated *Mecp2*$^{-/y}$ and *Mecp2*$^{+/y}$ mice cerebellum. There was no significant change or correlation in these comparisons, however there was a trend in correlation, particularly in *S100a9*. This could become significant using a larger sample size.

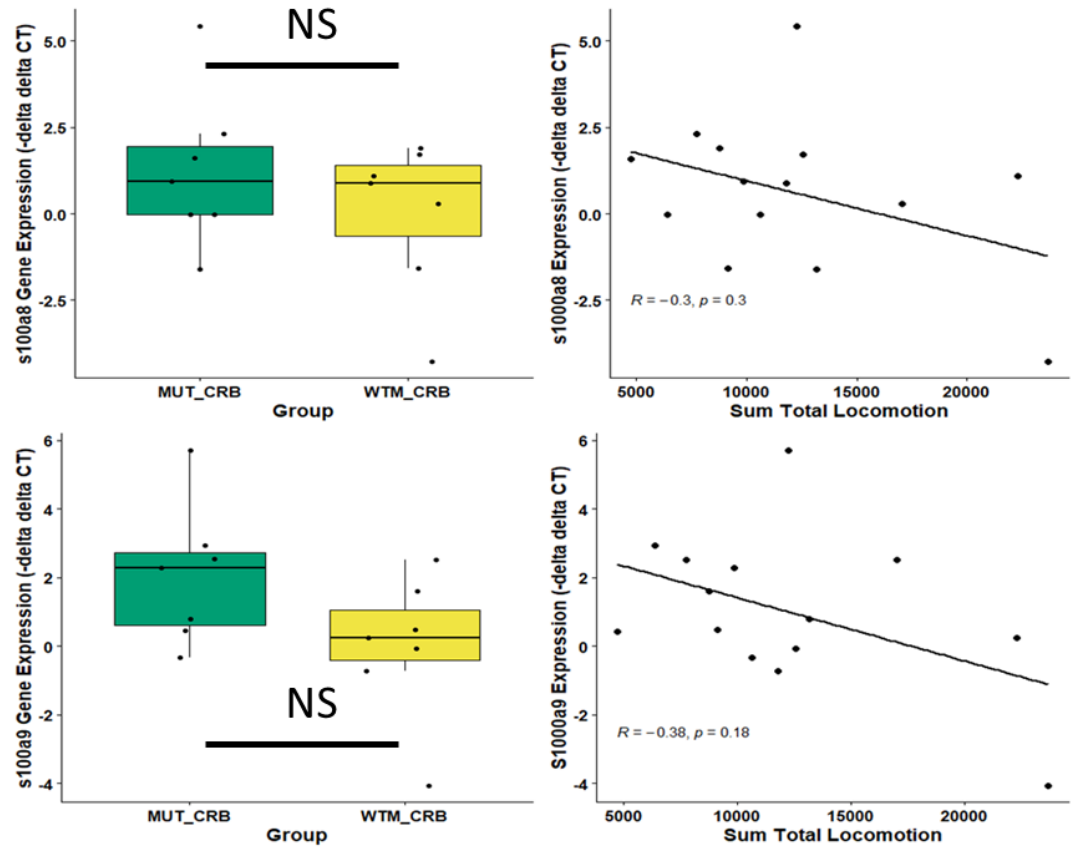

Figure 3.17 - Expression of *S100a8* and *S100a9* in untreated *Mecp2*$^{-/y}$ and *Mecp2*$^{+/y}$ mice plotted against locomotion

Difference in *S100a8* and *S100a9* expression in the cerebellum of *Mecp2*$^{-/y}$ and *Mecp2*$^{+/y}$ mice showing mean, and interquartile range as represented by boxplot with whiskers showing the maximum and minimum values (**A** and **C** respectively). Expression values of *S100a8* and *S100a9* were plotted against the sum of the sum

total locomotor activity as measured by beambreaks/hour during the night in scatter plot with linear regression line displayed (**B** and **D** respectively).
For test comparing the means Wilcoxon test unpaired was used and corrected for testing of multiple genes using the Benjamini-Hochberg method. For correlation between gene expression and locomotor activity spearman's test reporting R and P-values.
Legend:
WTM_CRB = Cerebellum of *Mecp2*$^{+/y}$, MUT = Cerebellum of *Mecp2*$^{-/y}$, NS = Non-Significant , -ddCT = - delta delta CT, sample size (WTM_CRB n = 7, MUT_CRB n = 7)

Figure 3.18 shows the gene expression and correlation to the total locomotor activity of *Tmem176b* and *Ube2v1* in untreated *Mecp2*$^{-/y}$ and *Mecp2*$^{+/y}$ mice cerebellum. There was no significant change or correlation in these comparisons.

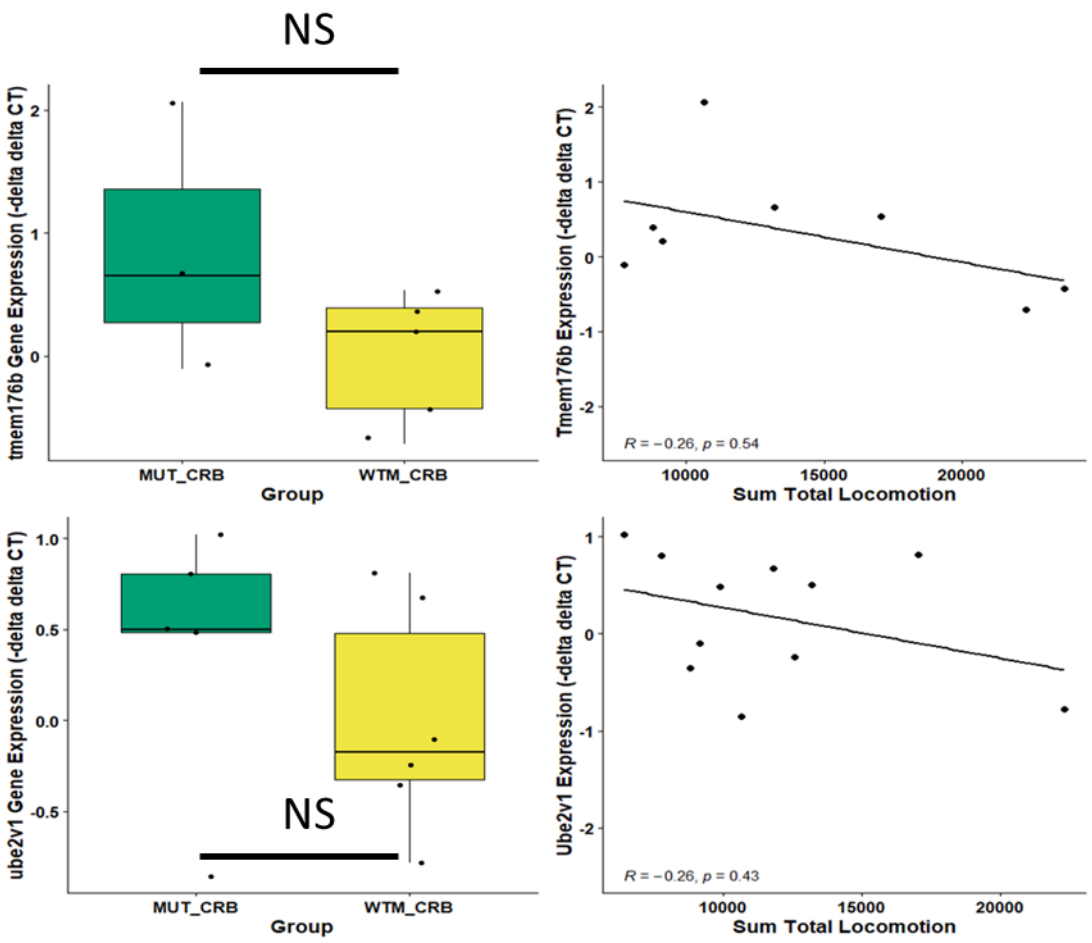

Figure 3.18 - Expression of *Tmem176b* and *Ube2v1* in untreated *Mecp2*$^{-/y}$ and *Mecp2*$^{+/y}$ mice plotted against locomotion

Difference in *Tmem176b* and *Ube2v1* expression in the cerebellum of *Mecp2*$^{-/y}$ and *Mecp2*$^{+/y}$ mice showing mean, and interquartile range as represented by boxplot with whiskers showing the maximum and minimum values (**A** and **C** respectively). Expression values of *Tmem176b* and *Ube2v1* were plotted against the sum of the sum total locomotor activity as measured by beambreaks/hour during the night in scatter plot with linear regression line displayed (**B** and **D** respectively).

For test comparing the means Wilcoxon test unpaired was used and corrected for testing of multiple genes using the Benjamini-Hochberg method. For correlation between gene expression and locomotor activity spearman's test reporting R and P-values.

Legend:

WTM_CRB = Cerebellum of *Mecp2*$^{+/y}$, MUT = Cerebellum of *Mecp2*$^{-/y}$, NS = Non-Significant, -ddCT = - delta delta CT, sample size (WTM_CRB n = 7, MUT_CRB n = 7)

3.2.13 Gene Expression and Locomotor Performance in Treated Female Mecp2-heterozygous Mice

Three target genes were assessed using rhIGF1 and vehicle treated *Mepc2*$^{-/+}$ and *Mecp2*$^{+/+}$ control mice. Here gene expression was compared in mice with different treatments groups and was plotted against the change in locomotor activity before and after treatment.

Figure 3.19 shows the analysis of *Igf1r*. Although not significant after multiple correction the raw p-value comparing vehicle treated *Mecp2*$^{-/+}$ mice with rhIGF1 treated *Mecp2*$^{-/+}$ and *Mecp2*$^{+/+}$ mice was significant. There was also a significant correlation between *Igf1r* expression and change in locomotor activity (R = -0.69, p-value = 0.0038).

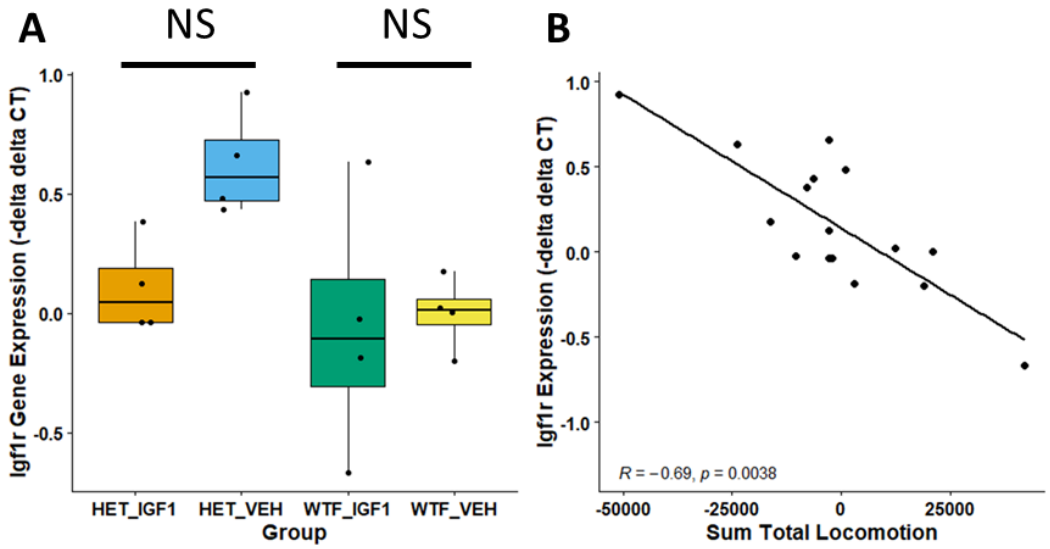

Figure 3.19 - Expression of *Igf1r* plotted against Locomotor change after rhIGF1 or Vehicle Treatment in the Cerebellum of *Mecp2*$^{-/+}$ and *Mecp2*$^{+/+}$ mice and plotted against change in locomotion

Difference in *Igf1r* expression in the cerebellum of *Mecp2-/+* and *Mecp2+/+* mice with boxplot representing mean and interquartile range and whiskers representing maximum and minimum values (**A**). This *Igf1r* expression was plotted against the

change in locomotor activity after rhIGF1 and Vehicle treatments. The sum of the total locomotor activity was measured by beambreaks/hour during the night represented as a scatter plot with linear regression line displayed (**B**).
For testing comparing the means Wilcoxon test unpaired was used, and for correlation between gene expression and locomotor activity Spearman's test was used, reporting R and P-value.
A Gene expression was plotted as –delta delta CT (-ddCT) in the cerebellum of treated female *Mecp2* mice. **B** –ddCT values were plotted against the change in locomotor activity at end of treatment compared to baseline.
Wilcoxon test unpaired and corrected for testing of multiple genes using the Benjamini-Hochberg method.
Legend:
HET_IGF1 = rhIGF1 treated *Mecp2*$^{-/+}$ mice, HET_VEH = Vehicle treated *Mecp2*$^{-/+}$ mice, WTF_IGF1 = rhIGF1 treated *Mecp2*$^{+/+}$ mice, WTF_VEH = Vehicle treated *Mecp2*$^{+/+}$ mice, NS = Non-significant, sample size (HET_IGF1 n=4, HET_VEH n= 4, WTF_IGF1 n = 4, WTF_VEH n=4)

Figure 3.20 shows the analysis of *S100a8* expression and change in locomotor activity in treated female mice. These results do not show any significant changes or correlation.

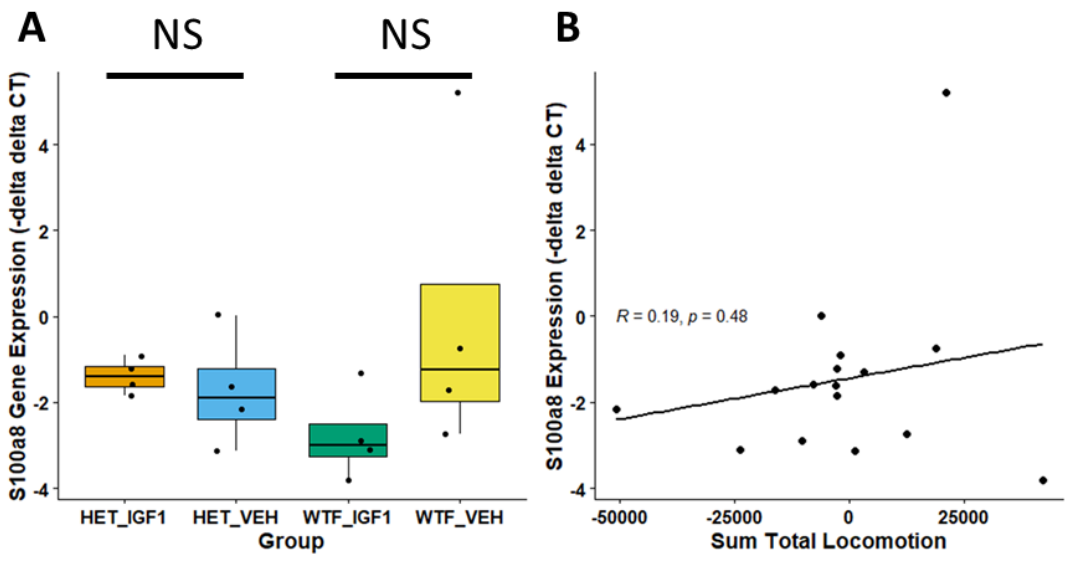

Figure 3.20 - Expression of *S100a8* compared to Locomotor change after rhIGF1 or Vehicle Treatment in the Cerebellum of *Mecp2*$^{-/+}$ and *Mecp2*$^{+/+}$ mice

and plotted against change in locomotion

Difference in *S100a8* expression in the cerebellum of *Mecp2*$^{-/+}$ and *Mecp2*$^{+/+}$ mice with boxplot representing mean and interquartile range and whiskers representing maximum and minimum values (**A**). This *S100a8* expression was plotted against the change in locomotor activity after rhIGF1 and Vehicle treatments. The sum of the total locomotor activity was measured by beambreaks/hour during the night represented as a scatter plot with linear regression line displayed (**B**).

For testing comparing the means Wilcoxon test unpaired was used, and for correlation between gene expression and locomotor activity Spearman's test was used, reporting R and P-value.

A Gene expression was plotted as –delta delta CT (-ddCT) in the cerebellum of treated female *Mecp2* mice. **B** –ddCT values were plotted against the change in locomotor activity at end of treatment compared to baseline.

Wilcoxon test unpaired and corrected for testing of multiple genes using the Benjamini-Hochberg method.

Legend:

HET_IGF1 = rhIGF1 treated *Mecp2*$^{-/+}$ mice, HET_VEH = Vehicle treated *Mecp2*$^{-/+}$ mice, WTF_IGF1 = rhIGF1 treated *Mecp2*$^{+/+}$ mice, WTF_VEH = Vehicle treated *Mecp2*$^{+/+}$ mice, NS = Non-significant, sample size (HET_IGF1 n=4, HET_VEH n= 4, WTF_IGF1 n = 4, WTF_VEH n=4)

Figure 3.13 shows the analysis of *S100a9* expression and change in locomotor activity in treated female mice. Again there is no significant change or correlation.

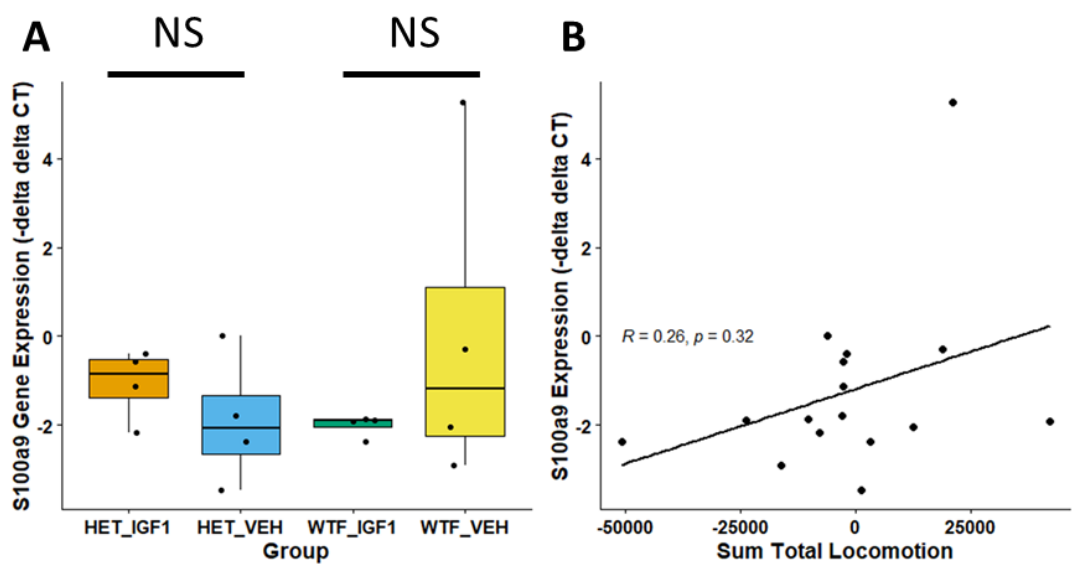

Figure 3.21 - Expression of *S100a9* compared to Locomotor change after rhIGF1 or Vehicle Treatment in the Cerebellum of *Mecp2*$^{-/+}$ and *Mecp2*$^{+/+}$ mice and plotted against change in locomotion

Difference in *S100a9* expression in the cerebellum of *Mecp2*$^{-/+}$ and *Mecp2*$^{+/+}$ mice with boxplot representing mean and interquartile range and whiskers representing maximum and minimum values (**A**). This *S100a9* expression was plotted against the change in locomotor activity after rhIGF1 and Vehicle treatments. The sum of the total locomotor activity was measured by beambreaks/hour during the night represented as a scatter plot with linear regression line displayed (**B**).

For testing comparing the means Wilcoxon test unpaired was used, and for correlation between gene expression and locomotor activity Spearman's test was used, reporting R and P-value.

A Gene expression was plotted as –delta delta CT (-ddCT) in the cerebellum of treated female *Mecp2* mice. **B** –ddCT values were plotted against the change in locomotor activity at end of treatment compared to baseline.

Wilcoxon test unpaired and corrected for testing of multiple genes using the Benjamini-Hochberg method.

Legend:

HET_IGF1 = rhIGF1 treated *Mecp2*$^{-/+}$ mice, HET_VEH = Vehicle treated *Mecp2*$^{-/+}$ mice, WTF_IGF1 = rhIGF1 treated *Mecp2*$^{+/+}$ mice, WTF_VEH = Vehicle treated *Mecp2*$^{+/+}$ mice, NS = Non-significant, sample size (HET_IGF1 n=4, HET_VEH n= 4, WTF_IGF1 n = 4, WTF_VEH n=4)

3.3 Discussion

3.3.1 Male and Female Mecp2 Mice Display Locomotor Deficiencies

Deficiencies in nocturnal locomotor activity were detected in both *Mecp2*$^{-/+}$ and *Mecp2*$^{-/y}$ mice compared to WT counterparts. These deficits were observed when comparing the sum of each variable (horizontal, vertical and total activity), shown in figures 3.1 and 3.2. Previous work in a different *Mecp2* KO model supports this finding [125], although this study did not make the distinction between horizontal and vertical activity. Horizontal activity measured beambreaks at ground level of the cage, and vertical activity measured beambreaks at the level of the metal grid holding the food pellets and water bottle. Therefore, vertical beam-breaking could be associated with feeding or exploration behaviour. A schematic figure of this experimental setup is displayed in figure 6.2.1.

When examining nocturnal activity over time in *Mecp2*$^{-/+}$ mice, impairment in the horizontal, vertical and total activity compared to WT during the night was detected. In *Mecp2*$^{-/y}$ mice, the first 7 hours of horizontal activity and in the first hour of total activity were significantly decreased compared to WT. These results suggested that *Mecp2*$^{-/y}$ mice had a more subtle change in activity. However, this may be due to the higher sample number used in female relative to male mice, or the fact that the female mice were much older than the male mice. The locomotor activity was measured at different age ranges to correspond with onset of symptoms, but this could also influence the results detected. Male mice were measured between p28-69 a period roughly corresponding to adolescence, while female mice were measured from p120 onwards and were considered matured mice. Mature mice were larger and therefore could easily reach the vertical beam plane, while smaller male mice, especially *Mecp2*$^{-/y}$ mice, would require greater effort to reach the vertical plane.

Hypoactivity has been observed in multiple RTT mouse models including; *Mecp2*$^{tm1.1Jae}$, *Mecp2*$^{308/y}$, and specific-peripheral *Mecp2*$^{-/y}$ mice [94,125,182]. The specific-peripheral *Mecp2*$^{-/y}$ mice model displayed fatigue in response to exercise [94]. This model is of particular interest, given the use of peripheral blood tissue in DGE analysis. *Mecp2*$^{-/y}$ mice have aberrant skeletal muscle growth which is linked to the IGF1/AKT/mTOR pathway [207], which may explain why these mice are prone to fatigue.

Nocturnal activity and age were not significantly correlated in *Mecp2*$^{-/y}$ and *Mecp2*$^{-/+}$ mice but the trends were informative. *Mecp2*$^{-/y}$ mice activity decreased with age while *Mecp2*$^{+/y}$ mice increased with age. This increase in WT mice would be expected given normal growth and stage of development in these mice. Rapid physical deterioration has been noted in *Mecp2*$^{-/y}$ mice, and ultimately leads to death between 8 and 10 weeks of age. Therefore, a decline in movement would also be expected in these mice [38,125]. The milder phenotype of *Mecp2*$^{-/+}$ relative to *Mecp2*$^{-/y}$ mice occurs in a number of models [173]. Therefore these results are consistent with the characteristic phenotypes of *Mecp2*$^{-/+}$ and *Mecp2*$^{-/y}$ mice; *Mecp2*$^{-/y}$ mice have early onset of motor symptoms and decline until death around 8-10 weeks, and *Mecp2*$^{-/+}$ mice phenotype is milder and have greater longevity.

3.3.2 rhIGF1 treatment protects against locomotor decline in Mecp2$^{-/+}$ *and Mecp2*$^{-/y}$ *mice*

rhIGF1 treatment in *Mecp2*$^{-/+}$ and *Mecp2*$^{-/y}$ mice appeared to protect against decline observed in locomotor activity, but male and female mice were affected differently. rhIGF1 treated *Mecp2*$^{-/+}$ mice were protected from decline in vertical activity, while rhIGF1 treated *Mecp2*$^{-/y}$ mice were protected from decline in horizontal and total activity.

In *Mecp2*$^{-/+}$ mice, vehicle treated mice declined in vertical activity to a greater extent than horizontal activity. The deficiency in vertical activity could be a result of a number of factors. As described in 3.3.1 vertical activity could be associated with more exploratory and food/water retrieval because of the location of the infrared beams. IGF1 is known to have many metabolic effects, including; protein synthesis, glucose and lipid homeostasis, skeletal muscle regulation, and secretion of Growth Hormone [208]. Central IGF1 overexpression in mice increases appetite, improves glucose tolerance and insulin sensitivity [209]. The IGF1/AKT/mTOR pathway is also linked to abnormal skeletal morphology and growth of *Mecp2*$^{-/y}$ mice [207].

In this analysis, rhIGF1 may be inducing metabolic affects such as increased appetite or muscle growth which could cause mice to seek out food and water more frequently, therefore increasing vertical activity. In GO analysis of *Mecp2*$^{-/y}$ cerebellum, the ontologies “negative regulation of feeding behaviour” in vehicle treated mice and

"Feeding behaviour" in rhIGF1 treated mice were over-represented. This further suggests that food intake may be affected in rhIGF1 treated *Mecp2*$^{-/y}$ mice.

Hind leg clasping and impaired motor function is a classic sign of RTT-phenotype in *Mecp2*$^{-/+}$ and *Mecp2*$^{-/y}$ mice, which is thought to mimic hand stereotypy and impaired fine motor control observed in patients [210]. These features affect overall mouse behaviour, and the ability to rear onto hind legs has been found to be impaired in *Mecp2*$^{-/+}$ mice compared to WT [37]. Here, rhIGF1 treatment may ameliorate hind leg clasping and motor deficiency, therefore allowing *Mecp2*$^{-/+}$ to rear more easily which would lead to an increase in vertical activity.

rhIGF1 treatment may be increasing exploratory behaviour in *Mecp2*$^{-/+}$ mice thus increasing vertical activity. Exploratory and anxiety behaviour was assessed in rhIGF1 treated *Mecp2*$^{-/y}$ mice using plus maze paradigm [151]. There was no significant change in exploratory behaviour but untreated *Mecp2*$^{-/y}$ mice had increased preference for open arm of the plus maze, implying deficiency to anxiety compared to WT. After rhIGF1 treatment, there was a reduction to time spent in open arm in both *Mecp2*$^{-/y}$ and *Mecp2*$^{-/+}$ mice [151]. This study suggests that exploratory behaviour *Mecp2*$^{-/+}$ mice was unlikely to be abnormal in these mice. However, behavioural measures are variable in mice, anxiety across different *Mecp2* models of RTT do not display a consistent phenotype [210–213]. Genetic background of *Mecp2*$^{-/+}$ mice contributes to anxiety phenotype [214].

Of course, all of these factors may have contributed to the observed improvement to vertical activity. Further battery of specific behavioural and experimental testing would be required to determine if and how rhIGF1contributes to these variables. These factors include:

- Improved motor functioning
- Improved glucose homeostasis
- Increased exploration and/or feeding behaviours
- Improved skeletal muscle synthesis and morphology
- Decreased anxiety

In *Mecp2*$^{-/y}$ mice, locomotor activity improvements were the opposite of female counterparts. There was significant improvement to both horizontal and total activity but no significant difference in vertical activity. As mentioned in section 3.3.1 male

mice were much smaller than the mature female mice and therefore may not have been as likely to trigger vertical beam breaking. All male WT mice showed increase in locomotor activity which is consistent with their age and developmental stage of life during measurement. Given IGF1's role in muscle hypertrophy and metabolism, it is unsurprising to see increased locomotor activity in developing *Mecp2*$^{+/y}$ mice [207,209,215].

The increased horizontal activity in rhIGF1 treated *Mecp2*$^{-/y}$ demonstrates these mice travelled an increased distance compared to vehicle treated mice. This improvement could have a number of explanations. While Castro and colleagues demonstrated that rhIGF1 generally improved locomotor activity [151], they did not examine more specific motor function. In *Mecp2*$^{stop/y}$ mice, a thorough investigation of motor dysfunction found impairments to balance, grip strength, swim speed, and gait. Re-expression of *Mecp2* could partially rescue many of these impairments [218]. This analysis highlights the complexity of motor dysfunctions in RTT which may all contribute to general hypoactivity.

The efficacy of rhIGF1 treatment in mice could be attributed to improved bioenergetics in these mice. Mitochondrial dysfunction has been observed in both RTT patients and in *Mecp2*$^{-/y}$ mice [132,217–219]. Given IGF1's role in glucose tolerance and metabolism [208,209], rhIGF1 treatment may have altered metabolism leading to improved mitochondrial functioning and allowing these mice to travel greater distance without fatigue. In Reactome analysis comparing rhIGF1 treated and vehicle treated *Mecp2*$^{-/y}$ mice, mitochondrial translation pathways were over-represented in the cerebellum. However, mitochondrial related pathways were not affected in the blood, which would have more relevance to bioenergetics of muscles and should be considered. The results of this study suggests that rhIGF1 may be improving bio-energetics and mitochondrial functioning in the cerebellum through mitochondrial protein synthesis. More direct studies are required to investigate the role of mitochondrial functioning both in the CNS and peripherally in *Mecp2* mutant mice and whether rhIGF1 can rescue any defects.

3.3.3 Effect of Mecp2 Mutation on Gene Expression

To determine the effects of *Mecp2* mutation in male and female mice, vehicle treated *Mecp2* –null and -heterozygous were compared to WT controls. The transcriptional profiles of these mice differed in both cerebellum and blood. This was not surprising

considering the different pathological presentations and differing ages of these mice. In the cerebellum of *Mecp2*$^{-/+}$ mice (Figure 3.14) there was roughly equal proportions of up- and down-regulated genes, while in *Mecp2*$^{-/y}$ mice (Figure 3.15) up-regulation of DEG was favoured. In blood female *Mecp2*$^{-/+}$ mice (Figure 3.14) two thirds of DEG were down-regulated while in male *Mecp2*$^{-/y}$ mice (Figure 3.15) the opposite pattern of expression was observed.

Previous gene expression analysis in *Mecp2*$^{-/y}$ mice at pre- and post-symptomatic ages found twice as many up-regulated as down-regulated genes compared to WT littermates [220]. This is consistent with the current analyses in both cerebellum and blood of *Mecp2*$^{-/y}$ mice favouring up-regulation, suggesting that MeCP2 is acting as a transcriptional repressor in male mice. However, there is also evidence of *Mecp2* acting as a transcriptional activator of gene expression [74]. In this thesis, analysis of DEG in *Mecp2*$^{-/+}$ supported this observation, since *Mecp2* can act as a transcriptional activator with cerebellum displaying equal numbers of up- and down-regulated genes, and in blood there was a bias towards down-regulation of DEG.

The mosaicism of *Mecp2*$^{-/+}$ mice has been proposed to account for much of the variability in this phenotype [173]. Reactome analysis in the cerebellum of *Mecp2*$^{-/+}$ and *Mecp2*$^{-/y}$ mice compared to WT found that "Transcriptional regulation by MECP2" and "MECP2 regulates transcription of neuronal ligands" were over-represented. This suggests that mosaic expression was not able to fully mitigate the expression changes induced by mutant *Mecp2*. XCI in *Mecp2*$^{-/+}$ mice was shown to be dependent on age, with more mutant *Mecp2* being expressed in older symptomatic mice compared to younger pre-symptomatic mice. Mice at 3 months of age showed no mosaicism but mice at 6 and 9 months showed increased levels of mosaic expression [221]. The female mice used in this analysis were roughly 5 months old and are therefore more likely to express both mutant and WT *Mecp2*.

Reactome and GO analysis in male and female mice revealed a small number of shared pathways and ontologies, 2 pathways (Out of 37 female and male 13 pathways) and 3 ontologies (Out of 206 female and 17 male ontologies). In cerebellum, the pathways and ontologies enriched in both *Mecp2*$^{-/+}$ and *Mecp2*$^{-/y}$ mice were "Transcriptional regulation of MeCP2" and "MeCP2 regulates transcription of neuronal ligands" in Reactome analysis and in GO analysis "Positive regulation of cellular processes",

"Response to nitrogen compound" and "Response to organonitrogen compound". In blood, there was a greater number of shared functions, 16 ontologies (Out of 506 female and 322 male ontologies) and 44 pathways (Out of 86 female and 72 male ontologies).

In Reactome analysis of blood there was a variety of pathways including "Regulation of Insulin-like Growth Factor transport and uptake by IGFBPs", "Platelet degranulation" and "MAP2K and MAPK activation". In GO analysis of blood similar immune functioning related ontologies were enriched as had been detected in RTT patient study in chapter I. These ontologies included: "Defense response", "Innate immune response" and "Neutrophil chemotaxis".

The response to nitrogen compounds, confirms what was initially reported by Andreas Rett "… Cerebral atrophy with hyperammonaemia in childhood", however, this may have been a secondary effect of liver failure rather than a feature of RTT pathology [32,222]. A more recent metabolic study in RTT patient plasma compared to non-effected siblings revealed a significant difference in nitrogen metabolism [223], and in *Mecp2*$^{-/y}$ mice found a decrease in enteric neuronal Nitric Oxide Synthase which was suggested as a mechanism for gastrointestinal dismobility [224]. DEG in both *Mecp2*$^{-/+}$ and *Mecp2*$^{-/y}$ mice suggest nitrogen metabolism is affected in the cerebellum, but whether this disruption is central to RTT pathology is not clear.

3.3.4 Differential Gene Expression in rhIGF1 Treated Mecp2-null and Heterozygous Mice

The overall expression pattern can be discerned from figures 3.14 and 3.15. In *Mecp2* –null and –heterozygous mice treated with rhIGF1 compared to vehicle treated mice showed a similar pattern of expression. Both female and male mice had a greater number of DEG in the cerebellum relative to blood; in female mice 127 DEG in the cerebellum and 8 DEG in blood and in male mice 225 DEG in the cerebellum and 75 DEG in blood were found. There was a bias toward down-regulation of genes in each of these comparisons. DEG in rhIGF1 treated *Mecp2*$^{-/+}$ blood was relatively low compared to *Mecp2*$^{-/y}$ DEG, this suggested minimal effect of rhIGF1 peripherally in female mice, but not *Mecp2*$^{-/y}$ mice. The DEG in WT mice treated with rhIGF1 compared to vehicle treated mice was lower relative to the same comparisons in *Mecp2*-null and –heterozygous counterparts. The samples from rhIGF1 treated *Mecp2*$^{+/+}$ blood were not

included in this analysis due to restricted number of samples per run. The number of DEG in male WT blood was only 9 genes, suggesting minimal effect. Altogether, these results suggest that rhIGF1 has a homeostatic function. Where there is no *Mecp2* mutation in WT mice rhIGF1 treatment has little effect, but in the presence of RTT pathology rhIGF1 affects both *Mecp2*$^{-/y}$ and *Mecp2*$^{-/+}$ mice targeting a different set of genes in each phenotype . Because the severity of *Mecp2*$^{-/y}$ mice is worse than *Mecp2*$^{-/+}$ mice, higher number of DEG is observed in *Mecp2*$^{-/y}$ tissues.

A subset of DEG that are found in *Mecp2*-null and –heterozygous compared to WT and are expressed in the opposite direction in rhIGF1 treated *Mecp2*-null and –heterozygous compared to vehicle treated mice. These DEGs represent likely targets of rhIGF1 action in RTT pathology, because they are basally dysregulated in RTT-like phenotype and their expression is reversed by rhIGF1 treatment. Interestingly, there was no overlap between male and female cerebellum or between male and female blood. Only one gene *Transthyrin* (*Ttr*) was targeted in both *Mecp2*$^{-/y}$ blood and *Mecp2*$^{-/+}$ cerebellum. *Ttr* showed the same pattern of expression initially being up-regulated but with rhIGF1 treatment causing *Ttr* to be down-regulated. *Ttr* encodes a thyroid binding hormone thought to transfer thyroxine from blood stream to brain. Hyperthryoxinemia, subclinical hypothyrodisma, and elevated Free-T4 levels have all been identified in a cohort of RTT patients implicating abnormal thyroid function in RTT patients [225]. Although an interesting finding, there is little evidence in this analysis of thyroid dysfunction.

The Reactome and GO analysis of rhIGF1 target genes were consistent with *Mecp2*$^{-/+}$ having effecting CNS functions and having no effect on peripheral blood. In *Mecp2*$^{-/y}$ mice rhIGF1 target genes affected metabolic functions, such as “Regulation of cholesterol biosynthesis by SREBP” and “TP53 regulates metabolic genes” in the cerebellum and “Metabolism of lipids” and “Plasma lipoprotein clearance” in blood. These results suggest that rhIGF1 action in *Mecp2*$^{-/y}$ mice occurs primarily in cerebellum, but effecting metabolic rather CNS-specific processes. Combining this observation with the proposed homeostatic effect of rhIGF1, it would appear that *Mecp2*$^{-/+}$ mice have a less compromised CNS phenotype, while the *Mecp2*$^{-/y}$ phenotype is more wide spread and affects cellular and metabolic processes.

3.3.5 IGF Signaling and Growth Hormone

As with RTT patients from Chapter 1, the basal activity of IGF1 signaling may be an important factor in modulating the effects of the treatment in mice. In *Mecp2*$^{-/+}$ mice both *Igf1* and *Igfbp4* were both decreased in blood and in *Mecp2*$^{-/y}$ mice *Igf2* expression was decreased in the cerebellum. These results suggest that *Mecp2*$^{-/y}$ and *Mecp2*$^{-/+}$ mice have perturbation to IGF signalling. Indeed, Reactome analysis found that "Regulation of IGF transport and uptake by IGFBPs" was over-represented in blood when comparing vehicle treated *Mecp2*$^{-/y}$ or *Mecp2*$^{-/+}$ mice versus WT counterparts, and in rhIGF1 treated *Mecp2*$^{-/y}$ or *Mecp2*$^{-/+}$ versus vehicle treated mice. Additionally, this pathway was also significant in the cerebellum of rhIGF1 treated *Mecp2*$^{-/y}$ versus vehicle treated *Mecp2*$^{+/y}$ mice. This result suggests that *Mecp2* mutation leads to abnormal peripheral IGF regulation, which persists after the administration of rhIGF1. A study using *Mecp2*$^{-/y}$ microglia, found *Igfbp3* expression was increased, suggesting that Igf1 regulation was abnormal centrally as well as in the periphery [184].

Importantly one of the few DEG that was observed in both rhIGF1 treated *Mecp2*$^{-/y}$ and *Mecp2*$^{-/+}$ mice cerebellum was the up-regulation of *Gh*. *Gh* was also considered a target of rhIGF1 in *Mecp2*$^{-/+}$ cerebellum because it reversed the down-regulation in vehicle treated *Mecp2*$^{-/+}$ mice to up-regulation after treatment. In the blood, *Mecp2*$^{-/+}$ had decreased expression of the *Gh receptor* (*Ghr*) the effector of *Gh* action. *Gh* expression was also increased in both rhIGF1 treated *Mecp2*$^{-/y}$ and *Mecp2*$^{+/y}$ mice suggesting a persistent abnormality in these mice.

As discussed in section 2.3.2 Growth Hormone controls the secretion of IGF1 from the liver and the interconnected regulation of GH and IGF1 through the GH-IGF1 axis. The GH-IGF1 axis has a variety of functions in skeletal muscle, liver function, lipid metabolism, glucose metabolism and bone growth [177,226]. Skeletal muscle growth in *Mecp2*$^{-/y}$ is disrupted via IGF1 signaling [207] and therefore may have contributed to locomotor improvements observed in *Mecp2*$^{-/y}$ and *Mecp2*$^{-/+}$. Metabolism of lipids was disrupted in *Mecp2*$^{-/+}$ blood treated with rhIGF1, however it was only a target pathway of rhIGF1 action in *Mecp2*$^{-/y}$ mice. These DEG need to be further examined to understand the effect of rhIGF1 on RTT pathophysiology.

3.3.6 Inflammation and Immune function

Abnormal expression of cytokines, chemokines, and inflammatory markers have been reported in both *Mecp2*$^{-/y}$ mouse models and in patients with RTT [227]. Transcriptional analysis of *Mecp2*$^{-/+}$ mouse models of microglia suggest that activation of M1 and M2 states were abnormal and identified a down-regulation in heat shock proteins [124]. Characterisation of expression to autoimmune challenge in *Mecp2*$^{308/y}$ mice revealed an exacerbated response with a chronic inflammatory state [193]. These studies confirmed that RTT pathophysiology is more susceptible to neuroinflammation in mice.

In this thesis, the proinflammatory genes *S100a8* and *S100a9* were increased in both *Mecp2*$^{-/y}$ and *Mecp2*$^{-/+}$ mouse blood compared to WT control. These genes were also increased in vehicle treated *Mecp2*$^{-/y}$ compared to *Mecp2*$^{+/y}$ in the cerebellum. Additionally, this increase was also observed comparing rhIGF1 treated *Mecp2*$^{-/y}$ versus both rhIGF1 and vehicle treated *Mecp2*$^{+/y}$ mice, suggesting a persistent increase in *S100a8* and *S100a9* in these mice.

S100a8 and *S100a9* encode EF-hand containing calcium binding proteins that act as alarmin molecules, initiating and promoting inflammation during stress. Imaging analysis has found that these molecules can act as a predictor of local sub-clinical inflammation and damage in mouse model of arthritis [228]. In this research group, *S100a9* gene expression was increased in the blood from *Mecp2*$^{-/y}$ mice [203]. Here in this thesis, it is confirmed that *S100a9* along with the related *S100a8* gene have increased expression in both *Mecp2*-null and –heterozygous blood. *S100a9* gene expression was found to be up-regulated in several brain regions of *Mecp2*$^{-/y}$ mouse, and a target of Mecp2 binding [203].

3.3.7 Synaptic Plasticity in Mecp2$^{-/+}$ *mice*

Reactome and GO analysis found a number of pathways associated with synaptic plasticity and neurotransmission in *Mecp2*$^{-/+}$ compared to WT mice. LTP is one the classic mechanisms of synaptic plasticity in the brain and was over-represented in GO and Reactome analysis in both vehicle treated *Mecp2*$^{-/+}$ compared to WT mice and rhIGF1 treated *Mecp2*$^{-/+}$ compared to vehicle treated control.

Previous studies by Castro and colleagues found that rhIGF1 treatment in *Mecp2*$^{-/+}$ mice stabilised abnormal activity dependant plasticity as measured by monocular deprivation and the shift in ocular dominance. This shift occurred at P60, representing an extension of the normal critical period of plasticity in the visual cortex which is typically identified around P28 [22,151]. Castro and colleagues found that rhIGF1 increased the level of PSD-95 in *Mecp2*$^{-/y}$ mice. PSD-95 levels are a marker involved in the incorporation of α-Amino-3-hydorxyl-5-methyl-4-isoxazolepropionic acid receptor (AMPAR) into the synapse during LTP and activity dependent plasticity [151,229]. PSD-95 transport at the synapse is mediated by signaling mechanisms PI3K-AKT after NMDA activation [229].

The ontology "NMDA selective glutamate receptor signaling pathway" was identified in the analyses for the effect of rhIGF1 treatment in in heterozygous mice and the comparison for the effect of *Mecp2* mutation. The NMDA receptor 2B (*Grin2b)* and Calcium Calmodulin-Dependent Kinase 2A (*Camk2a)* genes were both targets of rhIGF1 action. These genes were initially up-regulated in *Mecp2*-heterozygous cerebellum, but with application of rhIGF1 became down-regulated. MeCP2 has been proposed to form an auto-regulatory loop with CAMK2A and therefore plays a critical role in synaptogenesis [230].

These findings suggest alterations to synaptic plasticity in *Mecp2*$^{-/+}$ mice. In this thesis, the analyses were based on gene expression, but functional analysis, by electrophysiology, is needed for confirming synaptic plasticity. Much of what is known about electrophysiology in RTT, has been derived from recordings from mouse models due to the invasiveness of the technique. Studies report decreases in the ratio of excitation to inhibition in cortical layer 5 neurons and the primary visual cortex [281, 282]. However, there is contradictory evidence of this, one study found increased excitation-inhibition balance in pyramidal hippocampal neurons [106], and another found an increase in excitatory current with no change to inhibitory currents [283]. These changes may be a result of the region in the brain, the other inputs from surrounding neurons or even age-dependent defects. However, these alteration to excitation inhibition balance reflect the underlying changes in synaptic plasticity. Therefore, they are likely to be due to impaired synaptic maturity [90]. LTP and Long Term Depression (LTD) are two forms of synaptic plasticity that are well characterised. LTP is a long term strengthening of synaptic connections, while LTD is a weakening of synaptic connection. *Mecp2*$^{-/y}$ mice

have decreased levels of LTP [284-286], however studies find conflicting results on LTD with both reports of decreases [285] and no change in LTD [285].

Global and PV-specific *Mecp2*$^{-/y}$ mice display abnormal excitation inhibition balance was found to be restored by rhIGF1 treatment [111]. This study supports the results observed in this thesis, that rhIGF1 affects synaptic plasticity in *Mecp2*$^{-/+}$ mice.

3.3.8 Metabolic and Cellular Processing

There was a higher number of DEG detected in the cerebellum of *Mecp2*$^{-/y}$ mice relative to the same comparisons in female mice. Reactome and GO analysis did not reveal any synaptic or neurotransmission related pathways or ontologies in cerebellum of male mice. Instead, a wide variety of functions related to metabolic and cellular processes were observed. None of the genes that were considered targets of rhIGF1 action in cerebellum overlapped between *Mecp2*$^{-/+}$ and *Mecp2*$^{-/y}$ mice, which suggests rhIGF1 had a completely different set of transcriptional effects in female and male mice.

This result does not mean that treatment did not affect neuronal functioning. Indeed, there is direct evidence of physiological improvements in global and PV-specific *Mecp2*$^{-/y}$ mice after rhIGF1 treatment [111]. A recent metabolomics study in *Mecp2*$^{-/y}$ cortex found up-regulation of carbohydrate, amino acid, mitochondrial and lipid metabolites, while neurotransmitters such as acetylcholine, serotonin and dopamine were down-regulated [232]. Clearly, neuronal function will be impacted by abnormal metabolic processing.

Lipid metabolism was found to abnormal in the blood of both *Mecp2*$^{-/+}$ and *Mecp2*$^{-/y}$ mice, suggesting that the disruption to metabolism was not exclusive to male mice. Although the effects of rhIGF1 treatment on *Mecp2*$^{-/+}$ mice blood was thought to be minimal, 3 genes were identified in the same comparison in male mice. *Albumin (Alb),* *Apolipoprotein A2 (Apoa2),* and *Fatty acid binding protein 1* (*Fabp1)* are all down-regulated with rhIGF1 treatment and are involved the metabolism of lipids. However, these genes were only considered targets of rhIGF1 action in male mice because rhIGF1 treatment reversed the direction of expression. Therapeutics targeting cholesterol metabolism by statins has been shown to improve survival and motor symptoms in *Mecp2*$^{-/y}$ and *Mecp2*$^{-/+}$ mice highlighting the importance of lipid metabolism in RTT pathology [233].

3.3.9 Potential for Biomarkers

One of the greatest challenges in studying RTT is the inaccessibility of the CNS, the site of primary pathology. This has led to many studies examining peripheral blood as a potential source of molecular markers for the RTT pathology [166,183,204,234,235]. A conditional KO of *Mecp2,* where protein was functional in the brain knocked out in peripheral tissues, displayed a unique subset of symptoms including hypoactivity, exercise fatigue and bone abnormality [94]. The detection of changes in gene expression or protein concentration in blood correlating to disease severity or response to treatment could be vital for developing RTT therapeutics.

The observed differential expression in patients with RTT and mouse models treated with Mecasermin/rhIGF1, suggest that endogenous regulation of IGF1 signaling plays an important role in RTT pathophysiology. This observation is supported by a recent study using rhIGF1 as a treatment in neuronally differentiated ASD IPS cells found that response correlated to *IGFR* expression [171]. Based on these findings, gene expression of *Igf1r* was measured and plotted against the change in locomotor activity (Figure 3.11).

This was first assessed in the cerebellum of untreated male mice, 4 weeks of age and older, see figure 3.8. There was no significant difference in expression or correlation between expression and locomotor activity. Similarly, there was no significant change or correlation with *Igf1* expression. When *Igf1r* expression was measured in rhIGF1 and vehicle treated female mice there was a significant correlation between *Igf1r* and the change in locomotor activity before and after treatment. *Igf1r* was elevated in vehicle treated *Mecp2*$^{-/+}$ mice compared to rhIGF1 treated *Mecp2*$^{-/+,}$ although this was not significant after multiple testing correction. Considering the relatively low sample number of the experiment in treated female mice more biological replicates are needed to validate this finding. In order for *Igf1r* expression to be developed as a useful biomarker for response to rhIGF1 treatment, this experiment needs to be repeated in blood.

S100a9 and *S100a8* were up-regulated in the blood of *Mecp2*$^{-/+}$ and *Mecp2*$^{-/y}$ mice, and the literature had previously indicated elevated expression of *S100a9* [203,204]. Due to the utility of these genes as biomarkers of sub-clinical inflammation [228], *S100a9* and *S100a8* expression was plotted against locomotor activity to measure the correlation

between these variables. However, in the both untreated *Mecp2*$^{-/y}$ and treated *Mecp2*$^{-/+}$ mice there was no significant change in expression compared to WT or correlation with locomotor activity.

This analysis has displayed the potential for *Igf1r* gene expression in cerebellum to correlate with the change locomotor activity in *Mecp2*-heterozygous and WT mice. The sample size for this analysis should be expanded to determine if this relationship holds and a similar experiment should be carried out in blood to validate whether *Igf1r* expression could be developed as a biomarker for response to rhIGF1 treatment.

3.4 Conclusion

In Chapter II the molecular correlates of rhIGF1 administration were assessed *in vivo* using the *Mecp2* mouse model. This approach enabled DGE analysis of the cerebellum and blood understand how the RTT pathology is affected centrally in the CNS and in the periphery. The general motor behaviour of these mice was measured before and after treatment and demonstrated that *Mecp2*$^{-/+}$ and *Mecp2*$^{-/y}$ mice improved from treatment in different ways.

DGE analysis found that rhIGF1 treatment had a homeostatic role in *Mecp2* mice. The effects of treatment in the milder *Mecp2*$^{-/+}$ mouse based on synaptic and neurotransmitter functions, while in severely compromised *Mecp2*$^{-/y}$ mice treatment effected metabolic and cellular processes.

In concurrence with the findings of Chapter I, this mouse model highlights the importance of IGF1 signaling and regulation in the response to rhIGF1 treatment. Encouragingly, in the cerebellum of female treated mice the expression of *Igf1r* correlated significantly with the change in locomotor activity before and after treatment. This same gene was found to correlate with electrophysiological response to rhIGF1 treatment in ASD IPS derived neurons. In Chapter I, the hypothesis driven testing revealed a number of gene sets related to IGF1R signaling were over-represented, these were:

1. IGF receptor signaling pathway (GO: 0048009) at T1 in RVMSR (n = 4 versus 5).

2. IGF1 receptor signaling pathway (GO: 0048009) from T1 to T2 in Responders (n = 4).
3. Chronic response to IGF1 in ASD IPS derived neurons from the Linker study [171] from T1 to T2 in MSRs (n =5).

The results of Chapter II demonstrate that *Mecp2*$^{-/+}$ and *Mecp2*$^{-/y}$ mice can be used to successfully derive DEG involved in RTT pathology that overlaps with what is observed in patients with RTT. rhIGF1 treatment induced different functional processes in *Mecp2* model mice based on sex. While rhIGF1 treatment effected synaptic functions in *Mecp2*$^{-/+}$ mice, in *Mecp2*$^{-/y}$ mice treatment effected metabolic and cellular processes. This analysis is consistent with the homeostatic role of rhIGF1 proposed in Chapter I; rhIGF1 in unaffected WT mice had little effect on DEG compared to *Mecp2*-null and -heterozygous counterparts and DEG was higher in severely compromised *Mecp2*$^{-/y}$ mice relative to *Mecp2*$^{-/+}$ mice.

4.0 Chapter III: *In Vitro* Mechanism of rhIGF1 in SH-SY5Y Neuronal Cell Line

4.1 Introduction and Aims

There are many regulatory and compensatory mechanisms for IGF1R signaling. This tight regulation is needed due to the numerous biological functions linked to IGF1 signaling, and aberrant signaling, in particular overexpression of IGF1R, is associated with cancer and tumorigenesis[237,238]. Negative feedback mechanisms are known to occur in IGF1R signaling in 3 distinct ways;

1. Under physiological concentrations of IGF1 stimulation, IGF1R is internalised due to Mouse double minute 2 (Mdm2) -ubiquitination, a form of clathrin mediated endocytosis [179].
2. At higher non-physiological concentrations of IGF1 stimulation, IGF1R is internalised via caveolin mediated pathway [179].
3. IRS desensitisation occurs in response to IGF1 stimulation, which occurs through IRS-1. Therefore desensitisation of IRS decreases PI3K signalling but not MAPK [239].

As described in section 1.6.1, rhIGF1 and GPE-based therapeutics have achieved varying levels of success in RTT human clinical trials. However, at a systemic level, it is difficult to identify the mechanisms linked to each of these treatments. To explain the difference in trial outcome, it is necessary to explore signaling pathways of rhIGF1 and GPE treatments. *In vitro* cell line experiments are well suited to understanding molecular mechanisms due to being a simplified system with homogenous cell population. One study by Corvin and colleagues, which compared rhIGF1 and GPE directly in mouse primary culture, found that rhIGF1 primarily activated signaling in neuronal cells, while GPEs action occurred primarily in glial cells. GPE also induces increase in endogenous IGF1 levels which in turn caused activation of IGF1R [30].

Chapter III aims to investigate *in vitro* mechanisms of rhIGF1and GPE stimulation in the neuronally differentiated SH-SY5Y cell line. Canonical downstream signalling of PI3K/AKT and MAPK pathways will be assessed and specific blocker of IGF1R, PPP will be used to determine dependence on IGF1R activation.

4.2 Results

4.2.1 Blockade of IGF1R by Picropodophyllin Inhibitor

To be able to distinguish between IGF1R mediated effects of stimulation the specific IGF1R inhibitor was used. Picropodophyllin (PPP) has been demonstrated to be an efficient blocker of IGF1R activity, as well as reducing downstream pAKT and pERK level, PPP does not to have cytotoxic effects [239]. PPP has been used previously used in SH-SY5Y cells to investigate the role of IGF1R and p75NTR on amyloid-β oligomerisation [240]. In this chapter, it was established the blocking conditions of IGF1R on PPP on the basis of the methods of Ito and colleagues. 1μM of PPP was pre-incubated in cell media for 2hr prior to stimulations in order to block phosphorylation of IGF1R (pIGF1R) [240].

In order to determine that this level of PPP was sufficient to block pIGF1R, western blot of total proteins measured pIGF1R relative to β-actin loading control as shown in figure 4.1. Cell were treated with either 100ng/ml of rhIGF1 or vehicle (differentiation media) with either 1 μM of PPP in DMSO solvent or vehicle control (DMSO). The results of the western blot are displayed in figure 4.1.

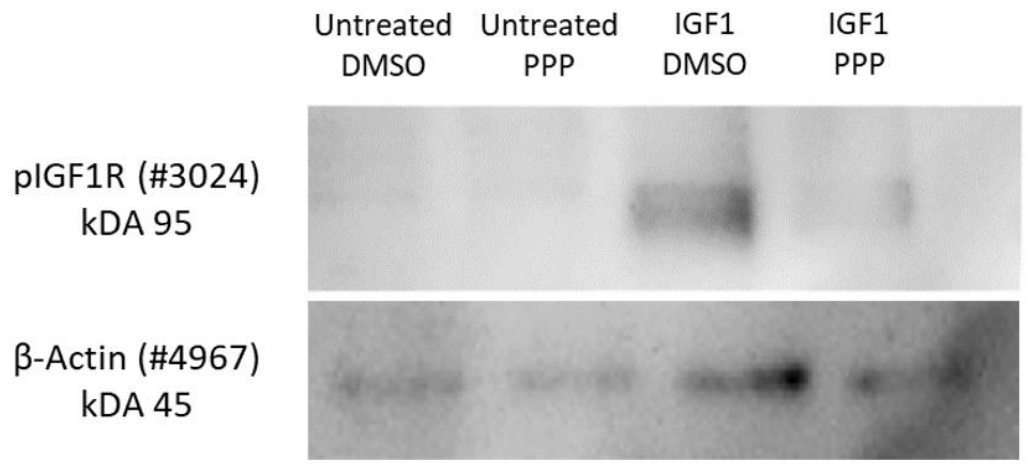

Figure 4.1 - Demonstration of blockade of pIGF1R by PPP Inhibitor
Neuronally differentiated SH-SY5Y cells were treated with 100ng of rhIGF1 or vehicle control for 24hr having been pre-incubated with 1μM PPP or vehicle control (DMSO) for 2hr. Protein extraction and western blot was performed. Protein containing membrane was stained using pIGF1R antibody (#3024, CST) and β-actin antibody (#4967, CST) as reference control. Blotting reveals that cells not treated

with rhIGF1 showed minimal levels of pIGF1R while cells treated with rhIGF1for 24hr without inhibitor showed a strong increase in pIGF1R, this phosphorylation was prevented largely by presence of PPP but not to as low a level as untreated cells. For this analysis 3 experiments were used (n = 3, pooled samples) but due to low concentrations of protein these replicates had to be pooled for blotting.

rhIGF1 stimulation induced pronounced increase in pIGF1R levels which was ameliorated by addition of PPP. Due to the low levels of protein yield from extraction, cells of the same condition were pooled together to ensure measurable levels of protein. This meant that although sample size of n = 3 was used, it was not possible to conduct statistical analysis. However, this was sufficient for proof of principle that PPP was efficiently blocked pIGF1R. This experiment should be replicated using GPE simulation, since previous studies have found that GPE can indirectly activate IGF1R by increasing the endogenous levels of IGF1 [30].

4.2.2 Effect of rhIGF1 on activation of AKT and ERK1/2

The cytoplasmic area of the cells was determined by staining cells for MAP2, a marker for neuronal differentiated cells [241]. The phosphorylation of AKT and ERK1/2 was measured in the cytoplasm of the cells after stimulation with 100 ng/mL rhIGF1 for 24hr. Cells were pre-incubated with either 1μM of PPP or vehicle DMSO for 2hr prior to stimulation.

Previous experiments in Cerebellar and P12 neuronal cell culture, determined that the pro-survival effects of IGF1 was induced through serine 473 [17,243]. Therefore, an antibody to measure phosphorylation of AKT at serine-473 (pAKT) was normalised to control and plotted in figure 4.2. This analysis found that rhIGF1 induced a decrease in pAKT, while addition of PPP blocked this decrease, relative to control. PPP by itself did not affect pAKT levels.

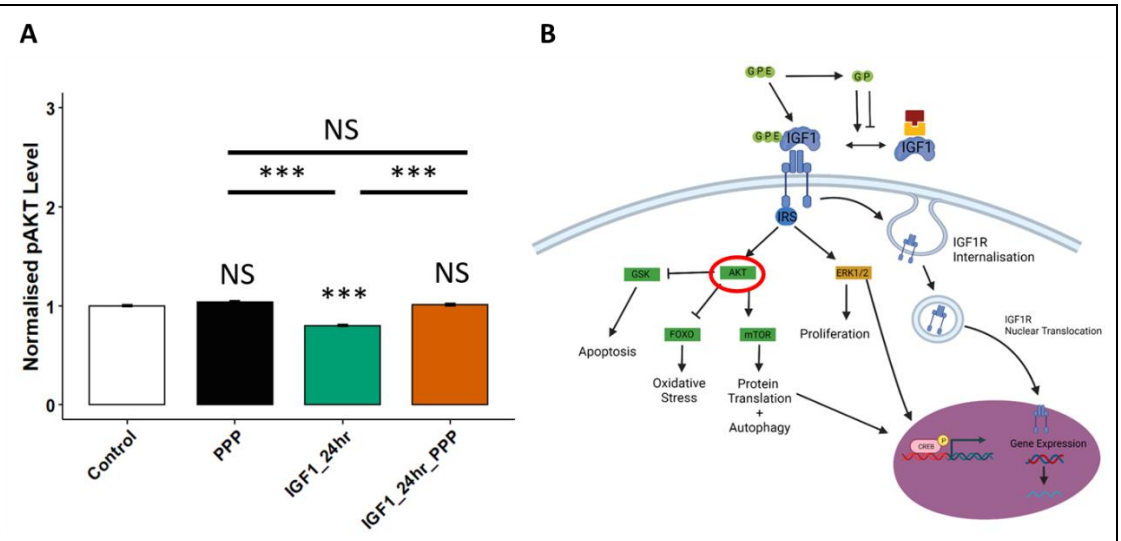

Figure 4.2 – Cytoplasmic pAKT Concentration after Stimulation with rhIGF1 in the Presence or Absence of IGF1R PPP Inhibitor

A – Shows the normalised levels of cytosolic pAKT as bar-graph with mean ± SE of the mean. PPP and rhIGF1 with PPP shows no significant difference in activation compared to control cells, while rhIGF1 by itself has reduction in pAKT compared to control cells. rhIGF1 treated cells are also decreased compared to PPP and rhIGF1 with PPP cells. This data suggests that activation of pAKT by rhIGF1 is IGF1R dependent. **B –** Schematic of IGF1 signalling pathway highlighting AKT in red.

Legend:

PPP = Cells pre-treated with 1uM PPP, IGF1_24hr = Cell treated with rhIGF1 for 24 hours, IGF1_24hr_PPP = Cells pre-treated with 1uM of PPP then treated with rhIGF1 for 24hr, *** = adjusted p-value <0.00005 (asterisks directly over individual bars were relative to control), NS = Non-Significant, tested using Kruskal-Wallis post hoc Wilcox test unpaired, sample size (n = 3).

Like AKT signalling, IGF1-dependent MAPK signalling also contributes to cell survival and DNA synthesis [8]. In peripheral blood mononuclear cells MAPK signalling potentiates proinflammatory response, via phosphorylation of ERK1/2 (pERK1/2) [193]. The results of pERK1/2 after rhIGF1 stimulation with or without PPP are displayed in figure 4.3.

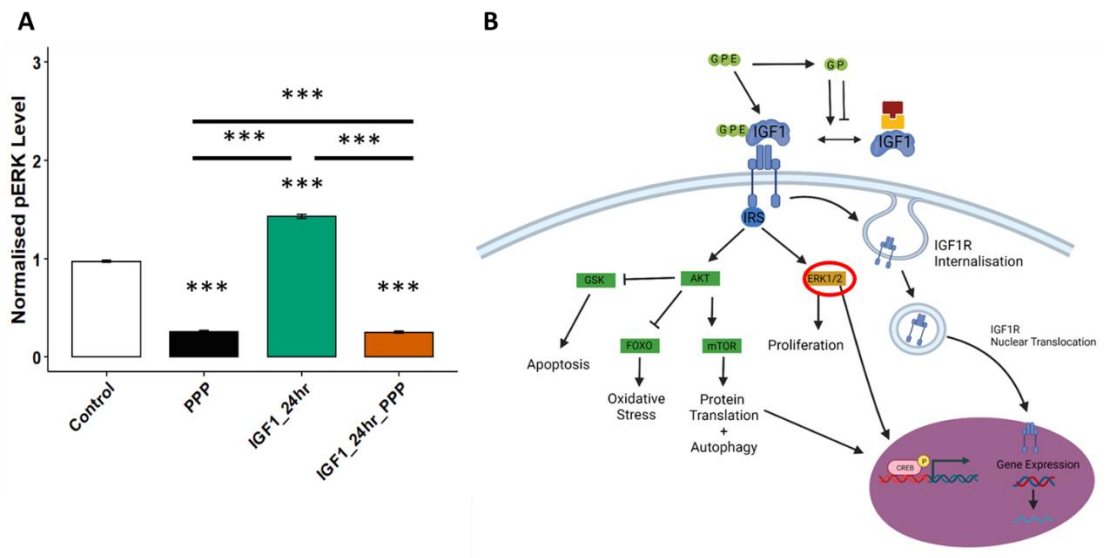

Figure 4.3 – Cytoplasmic pERK Concentration after Stimulation with rhIGF1 in the Presence or Absence of IGF1R PPP Inhibitor

A – Shows the normalised levels of cytosolic pERK 1/2 as bar-graph with mean ± SE of the mean. PPP and rhIGF1 with PPP show similar decreases in the levels of pERK 1/2 compared to control. rhIGF1 treatment induced an increase in the activation of ERK 1/2 compared to control. Additionally, rhIGF1 treatment was also significantly increased compared to PPP and rhIGF1 with PPP. This data suggests that activation of pERK 1/2 by rhIGF1 is IGF1R dependent. **B –** Schematic of IGF1 signalling pathway highlighting ERK 1/2 in red.

Legend:

PPP = Cells pre-treated with 1uM PPP, IGF1_24hr = Cell treated with rhIGF1 for 24 hours, IGF1_24hr_PPP = Cells pre-treated with 1uM of PPP then treated with rhIGF for 24 hours, *** = adjusted p-value <0.00005 (asterisks directly over individual bars were relative to control) tested using Kruskal-Wallis post hoc Wilcox test unpaired, sample size (n = 3).

This analysis showed that PPP with or without rhIGF1 stimulation decreased pERK1/2 relative to control cells. These results demonstrated that SH-SY5Y's endogenous levels of IGF1 are likely to be driving the ERK1/2 signaling. rhIGF1 stimulation induced an increase in the level of pERK1/2 compared to control.

4.2.3 Effect of GPE on activation of AKT and ERK1/2

Despite being derived from IGF1, GPE does not directly bind IGF1R [10], instead it can affect IGF1R signaling by stimulating endogenous IGF1 levels [30]. Additionally, the metabolite of GPE and IGF1, cGP affects the binding affinity of IGF1 and IGFBP3 in a homeostatic manner. In this study by Guan and colleagues [11] cGP was used as a treatment in two different contexts. First cGP was used to treat ischaemic head injury where it increased IGF1 to support vascular remodelling preventing neuronal damage. Second cGP was used to treat lymphatic tumours where tumour growth was inhibited, a process that was mediated by IGF1 [11]. Both these studies suggest that GPE functions by altering regulation of IGF1 signaling. In this thesis, GPE was used to stimulate SH-SY5Y cells with and without PPP inhibitor. The dose of GPE used was the molar equivalent of 100 ng/mL of rhIGF1, approximately 3.6 ng/mL to account for the different molecular masses of these compounds.

The results of pAKT levels in GPE stimulated cells are displayed in figure 4.4. GPE induced a strong increase in pAKT compared to control cells, this was inhibited to a large degree by PPP.

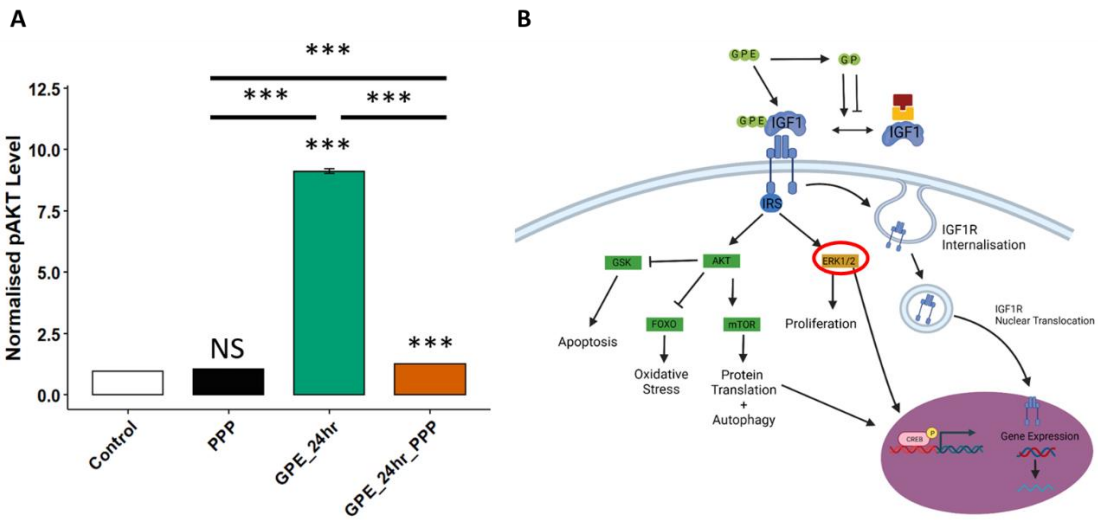

Figure 4.4 – Cytoplasmic pAKT Concentration after Stimulation with GPE in the Presence or Absence of IGF1R PPP Inhibitor

A - Shows the normalised levels of cytosolic pAKT as bar-graph with mean ± SE of the mean. PPP showed no significant difference compared to control. rhIGF1 treatment induced a large increase in the level of pAKT compared to control, PPP

prevented this increase suggesting that this activation of AKT was IGF1R dependent.

B – Schematic of IGF1 signalling pathway highlighting AKT in red.

Legend:

PPP = Cells pre-treated with 1uM PPP, GPE_24hr = Cell treated with GPE for 24 hours, GPE_24hr_PPP = Cells pre-treated with 1uM of PPP then treated with GPE for 24 hours, *** adjusted p-value <0.00005 (asterisks directly over individual bars were relative to control), NS Non-Significant, tested using Kruskal-Wallis post hoc Wilcox test unpaired, sample size (n = 3).

In figure 4.5, levels of cytoplasmic pERK1/2 were assessed after stimulation with GPE in the presence and absence of PPP. This experiment demonstrated, unlike rhIGF1, GPE treatment induced a decrease in the level of pERK. Additionally in the presence of PPP, GPE induced an increase in the level of pERK. This suggests that decrease induced by GPE treatment was not IGF1R dependent.

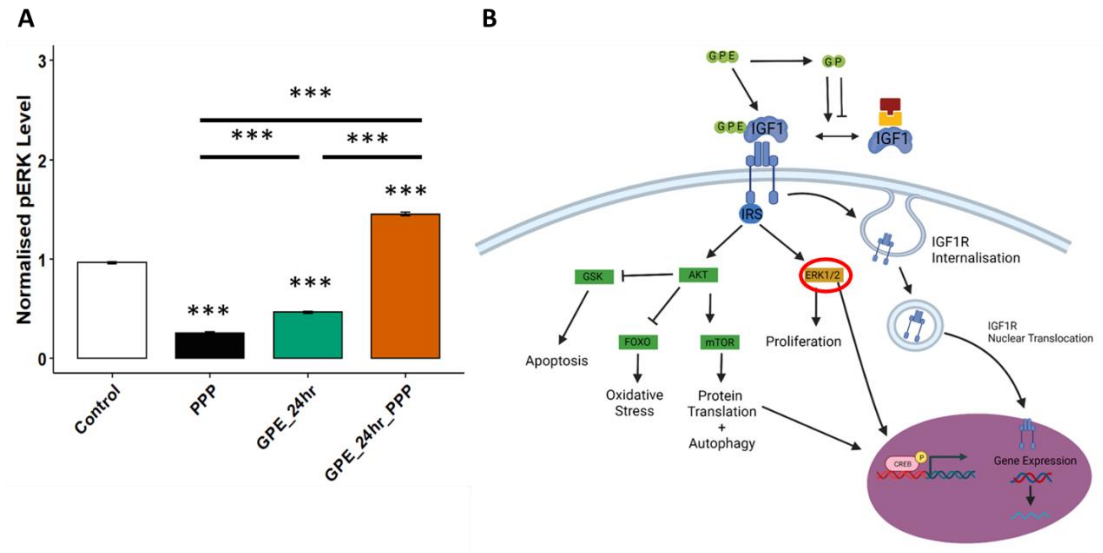

Figure 4.5 – Cytoplasmic pERK1/2 Concentration after Stimulation with GPE in the Presence or Absence of IGF1R PPP Inhibitor

A – Shows the normalised levels of cytosolic pERK 1/2 as bar-graph with mean ± SE of the mean. PPP showed a decrease in the levels of pEKR 1/2 compared to control, GPE also had a decrease in pERK1/2 levels but to a smaller extent than PPP. GPE

with PPP induced an increase in pERK1/2 levels compared to control, which is somewhat counterintuitive considering the canonical signalling of IGF1. This might be explained by the homeostatic role of cGP, the GPE metabolite, has on IGF1 signalling [27]. **B -** Schematic of IGF1 signalling pathway highlighting ERK1/2 in red.
Legend:
PPP = Cells pre-treated with 1uM PPP, GPE_24hr = Cell treated with GPE for 24 hours, GPE_24hr_PPP = Cells pre-treated with 1uM of PPP then treated with GPE for 24 hours, *** adjusted p-value <0.00005 (asterisks directly over individual bars were relative to control)

4.2.4 Effects of rhIGF1 and GPE stimulation on CREB activation

IGF1 stimulation is known to activate nuclear CREB in a MAPK dependent manner in PC12 neuronal cells [242]. CREB is expressed throughout the brain and acts as a transcription factor, and its transcription is associated with forms of synaptic formation, growth and plasticity [243].

Given that rhIGF1 and GPE has been shown to improve synaptic deficits in *Mecp2*$^{-/y}$ and *Mecp2*$^{-/+}$ mice [101,151], the concentration of nuclear pCREB was assessed after stimulation with rhIGF1 and GPE. The antibody used for pCREB staining detected specific phosphorylation at serine 133 which is activated through MAPK signaling, as well as Protein Kinase A (PKA), and calcium calmodulin-dependent kinase VI (CaMK VI) [242,243]. Hence, activation of CREB at serine 133 is activated by MAPK but not PI3K-AKT signalling.

Nuclear levels of pCREB were measured after stimulation with rhIGF1 with and without PPP inhibitor, the results of this analysis are shown in figure 4.6. In this analysis, PPP by itself induced a decrease in pCREB, while administration of rhIGF1 by itself and together with PPP increased pCREB levels in the nucleus. These results suggest that rhIGF1's activation of nuclear CREB is independent of IGF1R.

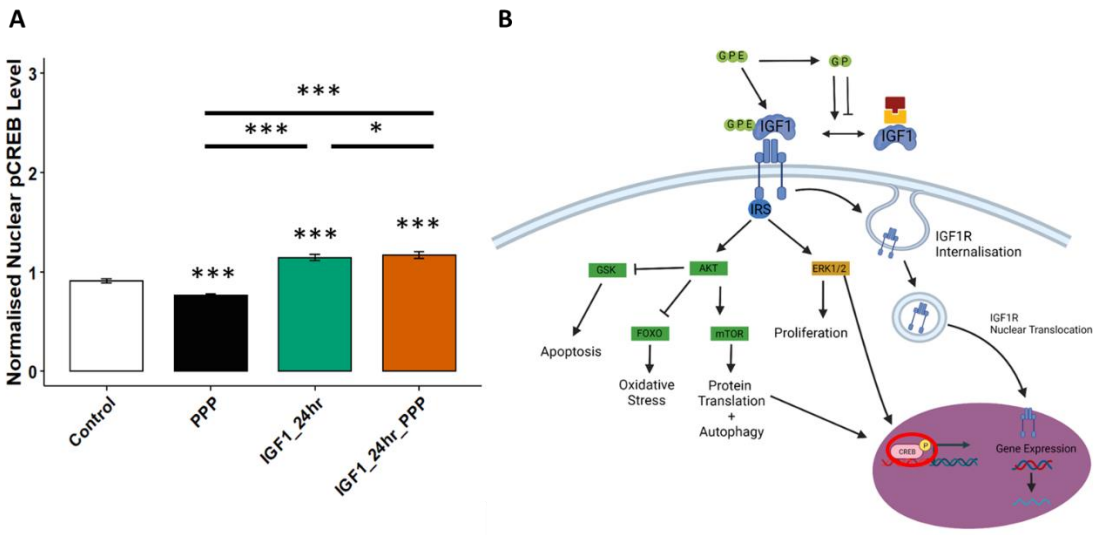

Figure 4.6 – Nuclear pCREB Concentration after rhIGF1 Stimulation in Presence or Absence of IGF1R PPP Inhibitor

A – Shows the normalised levels of nuclear pCREB as bar-graph with mean ± SE of the mean. Preincubation with PPP showed a decrease in pCREB, while rhIGF1 treatment induced increase in pCREB. This increase was not blocked with the addition of PPP suggesting that the mechanism of rhIGF1 increasing pCREB is independent of IGF1R.

B – Schematic of IGF1 signalling highlighting nuclear phosphorylated CREB in red.

Legend:

PPP = Cells pre-treated with 1uM PPP, IGF1_24hr = Cell treated with rhIGF1 for 24 hours, IGF1_24hr_PPP = Cells pre-treated with 1uM of PPP then treated with rhIGF1 for 24 hours, *** adjusted p-value <0.00005 (asterisks directly over individual bars were relative to control), * adjusted p-value <0.05 (asterisks directly over individual bars were relative to control)

In figure 4.7 the levels of nuclear pCREB are reported after stimulation with GPE in the presence and absence of PPP. GPE by itself increased levels of pCREB, while PPP by itself or in combination with GPE stimulation caused a significant decrease in pCREB levels compared to control. These results suggest that GPE induced activation of nuclear CREB was IGF1R dependent.

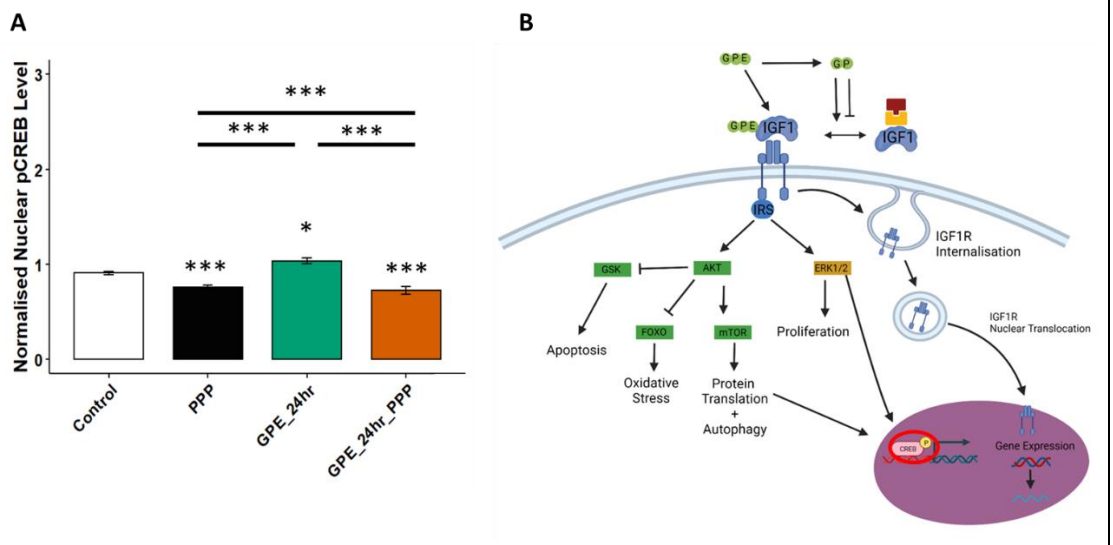

Figure 4.7 – Nuclear pCREB Concentration after GPE Stimulation in Presence or Absence of IGF1R PPP Inhibitor

A – Shows the normalised levels of nuclear pCREB as bar-graph with mean ± SE of the mean. Preincubation with PPP showed a decrease in pCREB, while GPE treatment induced increase in pCREB. This increase was blocked with the addition of PPP suggesting that, unlike rhIGF1, the mechanism of GPE increasing pCREB was IGF1R dependent.

B – Schematic of IGF1 signalling highlighting nuclear phosphorylated CREB in red.

Legend:

PPP = Cells pre-treated with 1uM PPP, GPE_24hr = Cell treated with GPE for 24hr, GPE_24hr_PPP = Cells pre-treated with 1uM of PPP then treated with GPE for 24hr, *** adjusted p-value <0.00005 (asterisks directly over individual bars were relative to control), * adjusted p-value <0.05 (asterisks directly over individual bars were relative to control)

Interestingly, all the mechanisms observed in this analysis, bar the activation of CREB induced by rhIGF1 and decrease in activation of pERK1/2 by GPE, were dependent on IGF1R. The activation of CREB by rhIGF1 could be explained by secondary effects of rhIGF1 on other signalling systems such as BDNF which could be contributing to CREB activation [243].

4.3 Discussion

In this analysis two potential treatments for RTT were directly compared in the neuronal cell model SH-SY5Y to identify the mechanisms of these drugs. PPP, a specific inhibitor of IGF1R, was used to block IGF1R activation and therefore to identify the intracellular mechanisms dependent of IGF1R activation. IGF1R signalling is not solely dependent on exogenous application of rhIGF1 or GPE, but is also stimulated by endogenous IGF1.

This analysis suggested that rhIGF1 and GPE stimulation have the opposite effects on the levels of pAKT and pERK1/2 at 24 hours, while both treatments increased the levels of nuclear pCREB. GPE treated cells showed a substantial increase in pAKT while rhIGF1 treated cells had decreased pAKT. Both these mechanisms were inhibited by PPP suggesting that these mechanisms are IGF1R dependent. In contrast rhIGF1 increased and GPE decreased the levels of pERK, both mechanisms occurred in IGF1R dependent manner.

Both rhIGF1 and GPE stimulation caused increases in nuclear pCREB in SH-SY5Y cells. For GPE, this increase could be prevented with blockade of IGF1R, while in rhIGF1 the presence of PPP was insufficient to block activation of CREB. These results suggest that GPE induced CREB activation in an IGF1R-dependent manner, but rhIGF1 induced CREB activation was independent of IGF1R. This may at first seem rather counterintuitive, as GPE is not able to bind IGF1R directly, although it can activate IGF1R by increasing endogenous IGF1 levels [10,30]. The metabolite of GPE and rhIGF1 cGP, is known to control the binding affinity of IGF1 and IGFBP3 in a homeostatic manner [11]. However, direct quantification of cGP and binding proteins would be required to understand its impact on the IGF1 signaling.

These results could have a number of different explanations. GPE is considered only a weak agonist for NDMAR [28], while rhIGF1 is known to activate IR and to a lesser extent IGF2R [7]. The results from this analysis represent the integration of all the signaling pathways in the SH-SY5Y system. Though SH-SY5Y culture is a simplified system, there is still a large degree of complexity to its signaling pathways. Therefore our results could be explained by other factors including IGF1 related regulation, promiscuity of the drugs for other receptors and compensatory signalling from other mechanisms using the same pathways.

4.3.1 Canonical signaling of rhIGF1 and GPE stimulation

The activation of the IGF1 signaling pathway occurs after IGF1R ligand binding and subsequent phosphorylation of the receptor, and these events lead to downstream canonical activation of PI3K-AKT and MAPK signaling [7,8]. The work of Corvin and colleagues found that rhIGF1 stimulation activated AKT and ERK1/2 in neurons, while GPE had an inhibitory effect on neuronal ERK1/2 and activated AKT in glial cells [30].

In this thesis, GPE but not rhIGF1 elicited a strong activation of AKT and both treatments decreased the MAPK activation. Though these findings conflict with the literature, it is important to consider that the levels of pERK1/2 and pAKT will be a result of many pathways and not only IGF1 related signaling. For example, BDNF signalling also affects both PI3K-AKT and ERK activation in the brain [231,244]. There were also a number of methodological differences between this thesis and the Corvin study that could account for the differing results, these were:

1. Different cultures. This thesis used neuronally differentiated SH-SY5Y cells which do not express a glial phenotype [241]. Corvin and colleagues use a primary neuronal culture from mouse which included a mixture of neuronal and glial cells [30].
2. Concentration of the drugs. The simulation of GPE in the Corvin paper was the same concentration as the rhIGF1 despite GPE be a fraction of the size of the IGF1 molecule. In this thesis the molar equivalent of GPE was used to control for this fact.
3. Duration of the stimulation. The stimulations in the Corvin paper were longer 48hr, than the stimulations used in this thesis 24hr.

While classically, rhIGF1 stimulation has been found to increase the PI3K-AKT and MAPK, the observed decreases may be explained by negative feedback mechanisms such as IRS desensitisation or internalisation. Phosphorylation of specific serine or tyrosine sites on IRS-1 by AKT or ERK1/2 can desensitise the protein to activation [20]. Long term stimulation (18hr) of L6 rat skeletal muscle cells with IGF1 (100ng/mL) decreases of IRS-1 and AKT activation [245]. Indeed adding of PPP prevented the rhIGF1 induced decrease of pAKT. The strong increase in pAKT induced by GPE stimulation

was largely blocked with presence of PPP. The effects of AKT by rhIGF1 and GPE are therefore IGF1R dependent.

The two members of the MAPK that were measured in this study, ERK1 and ERK2, have been shown to localise in the nucleus and activate immediate early gene transcription factors c-Fos and c-Jun, which are associated with growth functions [246].

rhIGF1 stimulation led to an increase in pERK1/2 levels while GPE induced a decrease in pERK1/2. Blockade of the IGF1R by itself induced a decrease of pERK1/2 to a greater extent than GPE. Somewhat counterintuitively GPE in the presence of PPP leads to an increase in pERK1/2, rather than a decrease. One explanation of this finding is while both PPP and GPE decrease pERK1/2 the addition of both at the same time disrupt the homeostatic balance that is maintained by IGFBPs and the metabolite cGP[11].

Another factor to take into account is the Internalisation of IGF1R. This process can happen via clathrin or caveolin pathway and it could mediate the decreases in AKT or ERK1/2 activation, therefore controlling the levels of bioavailable IGF1R to bind [179]. While clathrin mediated endocytosis was observed at physiological levels of IGF1, higher levels of IGF1 stimulation lead to caveolin mediated endocytosis of IGF1R [179]. Both pERK1/2 and pAKT are thought to target CREB in the nucleus after activation of NMDA receptor in striatal neurons [247]. MAPK signaling also activates CREB at Serine 133 through a downstream effector of ERK1/2, RSK2 [248]. Activation of CREB and inhibition of pro-apoptotic factor BAD, through IGF1 induced MAPK signaling increases cell survival [249]. Since the activation of CREB is associated with synaptic plasticity and intrinsic excitability [250], it is particularly interesting to find out if CREB activation is a target of rhIGF1 administration in relation to RTT.

In this thesis, the phosphorylation of serine 133 on CREB was measured in the nucleus, and was increased by both rhIGF1 and GPE stimulation. This increase persisted with the presence PPP and rhIGF1 stimulation but not with PPP and GPE, suggesting that GPE induced the increase in pCREB was dependent on IGF1R, while rhIGF1 stimulation did not.

4.3.2 Validity of PPP

PPP does not interfere with microtubules or induce cytotoxic effects and does not affect activation of IR [239]. PPP therefore represented a useful reagent to investigate blockade of IGF1R specifically. Previous studies using PPP in SH-SY5Y cell culture used a concentration of 1µM PPP that was pre-incubated with cells 2 hours before treatment to block the effects of IGF1 [240]. Western blot analysis demonstrated that PPP blocked the rhIGF1 associated activation of pIGF1R. This experiment displayed in figure 3.4 showed that the large increase in pIGF1R due to rhIGF1 stimulation was blocked by the action of PPP. Due the relatively low yield in protein from the extraction, the n = 3 experiments had to be combined in order to achieve detection of protein. Therefore statistical analysis was not possible.

Interestingly PPP inhibition by itself and combined with rhIGF1 did not fully block the pIGF1R. PPP inhibition interferes with the auto-phosphorylation of IGF1R through specific blocking of tyrosine at 1136 but not 1135 and 1131 [251]. Additionally, autophosphorylation has been proposed to only require tyrosine 1135 and 1131 [252], therefore PPP may not be causing a full blockade of IGF1R signaling. Further replications of this experiment and the effect of PPP blockade after GPE stimulation should be conducted to determine if PPP can fully inhibit IGF1R activation.

4.3.3 Regulatory Effect of GPE

GPE does not directly bind to the IGF1R [10] but instead is thought to increase endogenous levels of IGF1 which in turn leads to activation of IGF1R [30], and its metabolite of cGP regulates the bioavailability of IGF1 in a homeostatic manner [11], see section 4.3.2. This regulatory role of GPE on IGF1 signaling could mediate a more potent effect, which could explain the large increase in pAKT by GPE. In the context of RTT clinical trials, this regulatory role of GPE may have also contributed to the success of Trofinetide (a GPE derivative) during phase II clinical trial of RTT.

GPE's molecular mechanisms are thought to occur through glial cells more so than neuronal cells [30,253]. GPE and rhIGF1 have also been used to treat RTT IPS cells derived into an astrocyte phenotype co-cultured with WT interneurons. This study found morphological improvements were mutation dependent, and did not clearly show whether GPE out-performed rhIGF1 in this glial phenotype [140].

4.3.4 Graphic Summary of the Molecular Mechanisms of rhIGF1, GPE and PPP

Despite the relative simplicity of the neuronal SH-SY5Y cell model the results of *in vitro* experiments are nuanced and can be interpreted a number of ways. Though this analysis only scratches the surface of the mechanisms of rhIGF1 and GPE in neuronal cell culture, important questions can be asked from it. Additional experiments are needed to clarify the mechanisms of action of rhIGF1 and GPE, due to the restrictions and delays imposed by the SARS CoV2 pandemic such experiment were not completed for this thesis.

The results of Chapter III's analysis are complicated by two further factors that make it difficult to interpret the specific mechanisms:

1. rhIGF1 and GPE are interconnected. IGF1 can be broken down and metabolised to produce GPE [10] and GPE's metabolite cGP regulates bioavailability of IGF1 [11].
2. Endogenous IGF1 is present in these cultures and its activity can be driven by the application of treatments, for example the GPE induces increased endogenous IGF1 [30].

Therefore, care is needed when interpreting these findings and constructing a mechanism of action. To summarise the results of Chapter III, figure 4.8 displays a schematic of the effects of rhIGF1, GPE and PPP application on IGF1 signaling pathway. The signalling pathway of IGF1R has been previously described in section 1.1.2 of this thesis in figure 1.1. Graphical schematics were prepared using BioRender online platform, at BioRender.com.

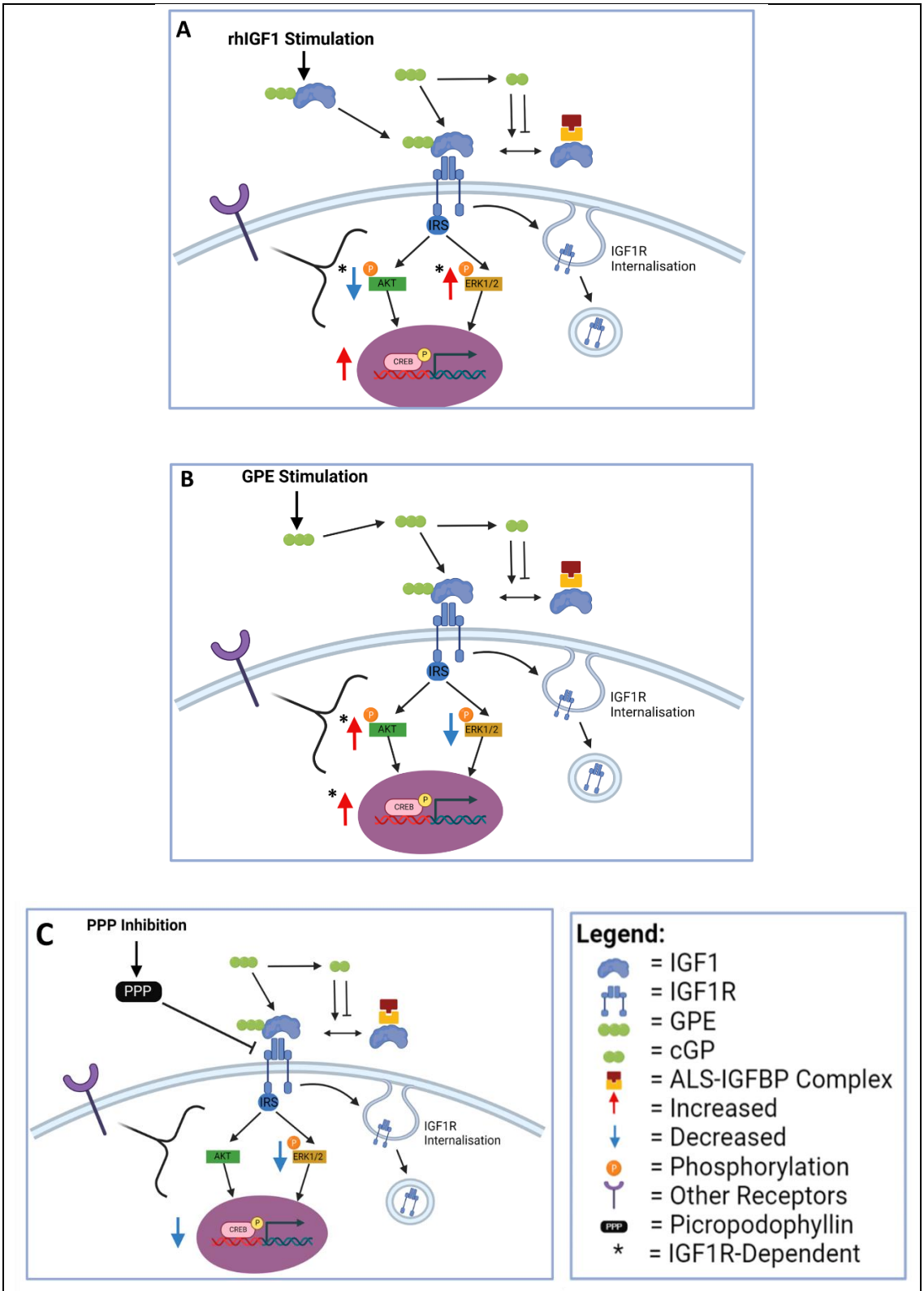

Figure 4.8 - Summary of rhIGF1, GPE and PPP Molecular Mechanisms in SH-SY5Y cell line

A – Stimulation of SH-SY5Y cells with 100ng/ml of rhIGF1 treatment for 24hr resulted in a decrease in pAKT and an increase in pERK1/2, both of which were IGF1R dependent mechanism. rhIGF1 treatment led to an increase in nuclear pCREB but this activation was found to be independent of IGF1R, suggesting involvement of other receptors or mechanisms. **B –** Stimulation of cells with 4ng/ml of GPE treatment for 24hr resulted in an increase of pAKT and a decrease in pERK1/2, the opposite of what happens after rhIGF1 treatment. GPE resulted in an increase in nuclear pCREB levels. Activation of pAKT and pCREB were both IGF1R dependent, the decrease in pERK1/2 was not. **C –** Inhibition of the IGF1R with PPP by itself had no effect on pAKT but decreased pERK1/2 and nuclear pCREB levels.

4.4 Conclusion

In this Chapter, experiments were conducted to clarify mechanisms of action of IGF1 by looking at the effect of rhIGF1 and GPE stimulation on the concentration of intracellular markers linked to pathways usually dependent on rhIGF1 and GPE administration. However, the experiments demonstrate rhIGF1 and GPE stimulation elicited different effects on the canonical downstream signaling pathways of IGF1R. GPE induced a strong AKT activation, while induced a decrease in AKT activation at 24hr. Both these results appeared to be IGF1R-dependents as they could be blocked by specific IGF1R inhibitor PPP.

rhIGF1 and GPE stimulation at 24hr decreased the levels of ERK1/2 activation. This decrease was significantly greater when combining stimulation with PPP blocker or by using PPP by itself. Decreased ERK1/2 activation, occurred in an IGF1R independent manner when induced by rhIGF1, and occurred in an IGF1R dependent manner when induced by GPE.

Finally, both rhIGF1 and GPE stimulations led to activation of nuclear CREB a transcriptional regulator associated with synaptic plasticity and long term potentiation [250].

Chapter III highlights the difference mechanism of rhIGF1 and GPE even in a simple system such as neuronal SH-SY5Y. While negative feedback and regulatory mechanisms may contribute to a decrease AKT and ERK1/2 activation after

rhIGF1 stimulation, GPE induced a strong activation of AKT suggesting a persistent or delayed activation mechanism in PI3K-AKT signaling.

5.0 General Discussion and Future Directions

The identification of IGF1 and its derivatives as a candidate treatment for RTT, has raised opportunities and challenges. While the treatment demonstrated improvements to apnoeic index in a phase I trial and to secondary measures of hand stereotypy and social communication in a phase II trial, the primary aims of the phase II trial failed to show efficacy [153,154]. The outcomes could be linked to the choice of primary outcomes or variability of RTT phenotype, which combined with the rarity of disease, impact the ability to validate a candidate treatment (NCT01253317). However, this class of compounds not only in RTT, but also for other neurodevelopmental disorders, since rhIGF1 is now in clinical trials for ASD (NCT01970345), and the GPE synthetic analogue, Trofinetide was efficacious in a phase II trial of RTT [156] and is continuing in phase III trials (NCT04181723 and NCT04988867).

These clinical studies suggest that IGF1 related are efficacious in treating RTT but in the case of rhIGF1/Mecasermin require optimisation. In this thesis data from patients with RTT, *Mecp2* mouse model and *in vitro* SH-SY5Y cell culture are used to help optimise rhIGF1/Mecasermin treatment.

A subset of patients with RTT showed improvements to apnoeic index and in the *Mecp2* mouse model nocturnal locomotor activity decline was prevented in rhIGF1 treated in *Mecp2*-null and –heterozygous mice. Analysing the gene expression illustrated many of the challenges of translational research. However, this analysis does provide a number of promising findings and indicate future directions that could help to help to predict patient responses to treatment.

This section will discuss, how these findings contribute to the understanding of rhIGF1/Mecasermin treatment in the context of RTT and discuss the details of future experiments that will help to validate these findings and hypotheses.

5.1 General Discussion

5.1.1 Mechanism of rhIGF1 Action

IGF1 signaling sits at the nexus of many cellular processes including growth, development, glucose metabolism, ageing, neuroprotection, and cancer. IGF1 signaling is highly regulated through IGFBP binding, negative feedback mechanisms (such as

desensitisation of IRS and endocytosis of IGF1R), IGF1 synthesis and secretion, and IGF1 transport across the blood brain barrier[7,13,177,178,245]. These regulatory mechanisms could mitigate the beneficial effects of exogenous rhIGF1 treatment in patients with RTT. Such mitigation was identified in ASD IPS derived neurons, where response to treatment positively correlated with *IGF1R* expression [171]. This research also showed that the magnitude of transcriptional response to rhIGF1 was significantly higher in acute treatment compared to chronic. This finding challenges the duration and posology of rhIGF1 treatment in order to evoke significant benefits.

In this thesis, both patients with RTT and RTT-like *Mecp2* mouse model data demonstrated IGF1 signaling was important in the response to rhIGF1/Mecasermin treatment. These analyses found several DEG and gene sets were associated with IGF1 signalling and regulation.

In patients with RTT, the IGF receptor signaling pathway (GO:0048009) was found to be differentially expressed comparing Responders to MSRs at T0 and T1. The only gene sets differentially expressed in HDT in patient subgroups were IGF receptor signalling pathway (GO: 0048009) in Responders (n=4) and chronic rhIGF1 treatment in ASD [171] MSRs (n = 5). These gene sets were both found during the off-treatment period (T1 to T2). In RTT-like mouse model, the "Regulation of IGF transport and uptake by IGFBPs" (R-HSA-381426) was over-represented in the blood of *Mecp2*$^{-/+}$ and *Mecp2*$^{-/y}$ versus WT and were also detected in the blood of these mice with rhIGF1 treatment compared to vehicle treated controls.

Together, these results suggest that IGF1 signalling genes may be associated with response to treatment, and therefore utilised as a potential biomarker for patient stratification. To investigate this possibility, further experiments using qPCR assessed *Igf1r* expression in the cerebellum of female mice treated with rhIGF1. This analysis revealed a significant correlation ($p = 0.0038$, $r = -0.69$) between *Igf1r* expression and change in nocturnal locomotor activity before and after treatment. There was increase in *Igf1r* expression in vehicle treated *Mecp2*$^{-/+}$ mice compared to rhIGF1 treated *Mecp2*$^{-/+}$ and vehicle treated *Mecp2*$^{+/+}$ mice. However, this change was no longer significant after testing for multiple correction (Figure 3.11). This experiment had a relatively low sample size (n = 4), so increasing the samples size is recommended. This is a promising

avenue, considering the evidence from sequencing experiments in both *Mecp2*-heterozygous and patients with RTT.

A homeostatic role of rhIGF1/Mecasermin treatment has emerged from analyses of the DEG in mice and patients with RTT. In mouse cerebellum, the greater the severity of phenotype the higher the level of DGE. Lower levels of DEG were observed in WT mice compared to diseased counterparts, and severely affected *Mecp2*$^{-/y}$ mice had higher number of DEG compared to milder *Mecp2*$^{-/+}$ mice. In the patients with RTT the DEG found comparing Responders and MSRs (RVMSR) decreased over the course of the trial as shown in figure 5.1. Total DEG was highest before treatment and decreased over subsequent timepoints. Similar pattern of expression was observed in HDT in RVMSR, the highest number of gene sets were differentially expressed at T0 and was lowest at T3. These data would support a homeostatic function of rhIGF1/Mecasermin in RTT. This relationship is depicted in figure 5.1.

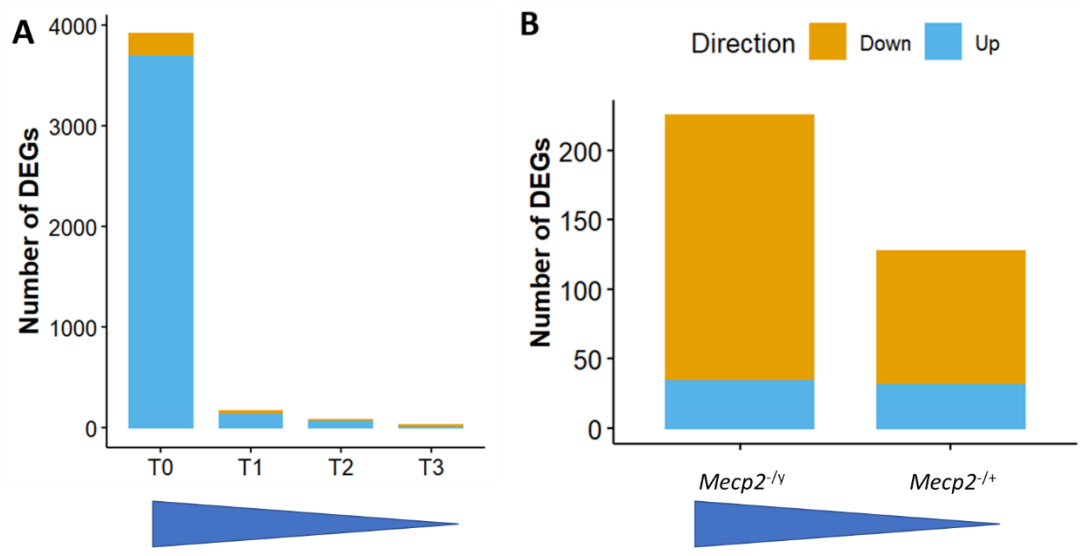

Figure 5.1 – Homeostatic Effect of rhIGF1/Mecasermin Treatment on Gene Expression in RTT patients and *Mecp2* Mice

The results from chapters I and II suggests that rhIGF1/Mecasermin treatment has a homeostatic effect on gene expression. **A –** Gene expression in blood comparing RVMSR at different time points across Mecasermin phase I clinical trial. As the trail progresses gene expression of Responders and MSR demonstrate less differential expression after initiating Mecasermin treatment. **B –** Gene expression comparing

rhIGF1 treatment versus vehicle in the cerebellum of *Mecp2*$^{-/y}$ and *Mecp2*$^{-/+}$ mice, shows that rhIGF1 had a greater effect in the more severely affected *Mecp2*$^{-/y}$ mice relative to *Mecp2*$^{-/+}$ mice. Gene expression in WT mice comparing rhIGF1 and vehicle was lower relative to *Mecp2*$^{-/y}$ and *Mecp2*$^{-/+}$ mice. These data suggest that rhIGF1treastment has a greater effect with increased severity of phenotype.

A Responder MSR distinction was found in this study but has also been made in other rhIGF1 studies, for example the distinction was observed measuring EEG resting state of patients with RTT treated with Mecasermin and measuring spontaneous neuronal activity in ASD IPS derived neurons treated with rhIGF1 [148,153,171]. Going forward with rhIGF1/Mecasermin treatment in RTT, it would be very beneficial to have a blood biomarker that could aid in patient stratification prior to treatment. Further experiments should be conducted to assess whether *Igf1r* could serve this purpose considering the correlation of cerebellar expression and locomotor performance.

The SH-SY5Y analysis found that GPE caused a strong increase in pAKT levels while rhIGF1 stimulation caused a decrease at 24hr, both effects on pAKT were IGF1R-dependent. Levels of pERK1/2 showed similar patterns of activation in rhIGF1 and GPE stimulation. PPP by itself and combined with stimulations caused decreased levels of pERK1/2, while rhIGF1 and GPE also caused a lesser decrease in pERK1/2 compared to PPP or PPP with stimulations. As rhIGF1 is known to activate AKT and ERK1/2 typically [7,8,30], these results suggest that the peak of rhIGF1 signaling happened prior to 24hr.

The increase of pAKT concentration induced by GPE suggests either a longer lasting activation of AKT, or a delayed activation of AKT signaling. The strong activation of AKT after GPE stimulation may have been induced by increased levels of endogenous IGF1, a mechanism that was observed in mouse primary culture [30]. Endogenous IGF1 levels have been found to be decreased in *Mecp2*$^{-/+}$ and *Mecp2*$^{-/y}$ mice serum compared to WT controls [151]. This is supported in Chapter II by DEG analysis, where *Igf1* expression was decreased in *Mecp2*$^{-/+}$ mouse blood. Though the results of this thesis contradict what was found in primary mouse culture [30] as described in section 4.3.1, there were key differences in experimental design between these studies.

5.1.2 Immune function and RTT

RTT patients and RTT-like mouse models have been found to display aberrant inflammatory responses [184,194,217,254]. The literature suggests that astrocytes and microglia are affected in RTT and their dysfunction contributes to the pathophysiology [115,118,120,121,255].

A number of immune related ontologies and pathways were over-represented in both *Mecp2*$^{-/+}$ and *Mecp2*$^{-/y}$ mouse blood compared to WT. These included innate immune system/response (R-HSA-168249, GO:0045087), neutrophil degranulation/chemotaxis (R-HSA-6798695, GO:0030593), and defense response (GO:0006952). This is consistent with what was found in MSRs; specifically, neutrophil degranulation (R-HSA-6798695), α-defensins (R-HSA-1462054), and antimicrobial humoral immune response mediated by antimicrobial peptides (GO:0061844), were all over-represented during the trial (T0 to T3). The results in *Mecp2*-null and –heterozygous mice and in MSRs treated with Mecasermin are complementary. The data suggest that innate response in RTT blood is not associated with beneficial response to Mecasermin treatment, and immune dysfunction could be abrogating the beneficial effects of Mecasermin.

5.1.3 Comparisons between blood and cerebellum

One of the primary challenges in studying RTT in patients is the inaccessibility of CNS samples outside of invasive procedures. *Mecp2*-null and –heterozygous mice allow researchers to study a RTT-like phenotype in neuronal tissues. Very few DEG were found overlapping between blood and cerebellum of *Mecp2*$^{-/+}$ and *Mecp2*$^{-/y}$ mice. Of the genes considered targets of rhIGF1 action, there was only one overlapping between blood and cerebellum. This was *Ttr* which was found in cerebellum of treated *Mecp2*$^{-/+}$ mice and blood of treated *Mecp2*$^{-/y}$ mice. These results highlight the fact that treatment in RTT blood is very different from what is observed in the central pathology.

DEG analysis in the blood of *Mecp2*$^{-/y}$ and *Mecp2*$^{-/+}$ mice show increased *S100a9* expression. Other studies in *Mecp2*$^{-/y}$ mice found that *S1000a9* had increased expression in brain and blood and additionally, determined that *S100a9* was a target of MeCP2 [203,204]. *S100a9* and the related *S100a8* expression was investigated in untreated *Mecp2*$^{-/y}$ mice and treated *Mecp2*$^{-/+}$ mice cerebellum. This analysis did not find any significant

change in expression or correlations with locomotor activity. *S100a9* and *S100a8* should be investigated in the blood and other brain regions such as cortex or midbrain to better assess the changes previously observed [203,204].

The genes *TMEM176A* and *TMEM176B* were found to be decreased in different intervals comparing all RTT samples (n = 9) in during off treatment period (T1 to T2), *TMEM176B* expression subsequently increased during OLE (T2 to T3). This was one of the few DEG identified using all RTT patients. *Tmem176b* was also decreased in the blood of rhIGF1 treated *Mecp2*$^{-/y}$ mice compared to vehicle treated *Mecp2*$^{-/y}$ mice. These genes are associated with maturation and potentially priming of dendritic cells by $CD4^+$ T-cell [185,186]. The expression of *Tmem176b* in untreated *Mepc2*$^{-/y}$ cerebellum using qPCR did not reveal significant changes or correlation to locomotor activity. Considering that this gene was also identified in all patients with RTT treated with Mecasermin, it would be interesting to know how this gene expression correlates with breathing abnormality in *Mecp2* mice.

The most promising results identified in blood and cerebellum were those implicating the signaling and regulation of IGF1 pathway, which were described in section 5.1.3. The significant correlation of *Igf1r* expression with change in locomotor activity after treatment suggests that this gene may have utility in assessing response to treatment. Higher expression of *Igf1r* correlated to decreased activity after treatment. Considering the decrease in *Igf1* expression in *Mecp2*$^{-/+}$ blood compared to WT, increased *Igf1r* may be a compensation mechanism to restore deficient Igf1 signaling.

These analyses show that *Mecp2*-null and –heterozygous can be used to find common mechanisms between blood and brain associated with RTT-like pathology. Further analysis of *Igf1r* and *S100a9* in cerebellum and blood is needed to validate the use of these genes as a blood biomarker for either efficacy of treatment.

5.1.4 Wider Implications for Neurodevelopmental Disorders

The results of clinical trials in RTT highlight the need for better understanding of the basic molecular mechanisms of rhIGF1 and GPE. While Trofinetide has been able to continue to phase III in treatment of RTT, Mecasermin did not succeed with in the selected primary aims at phase II trial. It is also important to identify different cohorts

of patients with RTT that respond differently to rhIGF1 treatment, to fully assess the rhIGF1 efficacy.

These results have implications not only in RTT but also other neurodevelopmental disorders. Currently there is an ongoing pilot trial using Mecasermin to treat ASD patients (NCT01970345). ASD IPS derived cells also show a Responder-Nonresponder distinction that correlates with *Igf1r* expression [171], therefore this thesis's analysis has direct implications for this trial. Trofinetide treatment in FXS was recently found to be efficacious in a phase II randomised double-blind placebo control trial [157]. Interestingly a recent study in *Fmr1*-null and *Mecp2*-null mice demonstrated a homeostatic relationship of these two proteins. MeCP2 levels were elevated in *Fmr1*-null mice and in *Mecp2*-null mice FMRP levels were decreased. Additionally, MeCP2 levels in *Fmr1*-null mice correlated with severity of hyperactivity [256]. A recent review by this research group was published comparing and contrasting the molecular mechanisms RTT and FXS [257]. It has been discussed at length in sections 5.1.1, and 3.3.2 how *Igf1r* expression appears to impact response to rhIGF1/Mecasermin treatment. These findings demonstrate that preclinical evidence in RTT can be used to inform and improve clinical trial based in other neurodevelopmental diseases.

5.1.5 Sex Differences in RTT

A confounding factor in the use of RTT-like mouse models is the impact of sex differences on the mouse phenotype, this thesis further highlights the impact of sex on DGE. In *Mecp2*$^{-/+}$ mice, the targets of rhIGF1 action were primarily identified in cerebellum with only a few genes in the blood (78 and 3 genes respectively), in *Mecp2*$^{-/y}$ mice there were more target genes in both cerebellum and blood (113 and 37 genes respectively). rhIGF1 action in *Mecp2*$^{-/y}$ mice appeared to effect metabolic and cellular processes, and in *Mecp2*$^{-/+}$ mice, treatment induced changes in synaptic plasticity and long term potentiation. Therefore, rhIGF1 is having entirely different effects on expression in male and female mice. Because *Mecp2*$^{-/+}$ and *Mecp2*$^{-/y}$ develop symptoms at different ages, it is not possible to dissociate the age-dependent and sex-dependent changes in these experiments.

The comparison of Responders and MSRs also suggested the importance of XCI, as *TSIX* was increased in Responders compared to MSRs at T0, T1 and T2. A greater level

mosaicism induced by increased *TSIX* would be expected to produce a less severe phenotype due to greater ratio of WT *MECP2*. Therefore, increased *TSIX* in Responders would contradict the fact that Responders have a more severe phenotype than MSRs. However, this could be a compensation in Responders due to increased severity. Double knock-out of *Tsix* and *Mecp2* in female mice showed increased severity of RTT-like symptoms and shortened lifespan akin to the phenotype of *Mecp2*$^{-/y}$ mice [152]. Considering how much research uses only *Mecp2*$^{-/y}$ mice, XCI could account for the difficulty translating preclinical finding to the human RTT condition.

5.1.6 Limitations of Studies

In each of the Chapters of this thesis there have been a number of limitations. Though they have been acknowledged and discussed throughout the thesis, it is important to keep them in mind when assessing the future directions of the project. A summary list of the main limitations is provided below:

Chapter I – Study in RTT patients:

- DEG analysis was conducted in whole blood and not CNS derived tissues, therefore may not reflect the pathology in the brain.
- There is no placebo control group in this analysis, therefore the placebo effect cannot be accounted for.
- Low sample numbers, particularly when assessing subgroups of RTT patients, (Responders n = 4, MSRs = 5).
- The complexity of the original clinical trial design. This trial was designed t to first measure pharmacokinetics and then provide preliminary assessment of efficacy. The 2 treatment phases are not equivalent length and initial MAD phase could influence the OLE phase.

Chapter II – Study in *Mecp2* mouse model:

- Levels of XCI in female mice add to variability in phenotype.
- Relatively low sample size used, sample sizes should be increased to n = 8-10 per group to increase statistical power.
- Limited number of samples per run during 3'DGE sequencing meant that rhIGF1 treated *Mecp2*$^{+/+}$ mouse blood was not included in DEG analysis.
- 3' DEG is a form of bulk RNA-Seq and therefore measures gene expression in complex cellular compositions that exist in blood or cerebellum.

- Severity of *Mecp2*$^{-/y}$ mice phenotype meant that the period of treatment varied in these mice and tended to be shorter than female mice.
- In the DEG analysis of treated *Mecp2*$^{-/y}$ mice treatment began at P21. In the locomotor analysis of treated *Mecp2*$^{-/y}$ mice this began at P28 because the animals had to be mature enough to be separated from their mother.

Chapter III - Study in *in vitro* neuronally differentiated SH-SY5Y:

- Certain groups had lower than n = 3 biological replicates these are marked in figures 4.3 to 4.5.
- While immunofluorescent confocal imaging is an excellent method for determining localisation of proteins, however, more appropriate quantitative and semi-quantitative methods such as ELISA or Western blot analysis should be used to validate the findings of this analysis.
- SH-SY5Y cells are a neuronal phenotype and does not capture the effects of rhIGF1 and GPE on glial cells.
- The effects of rhIGF1 and GPE may be different in the context of RTT pathology therefore effects measured in SH-SY5Y may not reflect this.

5.2 Future Directions

5.2.1 Chapter I: Gene Expression of RTT Patients Treated with Mecasermin (rhIGF1) from Whole Blood

As mentioned in limitations section 5.1.5 the phase I Mecasermin trial did not have a placebo control group. In the phase II trial there was a crossover placebo-control design to maximise the sample size to a total of 29 patients [154]. If whole blood samples from this trial were collected for both groups before and after crossover, sequencing using the same 3'DGE could be used. This cohort would also be an excellent means of hypothesis testing and validation based on the findings of this analysis. The additional measures of clinical performance in this phase II study, including several clinical severity scores, cardiorespiratory, and EEG assessment [154] would provide a detailed validation of Responders MSRs stratification if apnoea index was reported, observed in this thesis and other studies [148,154,171].

A similar analysis could be conducted using blood samples from the phase II Trofinetide study [156]. This cohort could test if the same Mecasermin related DEG were present in Trofinetide treated RTT patients. The DGE analysis may also reveal if Trofinetide does have a more regulatory effect on IGF1 signaling than Mecasermin, as was suggested by results from chapter III. Analysis of the effects of Trofinetide in RTT blood would also have direct implications for the ongoing phase III clinical trials (NCT04988867, NCT04776746, NCT04181723).

Another aspect of RTT patient response to treatment that was not assessed in this thesis, was the effect of Mecasermin treatment on neuronal function. Two obvious ways of investigating these properties without invasive measures would be, firstly to use EEG recordings to analyse patient response, secondly to use RTT IPS derived neurons and measure *in vitro* response to treatment with electrophysiological measures similar to the methods of the Linker study [171]. Frontal alpha band asymmetry was measured by EEG in the phase I Mecasermin trial and found a significant reversal before and after OLE phase. This correlated with ADAMS depressed mood index and has been used in other studies to correlate with anxiety and depression [153]. In a separate Mecasermin trial in RTT patients, resting state EEG was used to distinguish between responding and non-responding patients [148].

5.2.2 Chapter II: Behavioural and Molecular Correlates of Administration of rhIGF1 in Mecp2 Mouse Model

To validate the use of *Igf1r* as a potential biomarker for rhIGF1 treatment, blood samples should be tested before and after treatment to determine if expression of *Igf1r* can predict the response to rhIGF1 treatment. The sample size this analysis of treated mice should also be increased to at least n = 10 per group to ensure robustness of the data.

To mirror the analysis conducted in RTT patients, cardiorespiratory measurements should be measured in *Mecp2*$^{-/+}$ and *Mecp2*$^{-/y}$ mice. A previous study found improvement in the number of breath holds after rhIGF1 treatment in *Mecp2*$^{-/y}$ mice [151]. Oximeter sensor equipment can be used to detect heart rate and breathing patterns of mice after treatment.

Considering the results of the RTT clinical trials, the same experiments using rhIGF1 treatment should be repeated with GPE treated mice. rhIGF1 and GPE treatments have demonstrated functional improvements, but these studies focused primarily in *Mecp2*$^{-/y}$ mice [101,151].

To explore the relationship between immune function and rhIGF1/Mecasermin response, an immune challenge group could be added to RTT-like mouse model experiments. Prototypical immune challenges use established methods to induce an immune response in mice. LPS challenge induces a systemic inflammatory response in mice, this results in sickness behaviour, anhedonia, and neuroinflammation in adult mice [258]. LPS injection induces a neuroinflammatory response strong enough to detect increased TNFα up to 10 months post-injection [260].

Recently, Experimental Autoimmune Encephalomyelitis (EAE) challenge was used in *Mecp2*$^{308/y}$ mouse model of RTT and identified an exacerbated inflammatory response compared to WT mice [194]. The authors note that *Mecp2*$^{308/y}$ model displays a less severe phenotype than *Mecp2*$^{-/y}$ mice making them more suited to immune challenge experiments. It is possible that, due to the severity of RTT pathology, *Mecp2*$^{-/y}$ mice would not survive LPS or EAE challenges, therefore *Mecp2*$^{-/+}$ mice may be a better option to study. If *in vivo* experiments were to prove not viable, *ex vivo* immune challenge could be more appropriate [120].

The use of bulk RNA-Seq in this thesis was to allow for cross comparison of the current experiment in treated female mice with a previous experiment in treated male mice. This previous work was conducted by a member of this research group Albert Sanfeliu. Recent advances in sequencing technology has led to the development of the single nuclei RNA-Seq. Applying this technology to RTT can resolve the mosaic expression of *MECP2*$^{-/+}$. In a study which combined scRNA-Seq and ChIP-Seq data in RTT, DNA methylation was able to predict the degree of up-regulation of gene expression in neuronal cells [260]. This analysis in human neuronal cells supported a previous finding from *Mecp2* mouse models, that MeCP2 preferentially represses longer genes [260,261]. Applying cell-type-specific sequencing techniques to experiments conducted in this thesis, would enable measurement of sub-populations of cells in the brain, and also resolve variability of mosaic *Mecp2* expression. This would be a powerful tool in resolving the cellular mechanisms of rhIGF1 in RTT pathology.

5.2.3 Chapter III: In Vitro Mechanism of rhIGF1 in SH-SY5Y Neuronal Cell Line

In SH-SY5Y cells, rhIGF1 stimulations counterintuitively led to the decreased activation of AKT and ERK1/2, while GPE had a similar effect on ERK1/2 activation it induced a strong increase in AKT levels. Time series experiments in SH-SY5Y cells should be conducted to determine:

1. If rhIGF1 induced activation of AKT and ERK1/2 prior to 24hr.

2. If GPE induced activation of AKT was a persistent activation or a delayed activation, perhaps by endogenous IGF1 activation.

The findings in Chapter III contradict the common understanding of IGF1 signaling [7,8], however they could be explained by negative feedback mechanisms, such as internalisation of IGF1R or IRS desensitisation [20,179]. These mechanisms could be investigated using specific inhibitors of these processes. The inhibitor Dansylcadaverine was used by Solomon-Zemler and colleagues to block clathrin-mediated endocytosis, the physiological mechanisms for IGF1R endocytosis [179,262]. IRS desensitisation could be investigated using CRISPR-Cas9 system to induce specific mutations to desensitise IRS proteins. IRS1 has been shown to regulate endocytosis of IGF1R [263], so these mechanisms may be difficult to parse apart. Careful design and control groups would be needed for such experiments.

The mechanisms of rhIGF1 and GPE treatments may be completely different in the context of RTT. RTT IPS derived cell culture would provide closer representation of RTT pathophysiology than neuronal SH-SY5Y cells. RTT IPS cell culture experiments can also be designed to have mosaic expression of *MECP2* or isogenic populations of mutant or WT *MECP2* [264,265]. This allows researchers to control for the XCI, a variable that can often confound RTT experiments. This *in vitro* cell model provides an endophenotype that mimics the early development of RTT-like neurons and can be functionally assessed using techniques like transient calcium signaling or electrophysiological recordings [264]. Comparing the effects of rhIGF1 and GPE treatment in RTT IPS cells would be a much more relevant a setting than SH-SY5Y cell culture.

5.2.4 Concluding Remark

This thesis examined the mechanisms of rhIGF1/Mecasermin in the context of RTT using studies with three different approaches: systemic whole blood samples from RTT patients in a phase I clinical trial, to CNS and systemic derived samples from the *Mecp2* mouse model of RTT and finally a simple cell line model, neuronally differentiated SH-SY5Y cells. The results of each study were used to give a wholistic understanding of rhIGF1's mechanism. The results of these studies highlight three areas of interest that warrant further exploration and experimentation:

1. **The endogenous signaling of IGF1 is important for the response to treatment.** Gene expression from both RTT patient blood found that IGF1 signaling and gene sets from Linker and colleagues' study [171] on response to IGF1 in ASD IPSC were significantly differentially expressed depending on if patients were stratified as Responders or MSR. The level of *Igf1r* in *Mecp2* mice correlated significantly with changes in locomotor activity, vehicle treated *Mecp2*$^{-/+}$ mice trended towards up-regulated *Igf1r* levels. GPE treatment is known to effect endogenous levels IGF1, resulting in down stream activation of IGF1R [11]. In this thesis both rhIGF1 and GPE stimulation resulted in increases of pCREB, despite having differing effects on pAKT and pERK1/2 which are up-stream of pCREB. Additionally, GPEs affect on pCREB was IGF1R dependent despite not being able to bind the IGF1R [10]. These results all highlight the important role of endogenous IGF1 signaling in relation to rhIGF1/Mecasermin treatment.
2. **Immune modulation and rhIGF1/Mecasermin.** The results of gene expression analysis form both Chapter I and II highlight the potential role of immune function in relation to rhIGF1/Mecasermin treatment. In RTT patient's blood there is a decrease in *TMEM176A* and *TMEM17B* in the RVMSR comparison at T1, after MAD treatment period. In *Mecp2*$^{-/y}$ treated with rhIGF1 *Tmem176b* also decreased. These two genes are associated with dendritic cell maturation [185]. Additionally, the proinflammatory gene *S100A8* is decreased in RVMSR comparison at T0, before treatment, and in *Mecp2*$^{-/y}$ and *Mecp2*$^{-/+}$ cerebellum and blood *S100a8* and *S100a9* was increased. These results suggest that immune modulations occur in RTT and may be alter the effects of rhIGF/Mecasermin treatment.

3. **Homeostatic effect of rhIGF1/Mecasermin.** The results from Chapters I found that Responders and MSR blood samples become more homogenous as the clinical trial progressed. In Chapter II, rhIGF1 had a greater effect in the more severely affected *Mecp2*$^{-/y}$ compared to *Mecp2*$^{-/+}$, with lower levels of DGE in WT animals. In SH-SY5Y cells rhIGF1 and GPE treatments had the opposite effects on pAKT and pERK1/2, but both treatments increased pCREB, which is further downstream in the IGF1 pathway. This suggests there was a compensatory mechanism regulating the AKT and ERK1/2 signaling after IGF1 related treatments. These results highlight the fact that rhIGF1/Mecasermin has sophisticated regulatory mechanisms that need to be accounted for in the context of RTT.

These studies provide further insight in the mechanisms of rhIGF1/Mecasermin in the treatment of RTT and related developmental disorders and could inform the design of future experiments and clinical trails rhIGF1 related treatments.

6.0 Materials and Methods

6.1 Chapter I: Gene Expression of RTT Patients Treated with Mecasermin (rhIGF1) from Whole Blood

6.1.1 Clinical Trial design and Cohort Details

Chapter I was completed as part of a collaboration with MIT and Boston Children's Hospital (BCH). The cohort in the phase I open label mecasermin trial [153] included 9 patients with classic RTT and 3 with MECP2-related disorders (MRD; non-RTT clinical presentations in individuals with MECP2 mutations [31]. Details about the cohort, including individual MECP2 mutations, can be found in Table 6.1.1 and in the original publication on the trial by Khwaja and colleagues [153]. Due to the open-label design of this trail, there was no randomisation or blinding with regards to treatment in this study. The experimental unit for this thesis was whole blood samples from clinical trial participant.

The study consisted of two different components: a 4-week multiple ascending dose (MAD) period and a 20-week open label extension (OLE) period. The MAD and OLE periods were separated by a variable interval of 12-30 weeks. The MAD period was focused on assessment of safety and collection of serial pharmacokinetic (PK) data. The goal of the OLE period was to extend the evaluation of Mecasermin safety and to conduct a preliminary assessment of the drug's efficacy. Both MAD and OLE periods began with a dose of 40 µg/kg, which was increased by 40 µg/kg per week to a maximum dose of 120 µg/kg. The MAD lasted a total of 4 weeks and OLE last for 20 weeks in total

The design of the Trial was to determine pharmacokinetics, safety, and tolerability of Mecasermin treatment in the MAD phase and examine preliminary measures of efficacy in the OLE phase. Autonomic dysfunction was measured using a plethysmograph (BioRadio, Great Lakes Neurotechnologies) to assess breathing dysfunction and breath holding. This analysis revealed that five RTT patients in the trial suffered from clinically significant apnoea, episodes lasting longer than 10 seconds. Of these five patients, four decreased in severity from moderate-severe to mild by the end of OLE (from > 5 episodes per hour to < 5 episodes per hour).

Sample	Age	Mutation (Nucleotide change)	Mutation Domain	Mutation Type	Sample Timepoints
RTT1	3	R168X	ID, TRD	Non-Sense	T0, T1, T2, T3
RTT2	2	Deletion (c.790-808del19)	TRD-NLS	Deletion	T0, T1, T2, T3
RTT3	5	Deletion Exon 3 and 4, min 6.0kb- max 7.1kb	Multiple	Deletion	T0, T1, T3
RTT4	4	Deletion (c.1159-1273del114)	C-Terminal	Frameshift Insertion or Deletion	T0, T1, T2, T3
RTT5	8	R255X	TRD	Non-Sense	T0, T1, T2, T3
RTT6	4	R255X	TRD	Non-Sense	T0, T1, T2, T3
RTT7	8	T158M	MBD	Mis-Sense	T0, T1, T2, T3
RTT8	10	Deletion Exon 1 and 2	Start Codon	Deletion	T0, T1, T2, T3
RTT9	8	P322L	C-Terminal	Mis-Sense	T0, T1, T3
MRD1	7	P379T.fs	C-Terminal	Frameshift, Deletion	T0, T1
MRD2	7	P379T.fs	C-Terminal	Frameshift, Deletion	T0, T1
MRD3	3	R306C	TRD	Mis-Sense	T0, T1, T2, T3

Table 6.1 - Sample Cohort for Phase I Mecasermin Trial

Note MRD1 and MRD2 are monozygotic twins.

Abbreviations: RTT (Rett syndrome, n=9), MRD (MECP2-related disorder, n=3), ID (Interdomain), TRD (Transcriptional Repression Domain), NLS (Nuclear Localisation Signal), C-term (Carboxy-terminus), MBD (Methyl Binding Domain).

All Patients were recruited from Boston Children's Hospital by Dr. Mustafa Sahin and informed parental consent was obtained for each patient. Inclusion-exclusion and

details of can be found in supplementary methods of the original publication from Khwaja and colleagues [153].

6.1.2 Sample Collection

Whole blood samples were taken from the patients at four different timepoints denoted T0 to T3 (T0 and T1, corresponding to the beginning and end of the MAD, respectively; and T2 and T3, corresponding to the beginning and end of the OLE, respectively) using PAXgene blood collection tubes. RNA was extracted at BCH and samples were sequenced using 3'-DGE in the MIT BioMicro centre. Of note, for patients RTT3 and RTT9 samples were not obtained at T2. All patients (n = 12) were included in the multiple ascending dose (MAD) period while only those with RTT (n = 9) and one other patient with MRD progressed onto the open label extension (OLE) component. Patients were administered Mecasermin twice daily by subcutaneous injection. Timepoints when blood sampling was performed are denoted by T0 (start of MAD), T1 (end of MAD), T2 (start of OLE) and T3 (end of OLE). A schematic representation of the clinical trial design and subsequent DGE analysis is displayed in figure 2.1.

6.1.3 Principal Component Analysis

Principal component Analysis (PCA) was conducted by using prcomp function in RStudio, with scaling and centring applied. The package ggplot2 was used to plot the PCA.

6.1.4 EdgeR: Differential Gene Expression and Permutation based Analysis

The 3'DGE sequencing was conducted by MIT BioMicro Centre, details of the sequencing protocol can be found at https://openwetware.org/wiki/BioMicroCenter:RNA_HTL. In short samples were tagged using SMARTseq chemistry and Nextera tagmentation to create tagged libraries of 3' cDNA transcripts based on an adapted protocol from Soumillon and colleagues [266]. Sample libraries were then sequenced on NextSeq Illumina sequencer. Initial bioinformatics support was provided by BioMicro Center and the raw gene counts and

counts per million (CPM) were returned. The raw counts generated from the 3'DGE sequencing were filtered to remove genes with zero counts across all samples.

Differential expression was determined using edgeR software, biostatistical package that utilises empirical bayes methods to assess differential expression with low sample size [165]. The following generalised script was used for each comparison:

Library(edgeR)

data <- read.table('counts.txt', header = TRUE)

#Make Genes/Ensemble IDs the rownames of the data frame

genes<-data[c(1)]

row.names(data)<-genes

data<-data[-c(1)]

#Selection of a given comparison

group <- factor(c(2,2,2,1,1,1))

dge_object<-DGEList(counts = data, group = group)

dge_object <- calcNormFactorrs (dge_object)

dge_design <- model.matrix(~group)

dge_object <-estimateDisp (dge_object, design)

fit<-glmQLFit(dge_object, design)

qlftest <- (fit, coef = 2)

result <-topTags(qlftest, n = x) #where x is the total number of genes detected

write.csv(result, file = 'qlftest_result.csv')

To test whether these gene sets were differentially expressed across each comparison, we used the edgeR function fry(). This function uses rotations, an approach similar to fractional permutations to determine whether a gene set was considered significantly differentially expressed in a given a comparison [268,269]. Gene sets were obtained either directly from the list of significant results or were taken from the relevant ontology from the Gene Ontology (GO) data base. These gene sets were taken from functions

from 5 different categories; 1. IGF1 and BDNF pathways, 2. Metabolic homeostatic mechanisms including; mitochondria, protein ubiquitination and chromatin mediated processes [166,] 3. Inflammatory microglia responses [167], 4. Pathways linked to apnoeic phenotype i.e. Monoamine metabolism [168–170], and ASD IPS derived neuronal response to rhIGF1 form Linker study [171].

6.1.5 Pathway and Gene Ontology analysis

Gene Ontology (GO) and Reactome analysis was conducted [269–271] by inputting the list of significant DEGs for each comparison. Unrecognised genes were filtered out so as not to affect FDR correction.

6.2 Chapter II: Behavioural and Molecular Correlates of Administration of rhIGF1 in *Mecp2* Mouse Model

6.2.1 Mouse Colony Breeding and Animal Housing

The *Mecp2* mouse colony was maintained and all *in vivo* experimental procedures, tissue dissection and collection performed in Comparative Medicine Unit (CMU) in Trinity Biomedical Sciences Institute (TBSI). All procedures performed on these animals were authorized by the Health Product Regulatory Authority of Ireland and by the Department of Comparative Medicine in TBSI under the project authorisation of AE19136/P067 and AE19136/P085.

Mecp2 mutant mice were generated using *Mecp2*$^{tm1.1Bird}$ female mice cross-bred with Wild-Type (WT) C57/BL6 male mice. The resultant heterozygous *Mecp2* mutant female mice (*Mecp2*$^{-/+}$) were used to breed with WT C57/BL6 male mice to maintain the colony. Offspring of the breeding pairs were genotyped using ear-punch samples taken between p15-p25. Animals were kept in ventilated cages with up to 6 adult animals per cage, a 12 to 12 hour light dark ratio was maintained in the CMU. During the winter facility lights were on from 07:00 to 19:00 and during the summer lights were on 08:00 to 20:00. Access to food and water was provided *ad libitum*.

Restrictions and limitations on the Mecp2 mouse colony due to the SARS CoV2 pandemic meant that the numbers of Mecp2 mice used for this study was significantly reduced. The experimental unit for Chapter II was a treated or untreated mouse, rather

than a cage containing littermates to accommodate for the low numbers of animals available. Therefore, litter effects could not be controlled for in this study. Mice were randomly assigned to be treated with rhIGF1 or vehicle, ensuring equal numbers of treatments per group, to enable meaningful analysis with the low number of animals used

6.2.2 Mouse Genotyping

Ear-punch samples were kept at -20°C once taken from the mice. DNA was extracted by adding 75µl of alkaline lysis solution (25mM Sodium Hydroxide (NaOH), 0.2mM Ethylenediaminetetra acetic acid (EDTA)) to the sample and incubating for 30 minutes at 95°C. After incubation samples were neutralised with equal volume of 40mM Tris-Hydrochloric acid (Tris-HCl) solution and kept on ice. 4µl of DNA sample were used for subsequent Polymerase Chain Reaction (PCR). The following reaction mix was made using Taq DNA Polymerase kit (201203, QIAGEN) per sample; 5µl of 10X CoraLoad Buffer, 1µl 10mM deoxynucleoside triphosphate (dNTPs) (U151B, Promega), 2.5µl of 2.5µM forward (32255571, IDT), reverse-mutant (279662344, IDT) and reverse-WT *Mecp2* primer (279662343, IDT), 32.25ul molecular grade water (BE51200, Lonza), 0.25µl Taq Polymerase enzyme. The primers were provided by Integrated DNA Technologies (IDT) and consisted of the following sequences:

Forward - 5’ AAATTGGGTTACACCGCTGA 3’

Reverse WT – 5’ CTGTATCCTTGGGTCAAGCTG 3’

Reverse Mutant - 5’ CCACCTAGCCTGCCTGTACT 3’

Each sample-reaction mix was kept on ice and then placed on thermocycler running the PCR program displayed in Table 6.2,1. The PCR products were then kept on ice.

Step	Temperature	Time
1	94°C	2 minutes
2	94°C	20 seconds
3	65°C (decreasing 0.5°C per cycle)	15 seconds
4	68°C	10 seconds
5	Repeat steps 2-4	Repeat steps 2-4

	For 10 cycles	For 10 cycles
6	94°C	15 seconds
7	60°C	15 seconds
8	72°C	10 seconds
9	Repeat steps 6-8 For 28 cycles	Repeat steps 6-8 For 28 cycles
10	72°C	2 minutes
11	4°C	Hold

Table 6.2 - Thermocycler Program for Genotyping

Mutant PCR products produced were 240bp in size while WT PCR products were 465bp in size. These amplicons were then visualised through gel electrophoresis separation in 1.5% agarose gel stained with ethidium bromide. 20µl of PCR product were loaded into each well along with a 1kilobase ladder (01015347, Invitrogen) and run at 120V for 25 minutes to separate the bands. Bands were visualised ultraviolet transilluinator.

6.2.3 IGF1 Treatment of Mecp2 Mice Colony

Mice were treated with 0.25mg/g of recombinant human IGF1 (100-11, Peprotech) or vehicle saline solution, 0.9% Sodium Chloride (NaCl) (S7653, Sigma-Aldrich), 0.01% Bovine Serum Albumin (BSA) (A7030, Sigma-Aldrich) as per Castro and colleagues study [151]. Treatment and vehicle were injected subcutaneously with either 26 or 30 gauge syringe depending on the size of the animal. Animals were injected between 10 A.M. and 11 A.M., 6 days a week. The age when male and female mice began rhIGF1 treatment corresponded to the initial age of symptom onset in the two sexes; in male 3-4 weeks of age and in females approximately 4 months of age. Animals were treated for a maximum of 4 and half weeks (for female mice) and a minimum of 3 weeks (for male mice). Mice were treated for approximately 4 weeks. Shorter treatment time's for male mice were necessitated by severity of disease in *Mecp2*$^{-/Y}$ mice. Treatment of WT cage-mates was kept the same as mutant mice to account for this variation in treatment duration.

Mice were euthanized by CO_2 within 1 week of end of treatment. After confirmation of death, blood was extracted using cardiac puncture with a 26G needle. 100µL of blood was stored in RNAprotect animal blood tubes (76544, QIAGEN) and stored at -20°C for later use. The brain was removed and placed in sterile Phosphate Buffered Saline or PBS (P4417, Sigma-Aldrich) in a culture dish for dissection. All brain samples were snap frozen on dry-ice and stored at -80°C for later use. The Olfactory bulbs were removed, the brain was divided into left and right hemispheres by cutting down the longitudinal fissure. The left and right cerebellum were extracted, the basal nuclei of the cerebrum were removed and the exposed hippocampus were extracted, the remaining cerebrum was also kept and stored.

6.2.4 Locomotor Activity Assessment

Locomotor activity of the mice was assessed using infrared beam-breaking sensors (47420, Ugo Basille) which captured horizontal and vertical beam-breaks every hour. Mice were placed in a clean cage similar to their home cage with nesting, food diet and water provided *ad libitum*. The cage was placed between the horizontal and vertical transmitters and receivers and the mice were allowed to freely move in their cages for a maximum 24 hours in a room separated from the colony.

Nocturnal activity was considered the 12 hour period when the lights were off in the animal facilities. Habituation to the new cage was considered the sum of the first two hours of recording beam-breaking. This provided a proxy measure of stress response as the mice were separated from their cage-mates and placed in a novel environment. Locomotor activity was assessed a maximum of three time per mouse. Locomotor activity of treated mice occurred prior to starting treatment and after finishing treatment. A Graphic schematic of the experimental setup is displayed in figure 6.1. Graphical schematics were prepared using BioRender online platform, at BioRender.com.

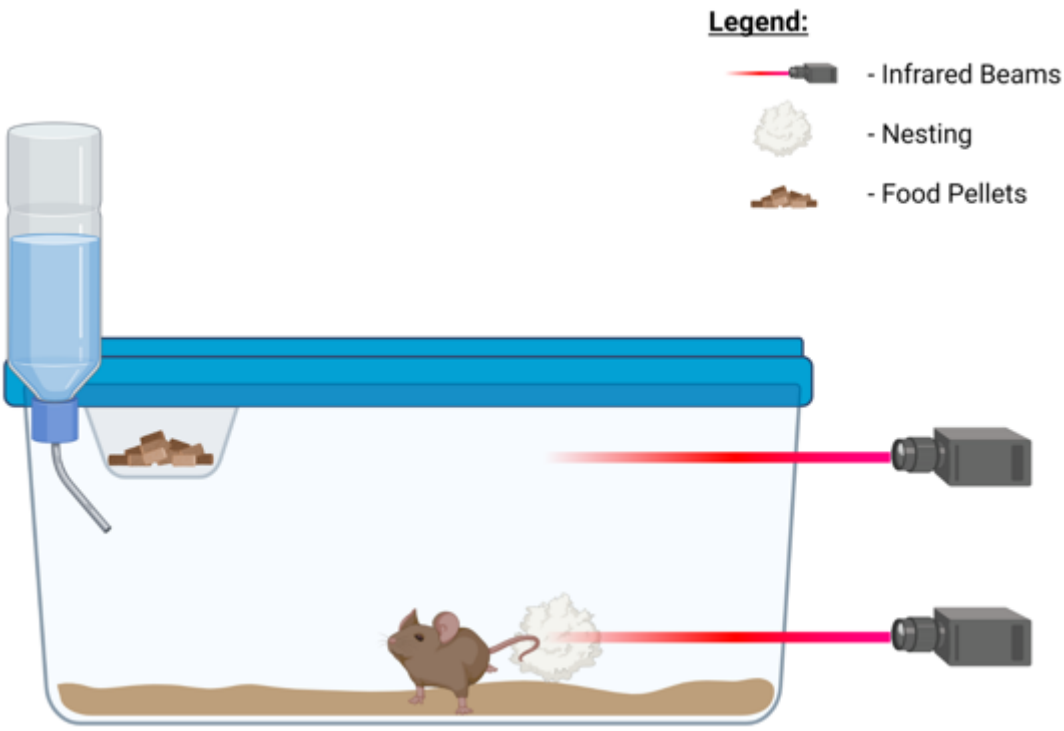

Figure 6.1 - Experimental Setup of Locomotor Activity Behaviour

Locomotor activity was measured in each mouse over the hours of the 12 hours of the night, when lights were turned off in the animal facility. Mice were placed in a clean cage containing the same nesting and bedding as provided in their home-cage, these mice were provided food diet and water *ad libitum*. Mice were placed in this cage at least 2 hours before being of recording, to allow the mice to habituate.

Locomotor activity was measured at infrared beam breaks per hour. One set of beams were aimed to run perpendicular to the bottom of the cage measuring horizontal activity and another set of beams aimed to run perpendicular with the gird at the top of the cage measuring vertical activity. Total activity was the sum of horizontal and vertical activity as beam breaks per hour.

6.2.5 RNA Extraction and quantitative Polymerase Chain Reaction

For quantitative Polymerase Chain Reaction (qPCR) RNA from mouse Cerebellum and Blood was extracted using RNeasy Mini Kit (1038703, QIAGEN) and RNeasy Protect Animal Blood (73224, QIAGEN), respectively. RNA concentration was determined using NanoDrop 8000 Spectrophotometer (Thermo Fisher Scientific).

Reverse transcription was performed using QuantiNova Reverse Transcription Kit (205411, QIAGEN) using 1µg of initial RNA. qPCR was performed in triplicate using 10µL reaction volumes in a 384 well plate (4309849, Applied Biosciences) with a 1:10 dilution of cDNA. Predesigned PrimeTime qPCR probe assays (Integrated DNA Technology) for loading control, *Glyceraldehyde 3-phosphate dehydrogenase* (*Gapdh*) and the gene of interest were measured in the same sample. *Gapdh* and gene of interest assays contained CY5 and FAM fluorescently labelled 5'nuclease probe and Iowa Black RQ and Iowa Black FQ 3' quenchers, respectively.

The sequences for the primers and probes for each gene were as follows:

Igf1 -

Primer 1 = AGTACATCTCCAGTCTCCTCAG

Primer 2 = ATGCTCTTCAGTTCGTGTGT

Probe (FAM) = TCCGGAAGCAACACTCATCCACAA

Igf1r -

Primer 1 = TCTCGTAGATGTCTCGTGTCA

Primer 2 = GCCTACCTCAATGCCAACA

Probe (FAM) = TTCGGCTACCATGCAGTTCCTAGC

S100a8 -

Primer 1 = CCACACCCACTTTTATCACCA

Primer 2 = ATGACTTCAAGAAAATGGTCACTAC

Probe (FAM) = TTCGATATTTATATTCTGCACAAACTGAGGACACT

S100a9 -

Primer 1 = CATCAGCATCATACACTCCTCA

Primer 2 = GGAATTCAGACAAATGGTGGAAG

Probe (FAM) = TGACATCATGGAGGACCTGGACACA

Tmem176a -

Primer 1 = CACAAGAAGGGTCCTCATCAG

Primer 2 = AGCCATGTATTCCGAAGGC

Probe (FAM) = CCAGCATAGCCACGATCCCAGTC

Tmem176b -

Primer 1 = CCGAAGTAGAGACATACTCCAAG

Primer 2 = CAGGCCAGAATCCACTATGG

Probe (FAM) = ACAGCTCACAAGCCCCAGCAATAT

Gapdh -

Primer 1 = GTGGAGTCATACTGGAACATGTAG

Primer 2 = AATGGTGAAGGTCGGTGTG

Probe (Cy5) = TGCAAATGGCAGCCCTGGTG

The following PCR cycle was used:

Step	Temperature (°C)	Time (Seconds)	Repeat Steps
1	50	120	
2	90	600	
3	95	15	
4	60	60	
5			3-4 for 40 cycles

Table 6.3 - Cycles for qPCR Quantification
The above cycles were used as a protocol for relative quantification of gene expression using Applied Biosystems Quantstudio 5 Real-time PCR system.

Samples Cycle Threshold (CT) values were obtained for both *Gapdh* and genes of interest. The average *Gapdh* CT values were subtracted from the average gene of interest CT value to provide delta CT (dCT). All sample values were normalised to control animals (WT animals or vehicle treated WT animals depending on the experiment) by subtracting dCT from average control dCT. This gives the delta delta

CT (ddCT) value, these values were converted to log2 fold change using the formula 2^{-ddCT}.

To determine if the was significant difference between expression levels, an unpaired Wilcoxon test was used and corrected for multiple comparisons by Benjamini-Hochberg method. Gene expression was plotted using –ddCT values so as up-regulation corresponded to positive values and down-regulation corresponded to negative values. These plots were generated using the ggpubr() software in RStudio

6.2.6 High-Throughput 3' Digital Gene Expression

Cerebellum RNA was extracted following the protocol for the QIAGEN RNeasy Mini Kit, for blood RNA the protocol for RNeasy Animal Blood System was followed. To measure RNA integrity and concentration RNA Nano 6000 chips were used on a Bioanalyser (Agilent Technologies). 25ng of RNA was submitted to the BioMicro Centre (Massachusetts Institute of Technology) with RNA integrity number of ≥ 7, in a 96 well plate shipped on dry ice (Polar Ice Ltd.).

Samples were limited to a run of 24. To ensure that this sequencing run could be compared to previous experiments, 2 previously sequenced samples were included, one cerebellum and one blood. Each sample is described in table 6.2.3

Sample Name	Sex	Genotype	Tissue	Treatment
HET_IGF1_CRB_1	Female	*Mecp2*$^{-/+}$	Cerebellum	IGF1
HET_IGF1_CRB_2	Female	*Mecp2*$^{-/+}$	Cerebellum	IGF1
HET_IGF1_CRB_4	Female	*Mecp2*$^{-/+}$	Cerebellum	IGF1
HET_IGF1_CRB_4	Female	*Mecp2*$^{-/+}$	Cerebellum	IGF1
HET_VEH_CRB_1	Female	*Mecp2*$^{-/+}$	Cerebellum	Vehicle
HET_VEH_CRB_2	Female	*Mecp2*$^{-/+}$	Cerebellum	Vehicle
HET_VEH_CRB_3	Female	*Mecp2*$^{-/+}$	Cerebellum	Vehicle
WTF_IGF1_CRB_1	Female	*Mecp2*$^{+/+}$	Cerebellum	IGF1
WTF_IGF1_CRB_2	Female	*Mecp2*$^{+/+}$	Cerebellum	IGF1
WTF_IGF1_CRB_3	Female	*Mecp2*$^{+/+}$	Cerebellum	IGF1
WTF_VEH_CRB_1	Female	*Mecp2*$^{+/+}$	Cerebellum	Vehicle
WTF_VEH_CRB_2	Female	*Mecp2*$^{+/+}$	Cerebellum	Vehicle

WTF_VEH_CRB_3	Female	*Mecp2*$^{+/+}$	Cerebellum	Vehicle
HET_IGF1_BL_1	Female	*Mecp2*$^{-/+}$	Blood	IGF1
HET_IGF1_BL_2	Female	*Mecp2*$^{-/+}$	Blood	IGF1
HET_IGF1_BL_3	Female	*Mecp2*$^{-/+}$	Blood	IGF1
HET_VEH_BL_1	Female	*Mecp2*$^{-/+}$	Blood	Vehicle
HET_VEH_BL_2	Female	*Mecp2*$^{-/+}$	Blood	Vehicle
HET_VEH_BL_3	Female	*Mecp2*$^{-/+}$	Blood	Vehicle
WTF_VEH_BL_1	Female	*Mecp2*$^{+/+}$	Blood	Vehicle
WTF_VEH_BL_2	Female	*Mecp2*$^{+/+}$	Blood	Vehicle
WTF_VEH_BL_3	Female	*Mecp2*$^{+/+}$	Blood	Vehicle
REF_CRB	Male	*Mecp2*$^{+/y}$	Cerebellum	Vehicle
REF_BL	Male	*Mecp2*$^{+/y}$	Blood	Vehicle

Table 6.4 – rhIGF1 Treated Female *Mecp2*$^{-/+}$ Mice and Reference Samples included for 3' DGE Sequencing

Differential Gene Expression, Gene Ontology and Reactome Analysis was conducted as described in sections 6.1.4 and 6.1.5. To understand the genes potentially rescued by IGF1 treatment, the gene overlapping between comparison of IGF1 versus vehicle treated *Mecp2* mutant mice and the comparison of vehicle treated *Mecp2* mutant and WT animals. DEG were considered potentially rescued by IGF1, if the logFC in the mutant versus WT comparison was the opposite in the mutant IGF1 versus vehicle comparison. A hypergeometric equation was used to determine the number of rescued genes was not identified by chance. This was computed in RStudio using phyper() function.

6.3 Chapter III: In Vitro Mechanism of rhIGF1 in SH-SY5Y Neuronal Cell Line

6.3.1 Cell Culture of SH-SY5Y Cell Line

Human neuroblastoma SH-SY5Y cells (CRL-2266, ATCC) were maintained at 37°C with 5% CO_2 and cultured under sterile conditions with appropriate aseptic technique. Cells were cultured in high glucose Dulbecco's Modified Eagle's Medium or DMEM (D5796, Sigma-Aldrich) with 15% heat inactivated Foetal Bovine Serum (F9665,

Sigma-Aldrich) in T25 tissue culture flask (83.3910.002, Sarstedt). Cells were passaged every 5-7 after reaching 70-80% confluency. For cell passage complete media was removed and cells were gently washed with sterile PBS. 0.5mL of TrypLE (12604-021, Gibco) was directly pipetted onto the adherent cells which were then incubated for 2 minutes at 37°C in 5% CO_2 to allow for trypsinisation. Trypsinisation was neutralised by adding 4.5mL of compete media. The cell suspension was pelleted down in centrifuge at 3000RPM for 5 minutes. The old media was replaced with fresh complete media and cells were vortexed to homogenise the suspension. A 1:5 to 1:10 dilution was made of the suspended cells in a new T25 flask with fresh complete media.

6.3.2 Neuronal differentiation of SH-SY5Y Cells

SH-SY5Y cells were differentiated into neuronal phenotype using all-trans Retinoic Acid or RA (R2625, Sigma-Aldrich) and Brain Derived Neurotrophic Factor or BDNF (130-093-811, Miltenyi Biotech) by a method adapted from Encinas and colleagues [241]. Cells were seeded on Poly-L-Lysine (P4707, Sigma-Aldrich) treated 12mm #1.5 coverslips (11846933, Fisher Scientific) at a density of 10^4 cells/cm^2. Cells were incubated in 10µM of all-trans RA in complete media for 5 days, and then washed with DMEM three times before incubating them in serum-free DMEM supplemented with 50ng/mL of BDNF for an additional 7 days to allow for full neuronal differentiation. The experimental unit for this analysis was a single culture well, which was assigned to one of the treatment groups using random block design to ensure equal sample number per treatment group.

6.3.3 Stimulations and Receptor Blockade of IGF1 System

Prior to conducting experiments on fully differentiated SH-SY5Y cells, fresh BDNF supplemented media was replaced to ensure the level of BDNF was kept constant. Cell were either treated with 100ng of recombinant human IGF1 (AF100-11, Peprotech) or the molar equivalent of GPE, approximately 3.6ng (Bachem Biosciences). Vehicle control cells were treated with BDNF serum-free media.

To specifically block IGF1R the inhibitor, Picropodopyllin or PPP (T9576, Sigma-Aldrich) was used. For experiments using PPP, cells were pre-incubated with 1 µM of

the inhibitor or vehicle control, dimethylsulfoxide or DMSO (D8418, Sigma-Aldrich) for 2 hours prior to stimulation. All cells were incubated for 24 hours before being fixed with 4% methanol-free Pierce Formaldehyde or PFA (28908, Thermo Scientific) for 20 minutes at room temperature. Cells were then washed 3 times in PBS. Fixed cells were maintained in PBS until ready for immunofluorescent staining.

6.3.4 Immunofluorescent Staining and Confocal Microscopy Analysis

Fixed cells were first blocked for 30 minutes at 37°C in PBS with 10% goat-serum (G9023, Sigma-Aldrich), 0.3% triton X-100 (T8787, Sigma-Aldrich) to permeabilize cell membrane. Cells were washed 3 times in PBS for 5 minutes each and primary antibody solution was added to be incubated overnight at 4°C. Antibody solution contained appropriate dilution of antibody in PBS with 5% goat serum. Cells were washed 3 times in PBS for 5 minutes each to remove unbound primary antibody. Secondary antibody solution contained 1:1000 dilution of fluorescent goat anti-mouse or goat anti-rabbit antibodies. Secondary antibody staining occurred at room temperature in the dark for 2 hours. Cells were washed in PBS for 3 times for 5 minutes each to remove excess secondary staining. Cells were then mounted on to glass slides with Prolong gold anti-fade mounting solution with DAPI nuclear staining (P36941, Bio-Sciences Ltd). The mounted cells were allowed to cure at room temperature for 24 hours in the dark before sealing with fast dry nail polish. The slides were kept at 4°C in the dark until ready for confocal analysis.

Primary and secondary antibodies and concentrations used for immunofluorescent staining are described in table 6.5.

	Primary Antibody			**Secondary Antibody**		
Antigen	**Species**	**Category**	**Dilution**	**Fluorescence**	**Category**	**Dilution**
IGF1R	Mouse	#05-656, Millipore	1:200	AlexaFluor 488 Gt anti-Ms	ab150077	1:1000
pCREB	Rabbit	#9198, CST	1:800	DL649 Gt anti-Rb	JIR 111-485-003	1:1000

pAKT	Rabbit	#4058, CST	1:200	DL488 Gt anti-Rb	JIR 111-485-003	1:1000
p44/42 MAPK (pErk1/2)	Rabbit	#4370, CST	1:200	DL488 Gt anti-Rb	JIR 111-485-003	1:1000
MAP2	Mouse	MAB3418, Sigma-Aldrich	1:500	DL649 Gt anti-Ms	JIR 115-495-003	1:1000

Table 6.5 – Antibodies used in Chapter III Experiments

Mounted immunostained cells were then imaged using Leica SP8 scanning confocal microscope using lasers at 405nm, 488nm and 638nm under oil immersion x40 objective. A secondary control was always included as part of the confocal analysis. The secondary control was treated exactly the same as experimental conditions except that primary antibody was not added. Secondary controls therefore measured the degree of non-specific background signal and controlled for variation in the laser intensity for a given experiment. 5 images per coverslip were taken with each experimental condition repeated a minimum of n = 3 times.

Images were analysed using Fiji software (https://imagej.net/software/fiji/). Images were opened in Fiji in .lif format as a file with channels for DAPI, bright-field, 488 and 649 staining. For nuclear (DAPI) or cytoplasmic staining (MAP2) a Gaussian blur filter was applied to smooth features and default thresholding was applied to provide a mask of nuclear or cytoplasmic areas. Nuclear or cytoplasmic areas were selected as regions of interest (ROI) and were measured. Fluorescence was determined by dividing the integrated density over the area of a ROI. Background signal from secondary control was subtracted from experimental conditions to give actual signal and ROI were normalised to average of experimental controls. Statistics and graphs were generated using RStudio software rstatix(), agricolae() and ggpubr() respectively.

6.3.5 Protein Extraction and Western Blot

Western blot was used to qualitatively demonstrate that PPP inhibited phosphorylation of IGF1R receptor in neuronally differentiated SH-SY5Y. After completion of

experiment, SH-SY5Y cells were washed once in ice cold PBS. Cell protein was extracted from culture using rubber scrapper on ice in 500µL of fresh RIPA buffer (150mM NaCl, 1% triton X100, 0.5% Sodium Deoxycholate, 0.1% Sodium Dodexyl Sulfate (SDS), in 50mM Tris-HCl pH 8.0) with cOmplete protease inhibitor cocktail (11836170001, Sigma-Aldrich) and PhosSTOP phosphatase inhibitor (04906845001, Sigma-Aldrich). Cell treated with same conditions were combined to ensure concentration of protein was high enough for detection and kept on ice so as not to effect the phosphorylation status of cell receptors. The cells were agitated on a rocker for 30 at 4°C and centrifuged at 16,000xg for 20 minutes at 4°C.

Acrylamide (A3699, Sigma-Aldrich) electrophoresis gel was made using a 12% stacking gel (0.375M Tris-HCl pH 8.8, 0.1% SDS, 0.1% Ammonium persulfate (APS), 0.0004% Tetramethylethlenediamine (TEMED)) and a 6% stacking gel (0.165M Tris-HClCl pH 6.8, 0.09% SDS, 0.09% APS, 0.0004% TEMED) approximately 1cm from the top of the gel cast with 12 well comb insert. 15µL extracted protein was added to 5µL loading buffer (0.24M Tris-HCl 6.8pH, 8% SDS 4% Glycerol, 0.05M EDTA, 0.04% Bromophenol Blue, 5% β-mercaptoethanol) and was heat denatured at 95°C for 5 minutes. The protein samples were loaded into gel electrophoresis chamber with running buffer (0.025M Tris base, 0.192M Glycine, 0.1% SDS) along with precision plus dual colour molecular weight ladder (#1610374, BioRad). The samples were run down the gel with 150 volts so as to separate the proteins sufficiently. The gel was then removed from the electrophoresis chamber and a transfer sandwich was prepared for wet transfer using Polyvinylidene Fluoride (PVDF) membrane. PVDF membrane was activated in methanol for 1 minute and the washed in transfer buffer (0.025M Tris base, 0.192M Glycine, 0.1% SDS, 20% Methanol), the acrylamide gel containing the proteins and two sets of chromatography paper (3001-861, GE) 5 layers thick was also washed in transfer buffer. The sandwich consisted of chromatography paper, activated membrane, acrylamide gel and another set of chromatography paper. The sandwich placed into a clamp with sponges on either side of the sandwich in wet transfer tank (BioRad) so as the protein could transfer from the gel (closer to cathode) to the membrane (closer to the anode). The transfer was run at 100 volts for 1 hour. After transfer membrane was placed in Tris Buffered Saline with tween or TBSt (150mM NaCl, 50mM Tris pH 7.6, 0.1% Tween 20). The membrane was cut to separate the target protein pIGF1R kDA 95 (#3024, CST) and reference protein β-Actin, kDA 45

(#4967, CST). Membranes were blocked at 37C for 30 minutes using 5% BSA in TBSt and then left to incubate overnight at 4C in 1:1000 dilution of primary antibody in TBSt 5% BSA. Membranes were washed 3 times for 5 minutes each in TBSt to remove primary antibody solution and then incubated at room temperature for 1 hour in anti-Rb Horseradish Peroxide (HRP) antibody (#7074, CST) at a dilution of 1:5000 in TBSt with 5% BSA. The membrane was washed 3 times in TBSt for 5 minutes each to remove secondary antibody solution. Prior to imaging in Fusion FX Imaging System (Vilber Lourmat) the membranes were incubated in Immobilon Western Chemiluminescent HRP substrate (P90720, Millipore) for 1 minute. Intensity of Staining was measured using Fiji software, the intensity of target protein (pIGF1R) was divided by the intensity of the reference control protein (β-Actin).

References

1. Llorens-Martín, M., Torres-Alemán, I. & Trejo, J. L. Mechanisms Mediating Brain Plasticity: IGF1 and Adult Hippocampal Neurogenesis. *The Neuroscientist* **15**, 134–148 (2009).

2. Netchine, I., Azzi, S., Le Bouc, Y. & Savage, M. O. IGF1 molecular anomalies demonstrate its critical role in fetal, postnatal growth and brain development. *Best Pract Res Clin Endocrinol Metab* **25**, 181–190 (2011).

3. Dyer, A. H., Vahdatpour, C., Sanfeliu, A. & Tropea, D. The role of Insulin-Like Growth Factor 1 (IGF-1) in brain development, maturation and neuroplasticity. *Neuroscience* **325**, 89–99 (2016).

4. Junnila *et al.* The GH/IGF-1 axis in aging and longevity. *Nat Rev Endocrinol* **9**, 366–376 (2014).

5. Bondy, C. A. & Lee, W. Patterns of Insulin-like Growth Factor and IGF Receptor Gene Expression in the Brain. *Annals New York Academy of Sciences* **692**, 33–43 (1993).

6. Philippou, A., Maridaki, M., Pneumaticos, S. & Koutsilieris, M. The complexity of the IGF1 gene splicing, posttranslational modification and bioactivity. *Mol Med* **20**, 202–14 (2014).

7. Fernandez, A. M. & Torres-Alemán, I. The many faces of insulin-like peptide signalling in the brain. *Nat Rev Neurosci* **13**, 225–239 (2012).

8. Hakuno, F. & Takahashi, S. 40 YEARS OF IGF1 IGF1 receptor signaling pathways. *J Mol Endocrinol* **61**, 69–86 (2018).

9. Hanks, S. K., Quinn, A. M. & Hunter, T. The protein kinase family: Conserved features and deduced phylogeny of the catalytic domains. *Science (1979)* **241**, 42–52 (1988).

10. Sara, V. R., Drakenberg, K. & Giacobini, M. B. The Biological Role of Truncated and the Tripeptide GPE in the Central Nervous System. *Anals New York Academy of Sciences* (1993).

11. Guan, J. *et al.* Cyclic glycine-proline regulates IGF-1 homeostasis by altering the binding of IGFBP-3 to IGF-1. *Sci Rep* **4**, 1–9 (2014).

12. Yamamoto, H. & Murphy, L. J. Enzymatic conversion of IGF-1 to des(1-3)IGF-1 in rat serum and tissues: A futher potential site of growth hormone regulation of IGF-1 action. *Journal of Endocrinology* **146**, 141–146 (1995).

13. Rajaram, S., Baylink, D. J. & Mohan, S. Insulin-Like Growth Factor-Binding Proteins in Serum and Other Biological Fluids: Regulation and Functions. *Endocr Rev* **18**, 801–831 (1997).

14. Allard, J. B. & Duan, C. IGF-binding proteins: Why do they exist and why are there so many? *Front Endocrinol (Lausanne)* **9**, 1–12 (2018).

15. Pandini, G. *et al.* Insulin/insulin-like growth factor I hybrid receptors have different biological characteristics depending on the insulin receptor isoform involved. *Journal of Biological Chemistry* **277**, 39684–39695 (2002).

16. Tartare-Deckert, S., Sawka-Verhelle, D., Murdaca, J. & Van Obberghen, E. Evidence for a differential interaction of SHC and the insulin receptor substrate-1 (IRS-1) with the insulin-like growth factor-I (IGF-I) receptor in the yeast two-hybrid system. *Journal of Biological Chemistry* **270**, 23456–23460 (1995).

17. Dudek, H. *et al.* Regulation of neuronal survival by the serine-threonine protein kinase Akt. *Science (1979)* **275**, 661–665 (1997).

18. Fukushima, T. *et al.* Phosphatidylinositol 3-Kinase (PI3K) Activity Bound to Insulin-like Growth Factor-I (IGF-I) Receptor , which Is Continuously Sustained by IGF-I Stimulation , Is Required for. **287**, 29713–29721 (2012).

19. Sun, Y. *et al.* Signaling pathway of MAPK/ERK in cell proliferation, differentiation, migration, senescence and apoptosis. *Journal of Receptors and Signal Transduction* **35**, 600–604 (2015).

20. Copps, K. D. & White, M. F. Regulation of insulin sensitivity by serine/threonine phosphorylation of insulin receptor substrate proteins IRS1 and IRS2. *Diabetologia* **55**, 2565–2582 (2012).

21. Liu, J. P., Baker, J., Perkins, A. S., Robertson, E. J. & Efstratiadis, A. Mice carrying null mutations of the genes encoding insulin-like growth factor I (Igf-1) and type 1 IGF receptor (Igf1r). *Cell* **75**, 59–72 (1993).

22. Tropea, D. *et al.* Gene expression changes and molecular pathways mediating activity-dependent plasticity in visual cortex. *Nat Neurosci* **9**, 660–668 (2006).

23. Baroncelli, L. *et al.* Early IGF-1 primes visual cortex maturation and accelerates developmental switch between NKCC1 and KCC2 chloride transporters in enriched animals. *Neuropharmacology* **113**, 167–177 (2017).

24. Guan, J., Williams, C., Gunning, M., Mallard, C. & Gluckman, P. The effects of IGF-1 treatment after hypoxic-ischemic brain injury in adult rats. *Journal of Cerebral Blood Flow and Metabolism* **13**, 609–616 (1993).

25. Guan, J. *et al.* Neuroprotective effects of the N-terminal tripeptide of insulin-like growth factor-1, glycine-proline-glutamate (GPE) following intravenous infusion in hypoxic-ischemic adult rats. *Neuropharmacology* **47**, 892–903 (2004).

26. Yamaguchi, F. *et al.* Increase of extracellular insulin-like growth factor I (IGF-I) concentration following electrolytical lesion in rat hippocampus. *Neurosci Lett* **128**, 273–276 (1991).

27. Gluckman, P. *et al.* A role for IGF-1 in the rescue of CNS neurons following hypoxic-ischemic injury. *Biochem Biophys Res Commun* **182**, 593–599 (1992).

28. Vaaga, C. E., Tovar, K. R. & Westbrook, G. L. The IGF-derived tripeptide Gly-Pro-Glu is a weak NMDA receptor agonist. *J Neurophysiol* **112**, 1241–1245 (2014).

29. Aguado-Llera, D. *et al.* Improvement in inflammation is associated with the protective effect of Gly-Pro-Glu and cycloprolylglycine against Aβ-induced depletion of the hippocampal somatostatinergic system. *Neuropharmacology* **151**, 112–126 (2019).

30. Corvin, A. P. *et al.* Insulin-like growth factor 1 (IGF1) and its active peptide (1-3)IGF1 enhance the expression of synaptic markers in neuronal circuits through different cellular mechanisms. *Neurosci Lett* **520**, 51–56 (2012).

31. Neul, J. L. *et al.* Rett Syndrome: Revised Diagnostic Criteria and Nomenlcature. *Annual Neurology* **68**, 944–950 (2010).

32. Rett, A. On a remarkable syndrome of cerebral atrophy associated with hyperammonaemia in childhood. *Wiener Medizinische Wochenschrift* **166**, 322–324 (2016).

33. Hagberg, B. Clinical manifestations and stages of Rett syndrome. *Ment Retard Dev Disabil Res Rev* **8**, 61–65 (2002).

34. Amir, R. E. *et al.* Rett syndrome is caused by mutations in X-linked MECP2, encoding methyl-CpG-binding protein 2. *Nat Genet* **23**, 185–188 (1999).

35. Temudo, T. *et al.* Rett syndrome with and without detected MECP2 mutations: An attempt to redefine phenotypes. *Brain Dev* **33**, 69–76 (2011).

36. Suter, B., Treadwell-Deering, D., Zoghbi, H. Y., Glaze, D. G. & Neul, J. L. Brief report: MECP2 mutations in people without rett syndrome. *J Autism Dev Disord* **44**, 703–711 (2014).

37. Krishnaraj, R., Ho, G. & Christodoulou, J. RettBASE: Rett Syndrome Database Update. *Hum Mutat* **38**, 922–931 (2017).

38. Guy, J., Hendrich, B., Holmes, M., Martin, J. E. & Bird, a. A mouse Mecp2-null mutation causes neurological symptoms that mimic Rett syndrome. *Nat Genet* **27**, 322–6 (2001).

39. Valderas, J. M., Starfield, B., Sibbald, B., Salisbury, C. & Roland, M. Defining comorbidity: Implications for understanding health and health services. *Ann Fam Med* **7**, 357–363 (2009).

40. Julu, P. O. O. *et al.* Characterisation of breathing and associated central autonomic dysfunction in the Rett disorder. 29–37 (2001).

41. Ramirez, J. M., Ward, C. S. & Neul, J. L. Breathing challenges in Rett Syndrome: Lessons learned from humans and animal models. *Respir Physiol Neurobiol* **189**, 280–287 (2013).

42. Weese-Mayer, D. E. *et al.* Autonomic nervous system dysregulation: Breathing and heart rate perturbation during wakefulness in young girls with rett syndrome. *Pediatr Res* **60**, 443–449 (2006).

43. Julu, P. O., Kerr, A. M., Hansen, S., Apartopoulos, F. & Jamal, G. A. Immaturity of medullary cardiorespiratory neurones leading to inappropriate autonomic reactions as a likely cause of sudden death in Rett's syndrome. *Arch Dis Child* **77**, 464–5 (1997).

44. Motil, K. J., Mcnair, L., Skinner, S. A., Lee, H. & Ph, D. Gastrointestinal and nutrional problems occur frequently throughout life in Girls and women with Rett Syndrome. *J Pediatr Gastroenterol Nutr* **55**, 292–298 (2012).

45. Strati, F. *et al.* Altered gut microbiota in Rett syndrome. *Microbiome* **4**, 1–15 (2016).

46. Thapa, S. *et al.* Assessment of the gut bacterial microbiome and metabolome of girls and women with Rett Syndrome. *PLoS One* **16**, 1–22 (2021).

47. Glaze, D. G. *et al.* Epilepsy and the natural history of Rett syndrome. *Neurology* **74**, 909–912 (2010).

48. Operto, F. F., Mazza, R., Pastorino, G. M. G., Verrotti, A. & Coppola, G. Epilepsy and genetic in Rett syndrome: A review. *Brain Behav* **9**, 1–10 (2019).

49. Tarquinio, D. C. *et al.* Longitudinal course of epilepsy in Rett syndrome and related disorders. *Brain* **140**, 306–318 (2017).

50. Wong, K., Leonard, H., Jacoby, P., Ellaway, C. & Downs, J. The trajectories of sleep disturbances in Rett syndrome. *J Sleep Res* **24**, 223–233 (2015).

51. Zhang, X., Lin, J. S. & Spruyt, K. Sleep problems in Rett syndrome animal models: A systematic review. *J Neurosci Res* **99**, 529–544 (2021).

52. Sarber, K. M., Howard, J. J. M., Dye, T. J., Pascoe, J. E. & Simakajornboon, N. Sleep-disordered breathing in pediatric patients with Rett syndrome. *Journal of Clinical Sleep Medicine* **15**, 1451–1457 (2019).

53. Hagebeuk, E. E. O., Bijlmer, R. P. G. M., Koelman, J. H. T. M. & Poll-The, B. T. Respiratory disturbances in rett syndrome: Don't forget to evaluate upper airway obstruction. *J Child Neurol* **27**, 888–892 (2012).

54. Amaddeo, A. *et al.* Polysomnographic findings in Rett syndrome. *European Journal of Paediatric Neurology* **23**, 214–221 (2019).

55. Li, Q. *et al.* Circadian rhythm disruption in a mouse model of Rett syndrome circadian disruption in RTT. *Neurobiol Dis* **77**, 155–164 (2015).

56. Fehr, S. *et al.* The CDKL5 disorder is an independent clinical entity associated with early-onset encephalopathy. *European Journal of Human Genetics* **21**, 266–273 (2013).

57. Jakimiec, M., Paprocka, J. & Smigei, R. CDKL5 Deficiency Disorder — A Complex Epileptic Encephalopathy. *Brain Science* **10**, 1–9 (2020).

58. Renieri, A. *et al.* Diagnostic criteria for the Zappella variant of Rett syndrome (the preserved speech variant). *Brain Dev* **31**, 208–216 (2009).

59. Mencarelli, M. A. *et al.* Novel FOXG1 mutations associated with the congenital variant of Rett syndrome. *J Med Genet* **47**, 49–53 (2010).

60. Ariani, F. *et al.* FOXG1 Is Responsible for the Congenital Variant of Rett Syndrome. *Am J Hum Genet* **83**, 89–93 (2008).

61. Philippe, C. *et al.* Phenotypic variability in Rett syndrome associated with FOXG1 mutations in females. *J Med Genet* **47**, 59–65 (2010).

62. Artuso, R. *et al.* Early-onset seizure variant of Rett syndrome: Definition of the clinical diagnostic criteria. *Brain Dev* **32**, 17–24 (2010).

63. Archer, H. L. *et al.* CDKL5 mutations cause infantile spasms, early onset seizures, and severe mental retardation in female patients. *J Med Genet* **43**, 729–34 (2006).

64. Nan, X., Campoy, F. J. & Bird, A. MeCP2 is a transcriptional repressor with abundant binding sites in genomic chromatin. *Cell* **88**, 471–481 (1997).

65. Lewis, J. D. *et al.* Purification, sequence, and cellular localization of a novel chromosomal protein that binds to Methylated DNA. *Cell* **69**, 905–914 (1992).

66. Shahbazian, M. D., Antalffy, B., Armstrong, D. L. & Zoghbi, H. Y. Insight into Rett syndrome: MeCP2 levels display tissue-and cell-specific differences and correlate with neuronal maturation. *Hum Mol Genet* **11**, 115–124 (2002).

67. Kriaucionis, S. & Bird, A. The major form of MeCP2 has a novel N-terminus generated by alternative splicing. *Nucleic Acids Res* **32**, 1818–1823 (2004).

68. Zachariah, R. M. & Rastegar, M. Linking epigenetics to human disease and rett syndrome: The emerging novel and challenging concepts in MeCP2 research. *Neural Plast* **2012**, (2012).

69. Klose, R. J. *et al.* DNA binding selectivity of MeCP2 due to a requirement for A/T sequences adjacent to methyl-CpG. *Mol Cell* **19**, 667–678 (2005).

70. Nan, X. *et al.* Transcriptional repression by the methyl-CpG-binding protein MeCP2 involves a histone deacetylase complex. *Nature* **393**, 386–389 (1998).

71. Lagger, S. *et al.* MeCP2 recognizes cytosine methylated tri-nucleotide and di-nucleotide sequences to tune transcription in the mammalian brain. *PLoS Genet* **13**, 1–26 (2017).

72. Lyst, M. J. *et al.* Affinity for DNA Contributes to NLS Independent Nuclear Localization of MeCP2. *Cell Rep* **24**, 2213–2220 (2018).

73. Lyst, M. J. *et al.* Rett syndrome mutations abolish the interaction of MeCP2 with the NCoR/SMRT co-repressor. *Nat Neurosci* **16**, 898–902 (2013).

74. Ben-Shachar, S., Chahrour, M., Thaller, C., Shaw, C. A. & Zoghbi, H. Y. Mouse models of MeCP2 disorders share gene expression changes in the cerebellum and hypothalamus. *Hum Mol Genet* **18**, 2431–2442 (2009).

75. Mellén, M., Ayata, P., Dewell, S., Kriaucionis, S. & Heintz, N. MeCP2 binds to 5hmC enriched within active genes and accessible chromatin in the nervous system. *Cell* **151**, 1417–1430 (2012).

76. Mellén, M., Ayata, P. & Heintz, N. 5-Hydroxymethylcytosine accumulation in postmitotic neurons results in functional demethylation of expressed genes. *Proc Natl Acad Sci U S A* **114**, E7812–E7821 (2017).

77. Skene, P. J. *et al.* Neuronal MeCP2 Is Expressed at Near Histone-Octamer Levels and Globally Alters the Chromatin State. *Mol Cell* **37**, 457–468 (2010).

78. Li, C. H. *et al.* MeCP2 links heterochromatin condensates and neurodevelopmental disease. *Nature* **586**, 440–444 (2020).

79. Ip, J. P. K., Mellios, N. & Sur, M. Rett syndrome : insights into genetic , molecular and circuit mechanisms. *Nat Rev Neurosci* **19**, 368–382 (2018).

80. Percy, A. K. *et al.* When Rett syndrome is due to genes other than MECP2. *Transl Sci Rare Dis* **3**, 49–53 (2018).

81. Fuchs, C. *et al.* Loss of CDKL5 impairs survival and dendritic growth of newborn neurons by altering AKT/GSK-3β signaling. *Neurobiol Dis* **70**, 53–68 (2014).

82. Mari, F. *et al.* CDKL5 belongs to the same molecular pathway of MeCP2 and it is responsible for the early-onset seizure variant of Rett syndrome. *Hum Mol Genet* **14**, 1935–1946 (2005).

83. Ma, M., Adams, H. R., Seltzer, L. E., Dobyns, W. B. & Paciorkowski, A. R. Phenotype Differentiation of FOXG1 and MECP2 Disorders: A New Method for Characterization of Developmental Encephalopathies. *Journal of Pediatrics* **178**, 233-240.e10 (2016).

84. Martynoga, B., Morrison, H., Price, D. J. & Mason, J. O. Foxg1 is required for specification of ventral telencephalon and region-specific regulation of dorsal telencephalic precursor proliferation and apoptosis. *Dev Biol* **283**, 113–127 (2005).

85. Dastidar, S. G. *et al.* Isoform-Specific Toxicity of Mecp2 in Postmitotic Neurons: Suppression of Neurotoxicity by FoxG1. *Journal of Neuroscience* **32**, 2846–2855 (2012).

86. Akbarian, S. The neurobiology of Rett syndrome. *Neuroscientist* **9**, 57–63 (2003).

87. Belichenko, N. P., Belichenko, P. V., Hong, H. L., Mobley, W. C. & Francke, U. Comparative Study of Brain Morphology in Mecp2 Mutant Mouse Models of Rett Syndrome. *Journal of Comparative Neurology* **508**, 184–195 (2008).

88. Bauman, M. L., Kemper Th., L. & Arin, D. M. Microscopic observations of the brain in Rett syndrome. *Neuropediatrics* **26**, 105–108 (1995).

89. Armstrong, D., Dunn, J. K., Antalffy, B. & Trivedi, R. Selective Dendritic Alterations in the Cortex of Rett Syndrome. *J Neuropathol Exp Neurol* **54**, 195–201 (1995).

90. Nguyen, M. V. C. *et al.* MeCP2 is critical for maintaining mature neuronal networks and global brain anatomy during late stages of postnatal brain development and in the mature adult brain. *Journal of Neuroscience* **32**, 10021–10034 (2013).

91. McGowan, H. & Pang, Z. P. Regulatory functions and pathological relevance of the MECP2 3'UTR in the central nervous system. *Cell Regeneration* **4**, 4:9 (2015).

92. Makedonski, K., Abuhatzira, L., Kaufman, Y., Razin, A. & Shemer, R. MeCP2 deficiency in Rett syndrome causes epigenetic aberrations at the PWS/AS imprinting center that affects UBE3A expression. *Hum Mol Genet* **14**, 1049–1058 (2005).

93. Guy, J., Gan, J., Selfridge, J., Cobb, S. & Bird, A. Reversal of Neurological Defects in Mouse Model of Rett Syndrome. *Science (1979)* **315**, 1143–1148 (2007).

94. Ross, P. D. *et al.* Exclusive expression of MeCP2 in the nervous system distinguishes between brain and peripheral Rett syndrome-like phenotypes. *Hum Mol Genet* **25**, 4389–4404 (2016).

95. Pozzo-miller, L. & Li, W. BDNF deregulation in Rett syndrome. **76**, 1–22 (2015).

96. Chang, Q., Khare, G., Dani, V., Nelson, S. & Jaenisch, R. The disease progression of Mecp2 mutant mice is affected by the level of BDNF expression. *Neuron* **49**, 341–348 (2006).

97. Sampathkumar, C. *et al.* Loss of MeCP2 disrupts cell autonomous and autocrine BDNF signaling in mouse glutamatergic neurons. *Elife* **5**, 1–23 (2016).

98. Zhou, Z. *et al.* Brain-Specific Phosphorylation of MeCP2 Regulates Activity-Dependent Bdnf Transcription, Dendritic Growth, and Spine Maturation. *Neuron* **52**, 255–269 (2006).

99. Picard, N. & Fagiolini, M. MeCP2: an epigenetic regulator of critical periods. *Curr Opin Neurobiol* **59**, 95–101 (2019).

100. Krishnan, N. *et al.* PTP1B inhibition suggests a therapeutic strategy for Rett syndrome. *Journal of Clinical Investigation* **125**, 3163–3177 (2015).

101. Tropea, D. *et al.* Partial reversal of Rett Syndrome-like symptoms in MeCP2 mutant mice. *Proc Natl Acad Sci U S A* **106**, 2029–2034 (2009).

102. Noutel, J., Hong, Y. K., Leu, B., Kang, E. & Chen, C. Experience-Dependent Retinogeniculate Synapse Remodeling Is Abnormal in MeCP2-Deficient Mice. *Neuron* **70**, 35–42 (2011).

103. Dani, V. S. *et al.* Reduced cortical activity due to a shift in the balance between excitation and inhibition in a mouse model of Rett Syndrome. *Proceedings of the National Academy of Sciences* **102**, 12560–12565 (2005).

104. Nelson, E. D., Kavalali, E. T. & Monteggia, L. M. MeCP2-Dependent Transcriptional Repression Regulates Excitatory Neurotransmission. *Current Biology* **16**, 710–716 (2006).

105. Wood, L., Gray, N. W., Zhou, Z., Greenberg, M. E. & Shepherd, G. M. G. Synaptic circuit abnormalities of motor-frontal layer 2/3 pyramidal neurons in an RNA interference model of methyl-CpG-binding protein 2 deficiency. *Journal of Neuroscience* **29**, 12440–12448 (2009).

106. Calfa, G., Li, W., Rutherford, J. M. & Pozzo-Miller, L. Excitation/inhibition imbalance and impaired synaptic inhibition in hippocampal area CA3 of Mecp2 knockout mice. *Hippocampus* **25**, 159–168 (2015).

107. Chen, C. Y. *et al.* Defective GABAergic neurotransmission in the nucleus tractus solitarius in Mecp2-null mice, a model of Rett syndrome. *Neurobiol Dis* **109**, 25–32 (2018).

108. Abdala, A. P., Toward, M. A., Dutschmann, M., Bissonnette, J. M. & Paton, J. F. R. Deficiency of GABAergic synaptic inhibition in the Kolliker-Fuse area

underlies respiratory dysrhythmia in a mouse model of Rett syndrome. *J Physiol* **594**, 223–237 (2016).

109. El-Khoury, R. *et al.* GABA and glutamate pathways are spatially and developmentally affected in the brain of Mecp2-deficient mice. *PLoS One* **9**, 25–29 (2014).

110. Chao, H. *et al.* GABAergic dysfunction mediates autism-like stereotypies and Rett syndrome phenotypes. *Nature* **468**, 263–269 (2010).

111. Banerjee, A. *et al.* Jointly reduced inhibition and excitation underlies circuit-wide changes in cortical processing in Rett syndrome. *Proceedings of the National Academy of Sciences* **113**, E7287–E7296 (2016).

112. Kahanovitch, U., Patterson, K. C., Hernandez, R. & Olsen, M. L. Glial dysfunction in meCP2 deficiency models: Implications for rett syndrome. *Int J Mol Sci* **20**, (2019).

113. Colantuoni, C. *et al.* Gene expression profiling in postmortem Rett Syndromerain: differential gene expression and patient classification. *Neurobiol Dis* **8**, 847–65 (2001).

114. Lioy, D. T. *et al.* A role for glia in the progression of Rett's syndrome. *Nature* **475**, 497–500 (2011).

115. Okabe, Y. *et al.* Alterations of gene expression and glutamate clearance in astrocytes derived from an mecp2-null mouse model of rett syndrome. *PLoS One* **7**, (2012).

116. Delépine, C. *et al.* Altered microtubule dynamics and vesicular transport in mouse and human MeCP2-deficient astrocytes. *Hum Mol Genet* **25**, 146–157 (2016).

117. Rakela, B., Brehm, P. & Mandel, G. Astrocytic modulation of excitatory synaptic signaling in a mouse model of Rett syndrome. *Elife* **7**, 1–23 (2018).

118. Wake, H., Moorhouse, A. J., Jinno, S., Kohsaka, S. & Nabekura, J. Resting microglia directly monitor the functional state of synapses in vivo and determine the fate of ischemic terminals. *Journal of Neuroscience* **29**, 3974–3980 (2009).

119. Nance, E. *et al.* Dendrimer-mediated delivery of N-acetyl cysteine to microglia in a mouse model of Rett syndrome. *J Neuroinflammation* **14**, 1–19 (2017).

120. Maezawa, I. & Jin, L. W. Rett Syndrome Microglia Damage Dendrites and Synapses by the Elevated Release of Glutamate. *Journal of Neuroscience* **30**, 5346–5356 (2010).

121. Derecki, N. C. *et al.* Wild type microglia arrest pathology in a mouse model of Rett syndrome. *Nature* **484**, 105–109 (2012).

122. Wang, J. *et al.* Wild-type microglia do not reverse pathology in mouse models of Rett syndrome. *Nature* **521**, 541–552 (2015).

123. Muffat, J. *et al.* Efficient derivation of microglia-like cells from human pluripotent stem cells. *Nat Med* **22**, 1358–1367 (2016).

124. Zhao, D. *et al.* Transcriptome analysis of microglia in a mouse model of Rett syndrome: differential expression of genes associated with microglia/macrophage activation and cellular stress. *Mol Autism* **8**, 1–12 (2017).

125. Chen, R. Z., Akbarian, S., Tudor, M. & Jaenisch, R. Deficiency of methyl-CpG binding protein-2 in CNS neurons results in a Rett-like phenotype in mice. *Nat Genet* **27**, 327–331 (2001).

126. Collins, A. L. *et al.* Mild overexpression of MeCP2 causes a progressive neurological disorder in mice. *Hum Mol Genet* **13**, 2679–2689 (2004).

127. Baker, S. A. *et al.* An AT-hook domain in MeCP2 determines the clinical course of Rett syndrome and related disorders. *Cell* **152**, 984–996 (2013).

128. Johnson, B. S. *et al.* Biotin tagging of MeCP2 in mice reveals contextual insights into the Rett syndrome transcriptome. *Nat Med* **23**, 1203–1214 (2017).

129. Dragich, J., Houwink-Manville, I. & Schanen, C. Rett syndrome: a surprising result of mutation in MECP2. *Human Molecular Genetics Review* **9**, 2365–2375 (2000).

130. Ren, Y. *et al.* siRecords: An extensive database of mammalian siRNAs with efficacy ratings. *Bioinformatics* **22**, 1027–1028 (2006).

131. Dana, H. *et al.* Molecular Mechanisms and Biological Functions of siRNA. *Int J Biomed Sci* **13**, 48–57 (2017).

132. Gibson, J. H. *et al.* Downstream targets of methyl CpG binding protein 2 and their abnormal expression in the frontal cortex of the human Rett syndrome brain. *BMC Neurosci* **11**, 53 (2010).

133. Lyu, J. W., Yuan, B., Cheng, T. L., Qiu, Z. L. & Zhou, W. H. Reciprocal regulation of autism-related genes MeCP2 and PTEN via microRNAs. *Sci Rep* **6**, 2–7 (2016).

134. Ananiev, G., Williams, E. C., Li, H. & Chang, Q. Isogenic pairs of wild type and mutant induced pluripotent stem cell (iPSC) lines from rett syndrome patients as In Vitro disease model. *PLoS One* **6**, (2011).

135. Neul, J. L. *et al.* Specific mutations in Methyl-CpG-Binding Protein 2 confer different severity in Rett syndrome. *Neurology* **70**, 1313–1321 (2008).

136. Tanaka, Y. *et al.* Transcriptional regulation in pluripotent stem cells by methyl CpG-binding protein 2 (MeCP2). *Hum Mol Genet* **23**, 1045–1055 (2014).

137. Chen, X. *et al.* Graded and pan-neural disease phenotypes of Rett Syndrome linked with dosage of functional MeCP2. *Protein Cell* **12**, 639–652 (2021).

138. Landucci, E. *et al.* iPSC-derived neurons profiling reveals GABAergic circuit disruption and acetylated α-tubulin defect which improves after iHDAC6 treatment in Rett syndrome. *Exp Cell Res* **368**, 225–235 (2018).

139. Ballas, N., Lioy, D. T., Grunseich, C. & Mandel, G. Non–cell autonomous influence of MeCP2-deficient glia on neuronal dendritic morphology. *Nat Neurosci* **12**, 311–317 (2009).

140. Williams, E. C. *et al.* Mutant astrocytes differentiated from Rett syndrome patients-specific iPSCs have adverse effects on wildtype neurons. *Hum Mol Genet* **23**, 2968–2980 (2014).

141. Gomes, A. R., Fernandes, T. G., Cabral, J. M. S. & Diogo, M. M. Modeling rett syndrome with human pluripotent stem cells: Mechanistic outcomes and future clinical perspectives. *Int J Mol Sci* **22**, (2021).

142. Gomes, A. R. *et al.* Modeling Rett Syndrome With Human Patient-Specific Forebrain Organoids. *Front Cell Dev Biol* **8**, 1–18 (2020).

143. Samarasinghe, R. A. *et al.* Identification of neural oscillations and epileptiform changes in human brain organoids. *Nat Neurosci* **24**, 1488–1500 (2021).

144. Chen, Y. *et al.* Modeling Rett Syndrome Using TALEN-Edited MECP2 Mutant Cynomolgus Monkeys. *Cell* **169**, 945-955.e10 (2017).

145. Wang, J. *et al.* White Matter Structural and Network Topological Changes Underlying the Behavioral Phenotype of MECP2 Mutant Monkeys . *Cerebral Cortex* 1–15 (2021) doi:10.1093/cercor/bhab166.

146. Pignataro, D. *et al.* Gene therapy approaches in the non-human primate model of Parkinson's disease. *J Neural Transm* **125**, 575–589 (2018).

147. Naidu, S. *et al.* Neuroimaging studies in Rett syndrome. *Brain Dev* **23**, 62–71 (2001).

148. Keogh, C., Pini, G., Gemo, I., Kaufmann, W. E. & Tropea, D. Functional network mapping reveals state-dependent response to IGF1 treatment in rett syndrome. *Brain Sci* **10**, 1–18 (2020).

149. Chahil, G., Yelam, A. & Bollu, P. C. Rett Syndrome in Males: A Case Report and Review of Literature. *Cureus* **10**, (2018).

150. Ribeiro, M. C. & MacDonald, J. L. Sex differences in Mecp2-mutant Rett syndrome model mice and the impact of cellular mosaicism in phenotype development. *Brain Res* **1729**, 146644 (2020).

151. Castro, J. *et al.* Functional recovery with recombinant human IGF1 treatment in a mouse model of Rett Syndrome. *Proc Natl Acad Sci U S A* **111**, 9941–6 (2014).

152. Carrette, L. L. G., Blum, R., Ma, W., Kelleher, R. J. & Lee, J. T. Tsix–Mecp2 female mouse model for Rett syndrome reveals that low-level MECP2 expression extends life and improves neuromotor function. *Proc Natl Acad Sci U S A* **115**, 8185–8190 (2018).

153. Khwaja, O. S. *et al.* Safety, pharmacokinetics, and preliminary assessment of efficacy of mecasermin (recombinant human IGF-1) for the treatment of Rett

syndrome. *Proceedings of the National Academy of Sciences* **111**, 4596–4601 (2014).

154. O'Leary, H. M. *et al.* Placebo-controlled crossover assessment of mecasermin for the treatment of Rett syndrome. *Ann Clin Transl Neurol* **5**, 323–332 (2018).

155. Oosterholt, S. P., Horrigan, J., Jones, N., Glass, L. & Della, O. European Journal of Pharmaceutical Sciences Population pharmacokinetics of NNZ-2566 in healthy subjects. *European Journal of Pharmaceutical Sciences* 1–10 (2017) doi:10.1016/j.ejps.2017.05.032.

156. Glaze, D. G. *et al.* A Double-Blind, Randomized, Placebo-Controlled Clinical Study of Trofinetide in the Treatment of Rett Syndrome. *Pediatr Neurol* **76**, 37–46 (2017).

157. Berry-Kravis, E. *et al.* A Double-Blind, Randomized, Placebo-Controlled Clinical Study of Trofinetide in the Treatment of Fragile X Syndrome. *Pediatr Neurol* **110**, 30–41 (2020).

158. Samaco, R. C. *et al.* Loss of MeCP2 in aminergic neurons causes cell-autonomous defects in neurotransmitter synthesis and specific behavioral abnormalities. *Proceedings of the National Academy of Sciences* **106**, 21966–21971 (2009).

159. Paterson, D. S. *et al.* Serotonin Transporter Abnormality in the Dorsal Motor Nucleus of the Vagus in Rett Syndrome: Potential Implications for Clinical Autonomic Dysfunction. *J Neuropathol Exp Neurol* **64**, 1018–1027 (2005).

160. De Filippis, B. *et al.* Pharmacological Stimulation of the Brain Serotonin Receptor 7 as a Novel Therapeutic Approach for Rett Syndrome. *Neuropsychopharmacology* **39105**, 2506–2518 (2014).

161. Abdala, A. P. *et al.* Effect of sarizotan, a 5-HT1a and D2-like receptor agonist, on respiration in three mouse models of rett syndrome. *Am J Respir Cell Mol Biol* **50**, 1031–1039 (2014).

162. Enns, G. M. & Cohen, B. H. Clinical Trials in Mitochondrial Disease. *J Inborn Errors Metab Screen* **5**, 232640981773301 (2017).

163. Nissenkorn, A., Kidon, M. & Ben-zeev, B. A Potential Life-Threatening Reaction to Glatiramer Acetate in Rett Syndrome. *Pediatr Neurol* **68**, 40–43 (2017).

164. Abdala, A. P., Bissonnette, J. M. & Newman-Tancredi, A. Pinpointing brainstem mechanisms responsible for autonomic dysfunction in Rett syndrome: Therapeutic perspectives for 5-HT1A agonists. *Front Physiol* **5 MAY**, 1–8 (2014).

165. Robinson, M. D., McCarthy, D. J. & Smyth, G. K. edgeR: A Bioconductor package for differential expression analysis of digital gene expression data. *Bioinformatics* **26**, 139–140 (2009).

166. Pecorelli, A. *et al.* Genes related to mitochondrial functions, protein degradation, and chromatin folding are differentially expressed in lymphomonocytes of rett syndrome patients. *Mediators Inflamm* **2013**, (2013).

167. Lin, P. *et al.* Transcriptome analysis of human brain tissue identifies reduced expression of complement complex C1Q Genes in Rett syndrome. *BMC Genomics* **17**, 1–11 (2016).

168. Viemari, J. C. *et al.* Mecp2 deficiency disrupts norepinephrine and respiratory systems in mice. *Journal of Neuroscience* **25**, 11521–11530 (2005).

169. Toward, M. A., Abdala, A. P., Knopp, S. J., Paton, J. F. R. & Bissonnette, J. M. Increasing brain serotonin corrects CO2 chemosensitivity in methyl-CpG-binding protein 2 (Mecp2)-deficient mice. *Exp Physiol* **98**, 842–849 (2013).

170. Vogelgesang, S., Niebert, M., Bischoff, A. M., Hülsmann, S. & Manzke, T. Persistent expression of serotonin receptor 5b alters breathing behavior in male MeCP2 knockout mice. *Front Mol Neurosci* **11**, 1–7 (2018).

171. Linker, S. B., Mendes, A. P. D. & Marchetto, M. C. IGF-1 treatment causes unique transcriptional response in neurons from individuals with idiopathic autism. *Mol Autism* **11**, 1–13 (2020).

172. Amir, R. E. *et al.* Influence of mutation type and X chromosome inactivation on Rett syndrome phenotypes. *Ann Neurol* **47**, 670–679 (2000).

173. Ribeiro, M. C. & MacDonald, J. L. Sex differences in Mecp2-mutant Rett syndrome model mice and the impact of cellular mosaicism in phenotype development. *Brain Res* **1729**, 146644 (2020).

174. Fan, D., Krishnamurthi, R., Harris, P., Barber, P. A. & Guan, J. Plasma cyclic glycine proline / IGF-1 ratio predicts clinical outcome and recovery in stroke patients. (2019) doi:10.1002/acn3.743.

175. Fan, D., Krishnamurthi, R., Harris, P., Barber, P. A. & Guan, J. Plasma cyclic glycine proline/IGF-1 ratio predicts clinical outcome and recovery in stroke patients. *Ann Clin Transl Neurol* **6**, 669–677 (2019).

176. Mellios, N. *et al.* MeCP2-regulated miRNA control early human neurogenesis through differential effects on ERK and AKT signalling. *Mol Psychiatry* **23**, 1051–1065 (2018).

177. Laron, Z. Insulin-like growth factor 1 (IGF-1): a growth hormone. *Mol Pathol* **54**, 311–6 (2001).

178. Romero, C. J. *et al.* Insulin-Like Growth Factor 1 Mediates Negative Feedback to Somatotroph GH Expression via POU1F1/CREB Binding Protein Interactions. *Mol Cell Biol* **32**, 4258–4269 (2012).

179. Sehat, B., Andersson, S., Girnita, L. & Larsson, O. Identification of c-Cbl as a new ligase for insulin-like growth factor-I receptor with distinct roles from Mdm2 in receptor ubiquitination and endocytosis. *Cancer Res* **68**, 5669–5677 (2008).

180. Modarresi, F. *et al.* Inhibition of natural antisense transcripts in vivo results in gene-specific transcriptional upregulation. *Nat Biotechnol* **30**, 453–459 (2012).

181. Mellios, N. *et al.* β2-Adrenergic receptor agonist ameliorates phenotypes and corrects microRNA-mediated IGF1 deficits in a mouse model of Rett syndrome. *Proc Natl Acad Sci U S A* **111**, 9947–9952 (2014).

182. Shahbazian, M. D., Antalffy, B., Armstrong, D. L. & Zoghbi, H. Y. Insight into Rett syndrome: MeCP2 levels display tissue-and cell-specific differences and correlate with neuronal maturation. *Hum Mol Genet* **11**, 115–124 (2002).

183. Pecorelli, A., Cervellati, C., Cordone, V., Hayek, J. & Valacchi, G. Compromised immune/inflammatory responses in Rett syndrome. *Free Radic Biol Med* **152**, 100–106 (2020).

184. Cronk, J. C. *et al.* Methyl-CpG Binding Protein 2 Regulates Microglia and Macrophage Gene Expression in Response to Inflammatory Stimuli. *Immunity* **42**, 679–691 (2015).

185. Condamine, T. *et al.* Tmem176B and Tmem176A are associated with the immature state of dendritic cells. *J Leukoc Biol* **88**, 507–515 (2010).

186. Lancien, M. *et al.* Dendritic cells require TMEM176A / B ion channels for optimal MHC II antigen presentation to naive CD4 + T cells. (2019).

187. Scholz, E. M. *et al.* Human leukocyte antigen (hla)-DrB1*15:01 and hla-DrB5*01:01 present complementary peptide repertoires. *Front Immunol* **8**, 1–12 (2017).

188. Yu, L. *et al.* Association of Brain DNA Methylation in SORL1, ABCA7, HLA-DRB5, SLC24A4 and BIN1 with Pathological Diagnosis of Alzheimer Disease. *JAMA Neurol* **72**, 15–24 (2015).

189. Caillier, S. J. *et al.* Uncoupling the roles of HLA-DRB1 and HLA-DRB5 genes in multiple sclerosis. *J Immunol* **181**, 5473–80 (2008).

190. Magdalon, J. *et al.* Complement System in Brain Architecture and Neurodevelopmental Disorders. *Front Neurosci* **14**, 1–14 (2020).

191. Ehrhart, F. *et al.* Integrated analysis of human transcriptome data for Rett syndrome finds a network of involved genes. *World Journal of Biological Psychiatry* **21**, 712–725 (2020).

192. Chu, Y. *et al.* Enhanced synaptic connectivity and epilepsy in C1q knockout mice. *Proceedings of the National Academy of Sciences* **107**, 7975–7980 (2010).

193. Wolters, T. L. J., Netea, M. G., Hermus, A. R. M. M., Smit, J. W. A. & Netea-Maier, R. T. IGF1 potentiates the pro-inflammatory response in human peripheral blood mononuclear cells via MAPK. *J Mol Endocrinol* **59**, 129–139 (2017).

194. Zalosnik, M. I., Fabio, M. C., Bertoldi, M. L., Castañares, C. N. & Degano, A. L. MeCP2 deficiency exacerbates the neuroinflammatory setting and autoreactive response during an autoimmune challenge. *Sci Rep* **11**, 1–15 (2021).

195. Spadaro, O. *et al.* IGF1 Shapes Macrophage Activation in Response to Immunometabolic Challenge. *Cell Rep* **19**, 225–234 (2017).

196. Mairet-Coello, G., Tury, A. & DiCicco-Bloom, E. Insulin-like growth factor-1 promotes G1/S cell cycle progression through bidirectional regulation of cyclins and cyclin-dependent kinase inhibitors via the phosphatidylinositol 3-kinase/Akt pathway in developing rat cerebral cortex. *Journal of Neuroscience* **29**, 775–788 (2009).

197. Ren, M. *et al.* Insulin-like growth factor-1 promotes cell cycle progression via upregulation of cyclin D1 expression through the phosphatidylinositol 3-kinase/nuclear factor-kB signaling pathway in FRTL thyroid cells. *Acta Pharmacol Sin* **30**, 113–119 (2009).

198. Zhang, W. *et al.* MeCP 2 deficiency promotes cell reprogramming by stimulating IGF 1 / AKT / mTOR signaling and activating ribosomal protein-mediated cell cycle gene translation. *J Mol Cell Biol* **10**, 515–526 (2018).

199. Shovlin, S. & Tropea, D. Transcriptome level analysis in Rett syndrome using human samples from different tissues. *Orphanet J Rare Dis* **13**, 1–15 (2018).

200. Krishnan, K., Lau, B. Y. B., Ewall, G., Huang, Z. J. & Shea, S. D. MECP2 regulates cortical plasticity underlying a learned behaviour in adult female mice. *Nat Commun* **8**, (2017).

201. Fintini, D., Brufani, C. & Cappa, M. Profile of mecasermin for the long-term treatment of growth failure in children and adolescents with severe primary IGF-1 deficiency. *Ther Clin Risk Manag* **5**, 553–559 (2009).

202. Li, Y. *et al.* Global transcriptional and translational repression in human-embryonic- stem-cell-derived rett syndrome neurons. *Cell Stem Cell* **13**, 446–458 (2013).

203. Urdinguio, R. G. *et al.* Mecp2-null mice provide new neuronal targets for rett syndrome. *PLoS One* **3**, (2008).

204. Sanfeliu, A., Hokamp, K., Gill, M. & Tropea, D. Transcriptomic Analysis of Mecp2 Mutant Mice Reveals Differentially Expressed Genes and Altered Mechanisms in Both Blood and Brain. **10**, 1–16 (2019).

205. Wang, S. *et al.* S100A8/A9 in inflammation. *Front Immunol* **9**, (2018).

206. Chen, J. & Chen, Z. J. Regulation of NF-κB by ubiquitination. *Curr Opin Immunol* **25**, 4–12 (2013).

207. Conti, V. *et al.* MeCP2 affects skeletal muscle growth and morphology through non cell-autonomous mechanisms. *PLoS One* **10**, 1–16 (2015).

208. Wrigley, S., Arafa, D. & Tropea, D. Insulin-Like Growth Factor 1: At the Crossroads of Brain Development and Aging. *Front Cell Neurosci* **11**, 14 (2017).

209. Hong, H. *et al.* Central IGF1 improves glucose tolerance and insulin sensitivity in mice. *Nutr Diabetes* **7**, (2017).

210. Stearns, N. A. *et al.* Behavioral and anatomical abnormalities in Mecp2 mutant mice: A model for Rett syndrome. *Neuroscience* **146**, 907–921 (2007).

211. Santos, M., Silva-Fernandes, A., Oliveira, P., Sousa, N. & Maciel, P. Evidence for abnormal early development in a mouse model of Rett syndrome. *Genes Brain Behav* **6**, 277–286 (2007).

212. Ricceri, L., De Filippis, B. & Laviola, G. Mouse models of Rett syndrome: from behavioural phenotyping to preclinical evaluation of new therapeutic approaches. *Behavioural pharmacology* **19**, 501–517 (2008).

213. Ure, K. *et al.* Restoration of Mecp2 expression in GABAergic neurons is sufficient to rescue multiple disease features in a mouse model of Rett syndrome. *Elife* **5**, 1–21 (2016).

214. Samaco, R. C. *et al.* Female Mecp2+/- mice display robust behavioral deficits on two different genetic backgrounds providing a framework for pre-clinical studies. *Hum Mol Genet* **22**, 96–109 (2013).

215. Glass, D. J. Skeletal muscle hypertrophy and atrophy signaling pathways. *International Journal of Biochemistry and Cell Biology* **37**, 1974–1984 (2005).

216. Robinson, L. *et al.* Morphological and functional reversal of phenotypes in a mouse model of Rett syndrome. *Brain* **135**, 2699–2710 (2012).

217. Pecorelli, A. *et al.* Cytokines profile and peripheral blood mononuclear cells morphology in Rett and autistic patients. *Cytokine* **77**, 180–188 (2016).

218. Kriaucionis, S. *et al.* Gene Expression Analysis Exposes Mitochondrial Abnormalities in a Mouse Model of Rett Syndrome. *Mol Cell Biol* **26**, 5033–5042 (2006).

219. De Filippis, B. *et al.* Mitochondrial free radical overproduction due to respiratory chain impairment in the brain of a mouse model of Rett syndrome: Protective effect of CNF1. *Free Radic Biol Med* **83**, 167–177 (2015).

220. Jordan, C., Li, H. H., Kwan, H. C. & Francke, U. Cerebellar gene expression profiles of mouse models for Rett syndrome reveal novel MeCP2 targets. *BMC Med Genet* **8**, 36 (2007).

221. Smrt, R. D., Pfeiffer, R. L. & Zhao, X. Age-dependent expression of MeCP2 in a heterozygous mosaic mouse model. *Hum Mol Genet* **20**, 1834–1843 (2011).

222. Justice, M. J., Buchovecky, C. M., Kyle, S. M. & Djukic, A. A role for metabolism in Rett syndrome pathogenesis: New clinical findings and potential treatment targets. *Rare Dis* **1**, e27265 (2013).

223. Neul, J. L. *et al.* Metabolic Signatures Differentiate Rett Syndrome From Unaffected Siblings. *Front Integr Neurosci* **14**, 1–10 (2020).

224. Wahba, G. *et al.* Activity and MeCP2-dependent regulation of nNOS levels in enteric neurons. *Neurogastroenterology and Motility* **28**, 1723–1730 (2016).

225. Stagi, S. *et al.* Thyroid Function in Rett Syndrome. *Hormone research in Pediatrics* **83**, 118–125 (2015).

226. Dehkhoda, F., Lee, C. M. M., Medina, J. & Brooks, A. J. The growth hormone receptor: Mechanism of receptor activation, cell signaling, and physiological aspects. *Front Endocrinol (Lausanne)* **9**, 1–23 (2018).

227. Aldosary, M. *et al.* Rett Syndrome, a Neurodevelopmental Disorder, Whole-Transcriptome, and Mitochondrial Genome Multiomics Analyses Identify Novel Variations and Disease Pathways. *OMICS* **24**, 160–171 (2020).

228. Vogl, T. *et al.* Alarmin S100A8/S100A9 as a biomarker for molecular imaging of local inflammatory activity. *Nat Commun* **5**, 1–12 (2014).

229. Ehrlich, I. & Malinow, R. Postsynaptic Density 95 controls AMPA Receptor Incorporation during Long-Term Potentiation and Experience-Driven Synaptic Plasticity. *Journal of Neuroscience* **24**, 916–927 (2004).

230. Yoshii, A. & Constantine-Paton, M. BDNF induces transport of PSD-95 to dendrites through PI3K-AKT signaling after NMDA receptor activation. *Nat Neurosci* **10**, 702–711 (2007).

231. Lee, L. C. *et al.* Association of CaMK2A and MeCP2 signaling pathways with cognitive ability in adolescents. *Mol Brain* **14**, 1–14 (2021).

232. Golubiani, G., Lagani, V., Solomonia, R. & Müller, M. Metabolomic fingerprint of mecp2-deficient mouse cortex: Evidence for a pronounced multi-facetted metabolic component in rett syndrome. *Cells* **10**, (2021).

233. Buchovecky, C. M. *et al.* A suppressor screen in Mecp2 mutant mice implicates cholesterol metabolism in Rett syndrome. *Nat Genet* **45**, 1013–1020 (2013).

234. Delgado, I. J., Kim, D. S., Thatcher, K. N., LaSalle, J. M. & Van den Veyver, I. B. Expression profiling of clonal lymphocyte cell cultures from Rett syndrome patients. *BMC Med Genet* **7**, 61 (2006).

235. Colak, D. *et al.* Genomic and transcriptomic analyses distinguish classic Rett and Rett-like syndrome and reveals shared altered pathways. *Genomics* **97**, 19–28 (2011).

236. Yuan, J., Yin, Z., Tao, K., Wang, G. & Gao, J. Function of insulin-like growth factor 1 receptor in cancer resistance to chemotherapy. *Oncol Lett* **15**, 41–47 (2018).

237. Werner, H., Sarfstein, R., LeRoith, D. & Bruchim, I. Insulin-like growth factor 1 signaling axis meets p53 genome protection pathways. *Front Oncol* **6**, 1–13 (2016).

238. Lee, A. V., Gooch, J. L., Oesterreich, S., Guler, R. L. & Yee, D. Insulin-Like Growth Factor I-Induced Degradation of Insulin Receptor Substrate 1 Is Mediated by the 26S Proteasome and Blocked by Phosphatidylinositol 3′-Kinase Inhibition. *Mol Cell Biol* **20**, 1489–1496 (2000).

239. Girnita, A. *et al.* Cyclolignans as Inhibitors of the Insulin-Like Growth Factor-1 Receptor and Malignant Cell Growth. *Cancer Res* **64**, 236–242 (2004).

240. Ito, S. *et al.* Involvement of Insulin-Like Growth Factor 1 Receptors Signaling in the Amyloid-β Peptide Oligomers-Induced p75 Neurotrophin Receptor Protein Expression in Mouse Hippocmapus. *Journal of Alzheimer's Disease* **31**, 493–506 (2012).

241. Encinas, M. *et al.* Sequential Treatment of SH-SY5Y Cells with Retinoic Acid and Brain-Derived Neurotrophic Factor Gives Rise. (2000) doi:10.1046/j.1471-4159.2000.0750991.x.

242. Zheng, W.-H. *et al.* Insulin-like growth factor-1 (IGF-1) induces the activation/phosphorylation of Akt kinase and cAMP response element-binding protein (CREB) by activating different signaling pathways in PC12 cells. *BMC Neurosci* **7**, 51 (2006).

243. Carlezon, W. A., Duman, R. S. & Nestler, E. J. The many faces of CREB. **28**, (2005).

244. Alonso, M., Medina, J. H. & Pozzo-Miller, L. ERK1/2 Activation Is Necessary for BDNF to Increase Dendritic Spine Density in Hippocampal CA1 Pyramidal Neurons. *Learning and Memory* **11**, 172–178 (2004).

245. Hakuno, F. *et al.* Constitutive expression of insulin receptor substrate (irs)-1 inhibits myogenic differentiation through nuclear exclusion of foxo1 in l6 myoblasts. *PLoS One* **6**, (2011).

246. Chen, R. H., Sarnecki, C. & Blenis, J. Nuclear localization and regulation of erk- and rsk-encoded protein kinases. *Mol Cell Biol* **12**, 915–927 (1992).

247. Perkinton, M. S., Ip, J. K., Wood, G. L., Crossthwaite, A. J. & Williams, R. J. Phosphatidylinositol 3-kinase is a central mediator of NMDA receptor signalling

to MAP kinase (Erk1 / 2), Akt / PKB and CREB in striatal neurones. 239–254 (2002).

248. Xing, J., Ginty, D. D. & Greenberg, M. E. Coupling of the RAS-MAPK Pathway to Gene Activation by RSK2, a Growth Factor-Regulated CREB Kinase. *Science (1979)* **273**, 959–963 (1996).

249. Bonni, A. *et al.* Cell survival promoted by the Ras-MAPK signaling pathway by transcription-dependent and -independent mechanisms. *Science (1979)* **286**, 1358–1362 (1999).

250. Benito, E. & Barco, A. CREB ' s control of intrinsic and synaptic plasticity : implications for CREB-dependent memory models. *Trends Neurosci* **33**, 230–240 (2010).

251. Vasilcanu, D. *et al.* The cyclolignan PPP induces activation loop-specific inhibition of tyrosine phosphorylation of the insulin-like growth factor-1 receptor. Link to the phosphatidyl inositol-3 kinase/Akt apoptotic pathway. *Oncogene* **23**, 7854–7862 (2004).

252. Favelyukis, S., Till, J. H., Hubbard, S. R. & Miller, W. T. Structure and autoregulation of the insulin-like growth factor 1 receptor kinase. *Nat Struct Biol* **8**, 1058–1063 (2001).

253. Sizonenko, S., Sirimanne, E. S., Williams, C. E. & Gluckman, P. D. Neuroprotective effects of the N-terminal tripeptide of IGF-1, glycine-proline-glutamate, in the immature rat brain after hypoxic-ischemic injury. *Brain Res* **922**, 42–50 (2001).

254. Cortelazzo, A. *et al.* Subclinical inflammatory status in Rett syndrome. *Mediators Inflamm* **2014**, 1–13 (2014).

255. Delépine, C. *et al.* Astrocyte Transcriptome from the Mecp2308-Truncated Mouse Model of Rett Syndrome. *Neuromolecular Med* **17**, 353–363 (2015).

256. Arsenault, J. *et al.* Interregulation between fragile X mental retardation protein and methyl CpG binding protein 2 in the mouse posterior cerebral cortex. *Hum Mol Genet* **29**, 3744–3756 (2021).

257. Bach, S., Shovlin, S., Moriarty, M., Bardoni, B. & Tropea, D. Rett Syndrome and Fragile X Syndrome: Different Etiology With Common Molecular Dysfunctions. *Front Cell Neurosci* **15**, 1–16 (2021).

258. Henry, C. J. *et al.* Minocycline attenuates lipopolysaccharide (LPS)-induced neuroinflammation, sickness behavior, and anhedonia. *J Neuroinflammation* **5**, 1–14 (2008).

259. Qin, L. *et al.* Advancing equity, equality and non-discrimination in food systems : Pathways to reform. *Glia* **55**, 453–462 (2007).

260. Renthal, W. *et al.* Characterization of human mosaic Rett syndrome brain tissue by single-nucleus RNA sequencing. *Nat Neurosci* **21**, (2018).

261. Sugino, K. *et al.* Cell-type-specific repression by methyl-CpG-binding protein 2 is biased toward long genes. *J Neurosci* **34**, 12877–12883 (2014).

262. Solomon-Zemler, R., Sarfstein, R. & Werner, H. Nuclear insulin-like growth factor-1 receptor (IGF1R) displays proliferative and regulatory activities in non-malignant cells. *PLoS One* **12**, 1–14 (2017).

263. Yoneyama, Y. *et al.* IRS-1 acts as an endocytic regulator of IGF-I receptor to facilitate sustained IGF signaling. *Elife* **7**, 1–34 (2018).

264. Marchetto, M. C. N. M. *et al.* A model for neural development and treatment of Rett syndrome using human induced pluripotent stem cells. *Cell* **143**, 527–39 (2010).

265. Cheung, A. Y. L. *et al.* Isolation of MECP2-null Rett Syndrome patient hiPS cells and isogenic controls through X-chromosome inactivation. *Hum Mol Genet* **20**, 2103–2115 (2011).

266. Soumillon, M., Cacchiarelli, D., Semrau, S., van Oudenaarden, A. & Mikkelsen, T. S. Characterization of directed differentiation by high-throughput single-cell RNA-Seq. *bioRxiv* 003236 (2014) doi:10.1101/003236.

267. Wu, D. *et al.* ROAST: Rotation gene set tests for complex microarray experiments. *Bioinformatics* **26**, 2176–2182 (2010).

268. Chen, Y., Lun, A. T. L. & Smyth, G. K. From reads to genes to pathways: differential expression analysis of RNA-Seq experiments using Rsubread and the edgeR quasi-likelihood pipeline. *F1000Res* **5**, 1438 (2016).

269. Consortium, T. G. O. The Gene Ontology resource: Enriching a GOld mine. *Nucleic Acids Res* **49**, D325–D334 (2021).

270. Consortium, T. G. O. Gene Ontology : tool for the unification of biology. *Nat Genet* **25**, 25–29 (2000).

271. Fabregat, A. *et al.* Reactome pathway analysis: A high-performance in-memory approach. *BMC Bioinformatics* **18**, 1–9 (2017).

272. Archer, H. *et al.* Correlation between clinical severity in patients with Rett syndrome with a p.R168X or p.T158M MECP2 mutation, and the direction and degree of skewing of X-chromosome inactivation. *J Med Genet* **44**, 148–152 (2007).

273. Jian, Le *et al.* p.R270X MECP2 mutation and mortality in Rett syndrome. *European Journal of Human Genetics* **13**, 1235- 1238 (2005).

274. Brown, K *et al.* The molecular basis of variable phenotypic severity among common missense mutations causing Rett syndrome. *Human Molecular Genetics*, **25**, 558-570 (2016).

275. Pitcher, M *et al.* Rett syndrome like phenotypes in the R255X Mecp2 mutant mouse are rescued by MECP2 transgene. *Human Molecular Genetics*, **24**, 2662-2672 (2015).

276. Merritt, Collins J *et al.* Pharmacological read-through of R294X Mecp2 in a novel mouse model of Rett syndrome. *Human Molecular Genetics*, **29**, 2461-2470 (2020).

277. Bebbington, A *et al.* Investigating genotype-phenotype relationships in Rett syndrome using an international data set. *Neurology*, **70**, 868-875 (2008).

278. Bebbington, A *et al.* Updating the profile of C-terminal MECP2 deletions in Rett syndrome. *Journal of Medical Genetics*, **47**, 242-248 (2010).

279. Neul, J *et al.* Specific mutations in Methyl-CpG-Binding Protein 2 confer different severity in Rett syndrome. *Neurology*, **70**, 1313-1321 (2008).

280. Xiol, C *et al.* X chromosome inactivation does not necessarily determine the severity of the phenotype in Rett syndrome patients. *Scientific Reports*, **9**, 1-9 (2019).

281. Sceniak, M *et al.* Mechanisms of Functional Hypoconnectivity in the Medial Prefrontal Cortex of Mecp2 Null Mice. *Cerebral Cortex,* **26**, 1938-1956 (2016).

282. Durand, S *et al.* NMDA Receptor Regulation Prevents Regression of Visual Cortical Function in the Absence of Mecp2. *Neuron*, **76**, 1078-1090 (2012).

283. He, L-j *et al.* Conditional deletion of Mecp2 in parvalbumin-expressing GABAergic cells results in the absence of critical period plasticity. *Nature Communication*, **5**, 1-15 (2014).

284. Asaka, Y *et al.* Hippocampal synaptic plasticity is impaired in the Mecp2-null mouse model of Rett syndrome. *Neurobiology of Disease*, **21**, 217-227 (2006).

285. Morretti, P *et al.* Learning and memory and synaptic plasticity are impaired in a mouse model of Rett syndrome. *Journal of Neuroscience*, **26**, 319-327 (2006).

286. Li, W *et al.* Excitatory synapses are stronger in the hippocampus of Rett syndrome mice due to altered synaptic trafficking of AMPA-type glutamate receptors. *Proceedings of the National Academy of Sciences of the United States of America*, **113**, 1575-1548 (2016).